# Tuning a bacteria-yeast transkingdom conjugation system toward *in situ* microbiome engineering

By

#### Kevin Stindt

A dissertation submitted in partial fulfillment of the requirements for the degree

#### **Doctor of Philosophy**

(Biophysics)

at the
UNIVERSITY of WISCONSIN – MADISON
2023

Date of final oral examination: 07 / 06 / 2023 This dissertation is approved by the following members of the Final Oral Committee:

Megan McClean, Advisor, Associate Professor, Biomedical Engineering
Ophelia Venturelli, Associate Professor, Biochemistry and Bacteriology
Jean-Michel Ané, Professor, Microbiology and Agronomy
Nancy Keller, Professor, Medical Microbiology & Immunology and Plant Pathology
Jo Handelsman, Vilas Research Professor, Howard Hughes Medical Institute Professor, and
Director, Wisconsin Institute for Discovery

© Copyright Kevin R. Stindt 2023

All Rights Reserved

## Acknowledgments

I must first thank my PI / mentor / boss Megan McClean, for so often pulling off the impeccable balance of being interested and knowledgeable while giving ample leeway for the learning process. I cannot count the number of times she responded to (asinine) experimental failures with sincere interest and apparent trust that I could solve the issues, making my time in lab scientifically constructive while disarming my stubborn doubts. Plus, she let me into the lab without a rotation or project in mind, so thanks for that. My fellow lab members were also instrumental to my success, especially Kieran (scaffolded the majority of my otherwise self-guided coding efforts), Renee (for all of the sanity-maintaining conversations), and Taylor, one of the rare people who is equal parts brilliant and kind; we need more like you, have some babies. My committee members, Ophelia, Jo, Nancy, Jean-Michel, have routinely subverted by fears of disaster at each discussion, instead showing enthusiasm and constructive feedback at every turn. Thank you. I also have to thank my former PI Tom Record, whom I respect tremendously, for supporting me during those early chaotic years of my Ph.D.

Many others help me on my way academically and professionally. Many thanks to Devin Wixon, Michel Wattiaux, Jess Maher, Dante Fratta, and Christina Othon for helping me to struggle through the Delta program on a limp leg (so to speak), and Jessica TeSlaa for offering me similar benefit of the doubt in WISCIENCE. In Life Sciences Communications, Dominique Brossard, Dietram Scheufele, and the ever-so-wonderful Shiela Reaves always offered fascinating points of view, lots of enthusiasm for the work, and gave me a desperately needed escape into the humanities. At 10x Genomics, thank you to Jessica Terry for being a constant source of support and encouragement, and thank you to Greg Tranah (UCSF and CPMC) and most especially Janelle Noble (CHORI), for taking a chance on a researcher with one Bio class under his belt; thanks, too,

to Julie Lane for generally being a joy to work with. The CaSPies, who kept me social in more ways than one—Nimu (kinda CaSP), Sam, Caitlin, Jenny, April, Chris, and many others—y'all are crazy and impressive. And the biggest thanks ever to Allison Lynch, who on multiple occasions kept me from walking by convincing me I could do it, and for bringing the program together, and for offering so much support—with work, with life, with kiddo—without reservation. Thank you.

Finally, I'm totally spoiled by the friends and family who've believed in this crazy scheme of mine over the (probably too many) years. To my parents, who always seemed confused by my selfdoubt; my brother, who was always game to take a pipe and song break; Olivia & Trent, who pretty much single-handedly (double-handedly?) showed me the appeal of Madison, and helped me get on my feet here; Travis & Carrin, for cutting the BS and being fantastic people; Terra & Ada for letting me flake on rehearsal and just show up to "play notes"; the Lancaster guys (& fams!) who gratefully got closer while I was 2000 miles away; the Elderberries, who kept my playing-fingers as busy as my dancin' feet, and kept me sane so much; and John Heron, for getting me started on this wacky route: thank you all. To my wife, Rachel, who has been almost (almost) as supportive scientifically—providing brilliant & thoughtful feedback with such ease—as she has been emotionally, truly being my rock during all of my roller-coastering: thank you for being thoughtful, brilliant, damnably optimistic, and my best friend. To my son, Aldo, thank you for giving me the most delightful perspective slap I could have ever hoped for at the end of each stressful day. I can't wait to see you make better decisions. Finally, a very, very special thanks to Todd Bradford and Shana McDevitt, for being so instrumental to all of this, at so many steps, in so many ways that couldn't possibly fit on this page, and for being there when it really mattered.

I love the hell out of these people. If it weren't for them, I would totally suck.

#### **Abstract**

Microbiomes play crucial roles in human health and ecosystems, though our understanding of the fungal members severely lags that of bacteria. And despite the rise in fungal infections, there are few treatments for them, and no fungal alternatives to bacteria-targeting phage therapies. Along with the myriad additional ways fungi interact with our agriculture, ecological, and food production systems, tools to engineer fungi in situ would be extremely valuable, whether to mitigate fungal infections or otherwise modify microbiome members. Transkingdom conjugation (TKC) offers a possibility for both, as the phenomenon of DNA transfer from bacterial cells to eukaryotes enables in situ modifications of yeasts. While such genetic transfers have been known to naturally occur in a wide range of eukaryotes, and are thought to contribute to their evolution, TKC has been understudied as a technique in synthetic microbial consortia or fungal treatment. One major obstacle to widespread use of TKC is its limited DNA transfer efficiency, due to the requirement for cell-to-cell contact. In this work, I utilize interactions between genetically tractable Escherichia coli and Saccharomyces cerevisiae to control the incidence of TKC. I test the landscape of population interactions between the bacterial donors and yeast recipients to find that bacterial commensalism leads to maximized TKC, both in culture and in mixed colonies. I demonstrate the capacity of cell-to-cell binding via mannoproteins to assist both TKC incidence and bacterial commensalism in culture, and model how these tunable controls can predictably yield a range of TKC outcomes. Further, I demonstrate that these lessons can be utilized to lastingly alter a recipient population, by both "rescuing" a poor-growing recipient population, and collapsing a stable population via a novel TKC-mediated CRISPR/Cas9 system. Finally, I demonstrate tools toward controlling TKC in space and time via optogenetic (light) control.

# Table of Contents

AcknowledgmentsAcknowledgments	i
Abstract	<i>iii</i>
Table of Contents	iv
A brief note on the organization of this text	1
Chapter 1: Introduction  1.1 Fungal pathogens, bioproduction, and the need for in situ perturbation	1 3
1.4 Figures	8
Chapter 2: Tunable population dynamics in batch culture affect TKC	
2.1 Introduction: levers of control	
2.2 Results	10
2.2.1 Tunable population dynamics in batch culture affect TKC outcomes	10 13 14
2.3 Discussion	
2.4 Figures and Tables	26
2.4.1 Figure 1: Batch culturing reveals relationships between population ratios and TKC	26 35 41 46
2.5 Materials and Methods	
2.5.1 Strain and plasmid construction 2.5.2 Batch culture and TKC counting 2.5.3 Flow cytometry 2.5.4 Microscopy of culture aggregates. 2.5.5 Clumping image analysis 2.5.6 Data analysis and figures 2.5.6 Table 3: Strains used in this study 2.5.6 Table 4: Plasmids used in this study	48 50 51 52 53 55
Chapter 3: Spatial dynamics of TKC in mixed colonies	57
3.1 Introduction: maximizing the boundary space of mixed colonies	
3.2.1 Building a TKC reporter for tracking transconjugants spatially	58 60
3.3 Discussion	
3.4 Figures	
3.4.1 Figure 1: Creation of TKC reporters.  3.4.2 Figure 2: Mixed colonies follow culture dynamics, show increased TKC with spatial mixing	67

3.4.3 Figure 3: Agar pad imaging of proto-colonies	79
3.5 Materials and Methods	81
3.5.1 Colony culturing and preparation	
3.5.2 Colony imaging and analysis	
3.5.3 Table 1: Strains used in this study	
3.5.4 Table 2: Plasmids used in this study	
Chapter 4: Altering recipient outcomes by tuning populations	86
4.1 Introduction	86
4.2 Results	87
4.2.1 Harnessing population dynamics to rescue a recipient population through TKC	
4.2.2 TKC-mediated CRISPR killing can be interrupted by mannose addition	
4.3 Discussion	90
4.4 Figures and Tables	95
4.4.1 Figure 1: TKC-mediated rescue of unhealthy recipient populations via population tuning	
4.4.2 Table 1: Rescue model parameters (values in green diverge from clump-model parameters)	
4.4.3 Figure 2: TKC-mediated killing drives recipient population collapse, is mannose-interruptible	
4.5 Materials and Methods	112
4.5.1 Rescue growth model	112
4.5.2 CRISPR-Cas9 plasmid and strain construction	
4.5.3 Determination of TKC count	
4.5.4 Batch culturing measurements	
4.5.5 Table 2: Strains used in this study	
4.5.6 Table 3: Plasmids used in this study	
Chapter 5: Optogenetic control of TKC	117
5.1 Introduction	117
5.2 Results	119
5.2.1 pDawn shows prolonged activation with low intensity, short-pulsed light signal	
5.2.2 Deletion of <i>TraJ</i> from T4SS genes leads to reduced TKC, toward opto-control	
5.2.3 Opto- <i>TraJ</i> donors fail to generate light-activated TKC	121
5.3 Discussion	122
5.4 Figures	
5.4.1 Figure 1: pDawn stimulation by automated blue-light batch culture system	
5.4.2 Figure 2: Opto-TKC control construction	128
5.4.3 Figure 3: Opto-TKC donors fail to conjugate with light activation	
5.5 Materials and Methods	134
5.5.1 Construction of opto-strains	
5.5.2 Blue-light stimulation in batch culture	
5.5.3 Intraspecies opto-TKC experiment.	
5.5.4 Table 1: Strains used in this study	
5.5.5 Table 2: Plasmids used in this study	
Chapter 6: Discussion	137
6.1 Summary of major findings, in brief	137
······································	
• •	138
6.2 Future directions and opportunities	

6.3 Concluding remarks	143
7 References	145
Appendix A: Secrete to Beat the Heat (News & Views Article)	162
A.1 Body text	
A.2 Figure 1: Cooperative secretion of glutathione extends the habitable temperature range for yeast	165
Appendix B: Give and Take in the Exametabolome (News & Views Article)	167
B.1 Body text	
B.2 Figure 1: SeMeCos to determine the effects of auxotrophs	
Appendix C: Protecting Soil Resources by Improving the Wisconsin Farmland Preserva	tion
Program (Policy Memo)	173
C.1 Executive Summary	173
C.2 Soil erosion and Wisconsin	173
C.3 Farmland Preservation Program	174
C.4 Farmland Preservation lacks sufficient tilling standards	
C.5 Policy recommendations	175
C.6 Appendix	176
Potential problems and solutions with minimal tilling	176

## A brief note on the organization of this text

A publication containing many of the findings here is forthcoming and will likely be submitted by the defense of this dissertation. But, given that it will span a variety of sub-projects, and that I considerably expand upon these topics below, I've opted to break paper contents into dissertation chapters based on subject matter instead of maintaining the flow of the manuscript. Moreover, I divide the introductory notes into those that are generic for all the findings—immediately following this—and those that are chapter-specific. I hope that this increases the narrative flow and avoids content repetition. That said, many findings will reference methods etc. across chapters, and for those purposes, I include hyperlinks within the text. The discussion is similarly split into chapters, with a brief cumulative summary, future directions, and concluding remarks at the end.

# Chapter 1: Introduction

#### 1.1 Fungal pathogens, bioproduction, and the need for *in situ* perturbation

Extraordinary advances have been made in recent years elucidating the composition and function of microbiome members, but the vast majority of this work has focused on bacterial species, and often overlooks fungal participants<sup>1</sup>. And even though the number of fungal cells in the human body is orders of magnitude less than that of bacteria, fungi play important roles in human and environmental health. Many fungal pathogens live as commensals in humans before becoming infectious, whether due to hospital-derived nosocomial infections or auto-immune disorders, both of which are on the rise<sup>2</sup>. *Candida* species cause many such nosocomial infections, resulting in a range of candidiasis symptoms that can lead to sepsis<sup>3</sup>. Common skin residents in the *Malassezia* genus have been implicated Chrohn's disease<sup>4</sup> and tumorigenisis<sup>5</sup>. Moreover, many fungi infect

plant and/or other animal species, often causing crop loss<sup>6</sup>. Some environmentally-important fungi can also infect humans through spore inhalation, such as *Aspergillus* and *Blastomyces* species<sup>7,8</sup>, the latter of which is endemic to the Great Lakes region and recently caused infections in dozens of paper mill workers in nearby Michigan, killing at least one<sup>9</sup>.

Unlike bacterial infections, for which we have several antibiotics, there are only four main classes of antifungals, largely due to the similarity of pathogenic fungi to their eukaryotic hosts, which makes antibiotic treatment strategies more difficult<sup>10,11</sup>. The most used classes—azoles and echinocandins—target membrane development, as one of the key differences between fungal and mammalian cells<sup>12,13</sup>. And while a growing field of phage therapies is promising for treating bacterial infections<sup>14</sup>, there are no known correlates to phages for fungal treatment<sup>15</sup>. Like many pathogenic bacterial species, antibiotic resistance among pathogenic fungi is on the rise, making this dearth of treatment options even more important. One possible solution to this growing concern is to harness the advances of synthetic biology to engineer bacteria for fungal perturbation in situ. Bacterial intervention is especially intriguing given the prevalence of bacterial-fungal interactions in the wild and in pathogenic mixed biofilms 16-18, suggesting that both mutualistic and antagonistic natural communications between such species can serve as scaffolds for engineered treatments. For example, natural antifungal activity of the gram-positive bacterium Rhodococcus rhodochrous has been harnessed to mitigate infection by Pseudogymnoascus destructans, which causes White-Nose Syndrome in bats<sup>19</sup> (which is a healthy reminder, too, of fungal risks to climatethreatened species<sup>20</sup>), but could hypothetically be enhanced and/or better controlled by synthetic modifications to this or other bacterial treatment strains.

Moreover, any system of fungal perturbation by bacteria would have myriad implications for synthetic microbial consortia and the bioproduction of useful products. Microbial consortia consisting of bacteria and yeast species has been engineered to produce a range of useful compounds, especially alcohols and organic acids such as ethanol, isobutanol, and lactic acid<sup>21</sup>, by making use of species' respective metabolic strengths. Mixed consortia with the common Saccharomyces cerevisiae, i.e. baker's and brewer's yeast, have been used to produce insulin and vaccine components<sup>22</sup>. Many food-related processes utilize mixed consortia, including kombucha<sup>23</sup> and lactic-acid-bacteria (LAB) products such as soy sauce<sup>24</sup>. Additionally, several other useful products generated from yeasts independent of bacterial involvement could feasibly be perturbed by synthetic bacterial inclusion, including biofuels, alcohols, and enzymes degrading cellulose and lignocellulose<sup>21</sup>. Importantly, the examples listed above utilize diffusible outputs from bacterial species, limiting their specificity in complex environments, in which a diversity of cells may encounter and respond to such molecules<sup>25</sup>. Most such cases are static changes to the bacteria strains, limiting dynamic control, too. This work therefore seeks to further develop bacterial tools that are more programmable, to expand upon the range of fungal perturbation options.

#### (Return to top)

#### 1.2 Bacterial mechanisms for targeted delivery of macromolecules in microbial consortia

Bacteria deploy a range of cell-to-cell communication mechanisms that can be—and in many cases *have been*—utilized to directly perturb recipient populations *in situ*. Collectively these mechanisms are known as secretion systems, and there are at least seven major types, characterized by membrane export machinery spanning bacterial membranes, and a proteinaceous pilus that connects to a recipient cell and deposits macromolecules<sup>26,27</sup>. Most of these secretion systems,

such as the Type VI Secretion System (T6SS), primarily export targeted proteins for bacterial defense. T6SSs have received notable attention recently toward this goal of targeting eukaryotes *in situ*, with examples including fungal death<sup>28</sup>. Moreover, T6SSs (more specifically, the similar eCIS) have been shown to be programmable by modifying their receptor targets, so as to specify cells into which killer payloads are delivered<sup>29</sup>.

Alternatively, bacterial conjugation utilizes the Type IV Secretion System (T4SS) to deliver DNA to recipient cells, offering a more-readily modified payload, given the diversity of tools researchers have for manipulating DNA, and the fact that conjugative DNA can vary widely in sequence length without impairment<sup>30</sup>. Conjugation is a form of horizontal gene transfer (HGT) that allows the exchange of genetic information among bacteria in the wild<sup>31</sup>, but has also been used to engineer organisms in situ<sup>32,33</sup>. It has been used for probiotics<sup>34</sup>, to modify crops for desired traits<sup>35</sup>, and to identify and alter function in undomesticated microbial species<sup>32,36</sup>. It can occur between bacteria and a variety of eukaryotic recipient cells, too, most commonly from bacterial donor Agrobacterium tumefaciens to plant cells<sup>37</sup>. While A. tumefaciens is uniquely well-studied in performing transkingdom conjugation (TKC) with plants in the wild, other highly genetically tractable bacteria, such as Escherichia coli, can be modified to perform TKC with diatoms<sup>38-41</sup>. mammalian cells<sup>42</sup>, and multiple yeast species<sup>43–47</sup>. Moreover, many *in situ* conjugative functions have been shown among bacterial species, that could feasibly be modified for use with eukaryotic recipients, including targeted killing<sup>3848,49</sup>, integration of plasmid DNA into recipient genomes<sup>32,36</sup>, and programmable activation via cell-to-cell adhesion<sup>50</sup>.

(Return to top)

#### 1.3 Conjugation to eukaryotes in the Type IV Secretion System

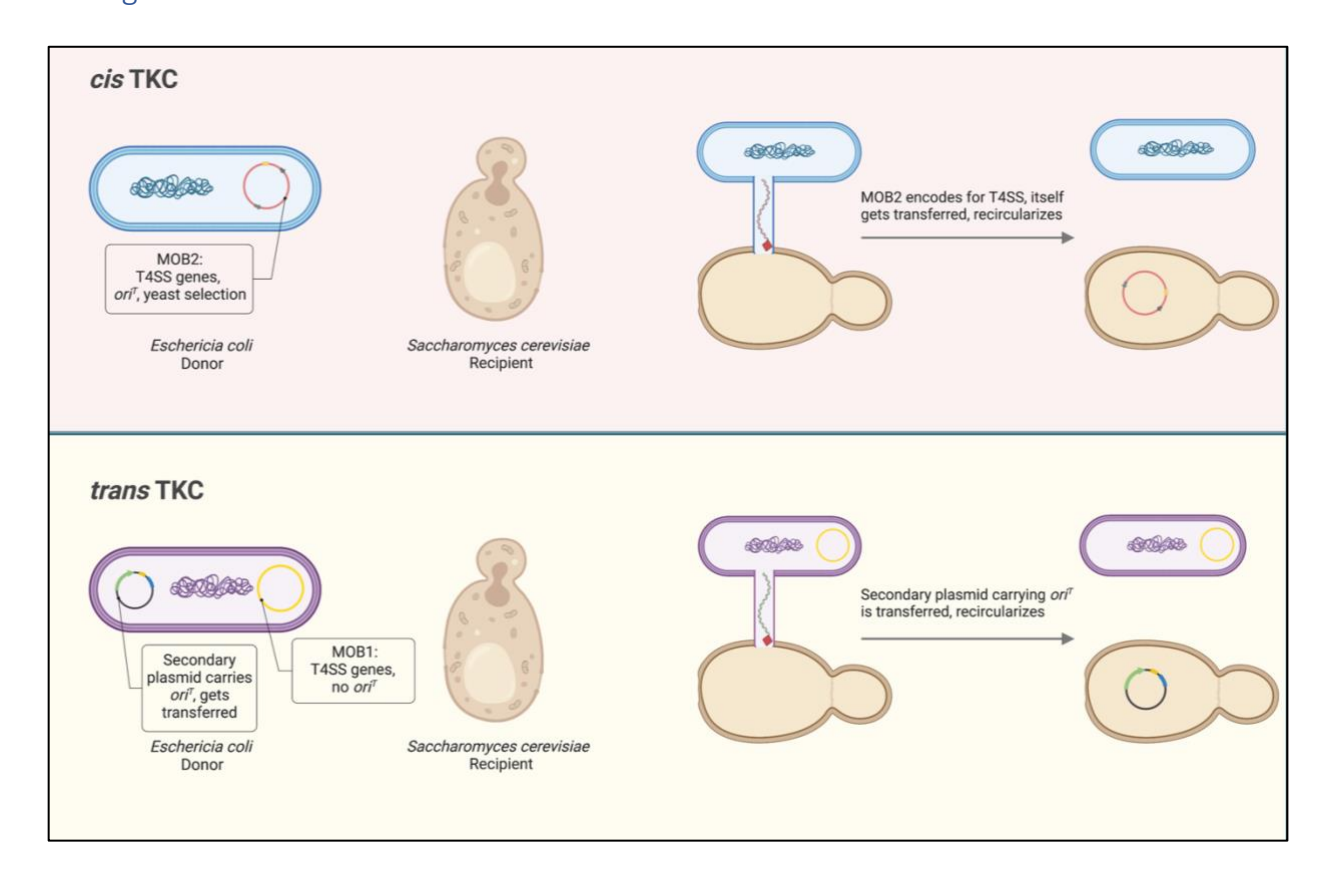
While the T4SS in Agrobacterium tumefaciens may be the best known natural conjugation system between bacteria and eukaryotic recipients, several similar donor species, especially those of the Rhizobium genus, can utilize the A. tumefaciens T4SS system if introduced to the bacteria artificially<sup>15</sup>. Moreover, it's thought that HGT occurs regularly in the wild, though the vast majority of such events are only elucidated post hoc, such as the evolutionary evidence of HGT to yeasts from other bacterial species, including relatives of E. coli<sup>51,52</sup>. The human bacterial pathogen Bartonella henselae is also thought to transfer genetic material to infected cells via a conjugationlike mechanism, after invading the host animal cell<sup>15</sup>. In E. coli, several conjugation systems have been discovered for interbacterial gene transfer—the first of which was the fertility "F plasmid" some of which have been synthetically adapted to allow transfer to eukaryotes. These systems are identified by incompatability type ("Inc-type", i.e. ability of the cell to maintain two such plasmids simultaneously) and mobilization genes used, but all include an origin of transfer sequence  $(ori^T)$ that flags the DNA for transfer into recipient cells<sup>53</sup>. For A. tumefaciens and related "Vir" systems, transferred DNA is in the form of a linear fragment, known as transfer DNA or T-DNA, that is first cut out of a large plasmid before transfer, and is protected by a series of proteins encoded by mobilization genes<sup>15</sup>. For B. henselae and modified E. coli systems, the  $ori^T$  resides on plasmid DNA, which is cut, linearized, transferred, and recircularized in the recipient cell. Expression of conjugative machinery and plasmid transfer has been shown to be growth stage-dependent for several Inc-types in E. coli<sup>53</sup>. In this work, I utilize an IncP-type T4SS system (aka RP4, RK2), first isolated from an infectious *Pseudomonas aeruginosa* hospital strain<sup>54</sup> which was shown to be remarkably stable across growth phases in the study listed above, and has a wide host range, i.e. it can be transferred to a large diversity of recipient cells<sup>55,56</sup>.

Conjugative transfer of DNA occurs in multiple stages in the bacterial cell. First, a complex of proteins called the "relaxosome", containing catalytic relaxases, nicks the conjugative plasmid at the origin of transfer  $(ori^T)$ , and transfers one strand of the plasmid DNA to the membrane-bound type IV secretion system (T4SS)<sup>57</sup>. Key genes for this process are included in the Tra1 region, including relaxase operon Tral-H, which together nick and bind to the ori<sup>T58-60</sup>. The T4SS transports the relaxosome-DNA complex through both membranes and a pilus connecting the donor and recipient cells. Some studies on the related F plasmid T4SS suggest that DNA only transfers upon cytoplasmic connection between donor and recipient cells, wherein donor cells receive molecular signals confirming this connection before initiating transfer<sup>61</sup>, though whether this is the case for transfers to eukaryotes in unknown. For E. coli T4SS, the DNA re-circularizes in the recipient cell to recreate the original plasmid<sup>62</sup>. While the exact mechanism of DNA recircularization in yeast recipients is not well understood<sup>15</sup>, studies have suggested that the required machinery is provided by the bacterial relaxosome itself, and doesn't depend on recipient DNA repair systems<sup>47</sup>. And unlike for A. tumefaciens T-DNA transfer, which includes associated proteins that enable transport through the nuclear envelope, it's less clear whether the E. coli relaxosome can transport its associated ssDNA into the recipient nucleus, or if passive transport occurs only after disruption of the nuclear envelope during cell division, as has been seen for B. henselae<sup>63</sup>. Conjugation can occur via either a cis mechanism, in which the plasmid carrying the relaxosome genes itself contains an  $ori^T$  and thus is transferred to a recipient cell, or a trans mechanism, in which the  $ori^T$  is on a separate plasmid, which gets transferred, enabling a wide range of possibilities of DNA that gets transported<sup>64</sup> (Fig 1).

TKC is currently limited as a tool for synthetic biology by its relatively low efficiency<sup>65</sup>. The vast majority of conjugation research has focused on lowering efficiency further<sup>66,67</sup>, in an effort to prevent the spread of antibiotic resistance, which occurs through conjugative transfer of resistance-coding genes<sup>68</sup>. Conjugation rates between *E. coli* and *Saccharomyces cerevisiae* are typically below 1 in 1,000 yeast cells<sup>69</sup>, though recent work has succeeded in generating >10x DNA-transfer rates by selectively mutating the T4SS machinery<sup>64</sup>. Another recent approach demonstrated increased conjugative efficiency between bacteria, but used glass beads to colocalize donor and recipient cells, limiting its wider usefulness<sup>49</sup>. TKC recipients are also unable to propagate conjugative plasmids, whereas bacterial recipients can act as conjugative donors, allowing logistic transconjugant growth over time<sup>49</sup>. Here, I've focused on IncP-based TKC between *E. coli* and *S. cerevisiae*, not because this consortium necessarily affords the greatest opportunities for pathogenic treatment or biotechnological production, but because these species are highly genetically tractable, and allow the greatest possible flexibility in generating foundational insights regarding how we might put TKC to use in any mixed consortium.

(Return to top)

#### 1.4 Figures



#### 1.4.1 Figure 1: methods of plasmid transfer in T4SS

For this IncP T4SS system, DNA transfer to recipient yeasts can either occur in cis or in trans. For cis TKC, the plasmid encoding the T4SS (pTA-Mob 2.0) also contains yeast centromeric DNA maintenance machinery, yeast selection genes HIS3 and URA3, and the transfer recognition sequence,  $ori^T$ , at which the relaxosome nicks plasmid DNA and transfers it through the pilus to the recipient. In trans TKC, the T4SS-encoding plasmid (pTA-Mob 1.0) lack the sequences for yeast maintenance, yeast selection, and the  $ori^T$  sequence. Thus, a second plasmid is required for trans-TKC, which carries these elements and is transferred to recipients.

(Return to top)

## Chapter 2: Tunable population dynamics in batch culture affect TKC

#### 2.1 Introduction: levers of control

One potential strategy to control TKC rates in a targeted way is to tune donor and recipient populations, since TKC rates have been shown to increase substantially with higher donor-torecipient ratios, at least at short time scales<sup>69</sup>. For intraspecies co-cultures, such control of steady state population ratios is achievable by engineering cross-feeding into strains, e.g. by making each strain auxotrophic for an essential amino acid that the other strain overproduces, allowing population tuning by manipulating these amino acid concentrations<sup>70</sup>. Other forms of metabolic dependency can be established for specific consortia, such as a 2015 study that created mutualism between E. coli and S. cerevisiae by using xylose as a carbon source, only consumable by E. coli cells, which then produce acetate, normally a bacterial toxin but for utilization by S. cerevisiae<sup>71</sup>. Such a strategy, while perhaps tunable (though it would appear to only have one experimental "knob" in the form of xylose concentration), cannot readily be extended to other consortia, whereas amino acid cross-feeding allows independent control of each amino acid's concentration, and can be extended to myriad consortia, since the nutrients are universally required for survival and have well-characterized genetic controls in many species. Much of this work thus utilizes strains of E. coli and S. cerevisiae mutated to allow tunable population control via engineered cross-feeding between E. coli and S. cerevisiae.

Complicating such a strategy for steady state culture, *E. coli* is capable of adhering to *S. cerevisiae* (and other eukaryotic cells) via the mannose-sensitive type I fimbriae, due to mannoproteins in yeast cell walls<sup>72–74</sup>. And because cross-feeding is highly dependent on spatial context of cells—due to the dependence of each strain on diffusible products<sup>75</sup>—aggregation between bacteria and

yeasts would alter any assumption of homogeneity in culture. This doesn't obviate the ability to tune population dynamics necessarily, but rather affords another opportunity to tune said dynamics, by controlling cell-cell adhesion in addition to metabolic cross-feeding. Such a strategy has recently been employed to show increased cross-feeding between aggregates of *E. coli* and *S. cerevisiae*, versus a co-culture in which mannose-supplemented media precludes aggregation<sup>76</sup>. Thus, this chapter focuses on 1) tuning co-cultures metabolically, by targeted cross-feeding mutations and environmental nutrient limitation, 2) changing aggregation, or "clumping" between cells, by mannose addition, and 3) modeling interactions to discern the effects of these tunable experimental knobs, and to predict unknown facets of the system.

#### (Return to top)

#### 2.2 Results

#### 2.2.1 Tunable population dynamics in batch culture affect TKC outcomes

To determine if we can control TKC frequencies by tuning steady state population growth, we designed strains of  $E.\ coli$  and  $S.\ cerevisiae$  to be obligate mutualists when deprived of nutrients. We utilized a previously studied yellow-fluorescent yeast strain<sup>77</sup> that's tryptophan auxotrophic (Trp<sup>-</sup>,  $\Delta trp2$ ) and leucine overproducing (Leu<sup>++</sup>,  $LEU4^{FBR}$ )<sup>78</sup>, and developed a corresponding leucine-auxotrophic, tryptophan-overproducing cross-feeder  $E.\ coli$  that expresses mCherry. Because we hoped to tune nutrients (especially amino acids) in batch culture media, we sought to use minimal media for growing co-cultures containing  $E.\ coli$  and  $S.\ cerevisiae$ . Initial experiments were performed in equal parts M9 bacterial minimal media and synthetic complete (SC) yeast media, with glucose levels at the higher SC-media concentration of 2%. These experiments

resulted in co-cultures heavily dominated by bacteria, with no stable obligate mutualism at 0% leucine and tryptophan.

Thus, we screened four experimental conditions for steady-state maintenance of each strain over several days, via Tecan Spark fluorescence plate reader (Fig 1a), especially looking for maintenance of obligate mutualism at 0% LW (Fig 1b). 1) A range of L and W concentrations at 50:50 SC:M9 were used to get a full sense of whether any benefit between cross-feeding strains could be found, even at [LW] > 0%. Minimal benefits were seen for crossB grown in co-cultures, but they were inconsistent over time. 2) We increased initial cell densities, with each strain combined in equal proportions, from 2-fold overall density (2E7 each cell type per well) to 5-fold density (5E7 each strain). All samples in this and subsequent conditions were grown at 0% LW. At each increased density, cross-feeder bacteria showed an ability to survive off of yeast, especially cross-feeder yeast, but cross-feeder yeast weren't able to survive off bacteria. 3) We varied the input ratio of cells from 10:1 yeast-to-bacteria to 1000:1 yeast-to-bacteria, all up from the previous 1:1. These results showed varying levels of crossB survival in co-culture, but as before, no corresponding crossY survival. 4) We changed the proportion of minimal media from equal parts SC-to-M9, to a range of SC:M9 ratios: 60:40, 75:25, 90:10, and 100:0. All ratios showed an improved ability for crossY to survive in culture at 0% LW, though all bacteria were unable to survive in 100% SC; this latter observation proved very useful in selecting for yeast, as TKCselection plates didn't require any bacterial antibiotics at 100% SC agar. Of the media ratios tested, the 75:25 SC:M9 results showed the best ratio of cross-feeder paired growth vs. pairings with a WT strain, and so that media type was used in all subsequent experiments. Importantly, though, this ability of crossY to survive at 0% W was never seen again, though the steady state

concentrations of yeast cells in other conditions were much more favorable to yeast and allowed better population tuning than 50:50 SC:M9.

After screening for optimal co-culture conditions, we batch cultured cells for six days in minimal media with a range of strain-dependent leucine and tryptophan concentrations. Relative growth was measured in 15-minute intervals using a Tecan fluorescence reader, and in most cases, additionally measured at day-ends via flow cytometry (Fig 1a). In most cases, bacterial and yeast populations failed to establish stable cross-feeding with leucine and tryptophan fully removed from media, and competition between species acted as the primary driver of population outcomes. Cross-feeding bacteria ("crossB") temporarily survived via leucine secreted by cross-feeding yeast ("crossY") before the latter was outcompeted, driving down both populations; in contrast, auxotrophic yeasts did not benefit similarly from Trp-overproducing bacteria. Moreover, auxotrophic bacteria survived from WT yeasts ("wtY") at 0% leucine and tryptophan (0% LW), in an apparent commensal relationship, suggesting either a low but significant level of basal leucine secretion from wtY or sufficient yeast lysate for crossB survival. WT bacteria ("wtB") did not provide a similar benefit for cross-feeding yeasts (Fig 1c,d).

We quantified TKC between bacteria and yeasts by plating 100uL of each batch culture condition onto TKC-selective media at ~24-hour intervals. We measured population effects on TKC both in *cis*—with the self-transferring plasmid pTA-Mob 2.0—and in *trans*, via a two-plasmid system including the *ori*<sup>T</sup>-lacking pTA-Mob 1.0 and a separate, yeast-selectable transfer plasmid (see <u>Intro Figure 1</u>). Contrary to previous work demonstrating higher TKC rates with more donor bacteria<sup>69</sup>, we found an inverse correlation between donor-to-recipient ratios and TKC counts (<u>Fig 1e</u>). This trend became more pronounced with time and manifested as a linear fit on a log-log plot (<u>Fig 1f</u>).

The correlation was weaker for *trans* TKC; as in previous work, we found markedly lower *trans* TKC rates relative to *cis* TKC<sup>30</sup>, which might have lessened the correlations in *trans* (Fig 1g). Importantly, the trend was not exclusively due to changes in recipient yeast populations, since the TKC-per-recipient rates also increased over this time (Fig 1h). These findings suggest that, despite the lack of stable cross-feeding at 0% LW, we can still control TKC by tuning populations, since steady-state ratios of donors-to-recipients are inversely correlated to TKC counts.

#### (Return to top)

#### 2.2.2 Mannoprotein-based cell adhesion mediates TKC

Since TKC depends on cell-cell collisions in culture, we explored how known adherence mechanisms between *E. coli* and *S. cerevisiae* affect TKC. Mannoproteins are ubiquitous in fungal cell walls<sup>74</sup>, and type I fimbriae in *E. coli* bind to these<sup>72,73</sup>, forming bacteria-yeast "clumps" that can affect cross-feeding dynamics<sup>76</sup>. We thus repeated our batch culture experiments for population dynamics and TKC with- and without mannose added to the media, which saturates bacterial mannose receptors and reduces clumping. These cultures were measured for fluorescence as per previous experiments, but here were also imaged via fluorescence microscopy to measure the extent of clumping.

Fluorescence microscopy analysis replicated previous findings showing that adding mannose to growth media prevented most bacteria-yeast clumping (Fig 2a). Image analysis demonstrated that the size of yeast clumps—a proxy for number of yeast cells per clump—increased concurrent with the number of bacteria in a clump ("coincident bacteria"), implying that bacteria mediate cell clump formation (Fig 2b,c). Interestingly, we found that mannose-infused media prevented nearly

all TKC, with only a few samples yielding single-digit TKC counts by the end of a six-day time course, roughly 10 fold fewer than corresponding samples without mannose (Fig 2d). Moreover, mannose-supplemented samples showed fundamentally altered dynamics for crossB\_wtY pairings, with auxotrophic crossB cells unable to survive at 0% leucine, and with much lower growth at higher percentages of leucine relative to mannose-free samples (Fig 2e,f). Thus, mannose interrupted the commensal dynamics previously seen without mannose.

#### (Return to top)

#### 2.2.3 Deterministic models reveal limitations of key parameters: "free" cell model

To explore how the "knobs" of our system could be tuned to best affect population ratios and TKC, and to better understand the differences between clumping and non-clumping populations, we used a set of ordinary differential equations (ODEs) to deterministically model our experimental conditions, based on previous work modeling cross-feeding co-cultures<sup>70,79</sup>. We first fit the results from mannose-supplemented experiments to a system of two ODEs representing total bacteria and total yeast (including transconjugants). We ran Latin Hypercube Sampling iteratively to randomly sample all parameters within a predicted range and calculated total error between model outcomes and fluorescence data for bacteria and yeast. We then used this error to rank model parameters, which we adjusted and rerun until key results were demonstrated for each cell pairing: namely, susceptibility to amino acid supplementation, steady-state survival, and approximate donor-to-recipient ratio.

Growth equations for bacterial and yeast growth were derived from Pearl-Verhulst<sup>80</sup> logistic growth, for which cells' growth were determined by its (monoculture) growth rate R, carrying capacity K, and death rate D. Modifications for co-culture conditions included deviations from

monoculture carrying capacity term and amino acid secretion terms<sup>70,79</sup>. For the effect of one species on limiting the carrying capacity of the other, a multiplier c was used to account for incomplete ecological niche overlap. The global concentration of amino acid supplemented to media G and amino acid secretion  $\alpha$ —dependent on secreting cell's concentration—together modified the growth rate of each species. Monod term k determined a strain's susceptibility to amino acid changes.

Transconjugants grew similarly to yeast, and thus had a nearly identical growth equation. Transconjugants were also added to the system by bacterial and yeast collisions, as modified by TKC rate term  $\gamma$ . Note that because the growth equation for yeast dY/dt was compared to yeast fluorescence data (see below), Y was a representation of *all yeast*, including transconjugants, and thus had no term depleting cells proportionate to TKC rate  $\gamma$ , as has been modeled by others<sup>81,82</sup>.

Growth equations for bacteria (B), yeasts (Y), and transconjugants (T) in "free-cell" model:

$$\begin{split} \frac{dB}{dt} &= R_b * B \, \left(\frac{\alpha_b Y + G_b}{\alpha_b Y + G_b + k_b}\right) \left(1 - \frac{B}{K_b} - \frac{c_y Y}{K_y}\right) - D_b \left(\frac{B}{K_b}\right) \\ \frac{dY}{dt} &= R_y * Y \, \left(\frac{\alpha_y B + G_y}{\alpha_y B + G_y + k_y}\right) \left(1 - \frac{Y}{K_y} - \frac{c_b B}{K_b}\right) - D_y \left(\frac{Y}{K_y}\right) \\ \frac{dT}{dt} &= R_y * T \, \left(\frac{\alpha_y B + G_y}{\alpha_y B + G_y + k_y}\right) \left(1 - \frac{T}{K_y} - \frac{c_b B}{K_b}\right) - D_y \left(\frac{T}{K_y}\right) + \gamma \left(\frac{B * Y}{B + Y}\right) \end{split}$$

We first estimated growth rates R and carrying capacities K by fitting integrated versions of simplified monoculture growth equations (lacking amino acid terms, death rates, and co-culture modifications) to monoculture fluorescence data at 100% amino acids in solution. Global amino acid concentrations G were known (see Methods for molar values), and initial guesses for cell

secretion  $\alpha$  were based on literature values for similar strain mutants—0.022 g<sub>Trp</sub>/CDW\*hr for  $\Delta trp^R$  bacteria<sup>83</sup>, and 7\*10<sup>5</sup> molecules<sub>Leu</sub>/cell\*s for Leu<sup>++</sup> yeasts<sup>77</sup>—taken for 1 hour, with an assumed bacterial CDW = 3\*10<sup>-13</sup> g/cell. Using these, we arithmetically derived Monod terms k for cross-feeder monoculture fits using the equation  $R_{max} = R * [AA]/([AA] + k)$ , where [AA] = 1 limited amino acid concentration, over a range of supplemented values.

For all subsequent terms and fits, we used Latin Hypercube Sampling (LHS) to fit a MATLAB ODE solver. We set upper and lower bounds for each parameter, between which 100,000 random parameter guesses were generated, each of which was put through the ODE solver. Each model output, determined by that guess's randomized parameters, was compared to fluorescence data, error between the two was calculated, and random model guesses were ranked by lowest calculated error.

We then estimated niche overlap terms c using fluorescence of WT co-cultures at 100% amino acids, for each WT donor variant (plasmids carried). Original parameter ranges were set widely for simplified conditions—e.g. c was initially sampled between -1 and 2 for WT pairings (Fig 3a)—then tightened for full-model fitting.

For batch co-culture fitting, we compared fluorescence values to a modified version of ODE solver, in which we fed each days' model outputs into the next day's initial conditions. In this way, we were able to emulate batch culture dilutions at the times experimentally performed and keep the ODE solver in time units of hours. We ignored day 1 growth for both measurements and model, as variation in cell counts among strains initially adapting to batch culture conditions proved

extremely unpredictable and resulted in errant model fits. To allow for experimental variation, we incorporated noise into day-end outputs at a rate of +/- 20%, before feeding them fed back into the solver as next-day initial conditions. Initially, we only calculated error between model and measured data for bacterial and yeast growth signals (not TKC values), and we ranked fits according to those errors. We manually assessed means of each model's 1000 best fits (top 1%) for each cell pairing based on three criteria: 1) susceptibility of each strain to changes in amino acid concentration, 2) steady-state persistence of each strain, and 3) approximate D:R ratio of cells. We manually modified means to best reflect these priorities, and then fed them back into the solver. We repeated this process several times, until model outputs no longer improved upon experimental matches (Fig 3b). Model thus represented a local minimum for fitting parameters and is not meant to represent a unique fit.

Once a representative parameter set was acquired for each species' growth in co-culture, we fixed all parameters besides TKC rate  $\gamma$ , and we tested  $\gamma$  across a range of possible outcomes ( $10^{-6}-10^{-2}$ ) for each cell pairing and concentration of added leucine and tryptophan. Note that, unlike bacterial and yeast growth equations, each of which maintains a single fluorescence unit (mCherry or ymCitrine), transconjugant equations include a combination of each fluorescence type. To account for this, the transconjugant model converts each cell type from fluorescence to cell count before multiplying by  $\gamma$ —using conversion factors derived by comparing flow cytometry data (cell counts) to fluorescence data—after which the entire frequency term is multiplied again by ymCitrine/cell, to maintain units of ymCitrine for transconjugants. Because transconjugants were modeled in units of ymCitrine, and because half of each growth well's volume was plated for TKC counts, we divided model outputs for TKC by 2\*Citrine/cell. We incorporated averages from each

condition's TKC data into TKC-sweep plots by altering heatmap colormaps according to where color (row-fraction of total output range) matched TKC counts.

Once we found best-fit approximations of parameters in bacterial and yeast growth equations (Table 1), we tested a wide range of TKC rates ( $\gamma$ ) against data from mannose-supplemented experiments, to determine order of magnitude for TKC given random cell collisions in culture. Though this plasmid transfer term has been previously approximated at  $4*10^{-3}$  using a similar model for enteric bovine *E. coli*<sup>84</sup>, we found that  $\gamma$  would have to be significantly lower, roughly between  $7*10^{-6}$  and  $4*10^{-5}$ , to recapitulate our results in media containing mannose (Fig 3c). (Return to top)

#### 2.2.4 Deterministic models reveal limitations of key parameters: clumped cell model

After testing the free cell model against experimental data, we modified deterministic equations to capture aggregation ("clumping") dynamics between the species. Specifically, three equations were added to the system, tracking 1) formation of clumps, as determined by some constant rate of aggregation for every random free-cell collision; 2) total clumped bacteria, based on both growth of already-clumped bacteria, or additional collisions between clumps and free bacteria; 3) total clumped yeast, based on growth of already-clumped yeast or additional collisions between clumps and free yeast. The latter clumped-cell growth equation terms were similar to free-cell growth, except for modified growth rates (starting values  $\sim$ 1/3 free cell values) and proximity terms P, which allow for altered amino-acid feeding from opposing cell type in a clump. We additionally modified free-cell growth equations to be carrying capacity-limited by summing clumped and free cells in the total per species. Finally, we modified the transconjugant equation to

include a second TKC rate  $\gamma_c$ , based on total number of clumped-bacteria and clumped-yeast interactions. We also changed the growth rate for transconjugants to the clumped-yeast rate, to reflect the expectation that most transconjugants require clumping at some point.

Growth equations for bacteria (B), yeasts (Y), transconjugants (T), total clumps (C), clumped bacteria ( $C_b$ ), and clumped yeasts ( $C_v$ ) in "clumped-cell" model:

$$\frac{dB}{dt} = (R_b * B) \left( \frac{\alpha_b Y + G_b}{\alpha_b Y + G_b + k_b} \right) \left( 1 - \frac{(B + C_b)}{K_b} - \frac{c_y (Y + C_y)}{K_y} \right) - D_b \left( \frac{B}{K_b} \right)$$

$$\frac{dY}{dt} = \left( R_y * Y \right) \left( \frac{\alpha_y B + G_y}{\alpha_y B + G_y + k_y} \right) \left( 1 - \frac{(Y + C_y)}{K_y} - \frac{c_b (B + C_b)}{K_b} \right) - D_y \left( \frac{Y}{K_y} \right)$$

$$\frac{dT}{dt} = R_{cy} * T \left( \frac{\alpha_y B + G_y}{\alpha_y B + G_y + k_y} \right) \left( 1 - \frac{Y + C_y}{K_y} - \frac{c_b (B + C_b)}{K_b} \right) - D_y \left( \frac{T}{K_y} \right) + \gamma \left( \frac{B * Y}{B + Y} \right) + \gamma_c \left( \frac{C_b * C_y}{C_b + C_y} \right)$$

$$\frac{dC}{dt} = R_c \left( \frac{B * Y}{B + Y} \right)$$

$$\frac{dC_b}{dt} = (R_{cb} * C_b) \left( \frac{P_b \alpha_b Y + G_b}{P_b \alpha_b Y + G_b + k_b} \right) \left( 1 - \frac{C_b}{K_b} - \frac{c_y C_y}{K_y} \right) - D_b \left( \frac{C_b}{K_b} \right) + R_c \left( \frac{C * B}{C + B} \right)$$

$$\frac{dC_y}{dt} = (R_{cy} * C_y) \left( \frac{P_y \alpha_y B + G_y}{P_y \alpha_y B + G_y + k_y} \right) \left( 1 - \frac{C_y}{K_y} - \frac{c_b C_b}{K_b} \right) - D_y \left( \frac{C_y}{K_y} \right) + R_c \left( \frac{C * Y}{C + Y} \right)$$

We fit clumped-cell dynamics similarly to free-cell equations, using LHS and the ODE batch solver. We additionally modified model outputs in two ways. We limited clumped-bacteria outputs to 10 bacteria per clump (based on image analyses, see Methods), beyond which clumped bacteria counts were subtracted from clumped-bacteria model outputs for each day and added to free-bacteria counts, before the next day's growth was modeled. We also added final clumped-cell model outputs to total free-cell outputs before comparing to fluorescence data, which doesn't distinguish between the two.

We compared batch co-culture LHS model outputs similarly to free-cell LHS fitting, using error between the model and experimental data, but here we calculated error between each experimental result: total bacteria, total yeasts, TKC counts, number of clumps, clumped bacteria, and clumped yeast (Fig 3d). Upon deriving fits that recapitulated main experimental outcomes, we swept key clumping parameters P and  $\gamma_c$  across a range of values to find approximate viable values. TKC rate sweeps of  $\gamma$  and  $\gamma_c$  yielded several values of each that were able to recapitulate the data, though they roughly fell into two categories: low  $\gamma_c$  with  $\gamma$  in the range of  $3*10^{-4} - 6*10^{-4}$ , or low  $\gamma$  with  $\gamma_c$ in the range of  $2*10^{-5} - 4*10^{-5}$  (Fig 3e). P value sweeps show an apparent amino-acid secretion increase on the order of 50x from wtY, for crossB cells to be able to grow in 0% leucine (Fig 3f). While P mathematically serves to multiply the amino acid secretion term in the model, it could just as likely result from leucine in yeast cell lysate or some other mechanism of bacterial benefit. This model assumes that the vast majority of transconjugants result from clumped interactions, though it's not clear how transient clumps are, so the free-cell TKC transfer rate here accounts for TKC from cells measured to be "free" despite having previously been clumped at some time between measurements.

#### (Return to top)

#### 2.3 Discussion

I set out to control TKC rates by tuning donor and recipient populations. Largely, I think this was successful, though not in the way I intended. My efforts to engineer cross-feeding between *E. coli* and *S. cerevisiae* proved elusive, despite other researchers' success in similar systems<sup>70,76,85</sup>. Initially, experiments were performed on timescales < 24 hours, based on TKC-delivery protocols that show efficiency changes for different population ratios<sup>69</sup>, but I found that the populations

never reached steady-state on such timescales, complicating tests of my population-tuning hypothesis (data not shown). Moreover, keeping to the "long view" goals of microbiome *in situ* perturbation and fungal probiotics, understanding steady-state dynamics is key for any future prolonged application of donor cells in a system. E.g., how long must donors persist to achieve sufficient TKC for a given application? Thus, any ability to engineer variable steady-state ratios between the populations proved effective in testing this hypothesis—regardless of whether the populations achieved stable *obligate mutualism*—and the divergence of population outcomes between commensalism and competition served this function. That these outcomes had such a reproducible effect on transconjugant numbers, with lower donor-to-recipient ratios leading to increased TKC, bears two major implications: first, it shows that tuning TKC via population control is possible, and second, because so much of this control stems from a commensal relationship, it shows that it's possible to engineer *only the donor strain* to alter TKC. This latter point is significant toward the goal of applying donor cells to modify a microbial system.

It's important to note, too, that many recent works have measured TKC rates as a frequency of transconjugants per recipient cells<sup>30,64,69,86</sup>, though some examples exist of quantifying conjugation as a rate of cell coincidence, similar to the modeling I've done here<sup>81,82,87</sup>. While both quantifications have value, with the former being especially useful toward conjugative alternatives to yeast transformation and the latter useful for predictive modeling, I've taken a slightly different approach here and focused on net outcomes given both populations, and therefore have mostly reported raw transconjugant counts and changes in overall recipient population. (The modeling rate version does account for both populations, but doesn't intrinsically prescribe population outcomes, as rates such as  $\gamma$  are constant regardless of each population, more on that below). Still,

the frequency of transconjugants was important to track, as it naively would seem that lower-growing donors would allow better-growing recipients due to lower competition, and that that *alone* could account for increases in overall transconjugants. While recipients' ability to grow better does explain part of the phenomena observed in these experiments, a steady increase in the *frequency* of transconjugants demonstrates that TKC is continuing to occur in culture, versus a fixed percentage of transconjugant yeast growing on par with the rest of the yeast population.

Early co-cultures of E. coli and S. cerevisiae showed large amounts of aggregation between cells in many cases, enough for cells to quickly precipitate out of solution—though it was unclear the cause for this. Testing a variety of bacterial and yeast strains showed that it was not metabolicdependence based, i.e., several prototrophic strains clumped as much as auxotrophic ones. Growing co-cultures with a membranous "transwell" divider demonstrated that contact between the species was required to achieve aggregation, as separated co-cultures didn't form aggregates (data not shown). These early results suggested mannoprotein binding between cells—versus, e.g., intraspecies flocculation in yeast—but adding mannose to my growth media didn't seem to have a major effect. It wasn't until the serendipitous work by Scarinci and Sourjik<sup>76</sup> that I realized I simply added too little mannose (100 mM, vs. >200 mM for 4% w/v mannose) in these tests to successfully disrupt clumps. And while the clumping tests presented above recapitulated that nondependent cells still form clumps, the fitness benefit bestowed upon dependent bacteria by clumping was remarkable, whereby auxotrophic bacteria were only able to survive from WT yeast when allowed to clump. Not only does this comport with the work by Scarinci and Sourjik, it potentially adds to the incredible list of adaptive strategies E. coli have to metabolically benefit from cells in co-culture, many of which have been elucidated in recent years by work in the Kost lab<sup>85,88,89</sup>. In these cases, E. coli are found to form membranous nanotubes that connect to the cytoplasms of prototrophic cells, not only enabling direct resource sharing between cells, but actually increasing the production of said resources by disabling feedback control in the "feeder" cells, turning them into over-producers. While it seems unlikely that such nanotubes could disrupt fungal cell walls, there is a possibility that nutrients are exchanged through the conjugative pilus, as other secretion systems allow a diversity of macromolecular transport and share common ancestry<sup>124</sup>. Perhaps the simplest explanation—still revelatory in terms of bacterial adaptive strategies—is that binding to fungal mannoproteins brings bacteria in close enough proximity to diffusible goods to utilize them more effectively. Roughly speaking, if nutrients diffuse exponentially<sup>77</sup>, the 50x benefit to auxotrophic bacteria predicted by the clumping model above would correspond to ~4x proximity to a producer yeast (since ln(50)~4), an intuitively reasonable change for bound vs. free bacteria. A final possibility is that aggregation causes yeast cell death, allowing bacteria access to lysed nutrients, to which agar pad imaging (See 3.5.4.C) lends some support. And yet such an explanation would run against TKC results showing clumped cells persisting as transconjugants, so at least some fraction of clumped cells must survive. In any case, considering the ubiquity of mannoproteins in the cell walls of fungal species<sup>74</sup>, and the propensity of the type I fimbriae to bind to them<sup>72,73</sup>, it seems likely that this aggregation is a native adaptive strategy to increase fitness and/or parasitize eukaryotic hosts, and can thus be utilized for systems with other recipient species.

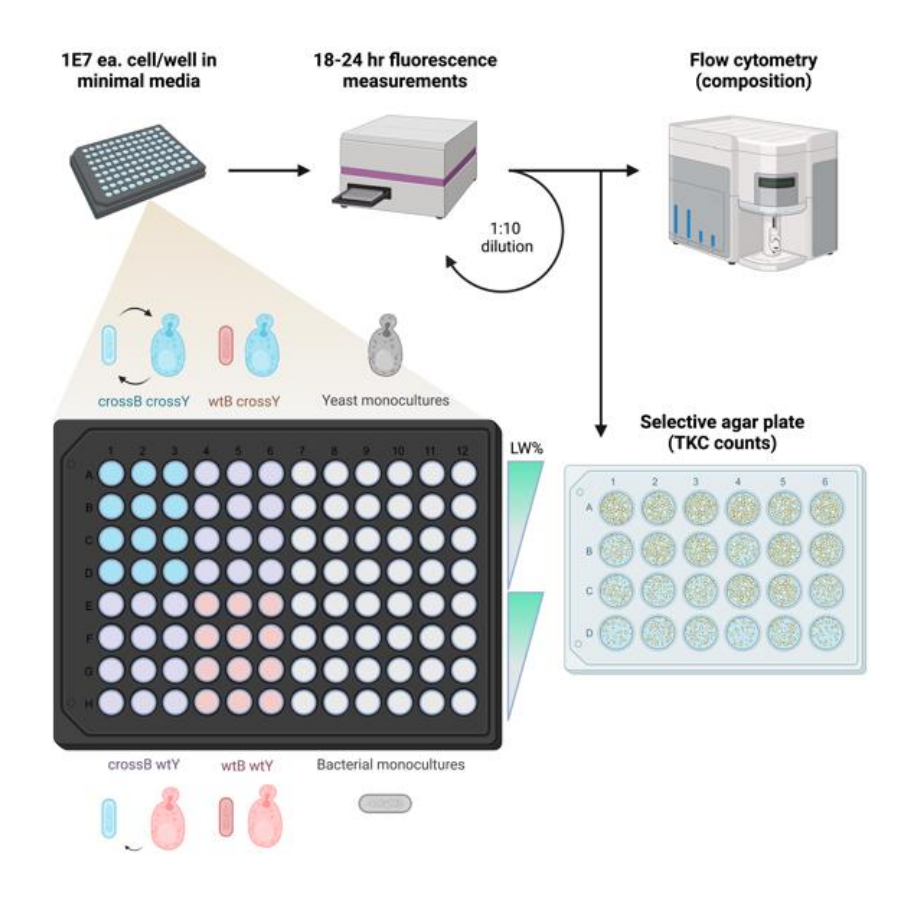
As stated above, my focus vis-à-vis TKC efficiency wasn't to explicitly maximize, or even determine, a TKC rate, but rather to find and control the conditions that modify recipient populations. Still, due to the complex nature of population dynamics—whether due to metabolic

demands, aggregation, or the black box of basal interactions between this synthetically-combined consortium—and the inherent difficulty in experimentally testing TKC outcomes for so many conditional possibilities, I sought to generate a model by which I could predict likely outcomes. While I attempted to match parameters to objective phenomena and literature values, and to be a rigorously logical about the terms included, the sheer number of parameters all but guarantees a fit to the data; in short, there's a strong possibility that the (clumped) model is overparameterized. This is especially the case for fitting clump data—number of clumps and clumped cells—given that these measurements were somewhat imputed from image data, and were only measured at endpoints. But as the adage goes, "all models are false, some models are useful," and these proved no exception, as I was able to predict the effect of commensalism in my rescue assay, and show that there could easily be more viable conditions to that end than I had the capacity to test. Moreover, sweeping TKC terms y against best-fit model parameters recapitulated many experimental outcomes, wherein transconjugant populations continued to grow unless yeast were driven out of co-culture. Predicting values for  $\gamma$  and proximity term P, while not an initial goal, allowed finer investigation of these key determinants, and hopefully contributes in an ever-sosmall way to the body of work focused on understanding these systems. While I'm far from the first to look at this—Levin et. al. set the stage for modeling conjugation in this way in 1978<sup>81</sup>, and many others have followed<sup>82,87</sup>, with the 0.04 y value used here provided by a more recent model of enteric bovine E. coli due to its similar modeling<sup>84</sup>—no research that I've found records such values for a transkingdom system, and indeed all of the work cited here is for single species, complicating any simple application of Levin's or similar models. Finally, it's worth pointing out the predominance of growth rates and ecological overlap terms (R and c, respectively, in models) on population outcomes, as opposed to, say, secretion of amino acids in cross-feeding. While the cross-species limitation on carrying capacity c was outlined for a two-species system by other researchers  $^{70,79}$ , it was theoretical in both cases, whereas here it's tangibly obvious how much the differences between R and c of the two species supersede other effects, demonstrating why, e.g., commensalism is possible for the faster-growing bacterial species, but not yeast. That said, both of these terms depend on a myriad of factors that aren't being modeled explicitly, such as sugar concentration, pH, secreted toxins, etc., and indeed multiple combinations of R and c are likely possible for fitting the data, together effectively forming a "consortial fitness" for a given co-culture. Thus, it could be said that E coli has a higher "consortial fitness" relative to S cerevisiae in co-culture (when clumping is allowed), by virtue of both its higher growth rate and the extent to which it limits yeast growth, relative to the converse.

(Return to top)

#### 2.4 Figures and Tables

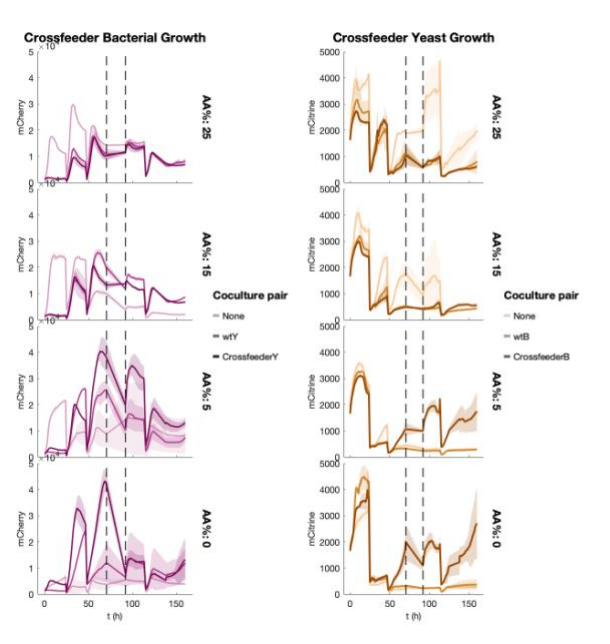
#### 2.4.1 Figure 1: Batch culturing reveals relationships between population ratios and TKC



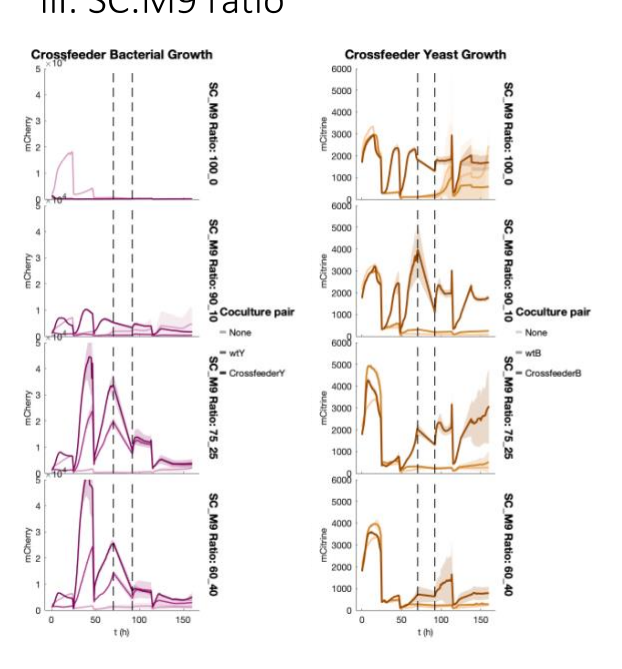
#### A. Experimental setup of batch cultures.

Cells are combined in a 96-well microplate with varying levels of amino acid in a minimal media cocktail. Co-cultures and monocultures are incubated at 30°C with continuous shaking and measured for fluorescence of each species every 15 minutes. After 18-24 hours of growth, cells are diluted 1:10 into new media to continue growing. Simultaneously, a 1:10 dilution of cells is prepared for flow cytometry, and an undiluted 100 uL is plated onto TKC-selective plates.

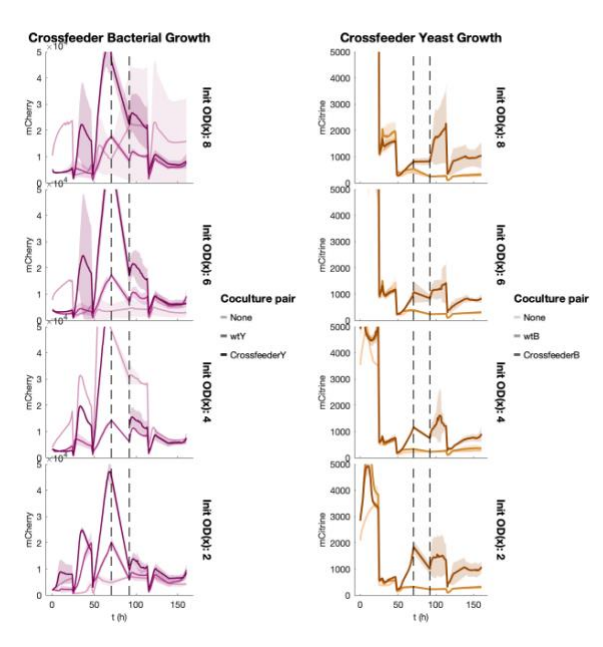
## i: Amino Acids



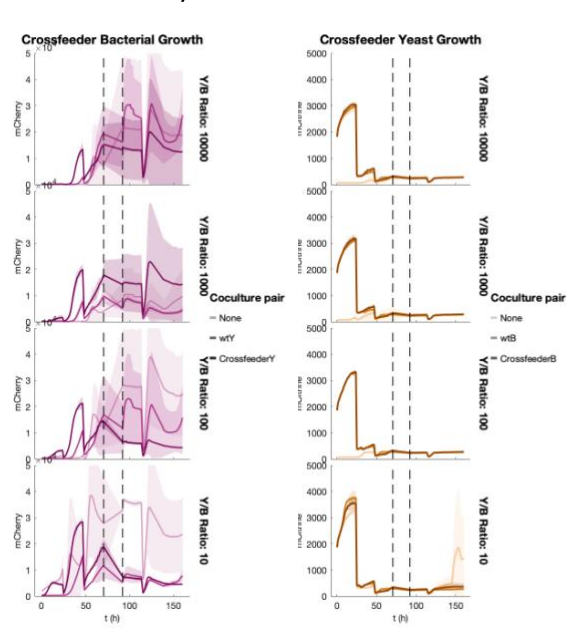
# iii: SC:M9 ratio



# ii: Initial cell densities

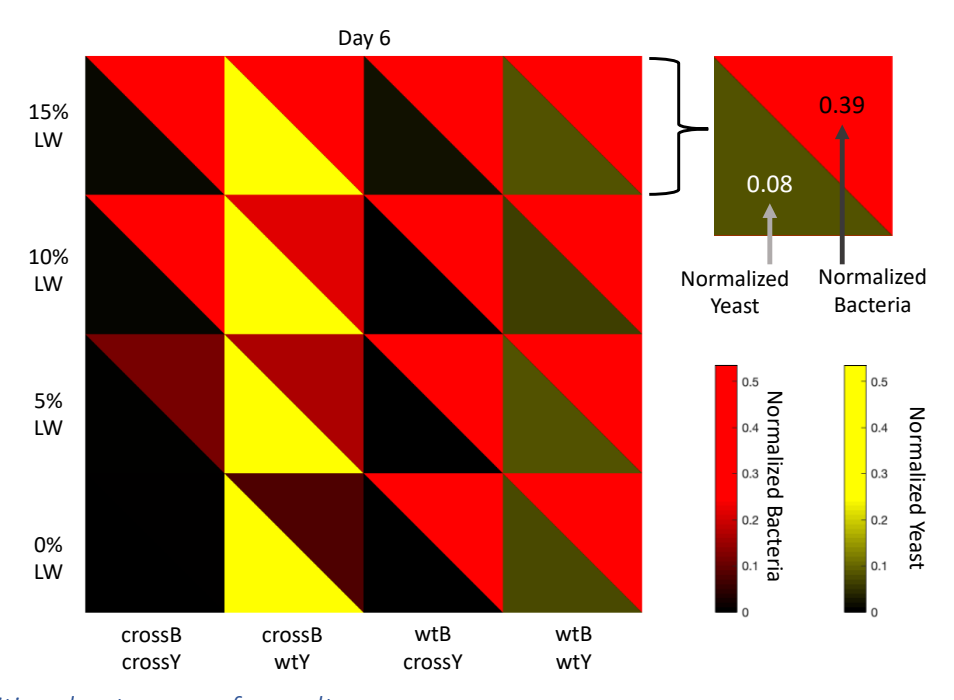


# iv: Initial yeast-to-bacteria ratio



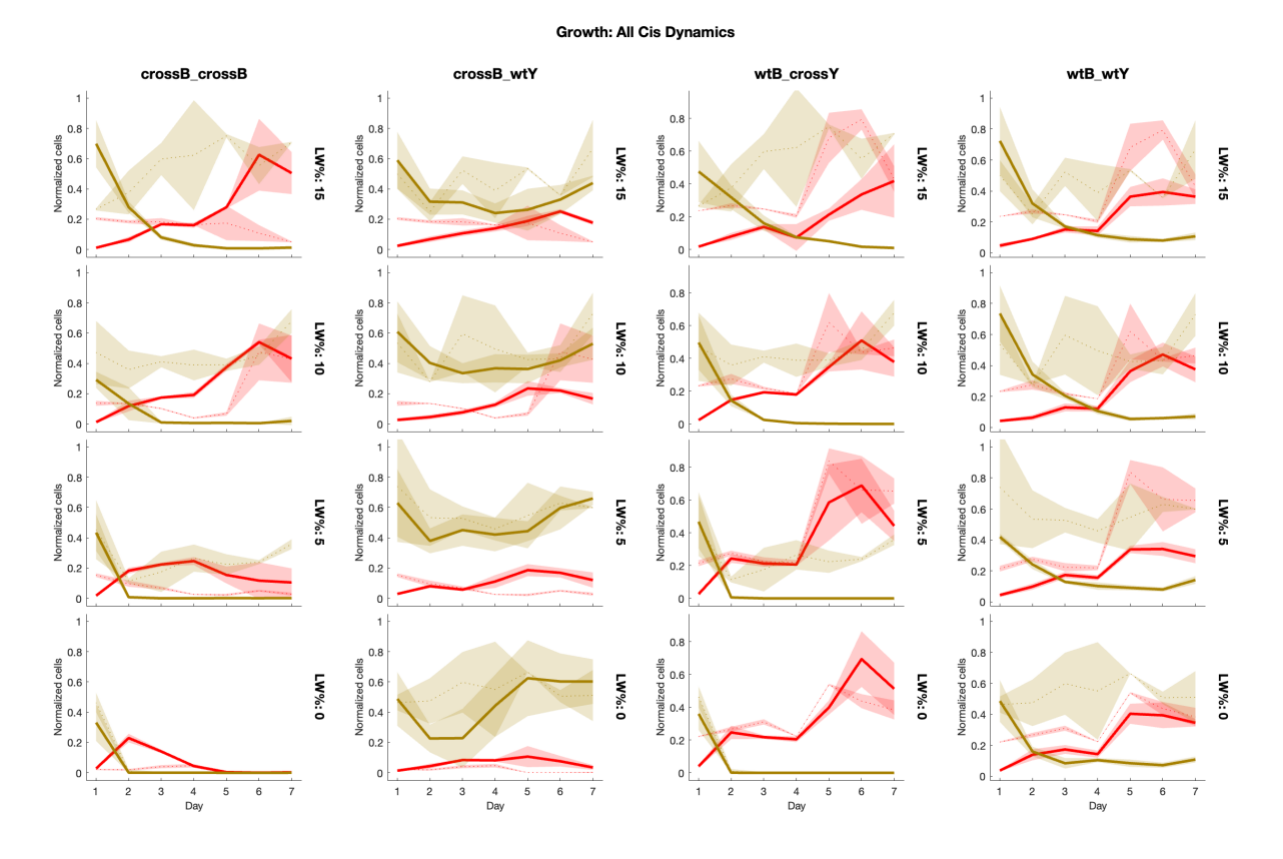
#### B. Condition screening for batch co-cultures

Fluorescence readings of cross-feeder bacteria (red traces) and cross-feeder yeast (brown traces) across several conditions during six days of batch culture. In each case, darkest traces pertain to co-culture with paired cross-feeder strain, mid-darkness traces with WT pair, and lightest traces monoculture (e.g. dark red is bacteria grown with cross-feeder yeast, mid-red trace is bacteria grown with WT yeast, light red trace is bacteria grown in monoculture); lines are means of three replicates, shading is 95% CI. (i) Cross-feeding strains grown across several limited amino acid concentrations (LW%, rows). (ii) Initial total cell density (rows), all 1:1 ratio between cell types, 0% LW. (iii) Ratios of SC (yeast minimal media) to M9 (bacteria minimal media, rows), all 0% LW. (iv) Initial ratio of yeast to bacteria (rows), all at 0% LW. Across all conditions of 0% LW, 75:25 SC:M9 (iii, 2<sup>nd</sup> row) showed the most promise for survival of both cross-feeders by the end of time course (dark traces). Vertical dotted lines represent gap in data.



C. Compositional outcomes of co-cultures.

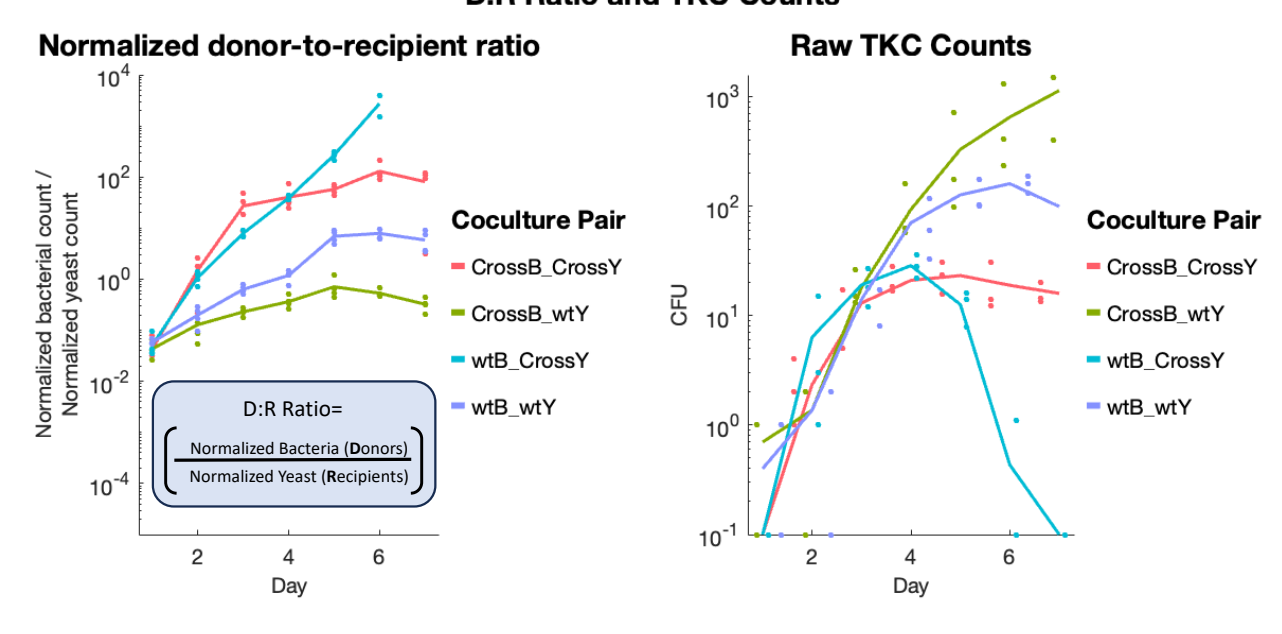
Split heatmap of bacterial cell counts (red) and yeast cell counts (yellow) for each co-culture pairing (columns) over a range of leucine and tryptophan (LW) concentrations (rows), from flow cytometry of batch culture day 6 (mean of four replicates). Counts are normalized to max cell counts per species—usually determined by input cell count, which is higher than carrying capacity—then multiplied uniformly to enhance color brightness, to better visualize low-growing populations. "crossX" pertains to cross-feeding cells (X = B for bacteria, X = Y for yeast), "wtX" to WT cells. At 0% LW, cross-feeding pairs' (crossB\_crossY) growth is imperceptibly small, crossB\_wtY bacterial commensalism, wtB\_crossY competitive exclusion of yeast. Experimental results are for *cis*-donors. Brightness is mean of four replicates.



D. Growth trajectories for all cis-cell pairings at various amino acid concentrations.

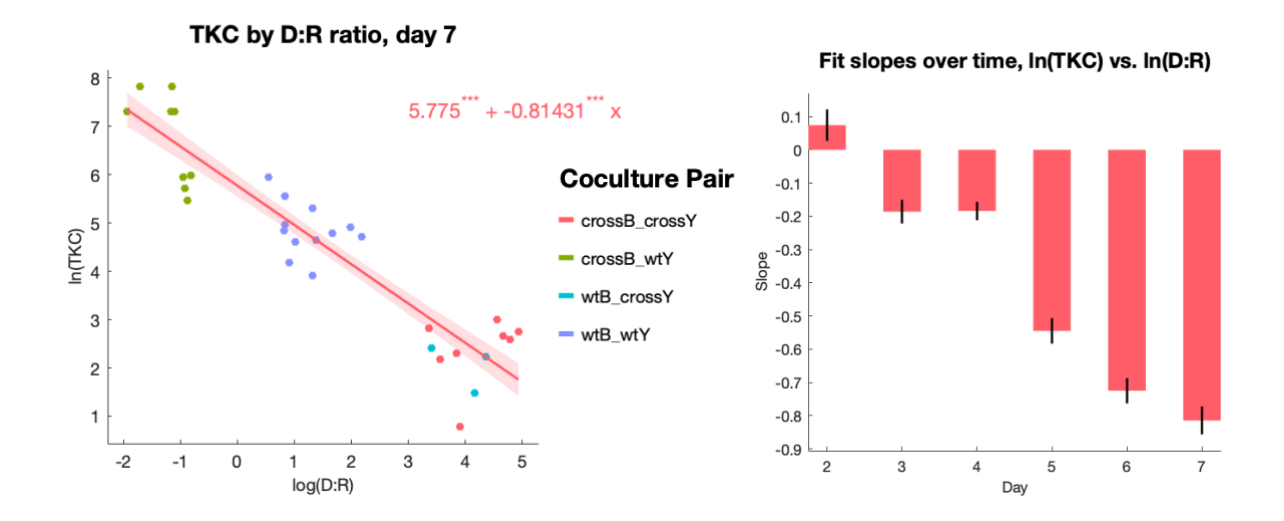
Normalized flow cytometry data for each cell pairing (columns) at four cross-fed amino acid concentrations (LW%, rows), for seven days' batch culturing. Bacterial cell counts shown in red, yeast counts in yellow. Solid lines represent co-culture traces, which are matched with each cell's monoculture traces (dotted) for comparison; shading is standard deviation (four replicates co-culture, two replicates monoculture). Representative outcomes at 0% LW range from parasitism (crossB crossY), commensalism (crossB wtY), and competitive exclusion (wtB crossY).

#### **D:R Ratio and TKC Counts**



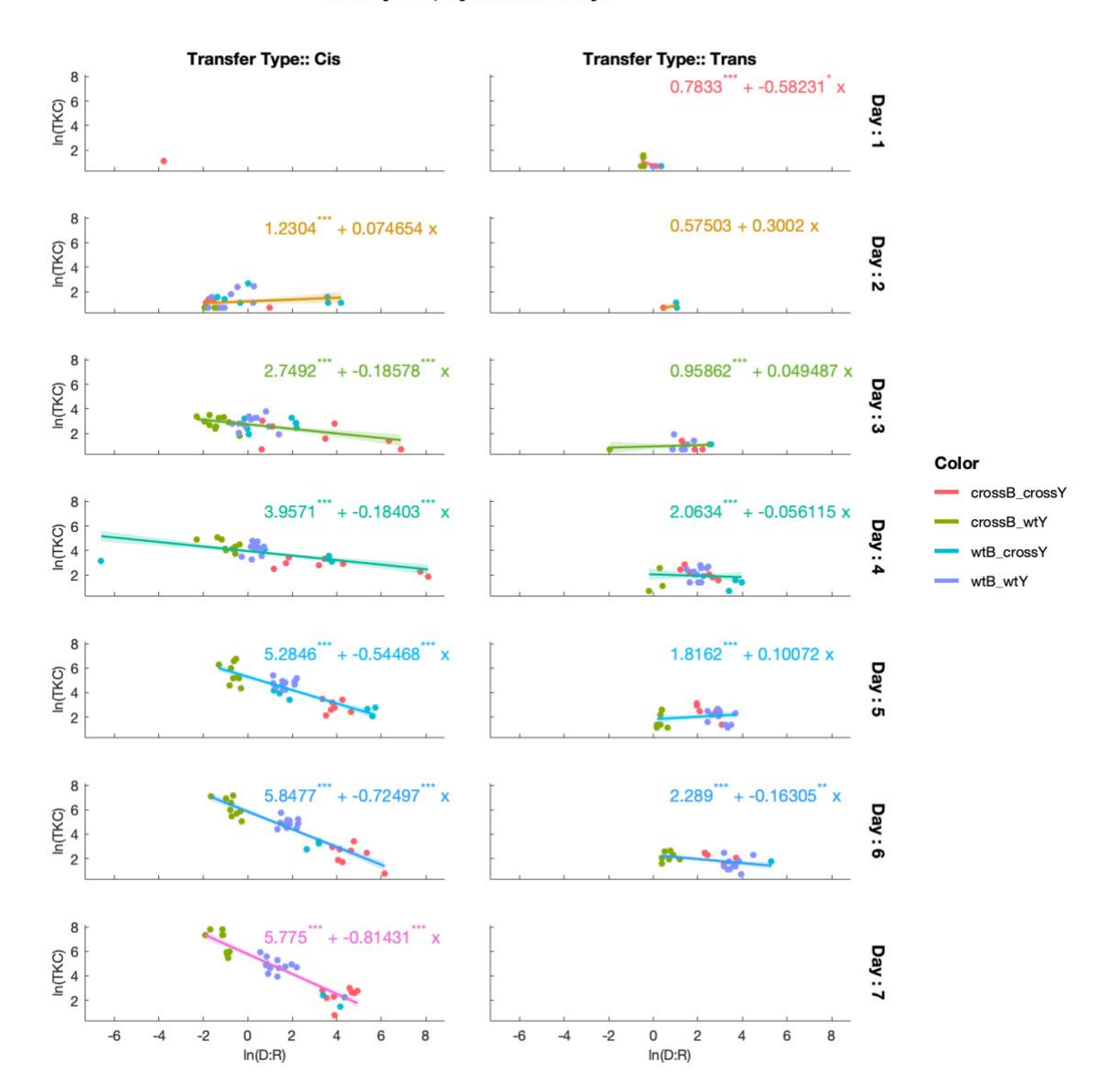
# E. Normalized donor-to-recipient ratios correspond inversely to TKC counts.

Ratios of normalized cell counts (cell count divided by maximum for that species across experiment) of bacterial donors and yeast recipients, calculated from flow cytometry data, plotted over time for each cell pairing, at 5% LW (left). Inset: determination of donor-to-recipient ratio ("D:R"), by dividing normalized bacterial (donor) count by normalized yeast (recipient) count. Raw TKC counts from colony forming units (CFU) on selectable media for the same conditions and cell pairings (right). Lines represent means of four replicates.



F. Inverse correlation between donor-to-recipient ratios and TKC increases in time.

Log-log distribution of donor-to-recipient ratio and TKC counts for each cell pairing at day 7, for all LW%, with linear fits (left). Slope of log-log fits of pairings on left, taken for all days of batch culture, showing decreasing slope over time (right). Black bars = standard error of mean.



TKC by D:R, Dynamics Assays

#### G. D:R ratios vs. TKC counts.

Log-log plots of donor-to-recipient ratios (D:R) and TKC, for *cis*-donor (left column) and *trans*-donor (right column) cultures, for each day's measurements (rows). Note that while *cis*-transfer conditions show a negative correlation between D:R and TKC, *trans*-cultures don't obviously follow this trend, possibly due to low TKC near the detection limit.

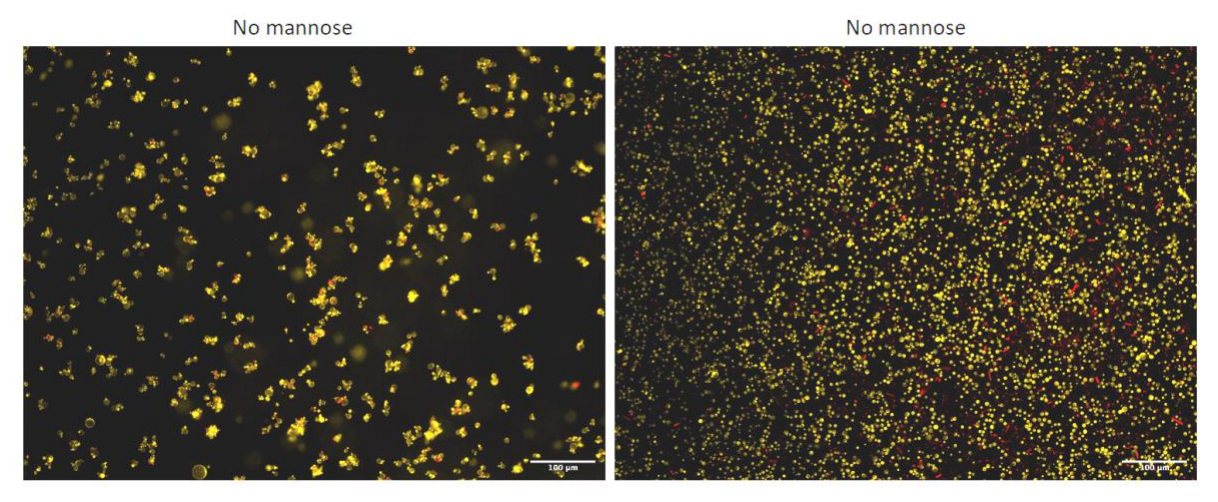
#### cis Culture trans Culture 10-2 10<sup>-4</sup> CFU/Yeast 01 LW%: 15 CFU/Yeast 10<sup>-</sup> 10<sup>-6</sup> 10<sup>-4</sup> 10<sup>-2</sup> CFU/Yeast LW%: 10 CFU/Yeast 10-4 **Coculture Pair Coculture Pair** 10<sup>-6</sup> CrossB CrossY crossB crossY crossB\_wtY 10<sup>-2</sup> 10<sup>-2</sup> wtB\_wtY wtB\_wtY CFU/Yeast LW%: 5 CFU/Yeast LW%: 5 10 10-10<sup>-6</sup> 10<sup>-4</sup> 10<sup>-4</sup> 10<sup>-2</sup> CFU/Yeast LW%: 0 10<sup>-6</sup> 10<sup>-4</sup>

**Transconjugant Fraction of Yeast** 

H. Transconjugants as fractions of yeast populations over time.

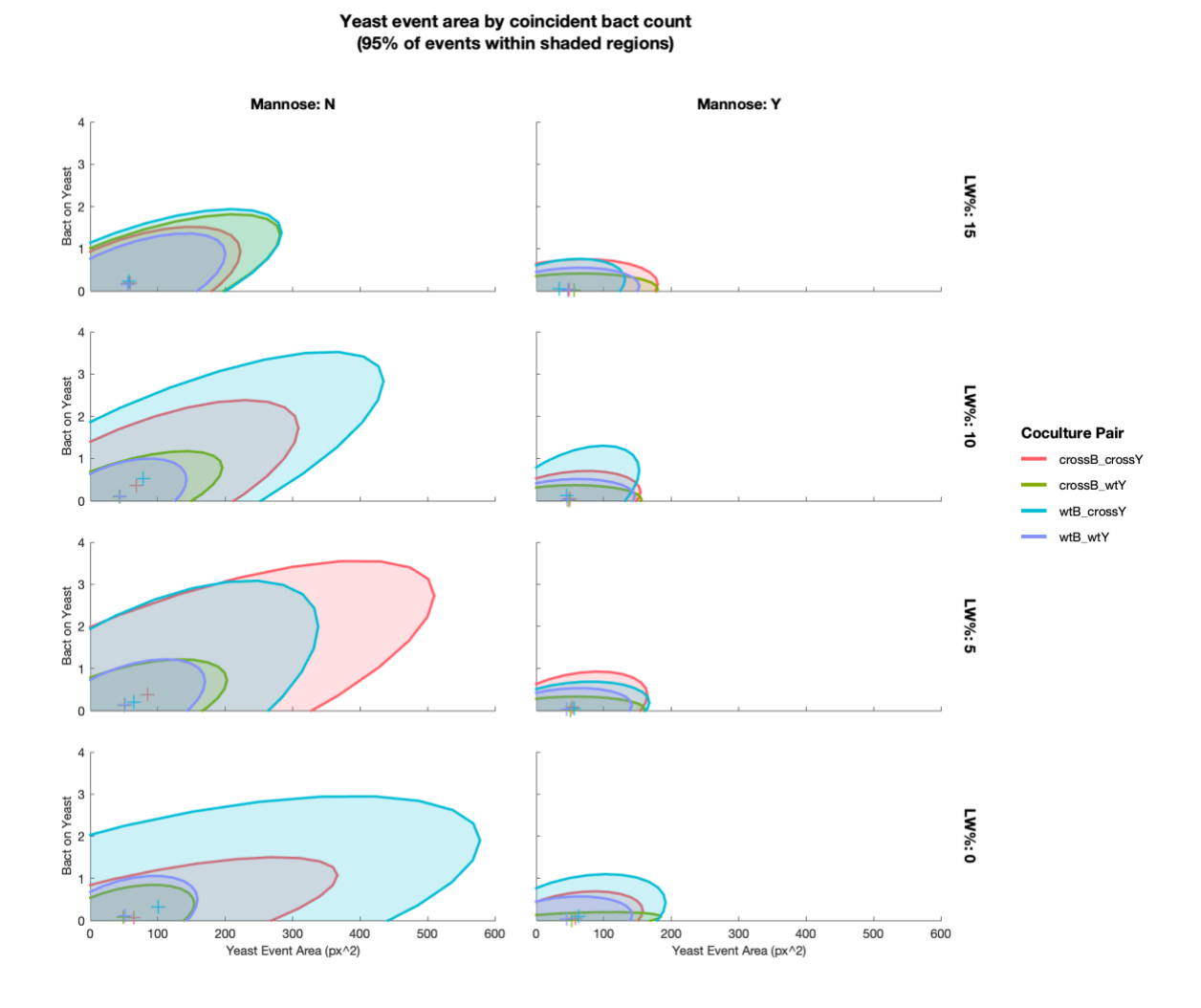
Percent transconjugants (per total yeast) for *cis*-donor cultures, *trans*-donor cultures, and *trans*-donor colonies over 6-7 days. Transconjugants measured as CFU per 100 μL culture or CFU per colony. Yeast counts from flow cytometry, back-calculated to represent 100 μL or entire colony. Note that, for both culture examples, transconjugant fractions increase for all pairings until leveling off at ~day 5, suggesting that increased TKC for certain pairings is not solely a function of higher yeast populations. Also note that *trans*-donor pairings show lower TKC in general.

2.4.2 Figure 2: Mannose disruption of cell aggregates lowers TKC, interrupts bacterial commensalism



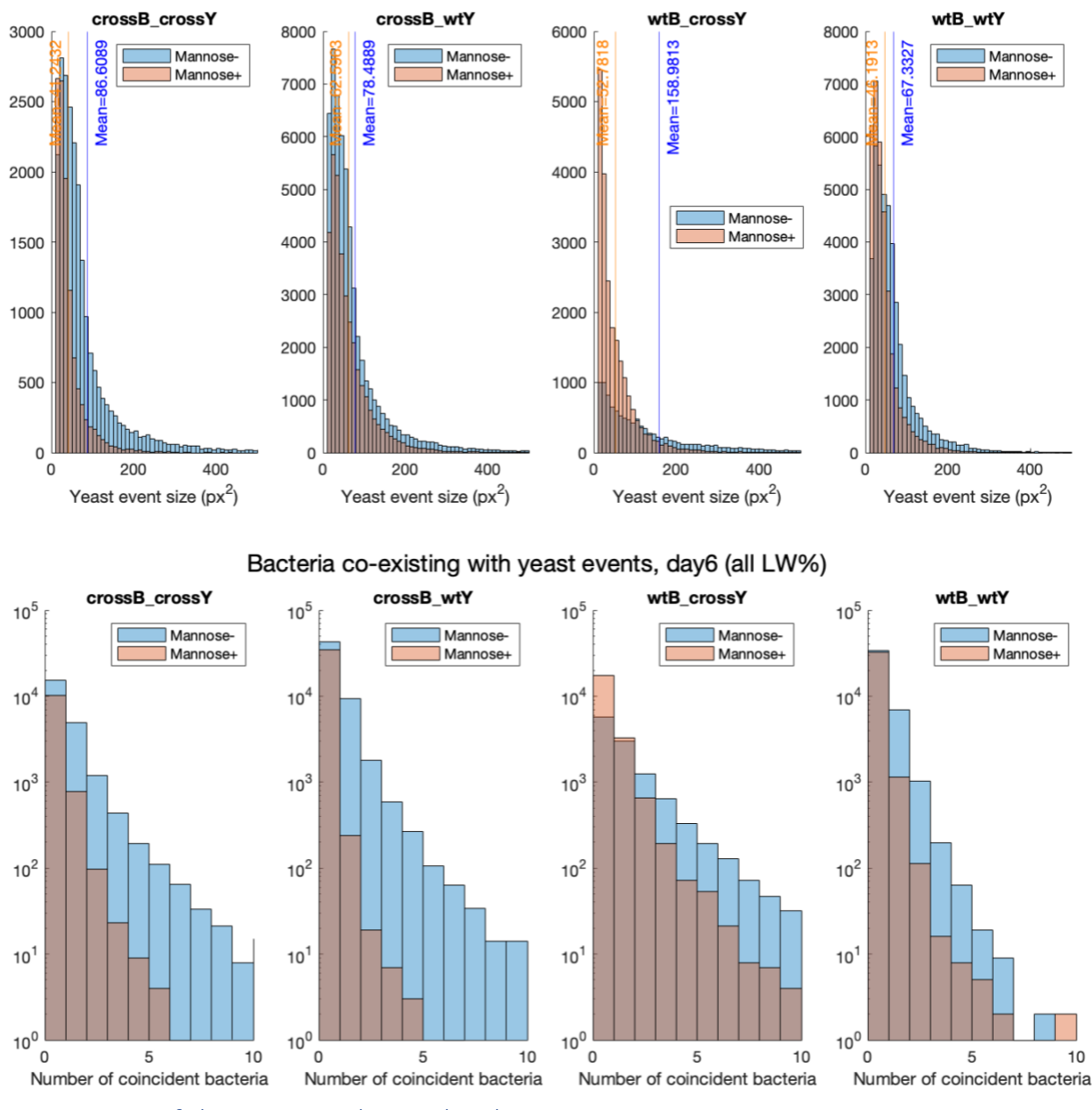
# A. Mannose interrupts mixed aggregates in culture.

Microscopy images of batch co-culture after six days, either without (left) or with (right) mannose supplemented in media. Cells shown are *trans*-WT bacteria (wtB) and cross-feeding yeast (crossY) at 15% LW, diluted 1:10, imaged with a 10x objective. Scale bar =  $100 \mu m$ .



# B. Clump sizes increase with coincident bacteria.

Sizes of clumps, as determined by image analysis, plotted against number of coincident bacteria (number of distinct bacteria identifiable in proximity to yeast events) after six days of batch culture. Ellipses are fit to include 95% of points for each cell pairing (color) and LW% (rows), for samples without mannose (left) or with mannose (right).

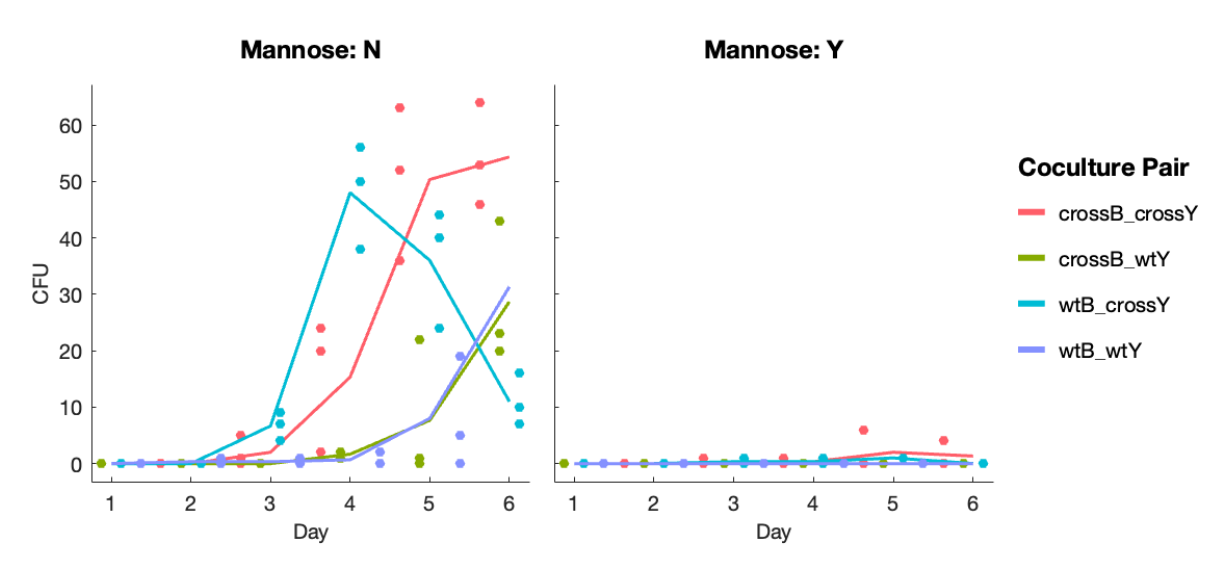


Yeast event areas, day6 (all LW%)

C. Histograms of clump sizes and coincident bacteria.

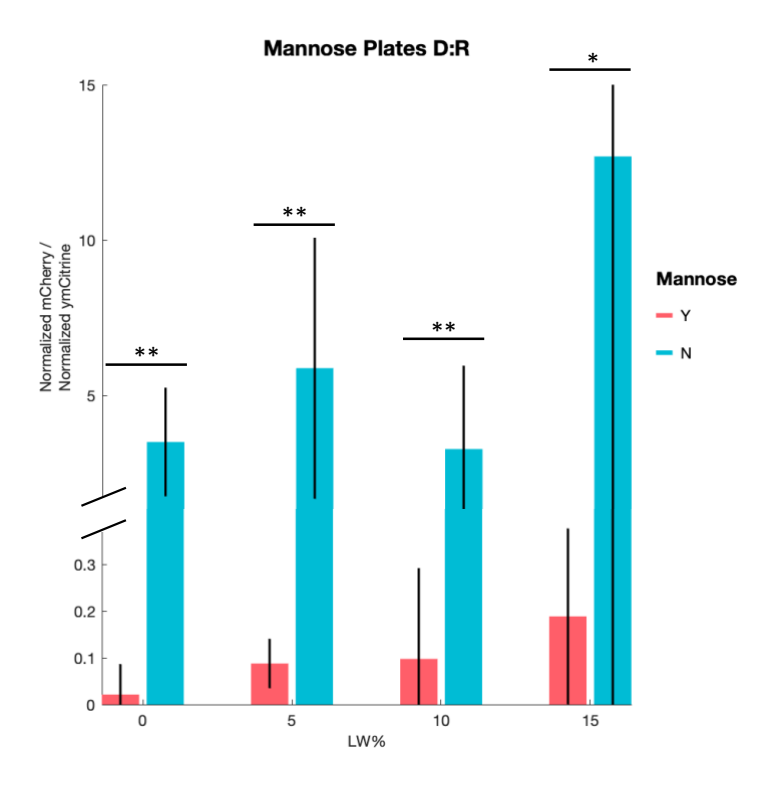
Histograms of clump sizes (top), as determined by image analysis, after six days of batch culture, either with mannose (orange) or without it (blue). Means of each distribution is shown in vertical lines. Log-frequency histograms of coincident bacteria shown at bottom for the same samples.

# **Mannose Plates TKC**



# D. Interrupting clumps with mannose depresses TKC.

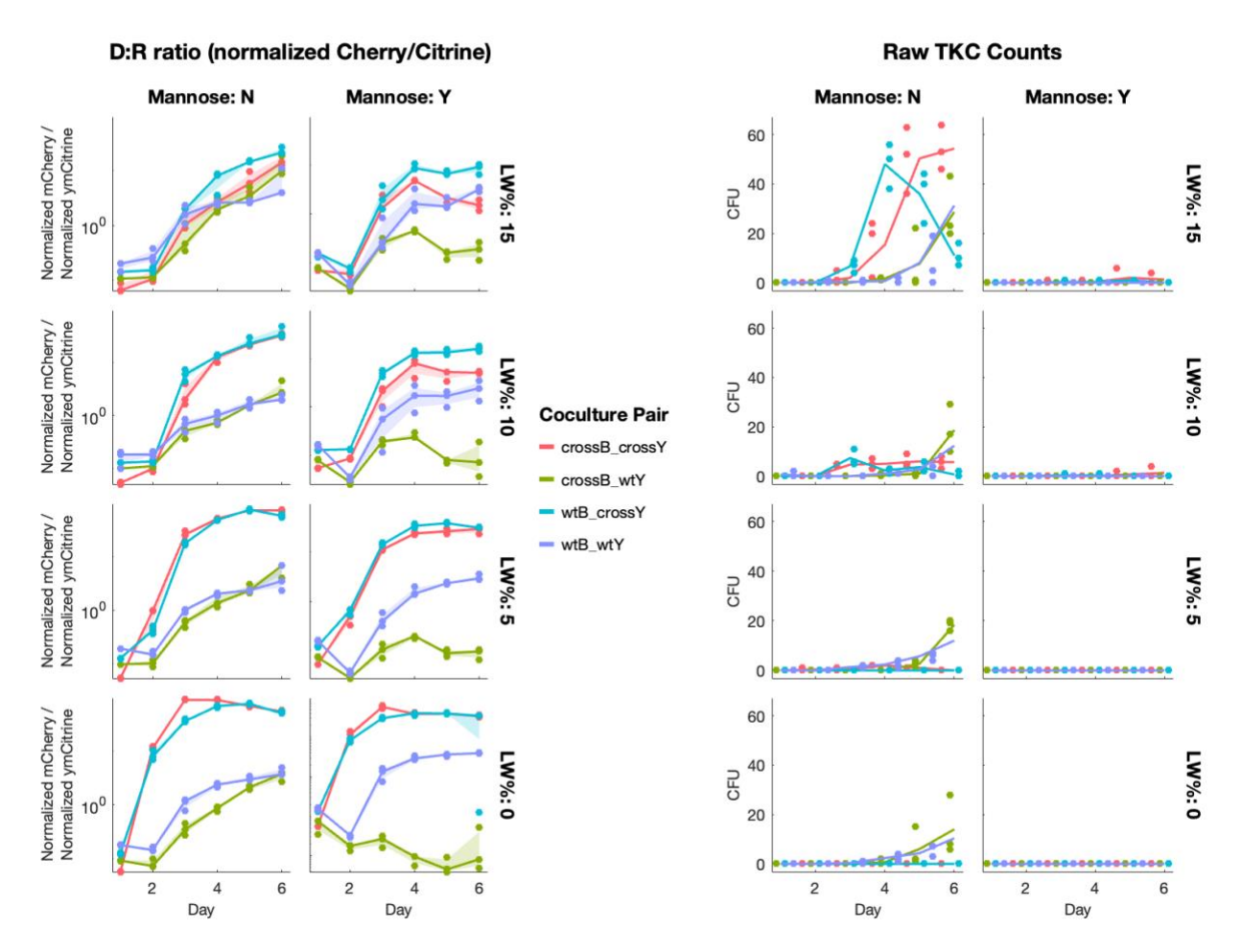
Raw TKC counts (CFU) for samples at four different %LW (rows) without mannose supplementation (left column) are  $\geq 10x$  those with mannose supplementation (right column). Data is colored by cell pairing, lines are means of three replicates.



E. Interrupting clumps with mannose prevents commensalism for cross-feeding E. coli.

Normalized donor-to-recipient ratios for commensal crossB\_wtY pairing, calculated from fluorescence data, for mannose-minus (blue) and mannose-plus (red) samples, shows that clumping is required to sustain cross-feeding bacteria with WT yeast, especially at lower LW%. Bars represent mean of three replicates, error bars 95% CI, significance via two-sample t test, p = 0.0010, 0.0041, 0.0071, and 0.018, for LW = 0%, 5%, 10%, 15%, respectively.

#### **Mannose Plates Cell Ratios and TKC**

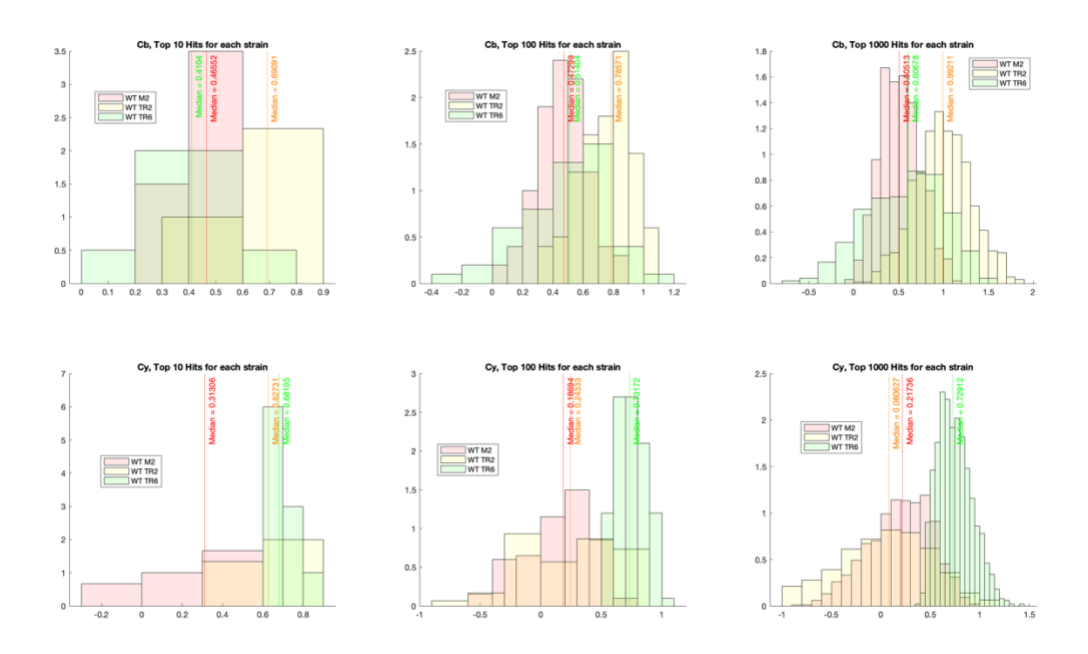


F. D:R ratios show increased commensalism for crossB in clumped cultures, decrease in TKC.

Left: donor-to-recipient ratios for each cell pairing (color) and LW% (row), for samples with or without mannose (columns) over six days' batch culture. Note how the crossB\_wtY pairing (green) ratio stays fairly consistent without mannose—wherein cells can clump—but drops with LW% in samples with mannose supplemented. Right: TKC counts from all days and % LW (rows), with or without mannose (columns).

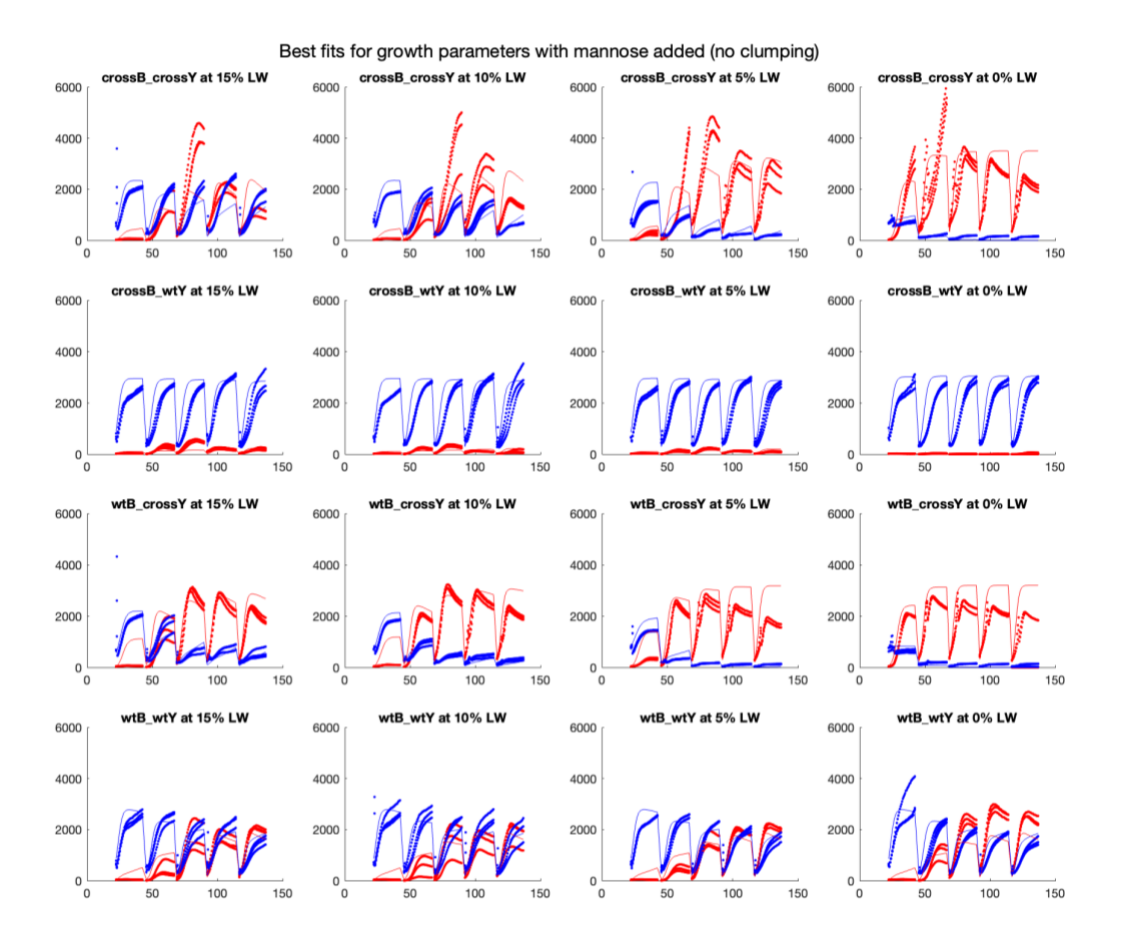
(Return to results)





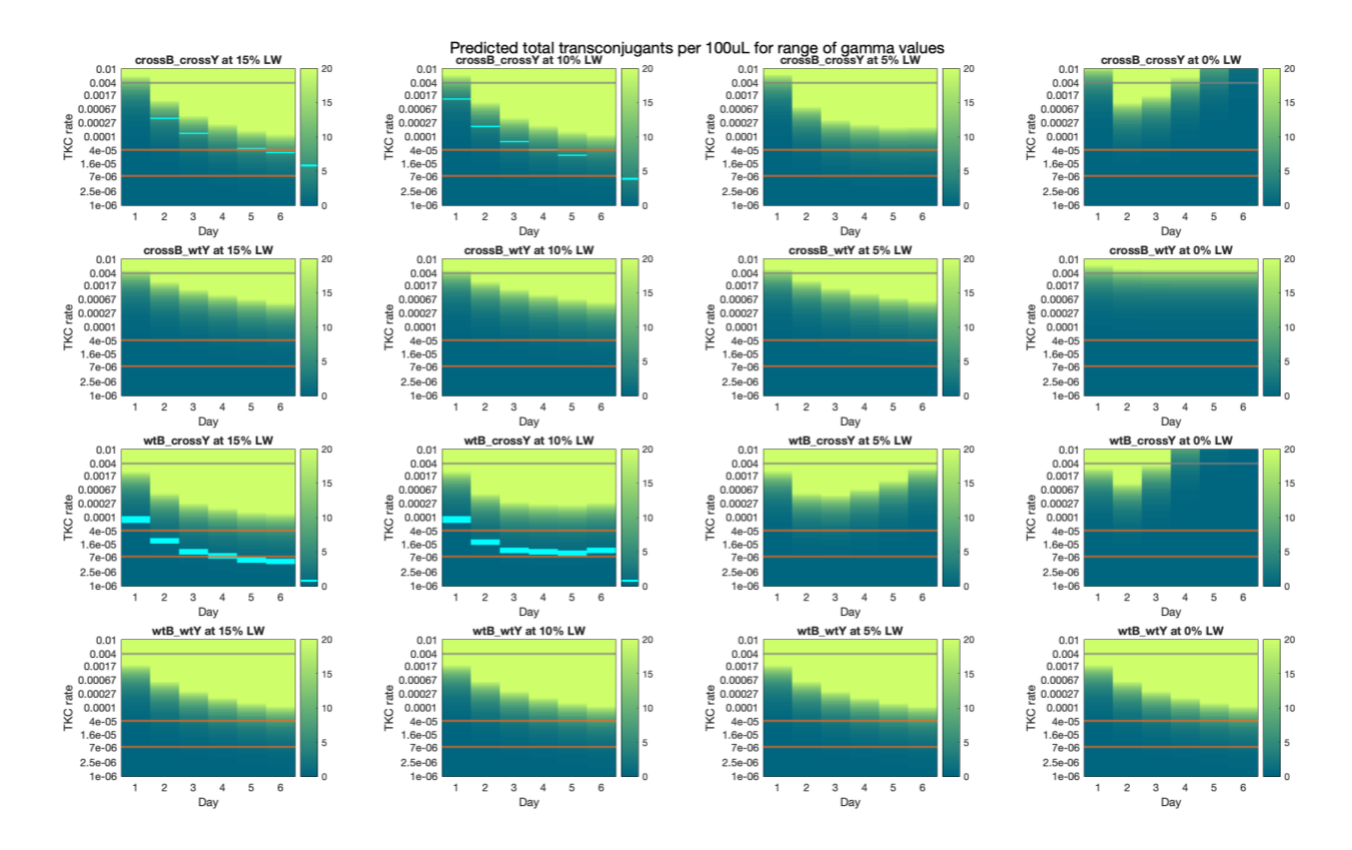
# A. Example parameter distributions for niche overlap terms c.

Example of parameter exploration using Latin Hypercube Sampling of ecological overlap terms c for each WT cell pairing at 100% LW. Each histogram color represents a different plasmid combination for WT donor cells, to account for slight fitness differences. Columns show top 10, 100, and 1000 parameter guesses for cb (top) and cy (bottom), based on a simplified version of free-cell model that omits amino-acid feeding, TKC, and death rates. Means of these distributions served as initial guesses in full free-cell model, and are meant to demonstrate the wider range of parameters explored before the full model was fit.



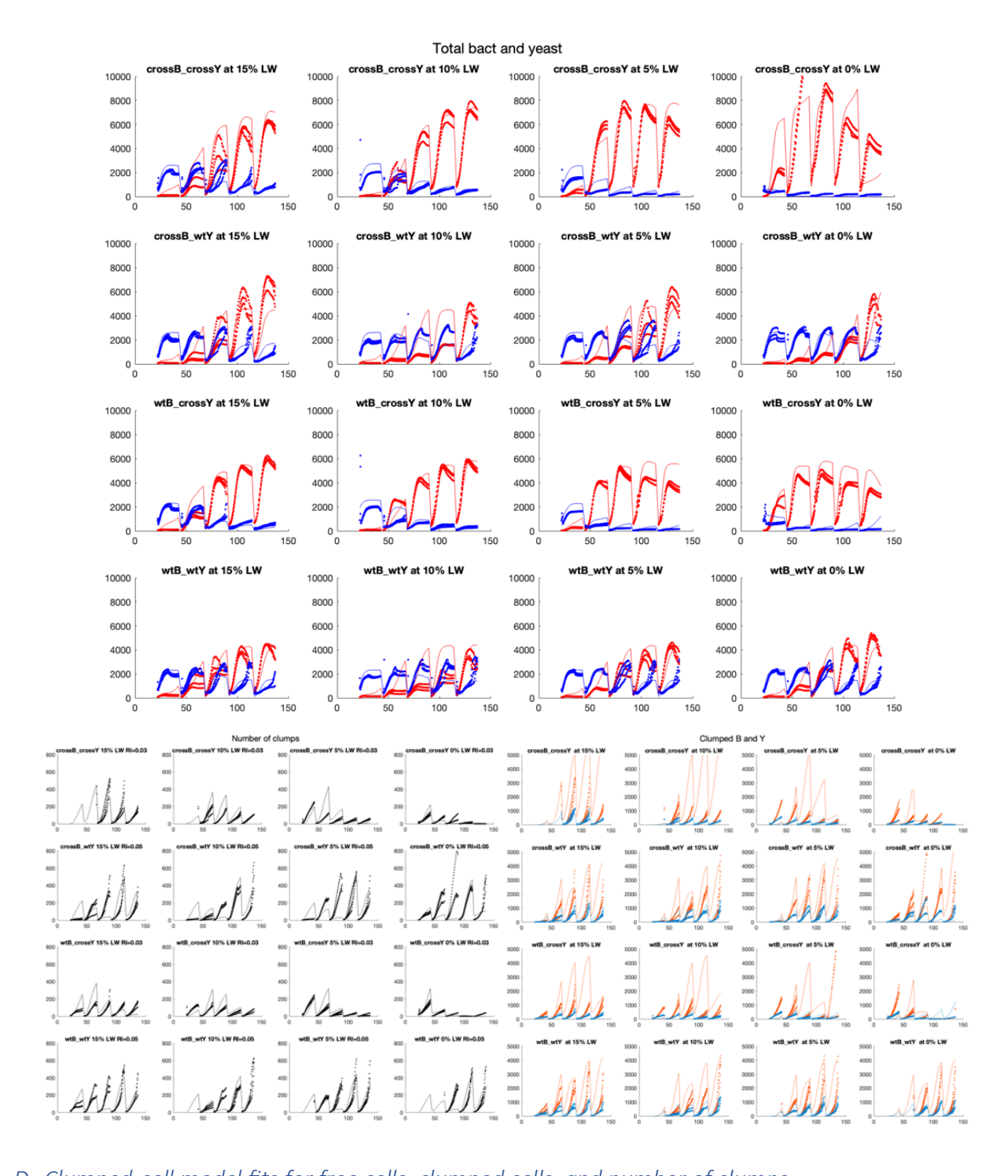
# B. Free-cell model fits for bacteria and yeast in co-culture.

Fluorescent data (dots) of bacteria (red) and yeast (blue) with mannose is compared to predictions (lines) from free-model, given parameters listed in Table 1. Each cell pairing (rows) and LW% (columns) are shown over six days of batch culturing. Free-cell model was fit to prioritize three specific outcomes: 1) susceptibility of each strain to changes in amino acid concentration, 2) steady-state persistence of each strain, and 3) approximate D:R ratio of cells.



C. TKC rate-term sweep for "free" cell model.

Heatmaps showing predicted number of transconjugants (color) for a range of TKC rates  $\gamma$  (y-axis) over six days' batch culturing, for all experimental conditions, assuming cells are unable to clump, and thus conjugate via random collisions. Cyan heat markers represent experimental TKC counts for the four conditions that had counts above zero with mannose, i.e. in the unclumped samples. Gray line at  $\gamma$ =0.004 represents literature prediction for enteric *E. coli* TKC rate, orange lines represent range of TKC-rate values matching data, roughly between 7\*10<sup>-6</sup> and 4\*10<sup>-5</sup>.

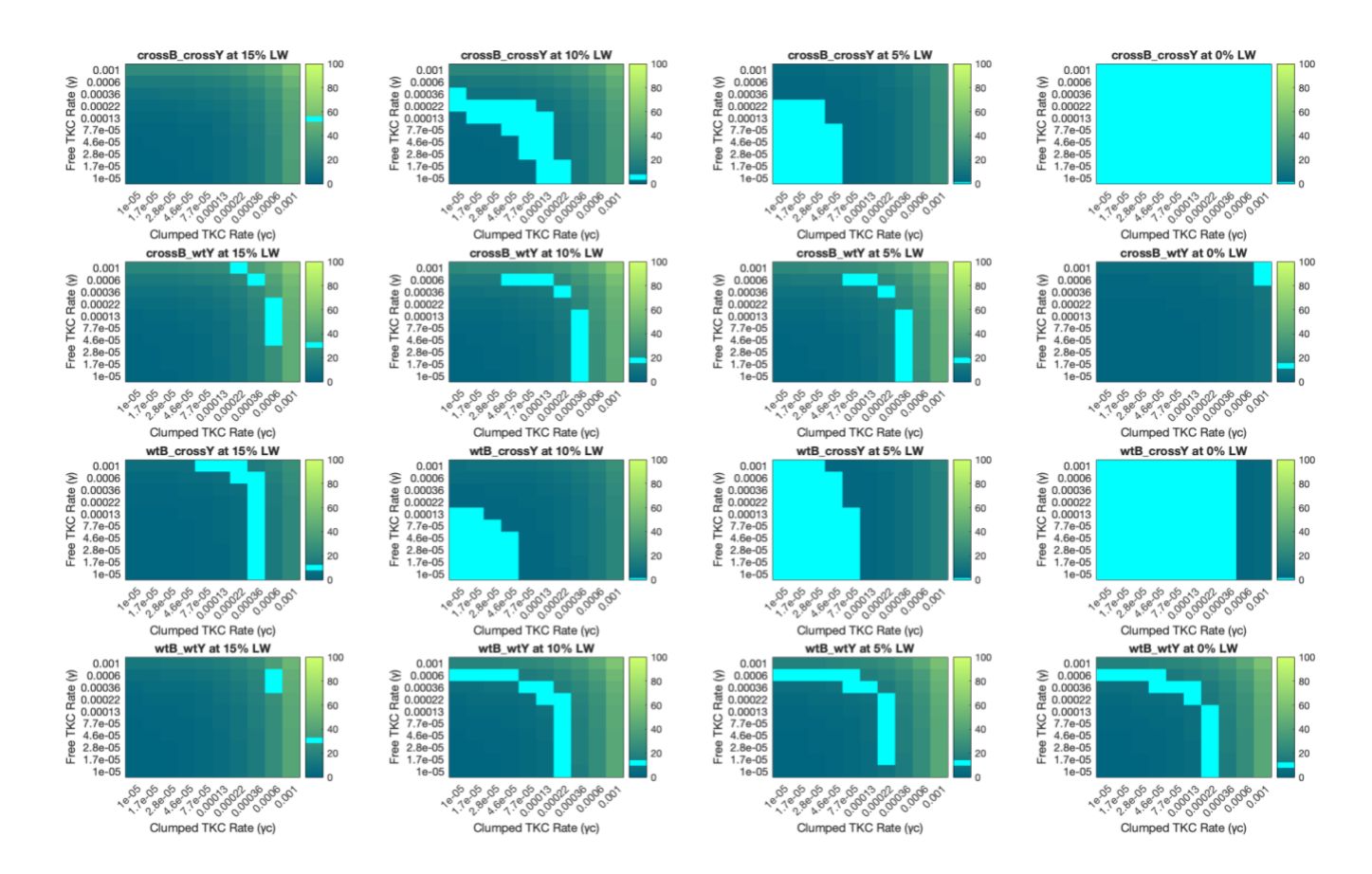


D. Clumped-cell model fits for free cells, clumped cells, and number of clumps.

Top: fluorescent data (dots) of free bacteria (red) and yeast (blue) without mannose is compared to predictions (lines) from clumped-model, given parameters listed in Table 2. Each cell pairing (rows) and LW% (columns) are shown over six days of batch culturing. Bottom left: image analysis

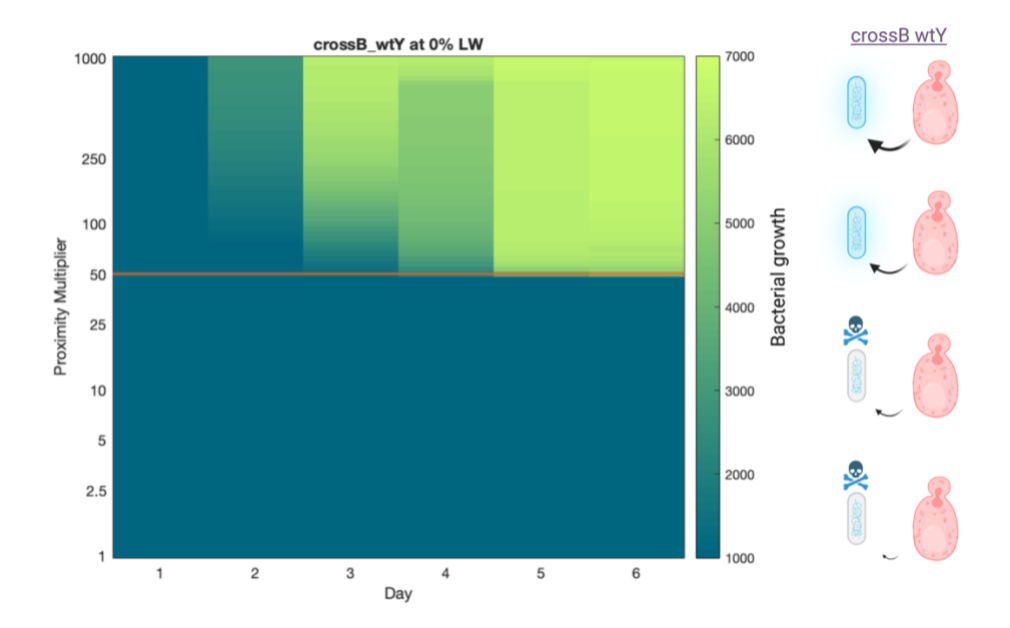
estimates for number of clumps (dots) with model predictions overlain (lines) for each condition.

Bottom right: image analysis estimates for clumped bacteria (orange) and clumped yeast (blue) with overlain model fits (lines) for each condition.



E. TKC rate-term sweep for "clumped" cell model.

Heatmaps showing predicted number of transconjugants (color) for a range of "free" TKC rates  $\gamma$  (y-axis) and "clumped" TKC rates  $\gamma$  (x-axis), for all experimental conditions at day six of batch culturing. Cyan cells represent experimental TKC counts from samples without mannose.



# F. Proximity term sweep for "clumped" model.

Heatmaps showing predicted bacterial fluorescence signal (color) for range of proximity-benefit multiplier P (y-axis) over six days, for crossB\_wtY condition at 0% LW. Orange bar shows approximate P value matching experimental co-culture data, i.e. a P value high enough (~50) to allow crossB growth solely from clumping to wtY.

# (Return to results)

2.5.4 Table 1: Free-cell model parameters

Var	Parameter	Unit	Unit Model Fits per Cell Pairing			
			crossB_crossY	crossB_wtY	wtB_crossY	wtB_wtY
$R_b$	Bacterial growth rate	hr <sup>-1</sup>	0.75	0.66	0.75	0.75
$R_y$	Yeast growth rate	hr <sup>-1</sup>	0.60	0.59	0.58	0.58
$K_b$	Bacterial carrying capacity	mCherry	3500	2987	3201	3500
$K_y$	Yeast carrying capacity	ymCitrine	2600	3044	3039	2998
Cb	Ecological niche overlap (effect of bacteria on yeast)	Unitless	0.80	0.84	0.80	0.80
$c_y$	Ecological niche overlap (effect of yeast on bacteria)	Unitless	0.95	0.99	0.90	0.90
$G_b$	Global amino acid (for dependent bacteria)	Molar	100% leucine = 7.622*10 <sup>-4</sup> M			
$G_y$	Global amino acid (for dependent yeast)	Molar	100% tryptophan = 2.449*10 <sup>-4</sup> M			
$\alpha_b$	Secreted amino acid (for dependent bacteria)	Molar/ mCitrine	1E-4	1E-10	1E-4	1E-10

$a_y$	Secreted amino acid (for dependent yeast)	Molar/ mCherry	1E-9	1E-9	1E-12	1E-12
$k_b$	Monod term for dependent bacteria	Molar	2E-6	2E-6	0	0
ky	Monod term for dependent yeast	Molar	2.5E-5	0	2.5E-5	0
$D_b$	Bacterial death rate	hr <sup>-1</sup>	0.455	0.455	0.455	0.455
$D_y$	Yeast death rate	hr <sup>-1</sup>	0.50	0.547	0.570	0.498
γ	TKC rate	Unitless	4E-5	Unknown	7E-6	Unknown

# 2.5.5 Table 2: Clumped-cell model parameters

Var	Parameter	Unit	Model Fits per Cell Pairing				
			crossB crossY	crossB_wtY	wtB_crossY	wtB_wtY	
$R_b$	Free bacterial growth rate	hr <sup>-1</sup>	0.75	0.75	0.75	0.75	
$R_y$	Free yeast growth rate	hr <sup>-1</sup>	0.58	0.58	0.58	0.58	
$R_{cb}$	Clumped bacterial growth rate	hr <sup>-1</sup>	0.25	0.25	0.25	0.25	
$R_{cy}$	Clumped yeast growth rate	hr <sup>-1</sup>	0.18	0.18	0.18	0.18	
$R_c$	Clumping rate	Unitless	0.03	0.05	0.03	0.05	
$K_b$	Bacterial carrying capacity	mCherry	7566	7269	5590	6790	
$K_{y}$	Yeast carrying capacity	ymCitrine	2822	2700	2637	2412	
Cb	Ecological niche overlap (effect of bacteria on yeast)	Unitless	0.80	0.69	0.90	0.70	
$c_y$	Ecological niche overlap (effect of yeast on bacteria)	Unitless	0.91	0.95	0.90	0.93	
$G_b$	Global amino acid (for dependent bacteria)	Molar	$100\%$ leucine = $7.622*10^{-4}$ M				
$G_y$	Global amino acid (for dependent yeast)	Molar	100% tryptophan = 2.449*10 <sup>-4</sup> M				
$\alpha_b$	Secreted amino acid (for dependent bacteria)	Molar/ mCitrine	9.2E-5	1E-8	9.2E-5	1E-8	
$\alpha_y$	Secreted amino acid (for dependent yeast)	Molar/ mCherry	1E-9	1E-9	1E-12	1E-12	
$P_b$	Proximity multiplier for $\alpha_b$	Unitless	50	50	1	1	
$\overline{P_y}$	Proximity multiplier for $\alpha_y$	Unitless	1	1	1	1	
$k_b$	Monod term for dependent bacteria	Molar	2E-6	2E-6	0	0	
$k_y$	Monod term for dependent yeast	Molar	1.2E-5	0	1.2E-5	0	
$D_b$	Bacterial death rate	hr <sup>-1</sup>	0.46	0.50	0.52	0.46	
$\overline{D_{v}}$	Yeast death rate	hr <sup>-1</sup>	0.46	0.39	0.45	0.48	
γ	Free TKC rate	Unitless	$\sim$ 2E-4 – 1E-3 (see Figure 4)				
$\gamma_c$	Clumped TKC rate	Unitless	$\sim 1E-4-6E-4$ (see Figure 4)				

(Return to results)

# 2.5 Materials and Methods

# 2.5.1 Strain and plasmid construction

Yeast cells in this study are derived from W303 strains developed by Müller et. al. (MATa canl-100 hmla\Delta::BLE leu9\Delta::KANMX6 his3\Delta::prACT1-ymCitrine-tADH::HIS3MX6, with S288C version of BUD1)<sup>77</sup>. Cross-feeding yeast strains ("crossY", yMM1430) have additional mutations to make them auxotrophic for tryptophan and leucine-overproducing: LEU4FBR trp2\Delta::NATMX4 prACT1yCerulean-tADH1@URA3, with leucine feedback resistance (FBR) resultant from deletion of codon 548 of LEU4. CrossY is also constitutively fluorescent for ymCitrine and yCerulean, whereas the baseline yeast used here (aka "WT yeast", "wtY", yMM1636) is only ymCitrine-fluorescent. Further mutations were introduced into these strains to make them auxotrophic for uracil and/or histidine, for TKC selection and CRISPR assay. Uracil was knocked out by amplifying a cassette of URA3 homology arms, transforming into yMM1430, and selecting for growth on 5-Fluoroorotic acid (5FOA). HIS3 was replaced with either KANMX6 or HPHMX6, depending on the strain (see Table 3 for list of strains and related experiments), by amplifying either resistance gene with overlap for HISMX6 regions.

Bacterial strains in this study are derived from Keio Collection strains of single-gene knockouts, based on BW25113 background (F-  $\Delta(araD-araB)$ 567  $lacZ4787\Delta$ ::rrnB-3  $\lambda$ - rph-1  $\Delta(rhaD-rhaB)$ 568 hsdR514)90. WT bacteria ("wtB") strains are simply BW25113, or Coli Genetic Stock Center (CGSC) #7636, containing different plasmids depending on the experiment (see Table 4 for list of plasmids and corresponding experiments). Cross-feeding mutations were introduced into CGSC #11110 ( $\Delta trpR789:kan^R$ ), which lacks the trp repressor gene, and has been shown to be tryptophan-overproducing<sup>85</sup>. Briefly, the kanamycin resistance gene at the trpR locus was

"flipped" out via flippase recognition target (FRT) sequences and flippase-expressing plasmid pMM0821<sup>91</sup>. Leucine auxotrophy was introduced by  $\lambda$ red recombination of PCR-amplified  $\Delta leuA781::kan^R$ , from CGSC #8373, using pMM0820, which expresses genes for  $\lambda$ red.  $kan^R$  was again flipped out to obtain kMM127, a double knockout of  $\Delta trpR$ ,  $\Delta leuA$ , with no antibiotic resistance. Note that we originally constructed crossB from  $\Delta leuA::kan^R$  (CGSC #8373), but it caused severe aggregation in co-culture, such that cells would precipitate out of media immediately, whereas the same mutation introduced from the  $\Delta trpR::kan^R$  strain did not produce this result. Moreover, we found that  $\Delta leuB::kan^R$  (CGSC #11943) proved prototrophic for leucine over long time periods, despite its similar function in the leucine biosynthesis pathway and previous experiments utilizing the knockout as an auxotroph<sup>92</sup>.

IncP-type TKC plasmids<sup>55</sup> pTA-Mob 1.0 (*trans*-transferring) and pTA-Mob 2.0 (*cis*-transferring) were generously provided to us by the Karas lab<sup>30</sup>. pTA-Mob 2.0 contains gentamicin resistance for bacterial selection, *URA3* and *HIS3* genes for yeast selection, *CEN6/ARSH4* for yeast maintenance, and the *ori*<sup>T</sup> sequence required for conjugative transfer of the plasmid into recipients, whereas pTA-Mob 1.0 only carries gentamicin resistance. Constitutive bacterial reporter pMM0819 contains *pProD:mCherry*, using a synthetic reporter meant to be high-expressing and minimally susceptible to cell phase<sup>93,94</sup>. TKC plasmids for *trans*-transfer were constructed using the Golden Gate-based Yeast MoClo Toolkit<sup>95</sup> (YTK), to modularly assemble a fluorescent yeast reporter (*pTDH3-yeBFP*), TKC selection (*HIS3*), and yeast replication machinery (*CEN6/ARSH4*). The *ori*<sup>T</sup> sequence was then added to the connector sequence downstream of yeBFP via Gibson assembly.

(Return to top)

# 2.5.2 Batch culture and TKC counting

Yeast and bacterial cultures used in each batch culture experiment were grown overnight in selective YPD or LB media, at 30°C or 37°C, respectively. After  $\geq$  16 hours' growth, bacterial strains were measured for OD600, yeast strains were measured for OD660, and each culture was washed at least 2 times with SC or M9 sans glucose or amino acids. Cells were then combined such that each reaction started with 1E7 cells, based on OD measurements. Growth media was composed of 200  $\mu$ L of a 75:25 mixture of SC:M9 minimal media (condition screening portion of Results) with 2% glucose, appropriate amino acids, and antibiotics to maintain each bacterial plasmid. Amino acid percentages in the text are based on the following molarities, considered 100%: L = 762  $\mu$ M, W = 245  $\mu$ M, U = 178  $\mu$ M, H = 95.4  $\mu$ M. For clumping experiment (Fig 2), half of the media was supplemented with 4% mannose. Upon spiking cells into 96-well CellVis back-walled optical glass-bottom plates (cat #P96-1-N), plates were sealed with gas permeable membranes (Fisher Scientific cat #50-550-304) seals to allow air flow for aerobic conditions.

Plates were grown in a customized Tecan Fluent automated plate handling robot, on a Bioshakes heater-shaker, kept at 30°C and rotating at 1000 rpm with a 2 mm orbital. In 15 minute intervals, the Fluent was programmed to transfer each 96-well plate to a connected Tecan Spark fluorimeter, in which each well was measured for OD600, mCherry (Ex=575nm, Em=620nm, 20nm bandwidth, gain=60), and ymCitrine (Ex=500nm, Em=545nm, 20nm bandwidth, gain=60). After each plate was measured, it was returned to the Bioshakes, where it grew for another 15 minutes until the next read. Each plate was grown in this way for roughly 18-24 hr., at which time plates were briefly spun (1 min at 1000xG) to remove condensate from plate seal. Each plate was then

diluted 1:10 in fresh media (180 µL media + 20 µL previous day's culture) for that day's growth, with another 20 µL diluted into a plate of PBS+0.1% Tween for flow cytometry (see below). Tecan data was consolidated in Excel format and imported into MATLAB via a custom script, which parses the Tecan Excel export format based on number of plates and channels measured. All further analyses were performed in MATLAB, including normalization, in which all fluorescence measurements were divided by the max reading of that channel; these normalized reads were used for D:R ratios in Fig 1 and in subsequent chapters.

An additional 100 μL of each day's culture was added, undiluted, to a 24-well plate containing TKC-selective SC with 2% agar: for *cis*-transfer experiments (Fig 1), SC-UH (lacking uracil and histidine) was used, whereas SC-H was used for *trans*-transfer experiments (Figs 2, 3). TKC plates were then placed in a culture shaker at 30°C for ~40 minutes, without lids, to dry. Once dried, TKC plates were incubated for ~3 days to grow countable transconjugant colonies. Individual transconjugant colonies were counted for CFU, unless wells were saturated, in which case estimates were generated based on density relative to countable wells, up to 500.

### (Return to top)

#### 2.5.3 Flow cytometry

After diluting cells from culture (see above) 1:10 into PBS+0.1% Tween (total volume=200 μL) in 96-well round-bottom plates (Fisher Scientific cat #07-200-760), samples were measured for cellular composition using a ThermoFisher Attune NxT V6 Flow Cytometer at UW-Madison's Carbone Cancer Center, which includes a 96-well compatible autosampler. Because the sizes of bacteria and yeast are so different, each co-culture was measured twice, with different forward and

side scatter voltages for each cell type (monoculture controls were generally measured using only that species' voltage settings, though at least two of the other species were included to get baseline counts). Each well was measured for ymCitrine (488 nm laser, 530/30 503LP filters, off target fluorescent) and mCherry (561 nm laser, 620/15 600LP filters), in addition to scatter, using a draw volume of 20  $\mu$ L, at a flow rate of 200  $\mu$ L/min.

FCS files exported from the Attune were processed via custom MATLAB tools modified for dual-voltage experiments. Gates were drawn per voltage setting to capture all cells of that species based on fluorescence and forward scatter. FCS files were imported, correlated with sample information, and queried for inclusion in each gate. Summary tables for each cell type were consolidated to combine all readings per experiment, upon which noise floors were calculated based on negative controls per voltage setting. Gate-defined cell counts for each species were subtracted by these baselines and converted to total cells per  $100~\mu L$ , to compare to TKC counts (see TKC prep in Batch Culture methods). Cell counts were further normalized by dividing by the max count for that experiment and cell type; normalized counts were used to generate D:R ratios.

# (Return to top)

#### 2.5.4 Microscopy of culture aggregates

Batch culture samples were diluted to various degrees (depending on day and sample density) in media lacking glucose and amino acids, but with mannose for samples grown with it, in a CellVis 96-well back-walled optical glass-bottom plates (cat #P96-1-N). Plates were loaded onto the stage of an inverted fluorescence microscope (Nikon TiE), enclosed by an opaque incubation chamber. A custom Nikon JOBS script was written to image each well of a plate in three random locations

distal to the well edges, with a two second wait time before each photo to allow cells to settle after moving the stage. All wells were imaged at 10x objective for mCherry (Chroma 96365, Ex = 560/40x, Em = 630/75m, 200 ms exposure), ymCitrine (Chroma 96363, Ex = 500/20x, Em = 535/30m, 600 ms exposure), and yeBFP (Chroma NC296093, Ex = 350/50x, Em = 460/50m, 500 ms exposure).

# 2.5.5 Clumping image analysis

Microscopy images from batch co-cultures with or without supplemented mannose were taken after each day's growth. Initially, samples were diluted 1:50 into corresponding media (mannose +/-) without glucose for imaging, though as day-end cell densities diverged between samples, additional dilutions were imaged, from 1:1 to 1:500, depending on the sample and day. A custom Nikon "JOBS" script imaged each well of dilution plates at three random locations, using filter cubes for mCherry, ymCitrine, and yeBFP, at 10x objective. All .nd2 files were converted to lossless .tif files using a custom ImageJ macro. Sample information for TIFF files were imported into a MATLAB table, including sample information, dilution, and whether mannose was included.

Each .tif file was binarized using MATLAB's adaptive thresholding, using thresholding values of 0.4 for both mCherry (bacteria) and ymCitrine (yeast). Binarized contiguous events were made solid by "filling" regions, and region properties were calculated via MATLAB's regionprops function: for yeast, event areas and bounding boxes (minimum rectangle that would fit event); for bacteria, centroids (center coordinates of each event). Yeast event areas less than 10 px^2 were filtered out as noise, and images with fewer than three such events, fewer than three bacteria, or more than 1000 yeast events were ignored. In this way, we only analyzed events that were truly

yeast, filtered out samples with too sparse or too concentrated cells, and corrected for optical defects which occasionally appeared as apparent single bright spots in a channel.

Coincident bacteria were calculated by comparing red-channel centroids and yellow-channel bounding boxes. For each yeast event bounding box, all bacterial positions for that image were queried for inclusion in the bounding box, with detectably proximal bacterial getting saved as "coincident" per each yeast event. Importantly, this technique depends on distinguishing individual bacterial cells to be counted accurately, which at 10x objective, probably isn't always the case, and so the coincident bacteria metric is likely a slight undercount in all cases.

To impute the number of yeast cells in each ymCitrine event, for use in modeling, a baseline single-cell size was estimated based on mannose-supplemented day 1 data. Because many yeasts in clumps appear rather small, a value on the low end of the single-yeast distribution was chosen: 20 px $^2$ . Each yeast event per image was categorized into number of predicted yeasts based on the square multiplier of this baseline area. E.g., events less than  $2^2*20$  px $^2$  were considered one cell, events greater  $2^2*20$  px $^2$  but less than  $3^2*20$  px $^2$  considered two cells, etc. Because of variability in yeast cell sizes, and because images don't account for yeast stacking in the z-plane (i.e., any cells obscured by those at the bottom of a plate well), we expect these yeast counts to mostly be underestimates. Clumps were defined as yeast events  $\geq$  two cells, and numbers of clumps and numbers of clumped cells, along with their frequencies per total yeast, were calculated from that designation. Similarly, coincident bacteria per clump were determined by comparing coincident bacteria to whether a yeast event was categorized as a clump.

To use image analyses of batch culture clumping as comparative data for the model, dynamic information on number of clumps, total clumped bacteria, and total clumped yeast were acquired by the following means. The total number of clumps was taken as a fraction of all yeast, based on determination of number of yeasts in each clump. Thus, a fractional term of clumps/total yeast could be multiplied by the ymCitrine fluorescence signal to get the number of clumps in units of ymCitrine, regardless of the fraction of cell culture was imaged to determine clump count. The number of clumped yeasts was calculated similarly, but tracking clumped yeast per total yeast, and multiplying by total yeast ymCitrine signal. For clumped bacteria, coincident bacteria on all clumped yeast (>2 yeast per event) was taken as a fraction of total clumps, to get clumped bacteria per clumps. Upon deriving number of clumps in terms of ymCitrine, this could be multiplied by clumped bacteria per clumps term to get clumped bacteria in terms of ymCitrine, which was then converted to mCherry by conversions described in the discussion of TKC sweeps for the free-cell model. All three metrics—each only determined at day-ends—were imputed for intermediate times as linear increases from 1/10th the previous day's metric (day 1 assumed = 0).

# (Return to top)

#### 2.5.6 Data analysis and figures

Unless otherwise specified, all data processing was performed using custom MATLAB scripts. Most data plots were generated with the gramm MATLAB toolbox<sup>96</sup> and flow diagrams were created with BioRender.com.

# 2.5.6 Table 3: Strains used in this study

ID	Species	Genetic features	Fluorescence	Source		Figures
yMM1585	Yeast	Leu <sup>++</sup> , Trp <sup>-</sup> , Ura <sup>-</sup>	ymCitrine, yCerulean	77,	this	1
				work		
yMM1636	Yeast	His-	ymCitrine	77,	this	All
				work		
yMM1720	Yeast	Leu <sup>++</sup> , Trp <sup>-</sup> , His <sup>-</sup>	ymCitrine, yCerulean	77,	this	2-3
				work		
kMM0011	Bacterium	None	None	90		All
kMM0127	Bacterium	Trp <sup>++</sup> , Leu <sup>-</sup>	None	90,	this	All
				work		

# 2.5.6 Table 4: Plasmids used in this study

ID	Species	Function / Features	Fluorescence	Source	Figures
pMM0819	Bacterium	pProD-mCherry	mCherry	Addgene 87144	All
pMM0820	Bacterium	$\lambda_{red}$ genes	None	91	None
pMM0821	Bacterium	Flippase	None	91	None
pMM0892	Bacterium	T4SS genes, Gent <sup>R</sup>	None	pTA-Mob 1.0 <sup>30</sup>	2-3
pMM1353	Both	T4SS genes, Gent <sup>R</sup> ,	None	pTA-Mob 2.0,	1
		URA3, HIS3,		Addgene 149662	
		CEN/ARS, $ori^T$			
pMM1437	Both	yeBFP, ori <sup>T</sup> , HIS3,	BFP	<sup>95</sup> , this work	2-3
		CEN/ARS			

(Return to top)

# Chapter 3: Spatial dynamics of TKC in mixed colonies

# 3.1 Introduction: maximizing the boundary space of mixed colonies

While studying TKC in laboratory culture conditions yields many insights, any application to natural microbiomes must take into account that microbes predominantly live in spatially constrained conditions, often in dense biofilms with low nutrient availability<sup>97</sup>, regardless of whether our target application is oral fungal infections or plant rhizospheres<sup>98</sup>. While a synthetic consortium of E. coli and S. cerevisiae doesn't intrinsically lend itself to studying mixed biofilms, since these species aren't known to form biofilms together in nature, we can still approximate such spatially constrained conditions by growing cells in mixed colonies. In fact, colony growth has been studied extensively for spatial outcomes of engineered cell interactions—mutualistic vs. antagonistic populations, etc.—for both E. coli<sup>99</sup> and S. cerevisiae<sup>77</sup>. In these examples, and in other studies utilizing range expansion assays developed by Hallatschek et. al., a dense mix of two fluorescent strains of a single species is plated on agar media and quantified for each strains' spatial distribution as the colony front expands 100-103. For isogenic (but for each fluorophore), i.e. neutrally-interacting strains, cells on the exterior of the original colony enjoy an advantage along the expanding colony front, preferentially growing their populations toward regions of higher nutrient density outside the colony center. These cells act as ecological founders for subsequent growth, forming uniformly colored segments based on whichever strain happened to be at the colony front for a given radius. But the width of these segments is highly dependent on the type of interactions between the strains, with obligate mutualists especially limited in their ability to grow distally from each other and thus forming highly mixed colonies, especially in yeast<sup>77</sup>. Competition between strains, moreover, vastly increases population widths in E. coli<sup>99</sup>.

Because these examples involve monospecies colonies, it's unclear how mixed colonies of *E. coli* and *S. cerevisiae* might spatially resolve, though naively it seems intuitive to expect more intermixing of populations the more the strains are interdependent, based on the conclusions from the referenced expansion studies. This is important for TKC dynamics in such a setting, because conjugation requires contact between donors and recipients, and so spatially resolved conjugation predictably occurs along population boundaries<sup>104</sup>, including in biofilms<sup>105</sup>. Thus, any interaction regime that increases intermixing between populations would hypothetically increase the occurrence of conjugation events. Several factors complicate such an investigation, including the difficulty of spatially resolving donors, recipients, and transconjugants simultaneously, and the stochasticity of cell interactions at colony fronts, which determines segment outcomes<sup>77,104</sup>. My research here therefore focuses on the effects of population interactions on spatial mixing and transconjugant abundance, while attempting to overcome the aforementioned challenges by creating a transconjugant reporter and quantifying populations at both the colony-wide and single-cell scale.

# (Return to top)

# 3.2 Results

#### 3.2.1 Building a TKC reporter for tracking transconjugants spatially

To compare colony experiments to batch culture experiments, which include both *cis* and *trans* TKC donors, I sought to create a TKC reporter—a fluorophore only active in transconjugant cells—for both transfer types. Because the strains used for this study carry ymCitrine (yeast) and mCherry (bacteria), I focused on implementing either iRFP or BFP to make transconjugants discernable from donors and recipients, though in the end iRFP proved worse than BFP for imaging colonies (see section 3.5.1). Generating a *cis* TKC reporter required modification of the ~60 kbp

pTA-Mob 2.0 T4SS plasmid, which was accomplished by  $\lambda_{red}$  recombineering<sup>91</sup> a cassette containing iRFP with a strong yeast promoter and spectinomycin resistance so as to replace the existing gentamicin resistance gene in pTA-Mob 2.0 (Fig 1a). This was accomplished twice, for slightly different landing sites within pTA-Mob 2.0. For each, iRFP fluorescence was verified by microscopy (Fig 1b) and sequence beyond insertion cassette verified by Sanger sequencing. In both cases, however, conjugative function was disabled for reasons still unresolved, as several attempts at side-by-side TKC experiments with unmodified pTA-Mob 2.0 gave zero transconjugants for the *cis*-TKC reporter. Any future attempts to create a *cis* reporter would benefit from whole-plasmid sequencing (versus sequencing the insertion region only) to rule out off-target recombination from  $\lambda_{red}$  or other mutations that could adversely affect the T4SS machinery.

A *trans*-TKC reporter was created by modular assembly of yeast-enhanced BFP (yeBFP) with a strong promoter, *CEN/ARS* yeast replication machinery, and *HIS3* TKC selection; the *ori*<sup>T</sup> sequence was subsequently added by Gibson assembly (Fig 1a). All functional regions were Sanger-sequence verified, and direct transformation of yeast cells were verified for blue fluorescence by microscopy (Fig 1c) and fluorescence plate reader. Unlike the *cis*-TKC reporters created, two constructions of *trans*-TKC reporter (with slightly different *ori*<sup>T</sup> landing sites) both conjugated successfully into yeast. Importantly, however, transconjugants were significantly dimmer for yeBFP than directly transformed yeast, even after selecting for and subculturing the brightest transconjugants. This phenomenon, along with the low occurrence of TKC (lower for *trans*-acting TKC, as has been shown previously<sup>30,64</sup>) prevented meaningful measurement of transconjugants in batch cultures, whether by fluorescence plate reading, flow cytometry, or microscopy. As with culture, transconjugant colonies were found to be dimmer for blue

fluorescence than their directly-transformed counterparts, even after several days' growth (Fig 1d). In mixed colony assay images, blue-fluorescent transconjugants were mostly indiscernible from autofluorescence from donors and recipients (Fig 2h), presumably due to brightness from the reporter as well as small transconjugant areas in most colonies. It's yet unclear why transconjugants should show lower fluorescence than direct transformants.

# (Return to top)

# 3.2.2 TKC in colonies follows feeding trends, with greater variability

We repeated batch culture initial conditions on 2% agar minimal media plates, except with 10-fold fewer initial cells. We pipetted  $\geq$  18 2 $\mu$ L mixed-cell droplets onto plates and allowed them to grow continuously for six days. We then imaged three colonies for 2D spatial distribution each day via wide-field fluorescence microscopy, and another three that were then scraped, washed, and diluted for composition and TKC measurements (Fig 2a,b).

As with batch cultures, there was an inverse correlation between donor-recipient ratios and TKC in most cases, though with greater noise (Fig 2c). However, TKC-per-recipient rates remained relatively constant, unlike cultures (Fig 2d). These differences from culture conditions might be due to "jackpot" populations, in which a genetic island of transconjugants finds a spatial niche among the stochastic colony front<sup>106</sup>, resulting in a wider range of TKC counts for each condition. Because conjugation has been shown to occur along population boundaries<sup>104</sup>, we determined relative population mixing by calculating colocalization<sup>107</sup> of bacterial and yeast fluorescence signals. While colocalization did positively correlate with overall TKC values, most mixed colonies had very low colocalization, suggesting once more that competition dominates population dynamics between these species (Fig 2e,f).

Metrics were also calculated radially, and show that, for most cases, bacterial growth is localized to the outer ring of the colony, where the greatest abundance of nutrients can be found<sup>77</sup>, while most of the yeast intensity is found within these bacterial boundaries (Fig 2g). This trend is subverted somewhat by crossY-pairings in low amino acid concentrations, for which bacteria are better able to grow within the colony center due to lowered competition from the yeast. Because yeast signals mostly drop off near the edge of the colony, where bacterial signals rise, the greatest colocalization between the channels can be found near the edge, too, though the exact radius of this spike depends on the conditions, with more divergence at lower amino acids, and the highest amino acid concentrations all showing similar colocalization at  $r \sim 3$  mm.

From this, we might infer that TKC occurs primarily near the border of colonies, especially for more segregated populations. Indeed, in one case this was observed explicitly, with a subpopulation of transconjugants detectable fluorescently via the BFP channel (Fig 2h). This subpopulation seems to grow from the bacterial-dense outer ring and extend beyond it, and the colony's TKC counts correspond to a "jackpot" TKC event (TKC ≥ 500 CFU)<sup>106</sup>. In general, the *trans*-TKC plasmid carrying yeBFP ("TKC reporter") proved unusable in most experiments due to its low signal, high autofluorescence, and infrequent TKC events (see Results section 1). In colonies, the blue signal was indistinguishable from a mixture of bacterial and yeast autofluorescence, with the former appearing stronger; thus, in general, the blue signal was brightest wherever the red signal was brightest. In this case, however, it's clear that the bright blue subpopulation along the outer edge doesn't align with the red signal, and thus is a true transconjugant population. More work on this reporter scheme might unlock the possibility of better tracking TKC events spatially and allow much better tracking of TKC distribution.

These experiments utilized 2% agar media plates to grow mixed colonies, for which bacteria are rendered non-motile. To gauge the effect of motility on colony separation, we also ran mixed colonies on semisoft 0.2% agar plates, on which bacteria are motile<sup>108</sup>. These mixed colonies were grown for eight days, and, like the 2% agar experiments, measured for flow cytometry and TKC, but unlike the 2% agar experiments, were not fluorescently imaged. Rather, they were imaged at low resolution in ambient lighting to gauge gross colony structure, since the mCherry fluorophore carried by bacteria is visible under ambient lighting. 0.2% agar (motile) colonies showed apparently greater separation of population versus the corresponding 2% agar colonies (Fig 2i), especially along the z-axis relative to the media, with bacteria preferentially growing furthest from the plate. This was true, too, for commensal *E. coli*, despite their dependence on yeast leucine secretion, suggesting a complex interplay between competitive forces and dependent forces (Fig 2i), upper left, green box). Corresponding to this apparent separation, motile mixed colonies yielded fewer overall transconjugants, and more colonies gave zero TKC CFU compared to their 2% agar counterparts.

# (Return to top)

# 3.2.3 Developing an agar pad protocol to elucidate colony genesis at single-cell resolution

To better understand the cell-to-cell interactions that result in the dynamics seen in mixed colonies, I developed an agar pad assay that could be used to image cells with single-cell resolution via fluorescence microscopy. This modified protocol utilized the ease of agar pad construction relative to, say, microfluidic chambers, which are better suited to experiments requiring nutrient flux <sup>109</sup>. Unlike other protocols, with limited sample throughput and imaging time before pads dry out or lose imaging focus <sup>109–111</sup>, this protocol provided 24 experimental conditions per experiment with

minimal media depletion. These factors were especially important for comparing to colony assays, as most experiments utilized at least 16 conditions—4 cell pairings, 4 monocultures, and  $\geq$  2 amino acid concentrations—and both species grow slowly on mixed minimal media, especially yeast at low amino acid concentrations. This was accomplished by first pipetting 3 mL 2% agar media into each well of a 24-well "mold" plate (CELLTREAT clear plastic, Dot Scientific # 229123) and allowing agar media to dry for ~15-30 minutes. Cells were prepared as for colony experiments (see Methods) but diluted to 1E6 cells/mL for each cell type, and 5 uL was used for each pad, for 5E6 cells (of each species) total. Samples were pipetted into each well of a separate 24-well imaging plate (CellVis #P24-1.5H-N glass-bottom optical plates) and agar pad molds were transferred to the imaging plate via flat micro spatula such that each well of imaging plate contained samples sandwiched between agar media and glass well bottoms (Fig 3a). Plates were then sealed with a gas-permeable membrane (Fisher Scientific cat #50-550-304) to prevent drying of agar by evaporation. The imaging plate was allowed to grow at 30°C for ~3 hours prior to imaging, so that the sample liquid could dry out and/or get absorbed to avoid cell migration during imaging. For imaging, a custom Nikon "JOBS" script was written to allow manual identification of three points per well such that at least one bacterium and one yeast were proximal in the frame. The plate was then imaged for all points for > 15 hours, at 30 minute intervals, using a Nikon Eclipse TI inverted microscope at 40x objective, while maintaining 30°C via an Okolab cage incubator.

While these experiments weren't used in any of the spatial assays presented here, this method did yield time courses that could resolve the genesis of spatial distribution between populations (Fig 3b), which, with further image processing, could help to develop spatial models that connect cell-

that are difficult to resolve at the colony scale, such as the death of bacteria-surrounded yeast (Fig 3c) and, with further development of TKC-reporters, the spatiotemporal dynamics of conjugation. Still, many options exist to improve on this assay, and spatially-resolved dynamics generally, such as hydrogels with lower optical noise, and confocal microscopy to resolve z-axis growth<sup>112</sup>. Moreover, this assay would benefit from starting with denser cell inputs and imaging at the edge of the spiked cells, corresponding to the colony front, where dynamics are most prominent.

# (Return to top)

#### 3.3 Discussion

With mixed colonies, I hypothesized that engineering population interactions would result in differences in population boundaries, which could be used to control TKC, since conjugation occurs exclusively at population boundaries<sup>104</sup>. More specifically, I reasoned that cross-feeding would lead to more population intermixing, as seen in single-species colonies for both *E. coli*<sup>99</sup> and *S. cerevisiae*<sup>77</sup>. But unlike those studies, for which the only separating "force" was genetic drift, these mixed colonies have complex forces at play both in separating and intermixing the populations. And as seen in culture, spatial distributions of populations show the predominant impact of competition between these species, as they primarily separate. Different, too, are the dynamics at the colony front, where cells with higher growth rate preferentially establish an ecological foothold: in cases where bacterial growth rates are high enough, they appear as a constraining halo, surrounding all other cells in the colony. Thus, a simplified model of population distribution (if any such models could be called "simple") will not suffice here, but that does not preclude investigating whether overall population intermixing leads to higher TKC. And in this regard the work was successful, as even in this competition driven regime, TKC does seem to

positively correlate to population intermixing. Contrary to my hypothesis however, this mixing is not very tunable, as the range of spatial outcomes is small, and mostly seen only at 0% amino acids. Moreover, the cell pairings that caused greater colocalization—my quantitative proxy for mixing—weren't cross-feeding pairs, but rather the commensal pair, followed by the WT pair (see 3.5.2.E). My interpretation of increased commensal colocalization is that the bacteria, which have a superior capacity to establish a spatial niche, will grow near a nutrient source such as secreting yeast, but starved yeast don't share the same capacity when paired with faster-growing bacteria, and so auxotrophic yeast pairings have the lowest colocalization. This conclusion needs further verification and would be well served by a predictive model that recapitulates these spatial distributions based solely on those factors I expect to be most important.

Multiple important features of the mixed colonies remain opaque as well. While I only measured fluorescence in two dimensions, I found that colonies had significant features along the z-axis, usually with bacteria dominating the highest (from the media) position and yeast preferentially growing along the media surface; the analogy I conjured often was of a layer cake (this can be seen somewhat in 3.5.2.1). And while the thickness of each species along the z-axis should pertain to its measured fluorescent brightness, those quantities are flattened in colocalization analysis. For example, if *E. coli* is uniformly layered atop *S. cerevisiae*, as seems to be the case for crossB\_wtY, the pixel intensities for each channel would imply that the populations are relatively well mixed, when it's more likely that a single uniform boundary exists between two otherwise isolated populations. That's not to say that colocalization is not worth measuring—indeed, the pairing cited here seems to have the highest TKC—but rather that it's one indirect method for gauging

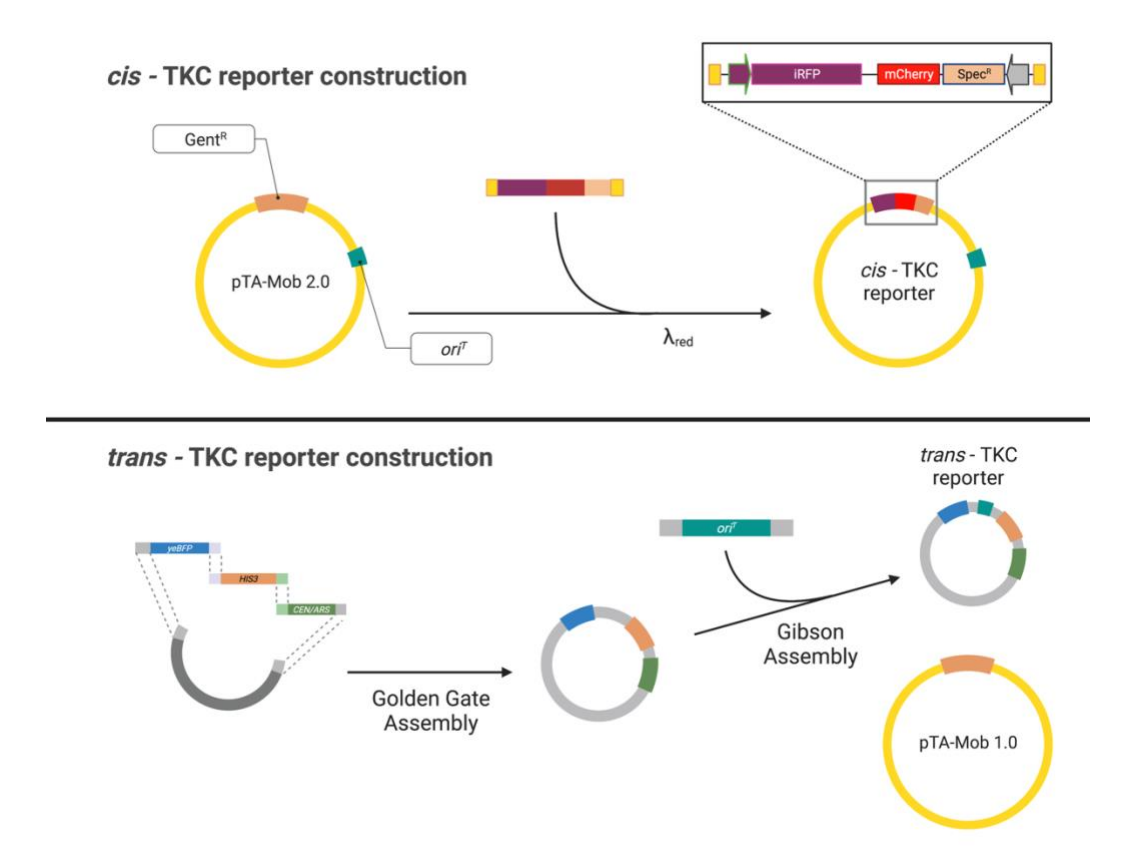
distribution from 2D measurements, and that a true measure of mixing would require resolving the third dimension, e.g. via confocal microscopy.

These mixed colony experiments were also limited by the lack of a reliable TKC-reporter, to resolve the spatial distribution of transconjugants, and whether they align with regions showing more or less colocalization. While the trans-TKC reporter I constructed with yeBFP did fluoresce, its dimness and the infrequency of TKC events, paired with autofluoresce common in the blue range<sup>113</sup>, resulted in blue-channel images that mostly resembled combined autoflorescence from each strain, especially E. coli. Short of spatial TKC resolution, colony-wide measurements of TKC were useful for relating to other colony-wide measurements such as species composition and colocalization, and I was able to deduce that the large variability of TKC outcomes between replicates (a much higher range than in culture) was likely due to jackpot events, wherein rare events occur early enough for a subpopulation—usually considered for mutations, but here considered for TKC—to establish an ecological foothold<sup>106</sup>. But it would be valuable to know exactly where and when such jackpots occur: are they mostly interior "bubbles" or do they correspond with segments formed by gene surfing (see Fig 3 in ref <sup>106</sup>)? Do they correspond spatially with high colocalization or a specific cell ratio? For example, for both higher-colocalizing pairings—the commensal pair and the WT pair (green and purple, respectively, in 3.5.2.E)—while there's greater TKC relative to the lower-colocalizing pairs, the correlation between these two seems reversed: the commensal pair has higher colocalization and lower TKC relative to the WT pair. It could be that the dependent crossB E. coli are better able to constrain expansion of yeast and thus prevent gene-surfing like TKC jackpots, while WT bacteria "allow" them; the singular likely case of TKC imaging seems to show such a segment in the WT pair (3.5.2.H). This is the type of hypothetical that's nearly impossible to answer without spatial resolution of all three populations: donors, recipients, and transconjugants.

#### (Return to top)

#### 3.4 Figures

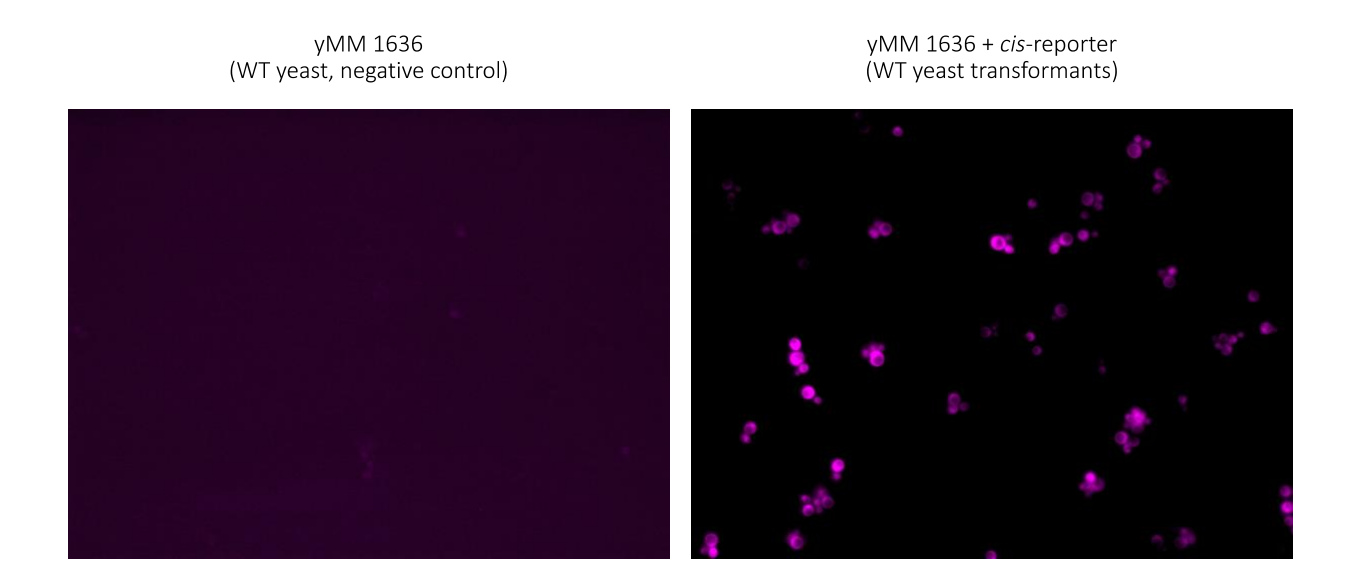
### 3.4.1 Figure 1: Creation of TKC reporters.



#### A. Design of TKC reporters.

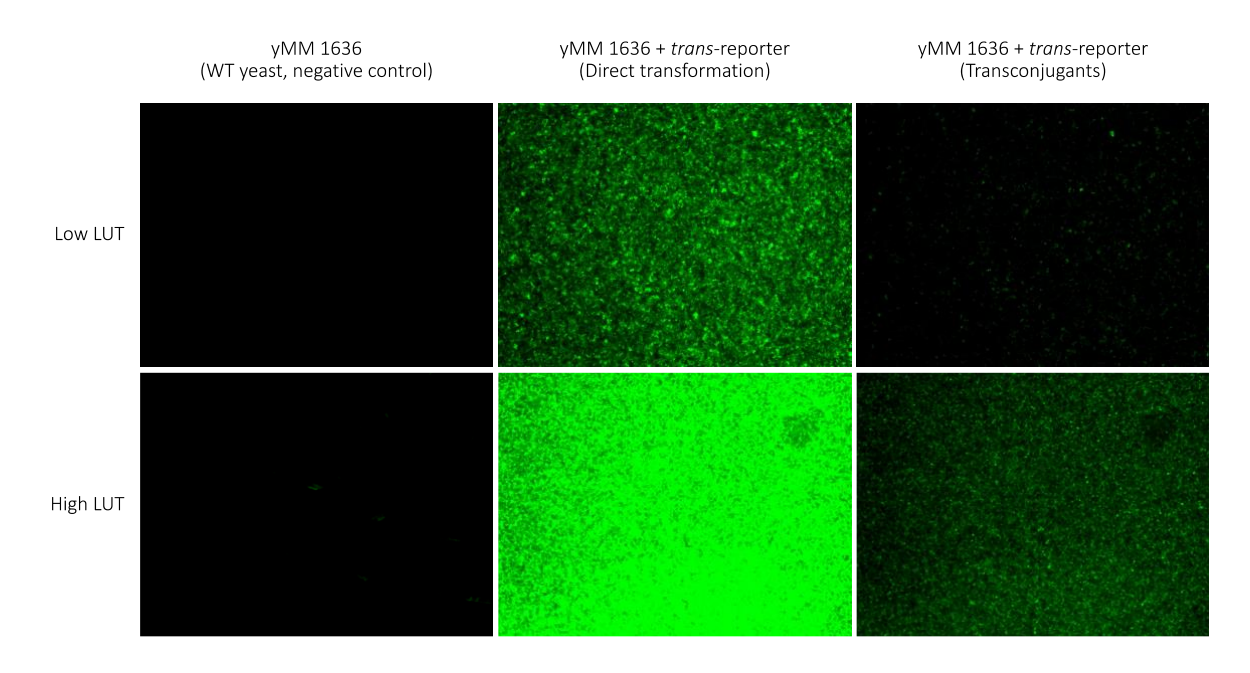
For *cis*-TKC reporters (top), a cassette of *pTDH3-iRFP*, mCherry and spectinomycin resistance was created via overlap PCR of yeast and bacterial components, with homology arms to pTA-Mob 2.0. Reporter cassette was inserted into pTA-Mob 2.0 via  $\lambda_{red}$  recombination so as to replace existing gentamicin resistance gene. For *trans*-TKC reporters (bottom), yeast components were

assembled via Golden-Gate based Yeast Toolkit components, after generating a part plasmid for yeBFP, and  $ori^T$  was subsequently added via Gibson assembly.



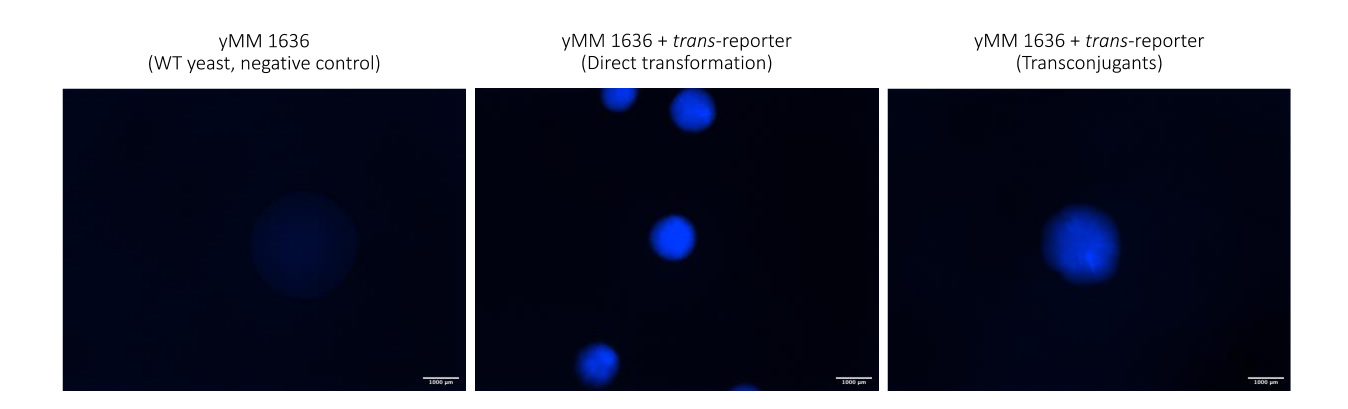
# B. Demonstration of iRFP fluorescence in cis-TKC reporter.

40x microscopy of WT yeast either with no plasmid (left) or directly transformed with *cis*-TKC reporter (right). *cis*-reporter shows bright iRFP fluorescence.



#### C. Demonstration of yeBFP fluorescence in trans-TKC reporter in culture.

10x microscopy of yeast with no yeBFP (left column), directly-transformed *trans*-reporter (center), or TKC-acquired *trans*-reporter (right), at two image brightnesses (rows) in liquid media. Yeast cells that obtain *trans*-reporter via TKC show dimmer yeBFP fluorescence than their directly-transformed counterparts.



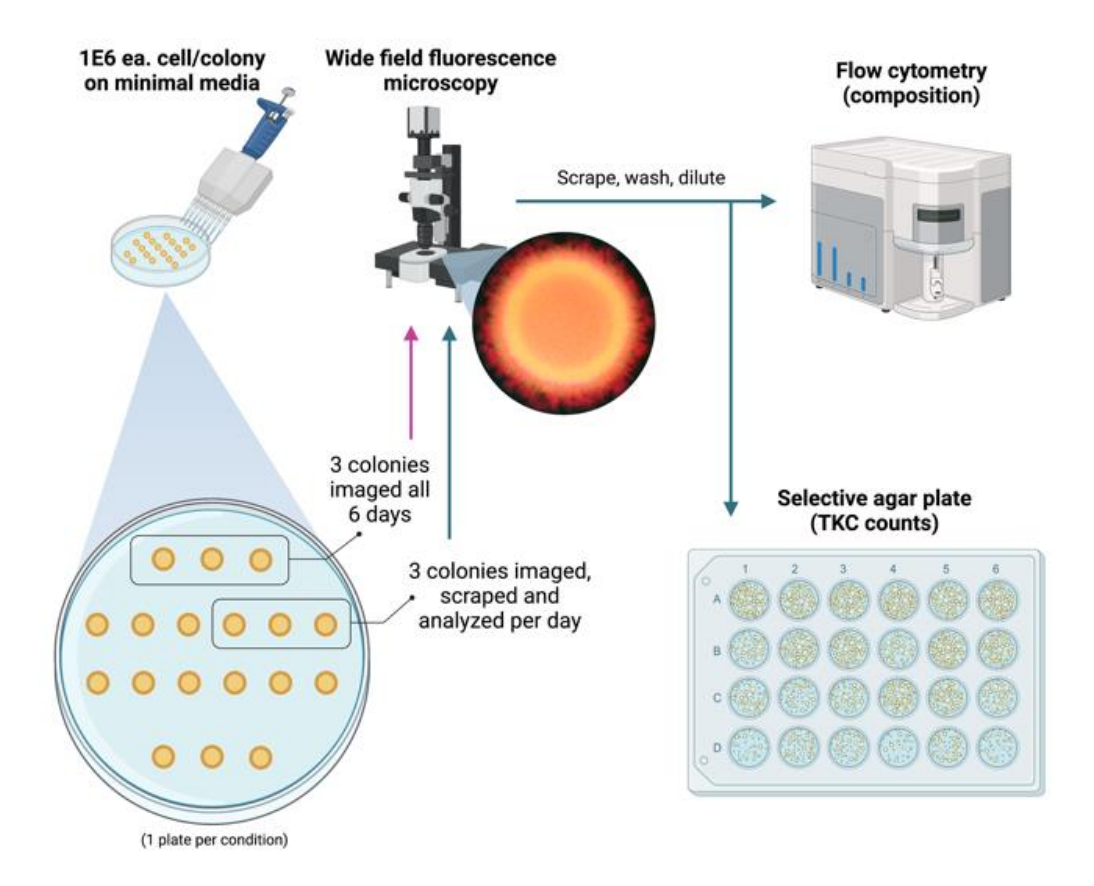
### E. Demonstration of yeBFP fluorescence in trans-TKC reporter in colonies.

8x zoom dissecting microscopy images of WT yeast with no yeBFP (left column), directly-transformed *trans*-reporter (center), or TKC-acquired *trans*-reporter (right), after 4 days of growth

on 2% agar media. Yeast cells that obtain *trans*-reporter via TKC show dimmer yeBFP fluorescence than their directly-transformed counterparts. Scale bars = 1 mm.

(Return to results)

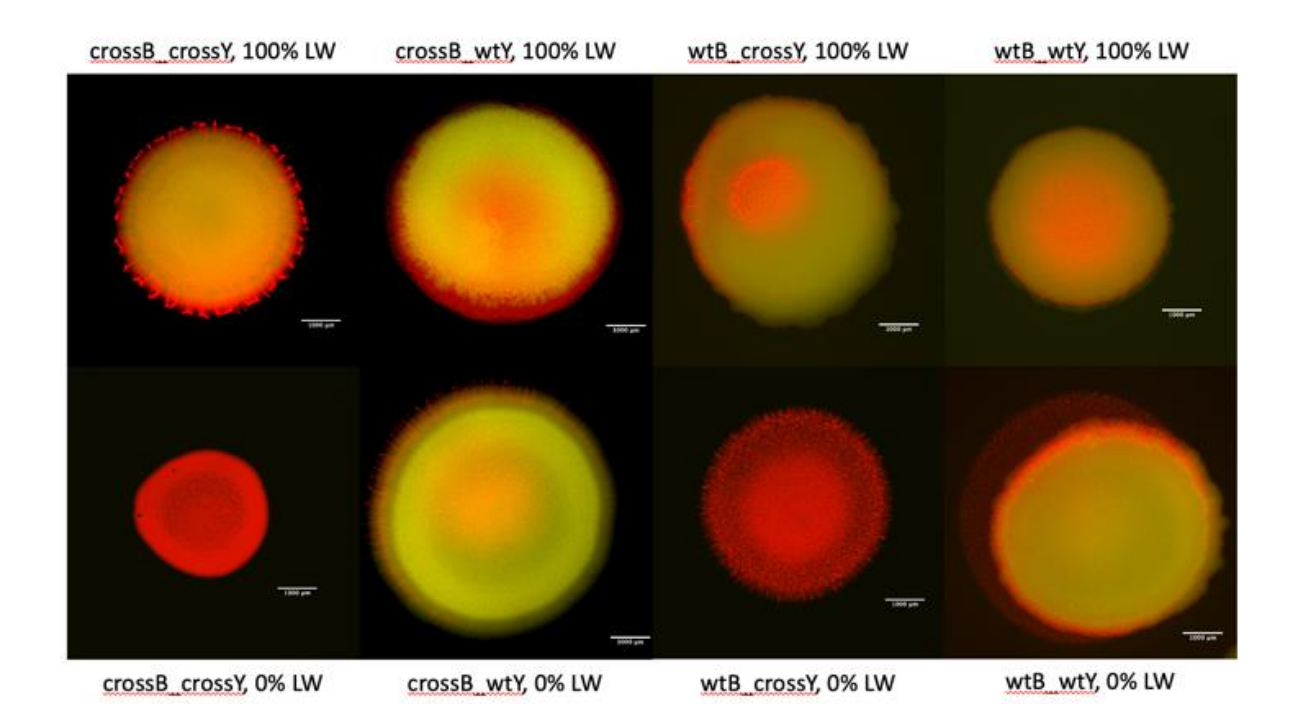
### 3.4.2 Figure 2: Mixed colonies follow culture dynamics, show increased TKC with spatial mixing.



# A. Experimental setup of colony assay.

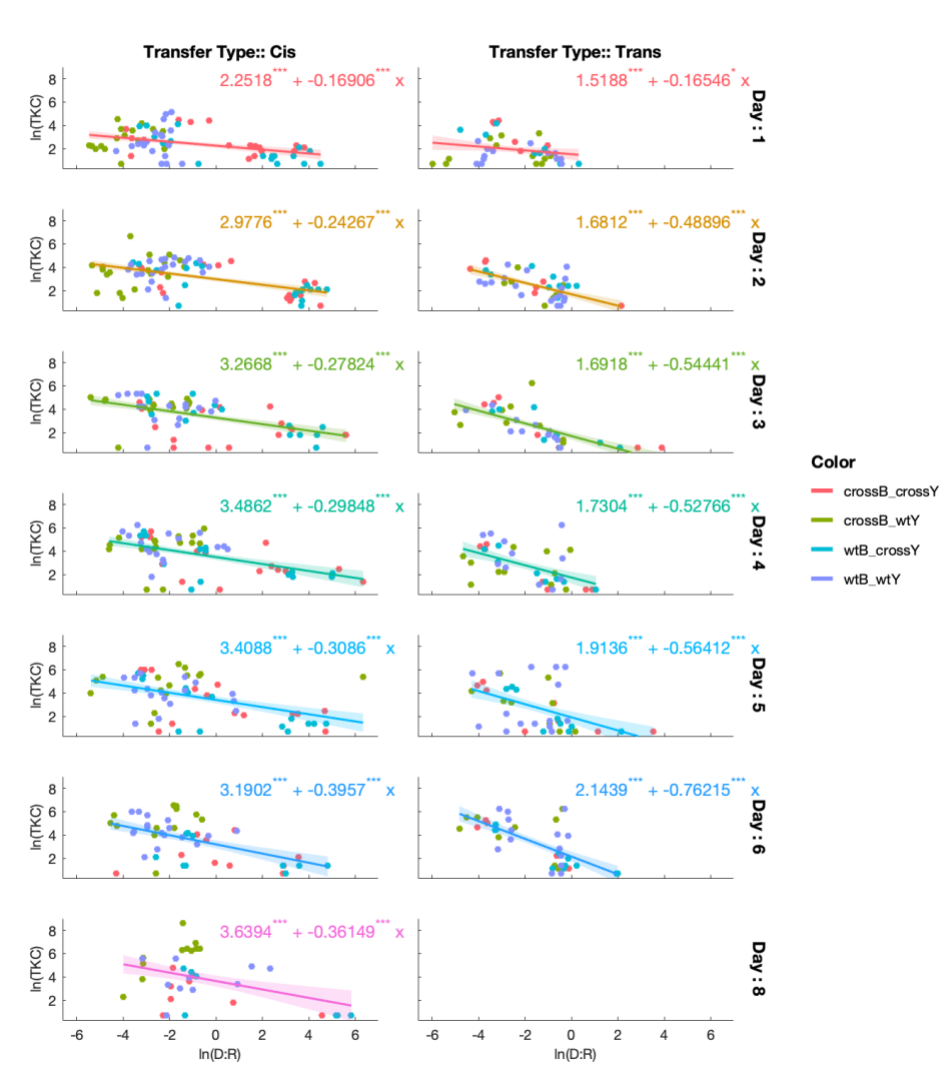
Cells are combined and pipetted in 2uL droplets onto minimal media with 2% agar. Each plate contains  $\geq 18$  colony replicates of one cell pairing, and one amino acid concentration. After each days' growth, 6 colonies are imaged with a wide-field fluorescence microscope. 3 of these

continue to be imaged daily, while the other 3 are scraped, washed, diluted for flow cytometry and TKC plating.



# B. Example of mixed colony cell distribution.

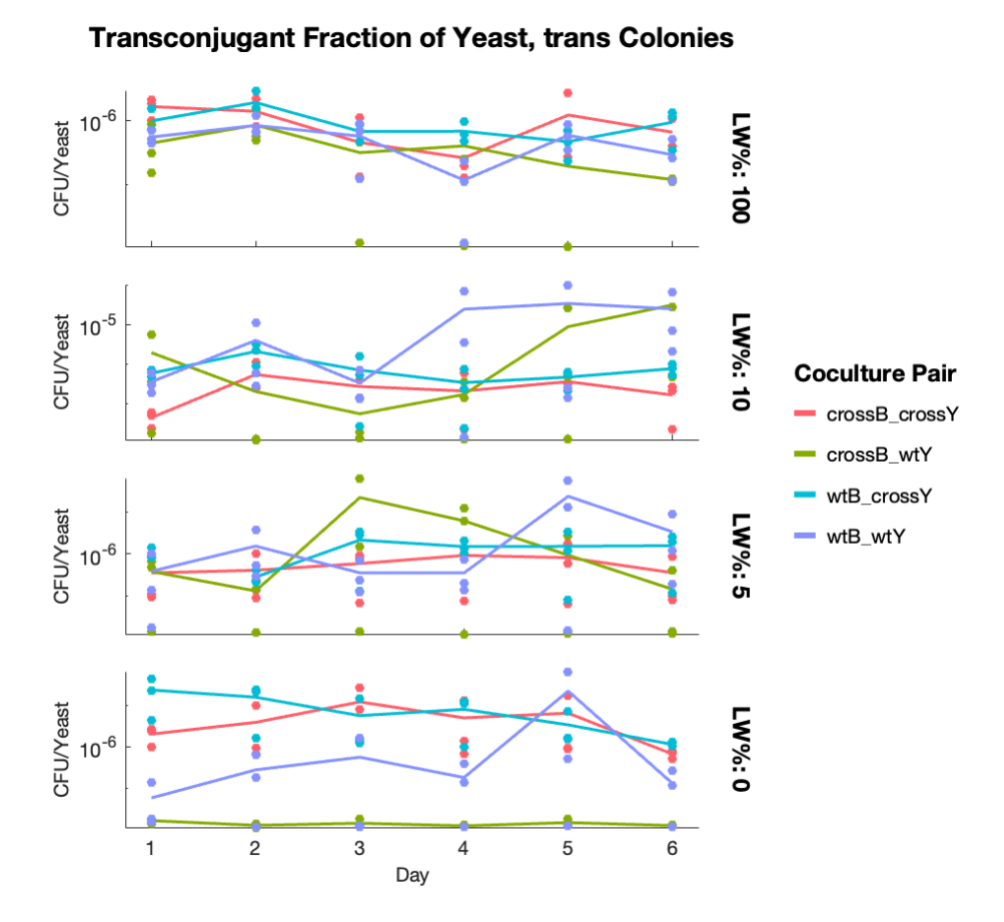
Fluorescence microscopy images for each cell pairing at 100% LW (top row) and 0% LW (bottom row). All pairings here include *cis*-donors. Yeast are displayed in yellow channel, bacteria in red. Channels are scaled for brightness to emphasize distribution, scale bar = 1000um.



#### TKC by D:R, Colony Assays

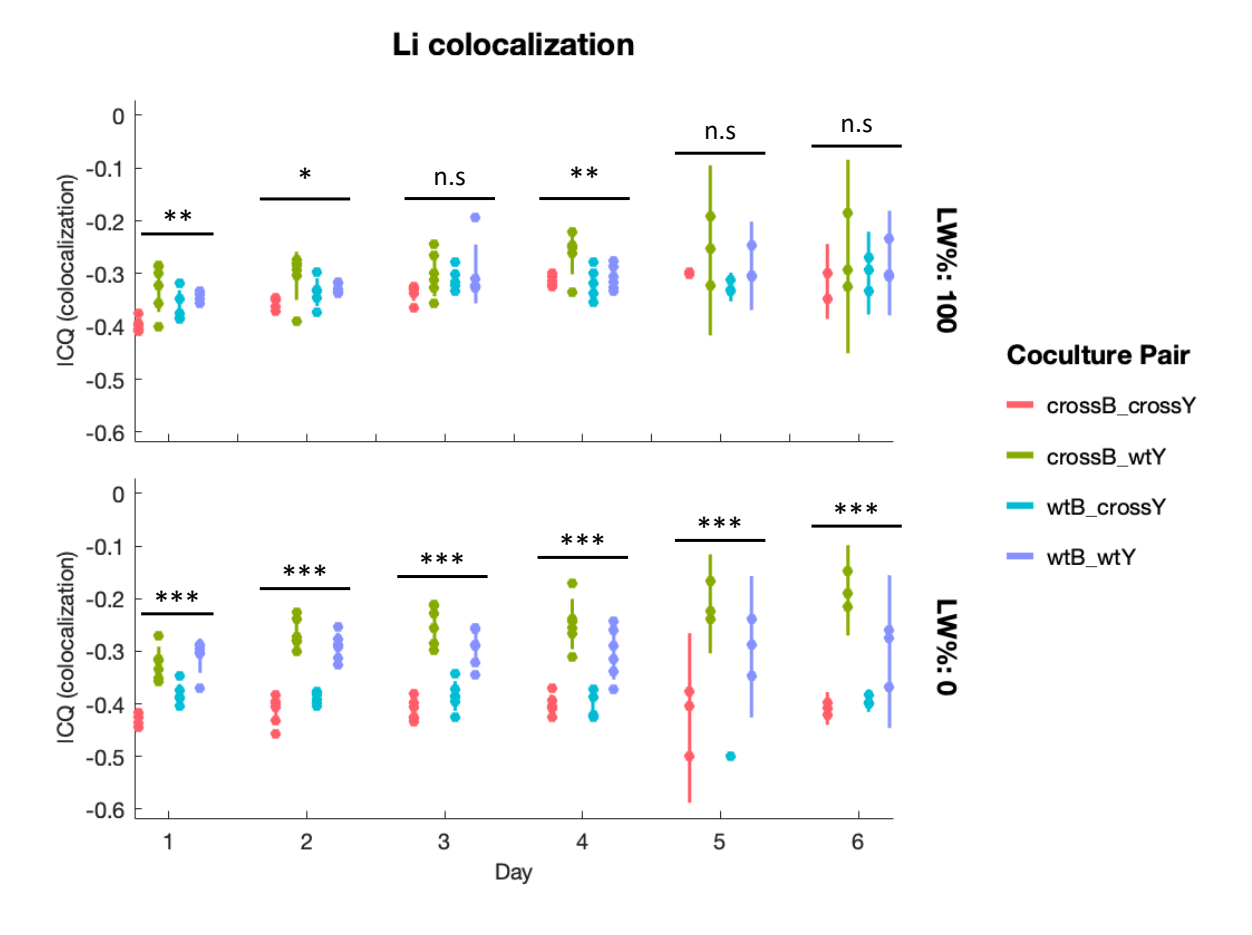
### C. Mixed colonies share relationship between D:R and TKC with co-cultures.

Log-log plots of TKC counts and donor-to-recipient ratios (D:R), for *cis*-donor (left column) and *trans*-donor (right column) mixed colonies, over 8 days (rows). Data points colored by cell combination (feeding type), linear fit lines colored by day. TKC measured by plating CFU, ratios by normalized flow cytometry counts.



### D. Transconjugant fraction of yeast population doesn't grow in mixed colonies.

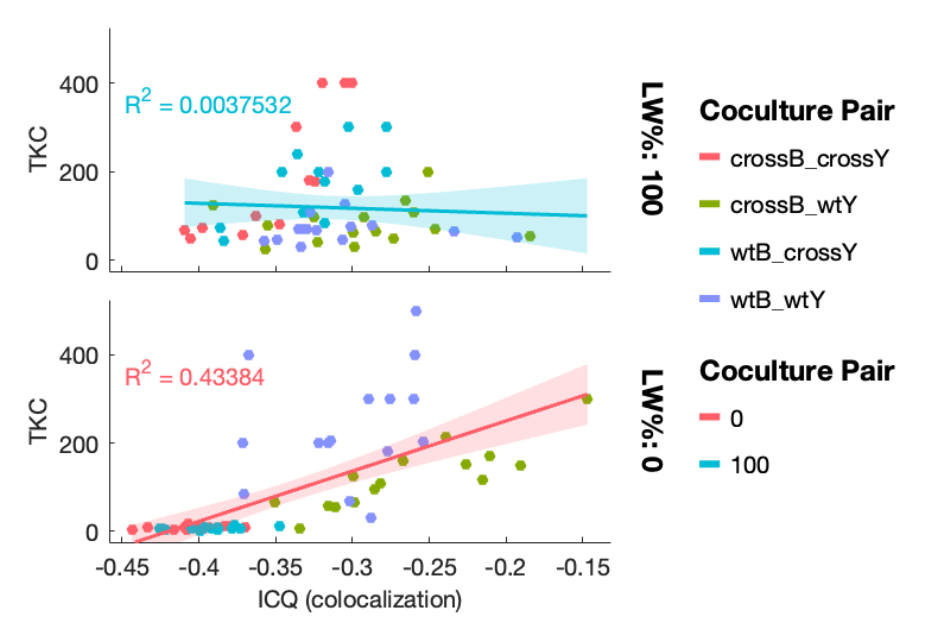
Colony fractions, on the other hand, are mostly constant, which could either result from a spatial population-stabilizing effect (i.e. there are few new interactions over time that could result in additional TKC events) or because each colony is measured separately—e.g. day 4's results don't relate to day 5, etc.—and counts are highly variable due to jackpot events.



E. Colocalization shows divergent intermixing at 0% amino acids, though competitive exclusion drives spatial distribution.

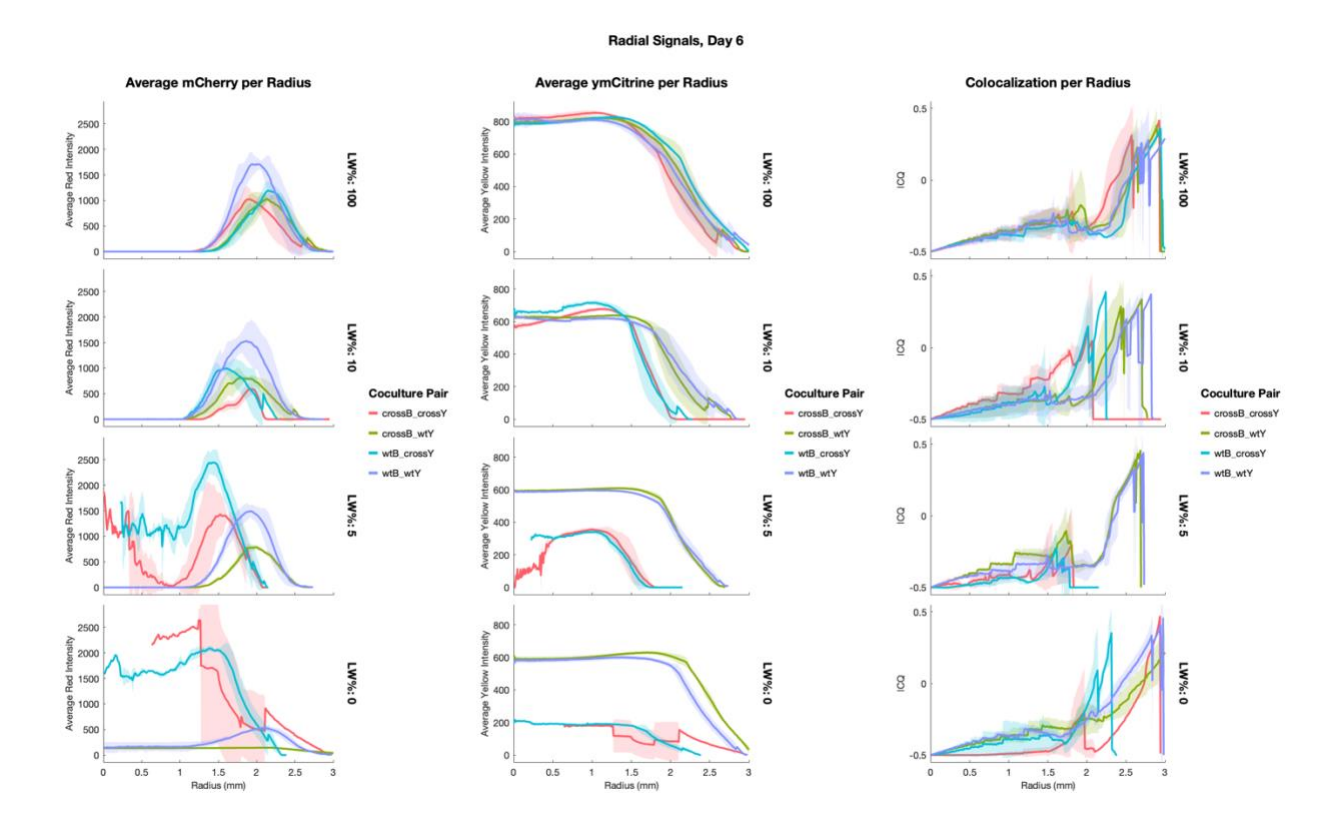
Li colocalization analyses of colonies (ICQ = 0.5 is complete colocalization between channels, ICQ = -0.5 is complete spatial segregation) show range of outcomes for 0% LW colonies, less so for 100% LW colonies. All ICQ values range from -0.1 – -0.5, implying competitive spatial segregation. Distributions shown are of *cis*-donor pairings. Calculated ICQ values for each replicate and condition represented by dots, 95% CI of the mean by vertical bars. Stars denote *p*-values from ANOVA 1-way test of 95% confidence between all 4 pairings using sum of squares test.





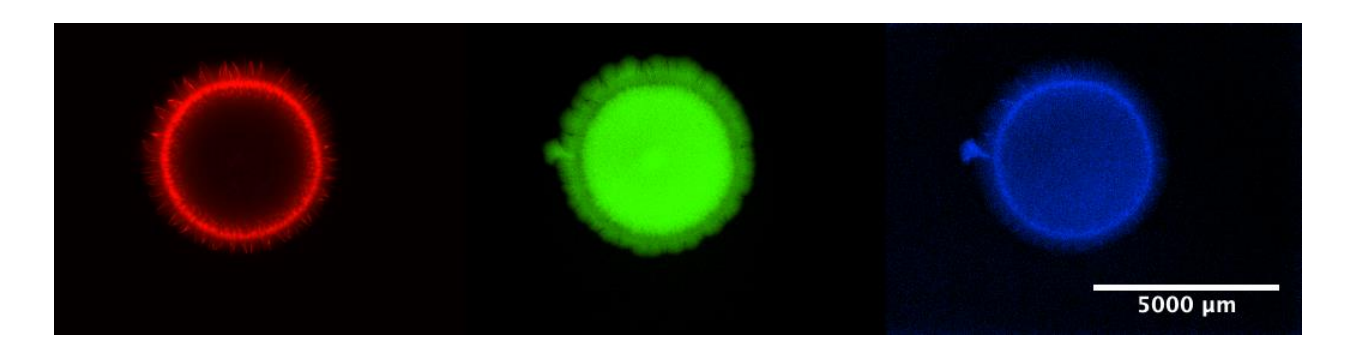
### F. Colocalization correlates positively with TKC values.

ICQ values plotted against raw TKC (CFU) counts for *cis*-donor pairings, at 0% and 100% LW, for TKC≥2. For the smaller range of ICQ values at 100% LW, TKC counts slow little divergence, whereas at 0% LW, TKC correlates positively with ICQ.



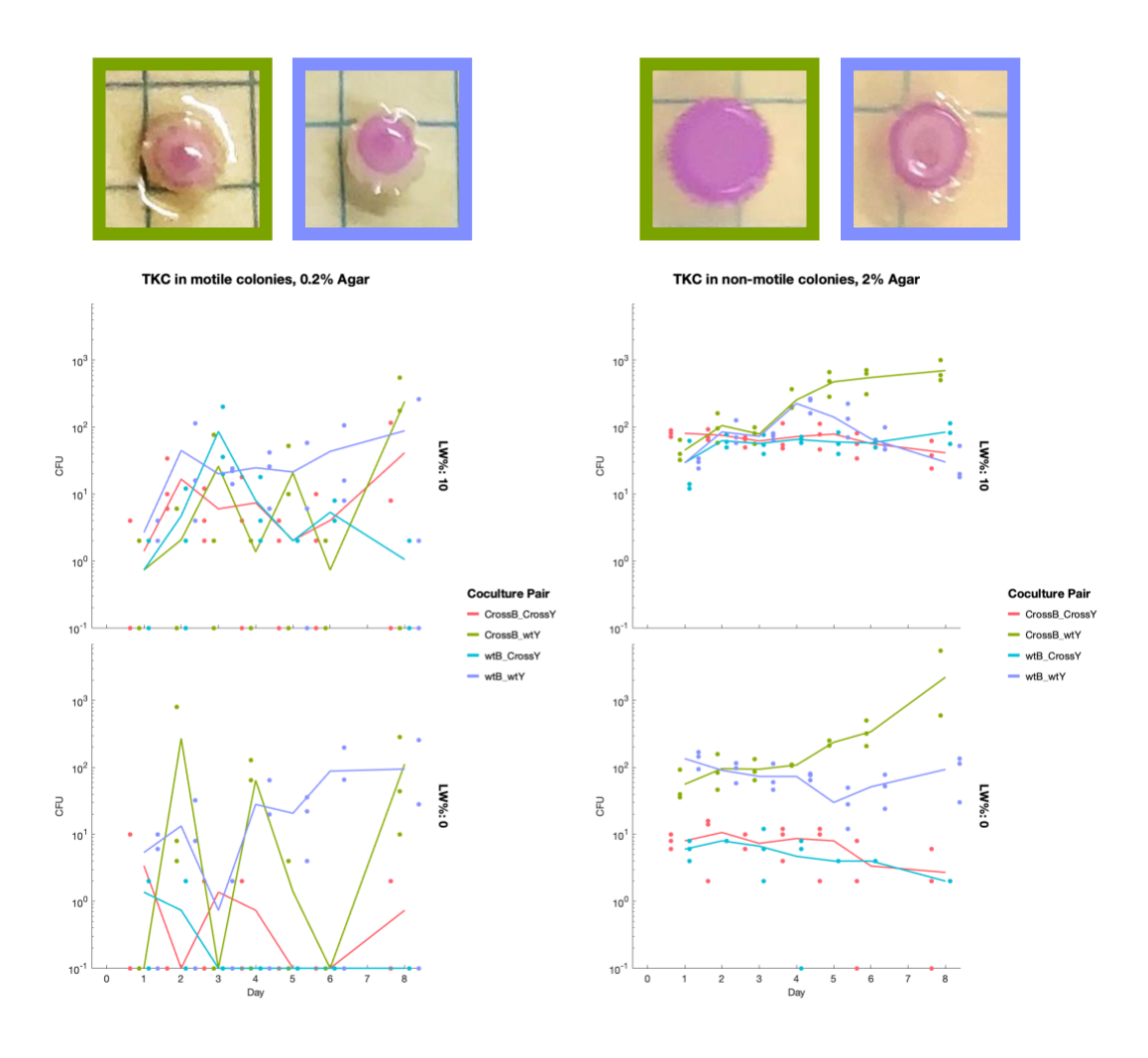
### G. Radial fluorescence measurements of mixed colonies.

Radial measurements of bacteria in mixed colonies (via mCherry, left column), yeast (via ymCitrine, middle column), and colocalization between the two cell signals (right column), for each pairing (color) and LW% (rows) after 6 days' growth. Lines are means of all pixels measured at a given radial shell, shading is standard deviation. Colocalization is measured by intensity correlation quotient (ICQ, see SI discussion) for each radius.



H. Jackpot transconjugant population along expansion front in mixed colony.

Fluorescence images of wtB\_wtY mixed colony at 10% LW, after six days' growth. Bacterial (mCherry, left), yeast (ymCitrine, middle), and TKC (yeBFP, right. See SI discussion on colony analysis for TKC-reporter details) channels are shown. Note that while yeBFP signal is largely convoluted by autofluorescence from bacteria (especially) and yeast, a protrusion on the left side of the colony shows some of the brightest yeBFP and doesn't correspond to bacterial signal. This colony showed "jackpot" TKC counts, > 500 CFU. Scale bar = 5 mm.



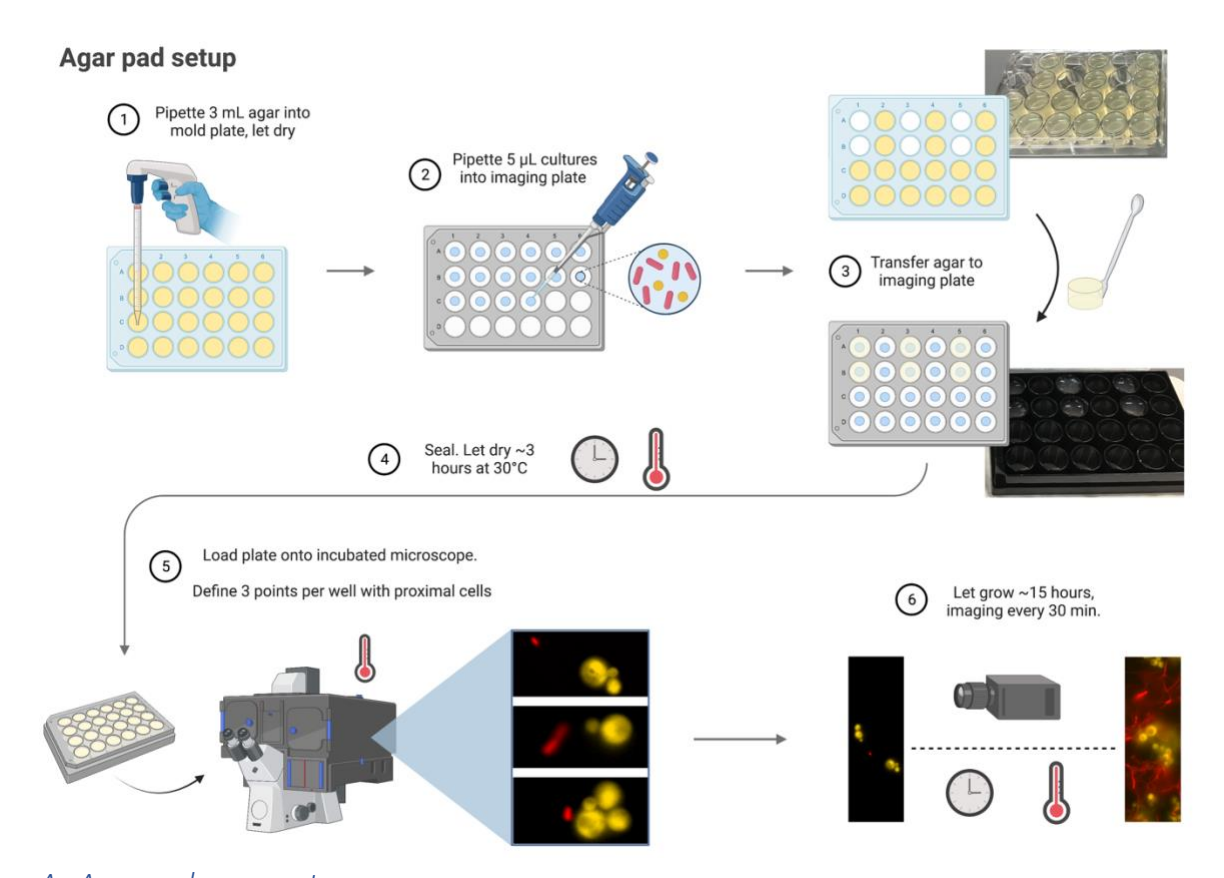
### I. Motile donors in mixed colonies show greater population separation, lower TKC.

Images of mixed colonies after 8 days' growth on 0.2% agar (top left), on which bacteria are motile, versus the same cell pairings on 2% agar (top right), on which bacteria are non-motile. Motility-enabled pairings of crossB\_wtY (green box) and wtB\_wtY (purple box) ostensibly show greater population segregation along the z-axis, with mCherry-carrying bacteria (visible as red in ambient lighting) preferentially growing along the top of the colonies (furthest from media). Yeast (white/uncolored in ambient lighting) preferentially grow along media surface, lower on z-axis. Grids in images are 1 cm<sup>2</sup>. Brightness and contrast adjusted to highlight morphology. TKC counts for 0.2% agar colonies (bottom left) and 2% agar colonies (bottom right) for two LW% (rows)

shown for 8 days, demonstrating lower TKC for 0.2% colonies, with more cases of zero TKC events.

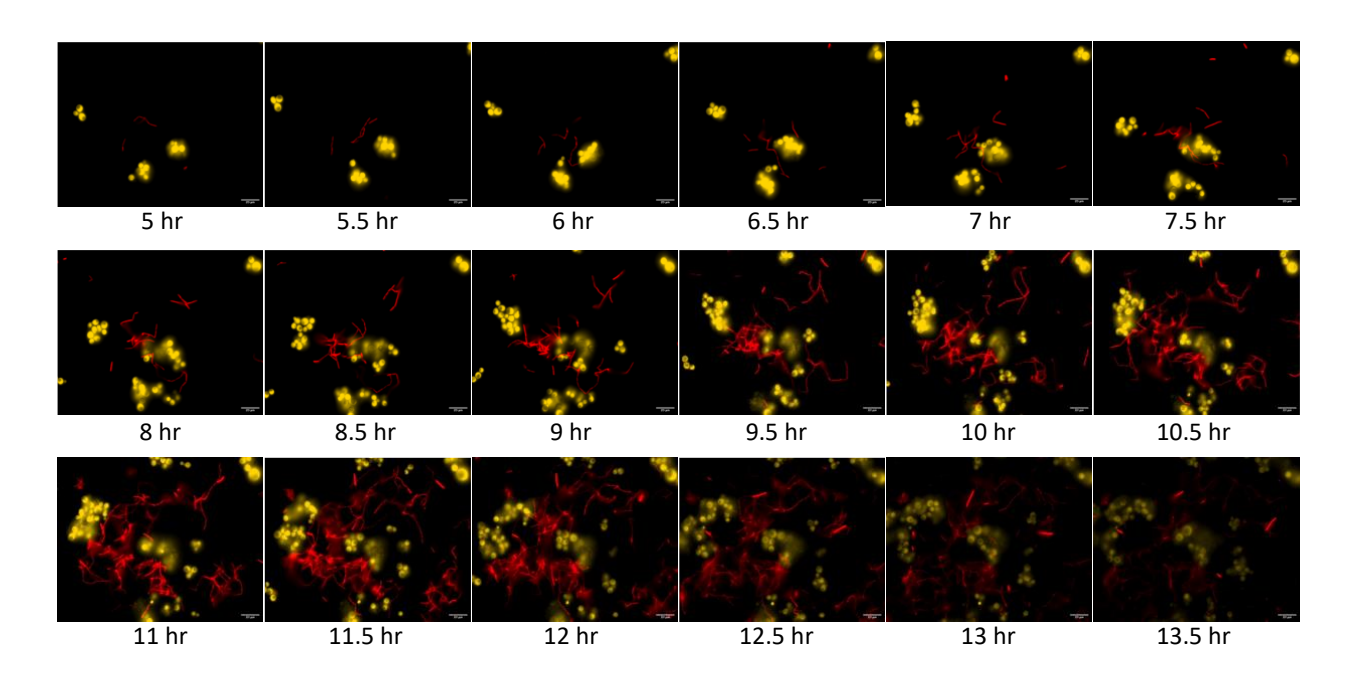
(Return to results)

#### 3.4.3 Figure 3: Agar pad imaging of proto-colonies



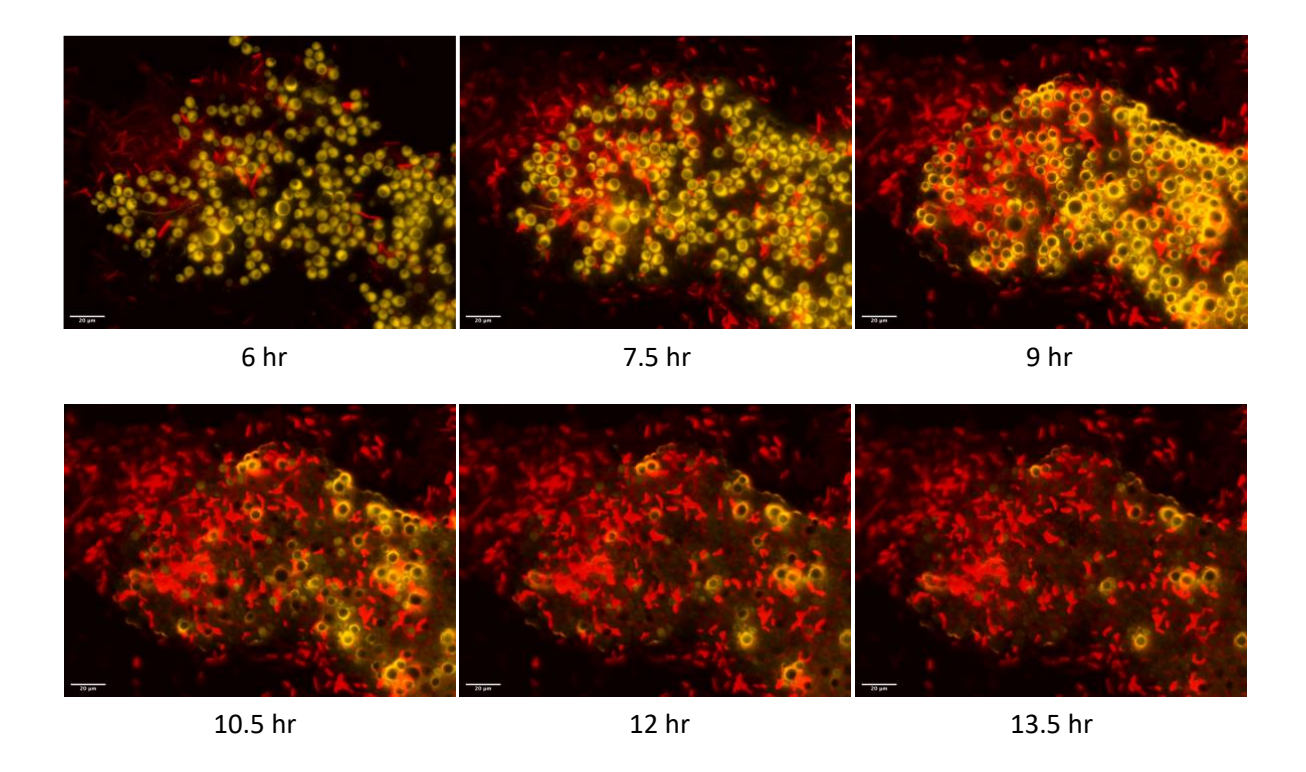
#### A. Agar pad assay setup.

3 mL 2% agar media is pipetted into a 24-well "mold" plate and allowed to dry. 5 uL cell mixtures are pipetted onto the surfaces of 24-well imaging plate glass, and molded agar is transferred on top of samples. Imaging plate is sealed with gas permeable membrane and incubated at 30°C for ~3 hr to let samples dry, after which it's imaged every 30 min for ~15 hr via fluorescence microscopy while maintaining 30°C.



B. Example time course demonstrates creation of population geography at single-cell resolution.

40x images of bacteria (red) and yeast (yellow) in a crossB\_crossY pairing at 100% LW. Times shown are based on when plate imaging began, and were selected and scaled for brightness to highlight spatial population changes. Scale bar =  $20 \mu m$ .



C. Agar pad images show yeast death via bacterial saturation.

40x images of bacteria (red) and yeast (yellow) in a crossB\_wtY pairing at 100% LW. Upon being fully surrounded by bacteria, fluorescence from yeast cells "turns off", apparently due to cell death. Time points selected to highlight population change. Scale bar =  $20 \mu m$ .

#### (Return to results)

#### 3.5 Materials and Methods

#### 3.5.1 Colony culturing and preparation

Each strain was grown, measured, washed, and diluted as in batch culture experiments. Because we wanted 2  $\mu$ L mixed culture droplets to seed each colony, we had to lower the input cell counts to 1E6 of each cell type. Strains were combined accordingly, then aliquoted into striptubes, from which we were able to multichannel-pipette  $\geq$  18 identical 2  $\mu$ L mixed colonies onto 2% agar minimal media plates, or 0.2% agar semi-solid plates, for motility testing. Each 60 mm plate

(Eppendorf cat #0030701011) contained 75:25 SC:M9 with appropriate bacterial antibiotics for plasmid maintenance, 2% or 0.2% agar, and one concentration of amino acids, such that each plate represented a single experimental condition; molten media was aliquoted to plates in equal (15 mL) portions. Once mixed colonies were added to plates, they were allowed to grow at 30°C for 6 days. For fluorescence-imaging assays, three representative colonies (by eye) were designated after the first day's growth to be repeatedly imaged over the entire time course, while another three were designated to be imaged that day only, after which they would be scraped, washed, and measured by flow cytometry and TKC-plating. All colonies were numbered, upon being selected, to correlate measurements.

After imaging, colonies were manually scraped off plates via micropipette tips and diluted into 1.5 mL tubes containing 1 mL water. Each diluted colony was vortexed for ~30 s to break up colonies and dilute residual agar, then spun at 3000xG for 5 min. 800 μL of water was removed from each tube, cells were resuspended in the remaining ~200 μL, 100 μL of which was plated for TKC-selection (see Batch Culture methods) and another 20 μL was aliquoted into 180 μL PBS+0.1% Tween for flow cytometry (see Flow Cytometry methods). After six days' growth, the colonies (1-3) designated for continual microscopy imaging were processed and measured in this way. (Return to top)

#### 3.5.2 Colony imaging and analysis

Plates were imaged for fluorescence using a Zeiss AxioZoom V16 dissecting microscope, at the Newcomb Imaging Center, Department of Botany, University of Wisconsin-Madison. Each *cis*-donor mixed colony was imaged for mCherry (Zeiss Set 43 BP 545/25, FT 570, BP 605/70, 200

ms exposure) and ymCitrine (Zeiss Set 46 HE, EX BP 500/20, BS FT 515, EM BP 535/30, 600 ms exposure), while *trans*-donor mixed colonies were additionally measured for yeBFP (Zeiss set 49: G365, FT395, BP445/50, 500 ms exposure). All images were taken at 8x zoom.

Output .czi files, each of which included all fluorescence images, were converted to .tif files via a custom ImageJ macro, with no brightness correction. A custom MATLAB scripts were written to import file information, read .tif files, background-correct images, identify colony circles, scan intensities of each channel, calculate radial metrics, and measure Li colocalization.

For red (bacteria) and yellow (yeast) channels, images were binarized via Otsu's method <sup>114</sup>. The blue channel corresponding to TKC-reporter yeBFP was imported using adaptive sensitivity of 0.5. "Filled" versions of bacterial and yeast channels—for which colony interiors were uniformly filled in—were used to automatically determine circular colony dimensions. Filled, binarized channels were added together and region properties were calculated for the combined binary image, as well as binarized bacterial and yeast samples, using MATLAB's regionprops function. If none of the three "images" was determined to have an event with length greater than 300 px and less than 1500 px, they were filtered out and defined as not having grown. Otherwise, whichever of the three showed the largest diameter was chosen for circle definition, based on its centroid and major axis length. All circle definitions were visually screened, and any images requiring circle modification—either due to inaccurate circles or lack of circles—were manually drawn and saved.

Images were background corrected by setting all pixels beyond the boundary of the circle definition to "nan". Background corrected images were then used to generate colony-wide metrics,

e.g., averages for each channel across the colony. Li colocalization 107 intensity correlation quotient (ICQ) was calculated colony-wide by the formula

$$ICQ = \frac{\sum_{N>0} (B_i - \bar{B})(Y_i - \bar{Y})}{\sum_{N} (B_i - \bar{B})(Y_i - \bar{Y})} - 0.5$$

Where  $X_i$  pertains to individual pixel intensities (B = bacteria, Y = yeast), from which we subtract the mean intensity for that channel. For each pixel, a product of each channel's difference is calculated, and the sum of these products is taken. ICQ calculates the proportion of these products that are positive (N>0), based on the idea that, for random distributions of intensities in each channel, the sum of products of differences should near zero, and thus how positive the sum is corresponds to how colocalized the two channels are. If both channels deviate from the mean similarly in space, more products of differences will be positive, and ICQ will be higher. Conversely, if the channels are highly segregated—e.g., if the bacterial signal is well above its average at the same location that the yeast signal is well below its average—more products will be negative, and the ICQ will be lower. The subtraction of 0.5 is an arbitrary way to get the metric to straddle 0 (corresponding to "random" distributions), with negative values corresponding to mostly segregated channels (-0.5 = perfectly segregated), and positive values mostly colocalized (0.5 = perfectly colocalized). In our case, all colonies presented as mostly segregated—ranging from -0.5 to -0.2—which agrees with both subjective assessment of the images and dynamics experiments that demonstrate strong competition between the species, which should result in spatial exclusion.

Metrics were also calculated radially, by defining a circumference along the colony circle's outer edge and taking intensity profiles for each unique radius from the circle center to pixels along the circumference. This yielded a matrix of pixel values in terms of radius r angle  $\theta$ , but rings closer to the center were overrepresented due to being measured as many times as there were circumference pixels. Thus, "nan" values were introduced in proportion to that r's fraction of the total radius R. Then metrics were calculated along each radial ring, including mean intensities and radial ICQ.

### 3.5.3 Table 1: Strains used in this study

ID	Species	Genetic features	Fluorescence	Source	Figures
yMM1585	Yeast	Leu <sup>++</sup> , Trp <sup>-</sup> , Ura <sup>-</sup>	ymCitrine, yCerulean	<sup>77</sup> , this	2-3
				work	
yMM1636	Yeast	His-	ymCitrine	<sup>77</sup> , this	2-3
				work	
yMM1720	Yeast	Leu <sup>++</sup> , Trp <sup>-</sup> , His <sup>-</sup>	ymCitrine, yCerulean	<sup>77</sup> , this	2
				work	
kMM0011	Bacterium	None	None	90	All
kMM0127	Bacterium	Trp <sup>++</sup> , Leu <sup>-</sup>	None	<sup>90</sup> , this	All
				work	

### 3.5.4 Table 2: Plasmids used in this study

ID	Species	Function / Features	Fluorescence	Source	Figures
pMM0819	Bacterium	pProD-mCherry	mCherry	Addgene 87144	2-3
pMM0820	Bacterium	$\lambda_{\rm red}$ genes	None	91	None
pMM0821	Bacterium	Flippase	None	91	None
pMM0892	Bacterium	T4SS genes, Gent <sup>R</sup>	None	pTA-Mob 1.0 <sup>30</sup>	2-3
pMM1018	Both	T4SS genes, Gent <sup>R</sup> , URA3, HIS3, CEN/ARS, <i>ori</i> <sup>T</sup> , iRFP	None	This work	1
pMM1066	Both	T4SS genes, Gent <sup>R</sup> , URA3, HIS3, CEN/ARS, <i>ori</i> <sup>T</sup> , iRFP	None	This work	1
pMM1353	Both	T4SS genes, Gent <sup>R</sup> , URA3, HIS3, CEN/ARS, <i>ori</i> <sup>T</sup>	None	pTA-Mob 2.0, Addgene 149662	2-3
pMM1437	Both	yeBFP, ori <sup>T</sup> , HIS3, CEN/ARS	BFP	<sup>95</sup> , this work	1-2

### (Return to top)

# Chapter 4: Altering recipient outcomes by tuning populations

#### 4.1 Introduction

Much of the work on TKC has focused on maximizing DNA transfer frequency in the pursuit of isolating single transconjugants a la yeast transformation protocols<sup>38,38,69,86</sup>, or else have exemplified novel HGT techniques without focusing on stable modification of recipient population fitness<sup>36,49</sup>. This could be because modifying a population's fitness is nontrivial, since microbes exhibit a range of strategies to adapt to any environmental stressors that would disturb its stability, and likewise, multispecies communities at steady state tend to resist any change to one member<sup>115</sup>. This latter point is especially relevant for any would-be probiotic treatment via TKC, as microbiomes have shown resistance to novel probiotic strain introduction, often requiring long-term or repeated exposure to the probiotici<sup>116</sup>, a community feature that usually works to prevent invasion from pathogens<sup>117</sup>. Still, engineered probiotics offer some of the best opportunities for specificity among *in situ* perturbation strategies<sup>25</sup>, so increasing the magnitude of their effect on recipient populations is worthwhile.

Population perturbation by HGT could be considered in two main ways, depending largely on the nature of the recipient cell modification encoded by the transferred DNA. If TKC-mediated modifications result in minor changes to the fitness of either species, we might consider any such effect as shifts along a stable fixed point for that consortium, i.e., minor shifts in steady-state community composition, deviating slightly from the homeostasis of that particular (synthetic) ecosystem. In this framing, significant changes in community composition would likely only occur if the consortium is already near a critical tipping point—sometimes called an unstable fixed point, such as in population collapse—due to the resilience of the established consortium<sup>118,119</sup>. But if the

genetic material introduced by TKC drastically altered the fitness of recipient cells, it might be better to consider the community disturbance as the introduction of a new species entirely, in which case the stable and unstable fixed points of the new consortium that includes transconjugants would be entirely different from that of the original ecosystem, as one additional community member independently competes for its niche among limited resources; in short, it would act as an invader 115. Indeed, both the would-be probiotic (donor) and the transconjugant strain could be considered invaders to any system into which the probiotic is introduced. To test the ability of TKC to alter recipient populations, I start with ostensibly basic population changes: improve recipient cell fitness, or cause recipient cell death. In both cases, I test near critical tipping points, i.e. near unstable fixed points for the original two-species consortium of donors and recipients.

#### (Return to top)

#### 4.2 Results

#### 4.2.1 Harnessing population dynamics to rescue a recipient population through TKC

To test whether population-control of TKC can be used to alter a recipient, we next sought to "rescue" starved yeast cells exhibiting poor or non-existent growth, via genes carried on the transferred DNA. We first tested this with the *cis*-TKC plasmid pTA-Mob 2.0, which carries *HIS3* and *URA3* and allows transconjugants to grow in media deficient for uracil and histidine. TKC from WT donors mostly failed to rescue U or H-auxotrophic yeast recipients growing in low concentrations of uracil and histidine (% UH), as the bacteria competed the yeasts to collapse before sufficient transconjugant growth could establish (Fig 1a).

Our previous results showed higher TKC for lower donor-to-recipient ratios, so to increase the likelihood of rescue, we used auxotrophic bacterial donors at 0% leucine. These donors can thus only survive if the paired yeasts metabolically support them. Remarkably, we found a drastic increase in TKC-rescue from crossB donors, for both crossY and wtY recipients, though this effect varied by uracil and histidine amounts (Fig 1b,c). crossB rescued both recipient strains with greater speed and efficiency than wtB did in all cases, though at 0% UH, paired cross-feeder populations collapsed (Fig 1a,c). The relationship between D:R ratio and TKC recapitulated population dynamics from previous experiments (see 2.4.1.G and 3.4.2.C), though with much higher TKC counts due to fitness changes for transconjugants in this experiment (Fig 1d). At intermediate concentrations of uracil and histidine—especially 5% UH—rescue showed high stochasticity, as some biological replicates were fully rescued while others collapsed (Fig 1e). We also used our clumping model to predict the range of possible rescue outcomes for each cell pairing over a range of amino acid concentrations. With minimal alterations to account for experimental differences, the model recapitulated our experimental results: for most concentrations of U and H, and with [L] kept low, bacterial competition is minimized, and greater TKC is possible, allowing for the increased rescue of yeast seen in these experiments (Fig 1f,g, see Methods discussion for model changes).

#### (Return to top)

### 4.2.2 TKC-mediated CRISPR killing can be interrupted by mannose addition

We next tested whether we could collapse or depress a recipient yeast population via TKC-mediated killing. We designed a conjugatable CRISPR/Cas9 system that can be transferred from bacteria to yeast, where it targets a blue fluorescent, *URA3*-carrying plasmid in recipients, such

that destruction of this plasmid would render recipient cells unable to grow in uracil deficient media. Unlike most Cas9 systems, which utilize a repair sequence to replace the cut DNA, we relied on repeated cutting of the target DNA with no repair, since our goal was simply to suppress the target cells' growth. Targeting an episomal sequence was also essential, to discern both TKC rates and cutting efficiency separately, without the lethality of cutting genomic DNA in recipient yeast (Fig 2a). After verifying that the TKC-Cas9 plasmid is efficient for cutting its target via both direct yeast transformation and TKC (Fig 2b), we batch cultured cross-feeding yeast (W auxotrophs) containing the *BFP-URA3* plasmid at low levels of tryptophan and 0% uracil, along with donor cells that either contained a functional TKC-Cas9 system, or one lacking an *ori*<sup>T</sup> sequence and thus unable to transfer DNA. At 1% W, all yeast cultures died out, while at higher levels of W (5% and 10%), competition resulted in depressed yeast levels relative to monoculture yeast growth (Fig 2c, d). Donors carrying TKC-Cas9 ("cutters") significantly depressed yeast growth beyond competition-mediated decreases, and at 5% W, yeast populations were wholly collapsed when co-cultured with the TKC-Cas9 donor (Fig 2e).

To gauge whether any effects of TKC could be reversed by interrupting cell clumps, we switched batch cultures to mannose-supplemented media after six days of growth and allowed them to grow for another six days (Fig 2f). In both co-culture pairings, subsequent yeast growth stopped declining after the media switch and persisted at steady-state levels from day six, ending trends of decline in both co-culture pairings, though never recovering recipients completely to previous (higher) levels (Fig 2d, e). From this data, we were thus able to discern the extent to which recipient populations are depressed by competition from co-culture with bacteria, versus TKC-mediated cutting, since the positive and negative donors are equivalent for fitness and ability to adhere and

form pili to recipients. TKC counts showed reversibility with mannose addition, with TKC dropping after day 6 (Fig 2f). Since transconjugants are terminal in 0% U, it should be noted that TKC counts are effectively transient "snapshots" of yeasts carrying TKC-Cas9 that have not yet been diluted out of batch-culture or died from starvation. Moreover, because the cut DNA is carried episomally in recipients, we were able to grow co-cultures in non-selective media to discern loss of *URA3* plasmid due to TKC-cutting (versus basal plasmid loss in monoculture yeasts, Fig 2g). Interestingly, TKC-cutting donors did apparently cause greater plasmid loss in 100% U media compared to negative donor pairings or yeast monocultures, even for conditions in which the corresponding 0% U recipient populations didn't collapse. This suggests either that the two conditions (100% vs. 0% U) aren't readily comparable, or that longer growth without mannose could have collapsed those populations, especially given that the trajectory of plasmid loss in 100% U reverses upon mannose addition.

#### (Return to top)

#### 4.3 Discussion

It's hard to know which facets of a complex system will matter for a tangible application until you actually try to apply it. With the goal of finding ways to perturb recipient populations *in situ*, and the awareness that TKC is limited by its contact dependence, I first sought to test basic functions for transferred DNA: either delivering an essential gene to salvage recipient growth ("rescue") or delivering DNA capable of killing the recipient (via TKC-Cas9). Naively, the rescue assay would seem quite simple, as TKC plasmids already carry essential yeast genes for the sake of selecting transconjugants, thus, I only needed to change the selective pressure on the recipients by limiting those nutrients encoded by the TKC plasmid. The transconjugants that would act as community

invaders to the two-strain consortium—as discussed in the Introduction to this chapter—would thus have drastically higher fitness than their non-conjugated counterparts, theoretically allowing them to fill the ecological niche left by poor-growing yeasts. But because the population dynamics between the species are complex and highly competition-driven, initial tests for rescue using only WT donors (with or without conjugative function) showed no rescue, as the low frequency of TKC was dwarfed by the competitive detriment from bacteria in co-culture. No "invader" transconjugant species could establish an ecological niche because the bacteria readily filled them. But increased TKC from lower-growing (commensal) donors provided a fruitful alternative, as starved donors proved exceptionally efficient in maximizing TKC events while minimizing competitive exclusion, so long as sufficient yeast were able to grow to sustain the donors.

Applying my deterministic (clumped) model to rescue conditions also demonstrated how this dynamic can result from time-independent changes to cell fitness, or as I call it above, "consortial fitness". E.g., the better-rescuing auxotrophic donors don't require time-sensitive clumping dynamics—in fact, fits of clumping rates were *lower* for crossB vs. wtB, see 4.5.3—or some other starvation phenotype; lowered donor consortial fitness was sufficient to recapitulate this phenomenon. Stochasticity seen in rescue capacity between replicates (especially at 5% UH) in such a deterministic system would thus appear to represent a critical transition in a conceptual phase space of the original two-species consortium, or to be more specific, an unstable fixed point<sup>118</sup>, above which both populations are resilient enough to allow rescue, and below which insufficient yeast growth causes collapse of both species. The model also implies that several additional conditions exist beyond what I've tested for here, so long as bacteria aren't so fit as to competitively exclude yeast including newly formed transconjugants. Moreover, it's worth noting

once again that there are likely other sets of parameters that could represent this system (see above), but it's my view that any set that sufficiently recapitulates the population dynamics will similarly show a conjugative benefit to lower-growing donors in rescue conditions.

While the rescue assay required little adaptation of batch culture experiments, TKC-mediated killing required a bit more engineering. Part of the complexity lie in my dual purposes: to depress recipient populations and to build a scaffold for future TKC-mediated applications. Thus, I sought to transfer a readily-programmable Cas9 system, versus a gene or toxin specific to S. cerevisiae. Most CRISPR-Cas9 systems, however, utilize a repair sequence to replace the cut DNA, and given TKC operates via plasmid DNA, incorporating a repair sequence is nontrivial. Some research has gotten around this inconvenience by including integrating genetic elements in their conjugative material<sup>32,36</sup>, but I found this unnecessarily complex for recipient killing, moreover, I wanted to control for Cas9-cutting efficiency without use of an inducer<sup>49</sup>. Thus, I strategized a scheme whereby the cut target resides on plasmid DNA in the recipient, so that cutting activity can be selected for, even with constitutive Cas9 nuclease activity (it's always "on" when in recipient cells) and no repair sequence provided; any similar scheme with genomic cut sites would likely kill any transconjugants regardless of selection, by disrupting the genome. To the best of my knowledge, such a CRISPR scheme hasn't been employed in yeast. I designed sgRNA to target a connector sequence in the Yeast Toolkit for modular assembly of yeast plasmids, designed by Lee, et. al. 95, a design feature that should allow for ready adaptation to other cut targets, so long as the same connector sequence is included in plasmid assembly. In these experiments, the cut target encoded the essential gene *URA3* and the fluorophore yeBFP. Thus, I was able to select for transconjugants separately from measuring cutting efficiency, while simultaneously tracking changes in blue

fluorescence relative to the total yeast population. And in this regard, I was able to successfully determine that all sgRNAs designed had 100% cutting efficiency within the detection limit, which was admittedly small due to low transconjugants in *trans*. It's also worth noting this strategy is limited to plasmid curing, and any introduced function not achievable by such cutting would require some integrating element, which could be plasmid-based or genomic.

Knowing that only a small percentage of yeast cells are converted to transconjugants in culture, especially with a trans-delivery system, I ran batch cultures with auxotrophic yeast at a range of low tryptophan concentrations, to test the lower limits of yeast growth for their susceptibility to TKC-mediated collapse. And even knowing the rates of TKC and cutting efficiency, it wasn't obvious that TKC-mediated cutting would have any effect on a population scale, as I naively assumed any loss of yeast cells due to killing would simply allow uncut yeasts to fill the ecological niche left by their cut counterparts. That's to say, it seemed TKC-cutting would have to outpace the recipient population's ability to recover and re-fill the ecological niche lost to cut cells. Thus, I was somewhat surprised to find a rather clear case of TKC-driven recipient collapse at 5% W. In this case, donor cells seem to have competitively filled the ecological niche left by deceased transconjugants, which comports decently well to the fits for resource niche overlap (c close to values of 1 in the models, see 2.4.5) and the fact that bacteria are able to grow and fill that niche more quickly than yeast. And while the fold-decrease in yeast cells was significantly different between TKC-Cas9 donors and negative control donors for most conditions (see 4.4.2.F), I only found recipient collapse at 5% W, suggesting that the population perturbations are still minor, with TKC events nudging the consortium away from its stable fixed point by "removing" yeast cells in small numbers, and only resulting in regime change when the stable fixed point is nearest the

unstable fixed point, i.e. when the population resilience is lowest (Fig 2i). It'd also be very interesting to test the effect of starved donors on this dynamic, as I would simultaneously expect higher TKC-mediated killing—due to increased TKC such as in the rescue assay—and a lower bacterial capacity to competitively fill ecological niches left open by cut recipients.

Because I had control over cut-selection, I was also able to duplicate my "killing" assay in non-selective media (100% U nonselective vs. 0% U selective) and measure the relative plasmid loss due to cutting. Interestingly, the growth of co-cultures in 100% U were uniformly worse for both species, a phenomenon that I still can't explain, though it doesn't seem to have affected the overall differences between non-conjugating donors, TKC-Cas9 donors, and yeast monocultures, in terms of plasmid loss. For the conditions in which yeast persisted—here, only 10% and 15% W—plasmid loss was fairly consistent between yeast monocultures and non-conjugating co-cultures, whereas TKC-Cas9 co-cultures showed markedly greater loss in these conditions.

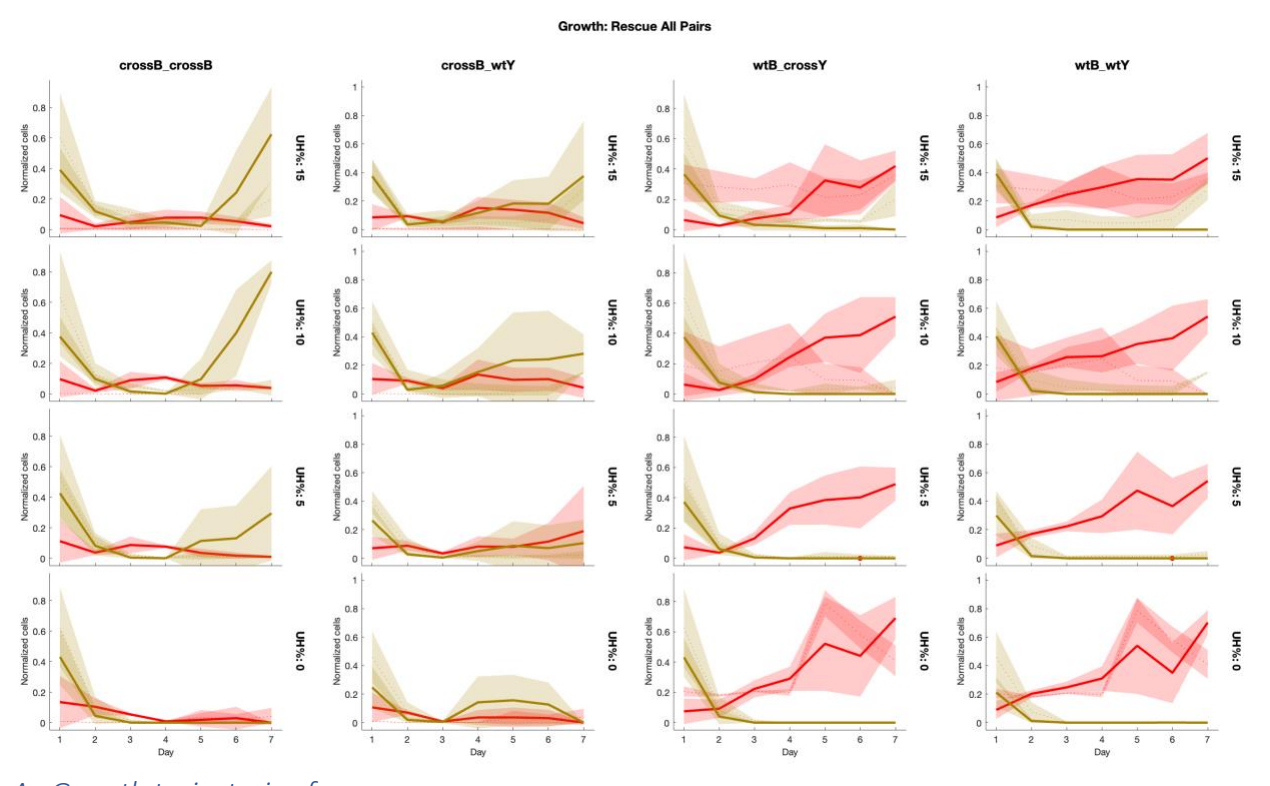
Finally, this experiment included several additional days of batch culture growth, after adding mannose to the media. While this was not an exhaustive test—it neither controlled for prolonged growth without mannose nor graded mannose concentrations—the reversal of trajectories across several measures is striking. Declining yeast populations in cut-selective media leveled off, TKC counts declined from their peaks, plasmid loss in non-cut-selective media reversed, and cells visibly showed less clumping via microscopy. This is very exciting for future applications, as it implies that TKC-mediated perturbations are largely interruptible via addition of a non-toxic sugar, but this result requires further validation and exploration of its limitations. Moreover, it might be possible to achieve *reversibility*—not just interruptibility—given different mannose

concentrations, as it's yet unclear whether the observation of post-mannose transconjugants were due to new TKC events (albeit at lower frequency) or persistent growth of transconjugants created pre-mannose.

# (Return to top)

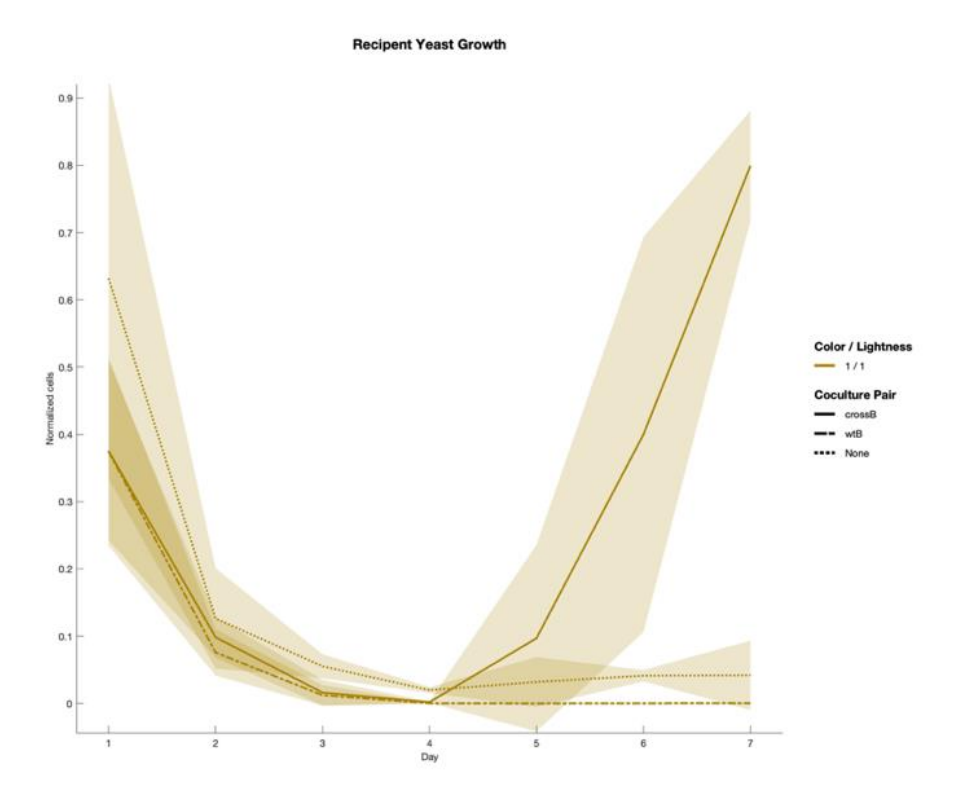
# 4.4 Figures and Tables

### 4.4.1 Figure 1: TKC-mediated rescue of unhealthy recipient populations via population tuning



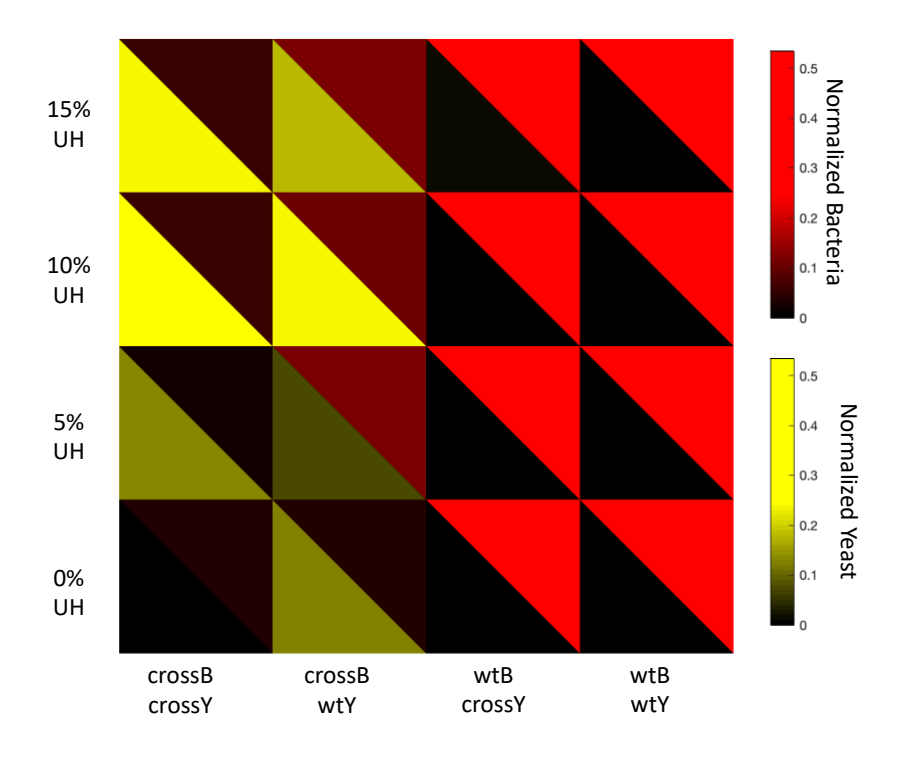
### A. Growth trajectories for rescue assay.

Normalized flow cytometry data for each cell pairing (columns) at four cross-fed amino acid concentrations (UH%, rows), for seven days' batch culturing. Bacterial cell counts shown in red, yeast counts in yellow. Solid lines represent co-culture traces, which are matched with each cell's monoculture traces (dotted) for comparison; shading is standard deviation (six replicates co-culture, five replicates monoculture).



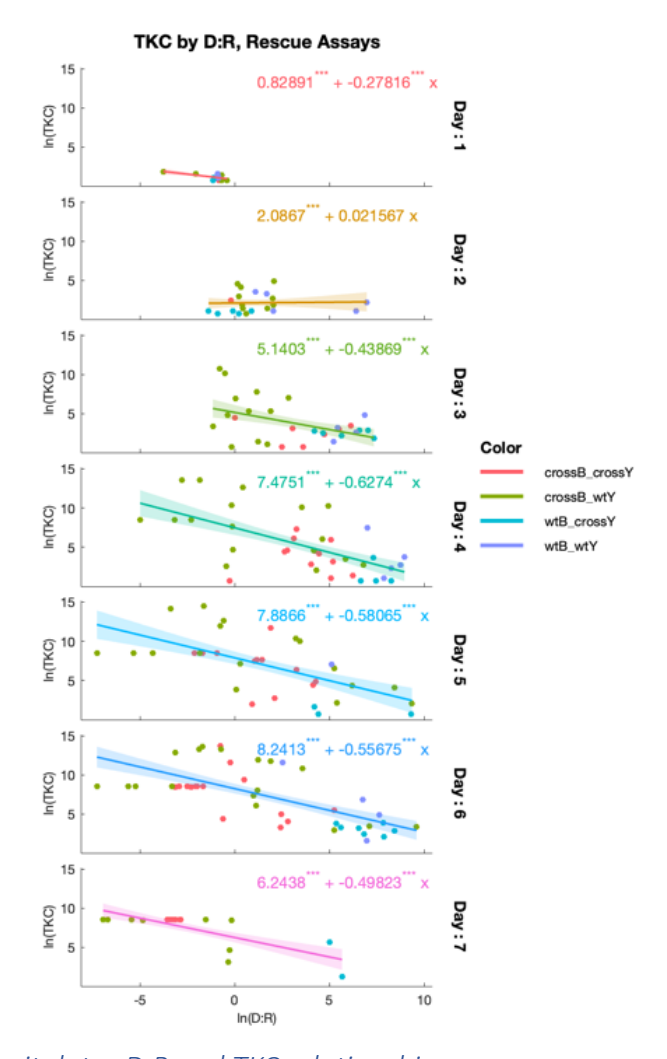
### B. Yeast growth is rescued by cross-feeding donor TKC.

Normalized yeast cell counts from flow cytometry for each cell pairing of crossY at 10% UH, 0% L. In monoculture (dotted line), crossY grows poorly at 10% UH. WT bacterial donors competitively exclude crossY (dot-dash line), despite their ability to transfer TKC plasmid that would rescue recipients. crossB donors, on the other hand, are able to transfer rescuing plasmid (solid line), allowing full crossY rescue. Means of six replicates over two experiments shown as traces, shading as standard deviation.



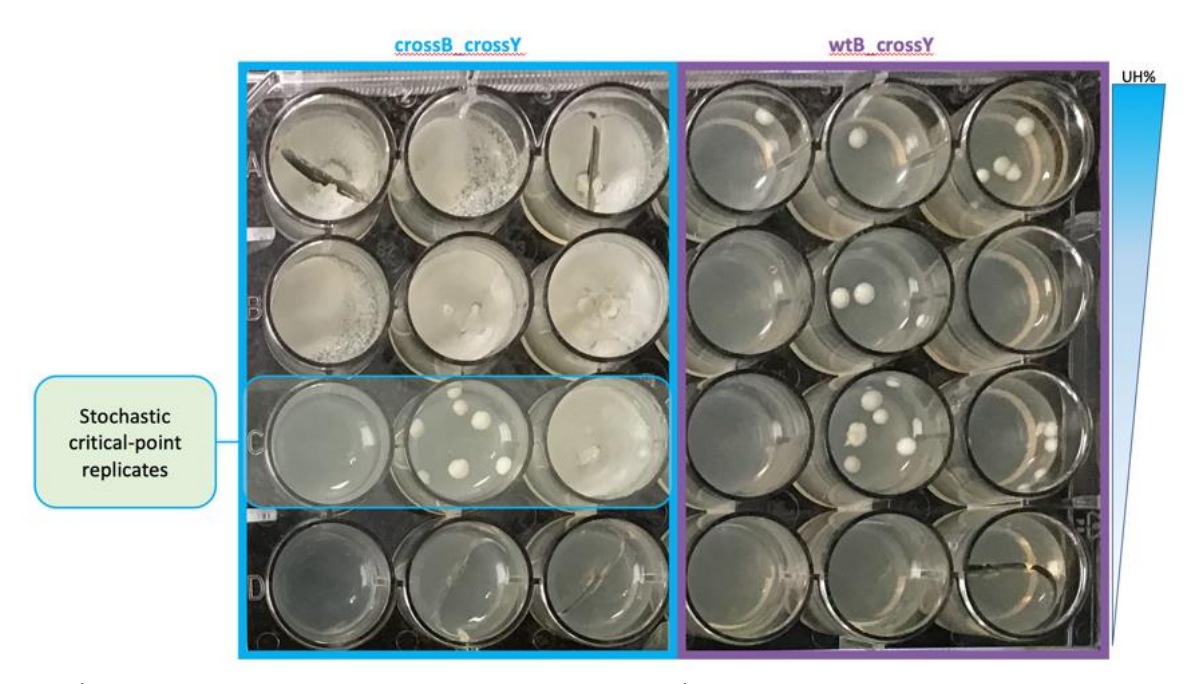
C. Batch culture growth in rescue assay shows greater success for starved donors.

Split heatmaps of normalized cell counts from flow cytometry for four cell pairings (columns) and four concentrations of uracil and histidine (rows). All samples grown with 0% leucine to starve crossB (bacteria in red). Yeast (yellow) auxotrophic for URA3 or HIS3, show greater growth upon receiving conjugated pTA-Mob 2.0 (*cis*), which is only significant when paired with crossB. Brightness is mean of six replicates across two experiments, normalized to max cell count per species and experiment, multiplied uniformly to visualize low-growing strains.



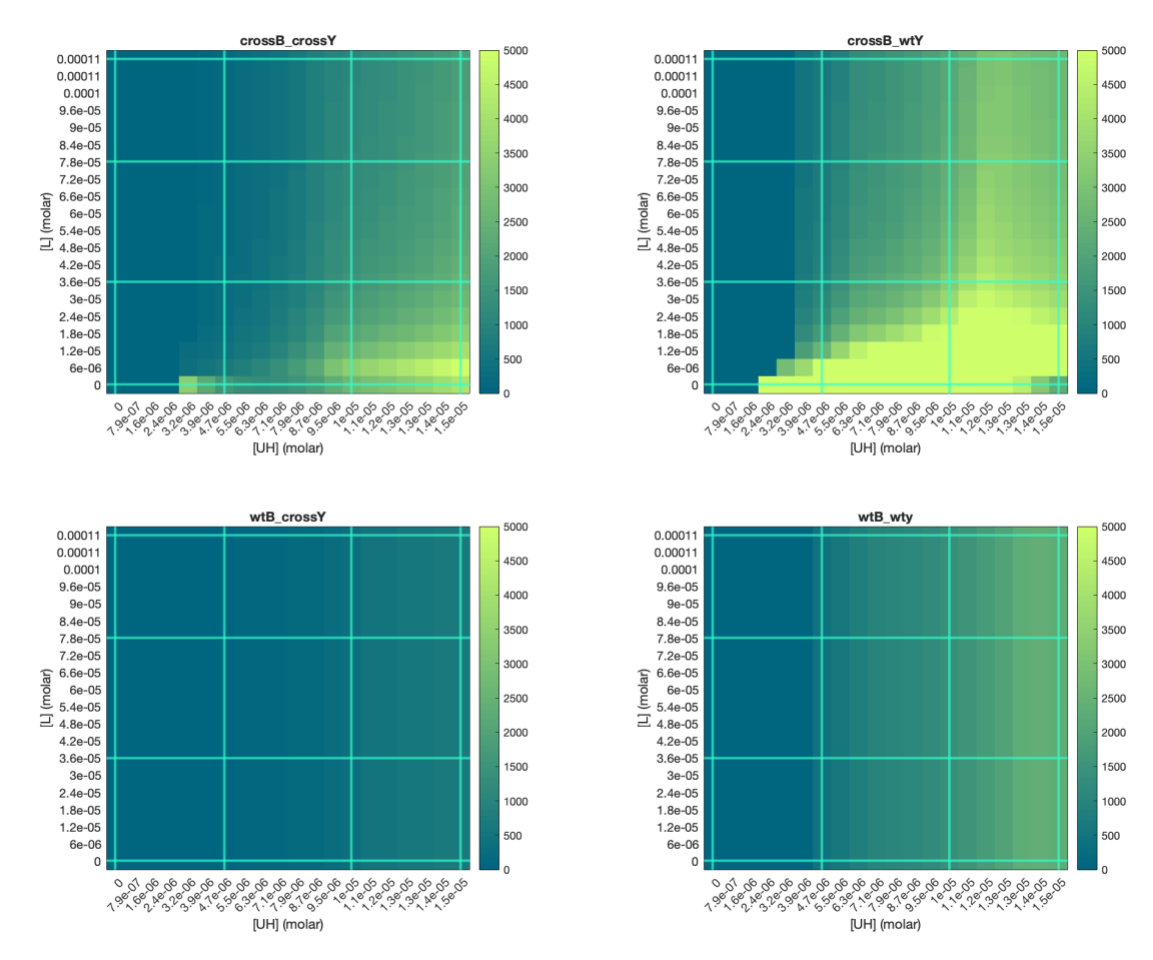
# D. Rescue assay recapitulates D:R and TKC relationship.

Log-log plots of donor-to-recipient ratios (D:R) and TKC, for rescue assay (*cis*) cultures, for each day's measurements (rows). Note that while the negative correlation between D:R and TKC recapitulates previous findings, the scale of the y-axis (TKC CFUs) far exceeds those from previous experiments due to differing selective pressure on transconjugants.



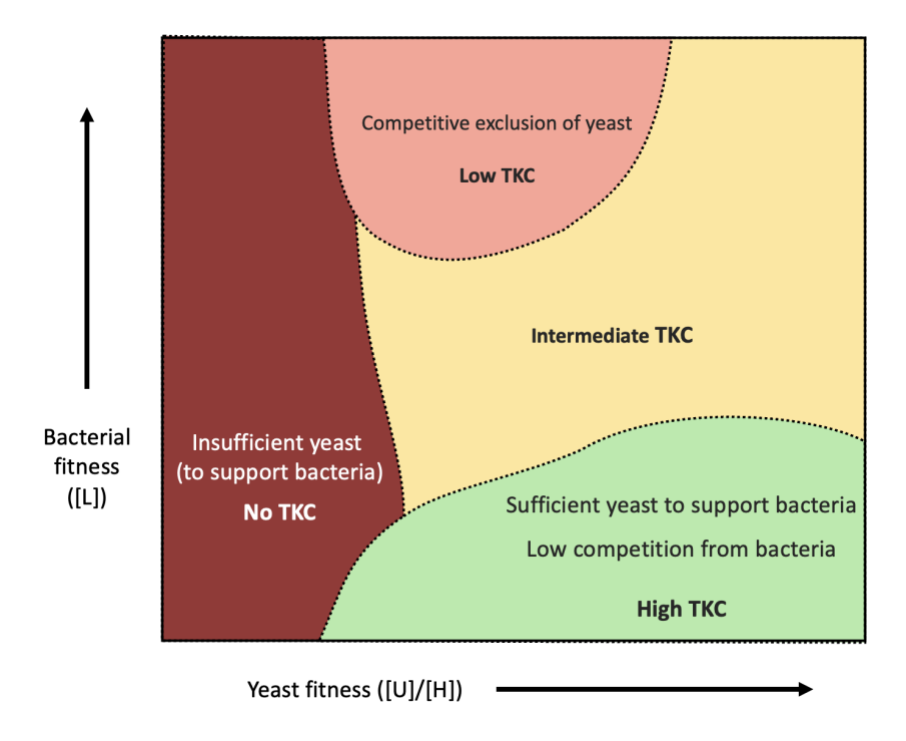
E. Stochasticity in rescue outcomes at apparent critical point.

TKC plate for one rescue experiment at day six. Left three columns are crossB\_crossY, right three columns wtB\_crossY, with each row a different UH% (top to bottom: 15, 10, 5, 0); each condition shown has three replicates. Note that at 5% UH (all samples have 0% L), three crossB\_crossY replicates give drastically different outcomes, ranging from collapse (well C1) to full rescue (well C3). We predict this corresponds to the boundary between red and green conditions in the phase map (Fig 1g).



#### F. Model prediction of rescue phase map.

Predictions for TKC counts based on clump model, adapted for rescue assay conditions. Concentrations of L (y-axis), U, and H (x-axis), for each cell pairing in rescue assay shown, with values 0%, 5%, 10% and 15% highlighted with cyan lines. Note that while rescue conditions don't include a range of leucine concentrations (only 0%), the model predicts a range of [L] over which crossB could rescue yeast more effectively than wtY.



# G. Conceptual phase map of TKC outcomes.

Comparing fitness of bacterial (y-axis) and yeast (x-axis) growth, as controlled in rescue assay by amino acid levels. At low enough fitness for both species, populations collapse before sufficient TKC can occur. When bacteria are sufficiently supplied with nutrients (or don't require them), competitive exclusion suppresses rescue of yeast by transconjugant growth. At low bacterial fitness, but moderately low yeast fitness, enough yeast cells are present to sustain growth of the starved bacteria for long enough to drive TKC, and the lack of competitive exclusion from the unhealthy donors allows for full rescue of recipient population.

(Return to results)

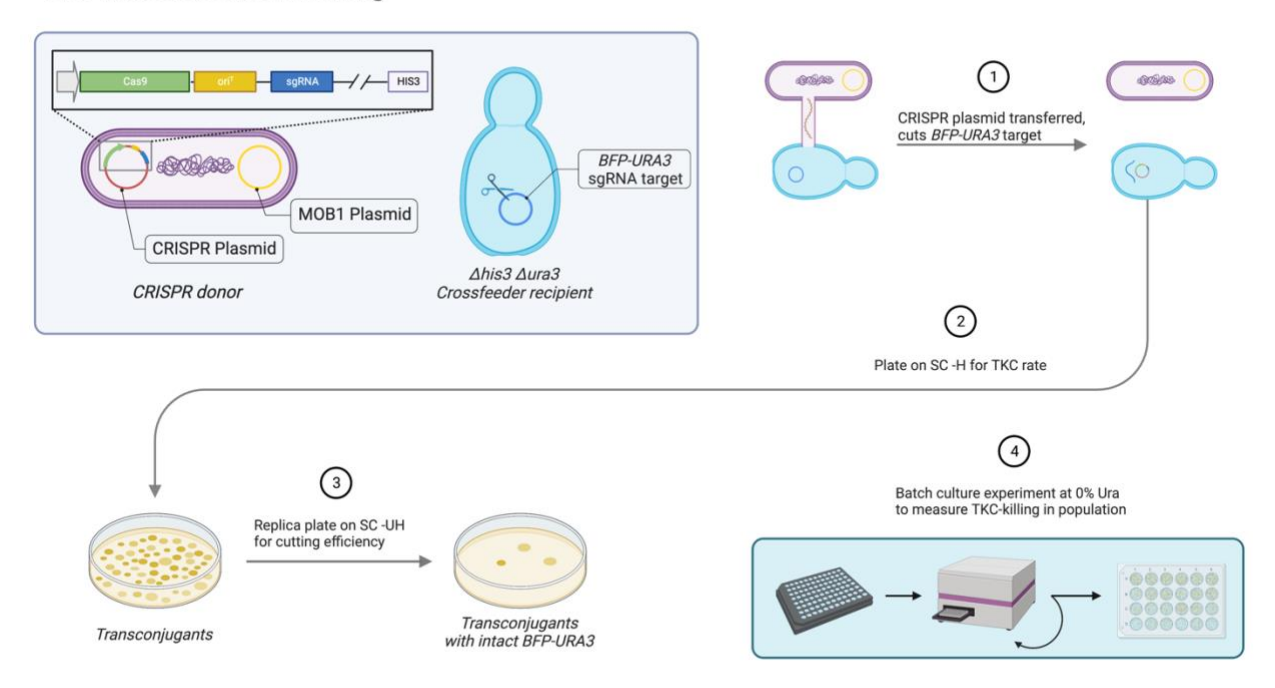
4.4.2 Table 1: Rescue model parameters (values in green diverge from clump-model parameters)

Var	Parameter	Unit	Model Fits per Cell Pairing			
			crossB_crossY	crossB_wtY	wtB_crossY	wtB_wtY
$R_b$	Free bacterial growth rate	hr <sup>-1</sup>	0.75	0.75	0.75	0.75
$R_y$	Free yeast growth rate	hr <sup>-1</sup>	0.58	0.58	0.58	0.58
$R_{cb}$	Clumped bacterial growth rate	hr-1	0.25	0.25	0.25	0.25
$R_{cy}$	Clumped yeast growth rate	hr <sup>-1</sup>	0.18	0.18	0.18	0.18
$R_c$	Clumping rate	Unitless	0.03	0.05	0.03	0.05
$K_b$	Bacterial carrying capacity	mCherry	7566	7269	5590	6790
$K_{\mathcal{V}}$	Yeast carrying capacity	ymCitrine	2822	2700	2637	2412
Cb	Ecological niche overlap (effect of bacteria on yeast)	Unitless	0.80	0.69	0.90	0.70
$c_y$	Ecological niche overlap (effect of yeast on bacteria)	Unitless	0.91	0.95	0.90	0.93
$G_b$	Global amino acid (for dependent bacteria)	Molar	$100\%$ leucine = $7.622*10^{-4}$ M			
$G_y$	Global amino acid (for dependent yeast)	Molar	100% Uracil/Histidine = 1.0*10 <sup>-4</sup> M			
$\alpha_b$	Secreted amino acid (for dependent bacteria)	Molar/ mCitrine	9.2E-5	1E-8	9.2E-5	1E-8
$\alpha_y$	Secreted amino acid (for dependent yeast)	Molar/ mCherry	1E-20	1E-20	1E-20	1E-20
$P_b$	Proximity multiplier for $\alpha_b$	Unitless	50	50	1	1
$P_y$	Proximity multiplier for $\alpha_y$	Unitless	1	1	1	1
$k_b$	Monod term for dependent bacteria	Molar	2E-6	2E-6	0	0
$k_y$	Monod term for dependent yeast	Molar	1.2E-5	0	1.2E-5	0
$D_b$	Bacterial death rate	hr <sup>-1</sup>	0.46	0.50	0.52	0.46
$D_{y}$	Yeast death rate	hr <sup>-1</sup>	0.46	0.39	0.45	0.48
γ	Free TKC rate	Unitless	1E-8			
$\gamma_c$	Clumped TKC rate	Unitless	2.5E-4			

(Return to results)

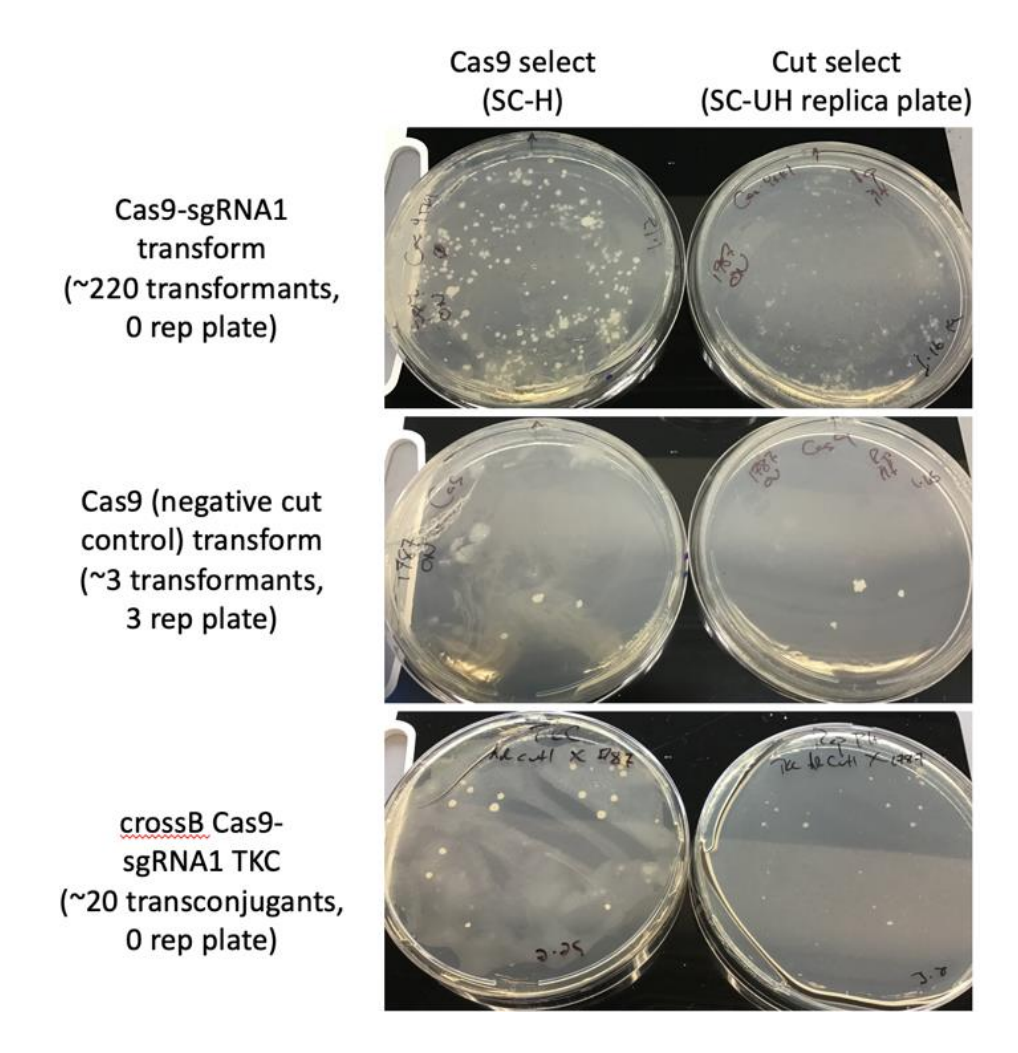
#### 4.4.3 Figure 2: TKC-mediated killing drives recipient population collapse, is mannose-interruptible.

#### **TKC-mediated CRISPR Killing**



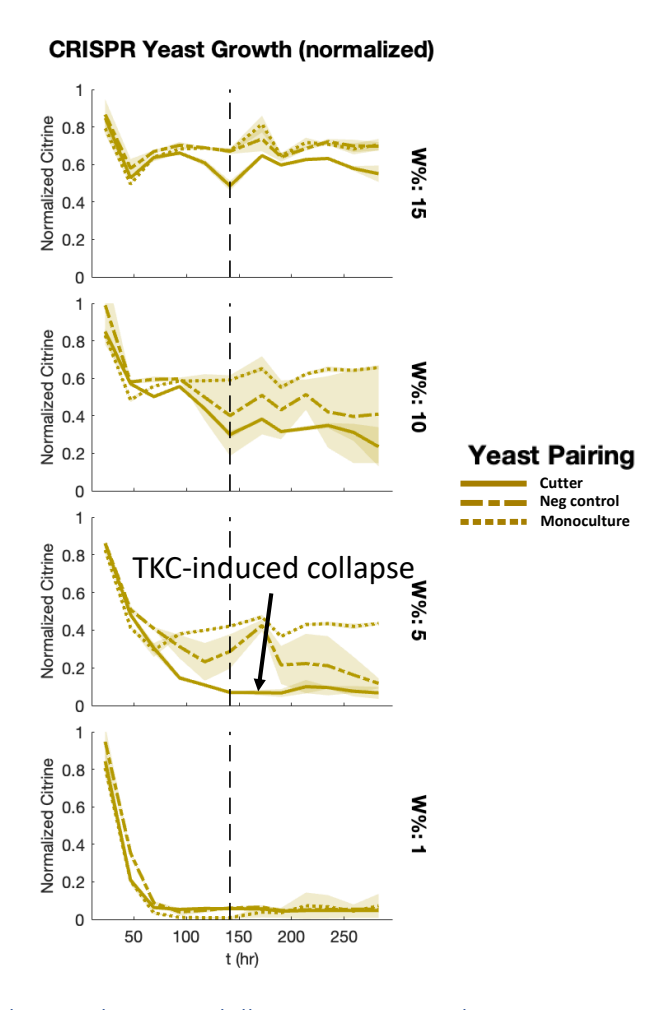
#### A. Design of TKC-mediated CRISPR system.

pTA-Mob 1.0 T4SS plasmid (trans) is paired with a Cas9 plasmid that contains the  $ori^T$  sequence (allowing for transfer), HIS3 yeast selection marker, and sgRNA coding for a connector region in BFP-URA plasmid. Recipient yeast are  $\Delta ura30$ ,  $\Delta his3::HPHMX6$  and carry BFP-URA plasmid. Upon TKC transfer, BFP-URA plasmid is continually cut via Cas9, with no repair template, but yeast can continue to grow in media supplemented with uracil. In this way, we can measure TKC efficiency independently from CRISPR cutting efficiency, but plating for TKC (SC -H) and then replica plating for cut yeast (SC -UH). Finally, cut-verified donors are grown in batch culture with CRISPR recipient yeast at 0% U to gauge ability to depress recipient population through TKC-killing.



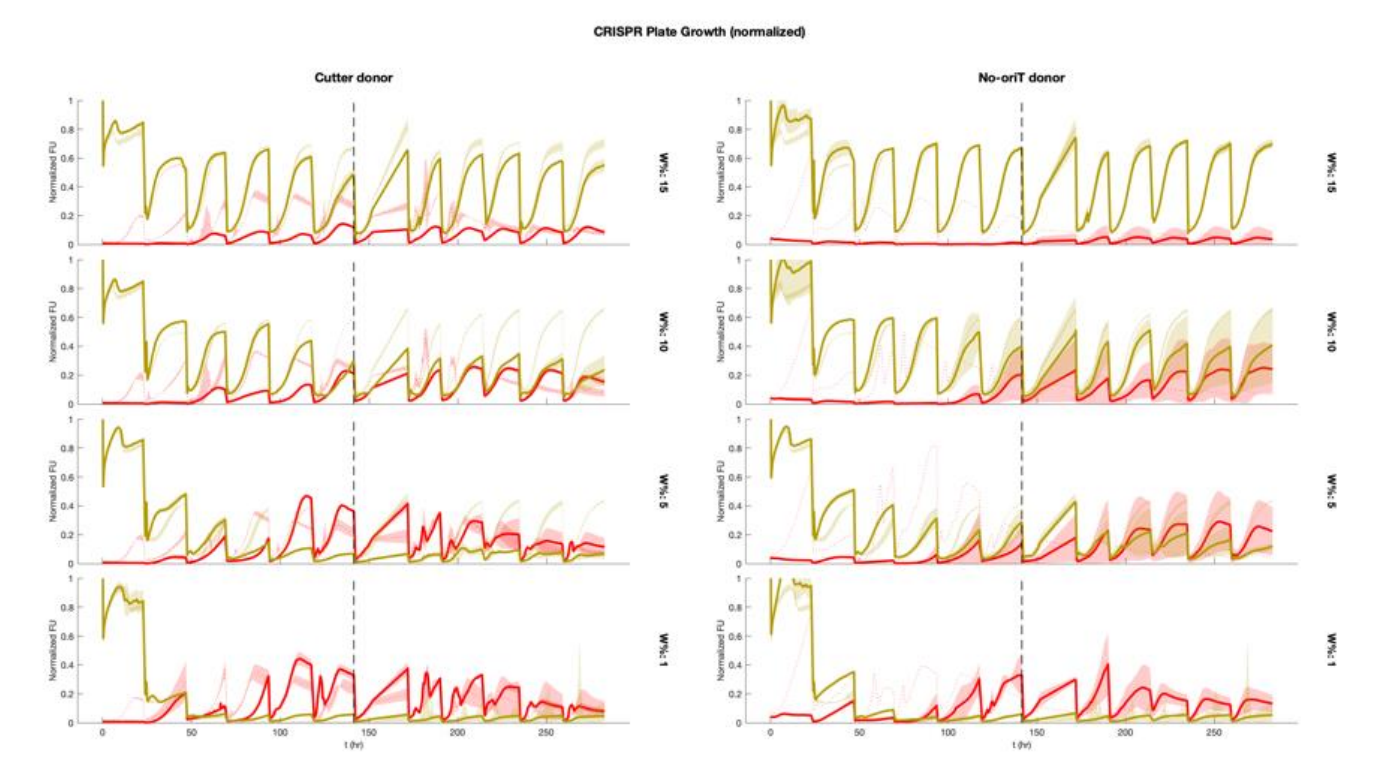
B. sgRNA testing for TKC-mediated killing.

Transformant/TKC selection plates (SC-H, left) and corresponding cut selection replica plates (SC-UH, right). Top row: Cas9-sgRNA was transformed directly into yMM1787, resulting in ~220 colonies on SC-H, none of which replica plated on SC-UH, demonstrating complete cutting of BFP-URA3 plasmid. Middle row: Cas9 (no sgRNA) negative control was transformed directly into yMM1787, showing only three colonies on SC-H, all of which replica-plated on SC-UH, demonstrating no cutting. Bottom row: Cas9-oriT-sgRNA was conjugated into yMM1787 via crossB TKC donor, showing ~20 transconjugants, none of which replica plated on SC-UH, demonstrating complete cutting of BFP-URA3 plasmid via TKC.



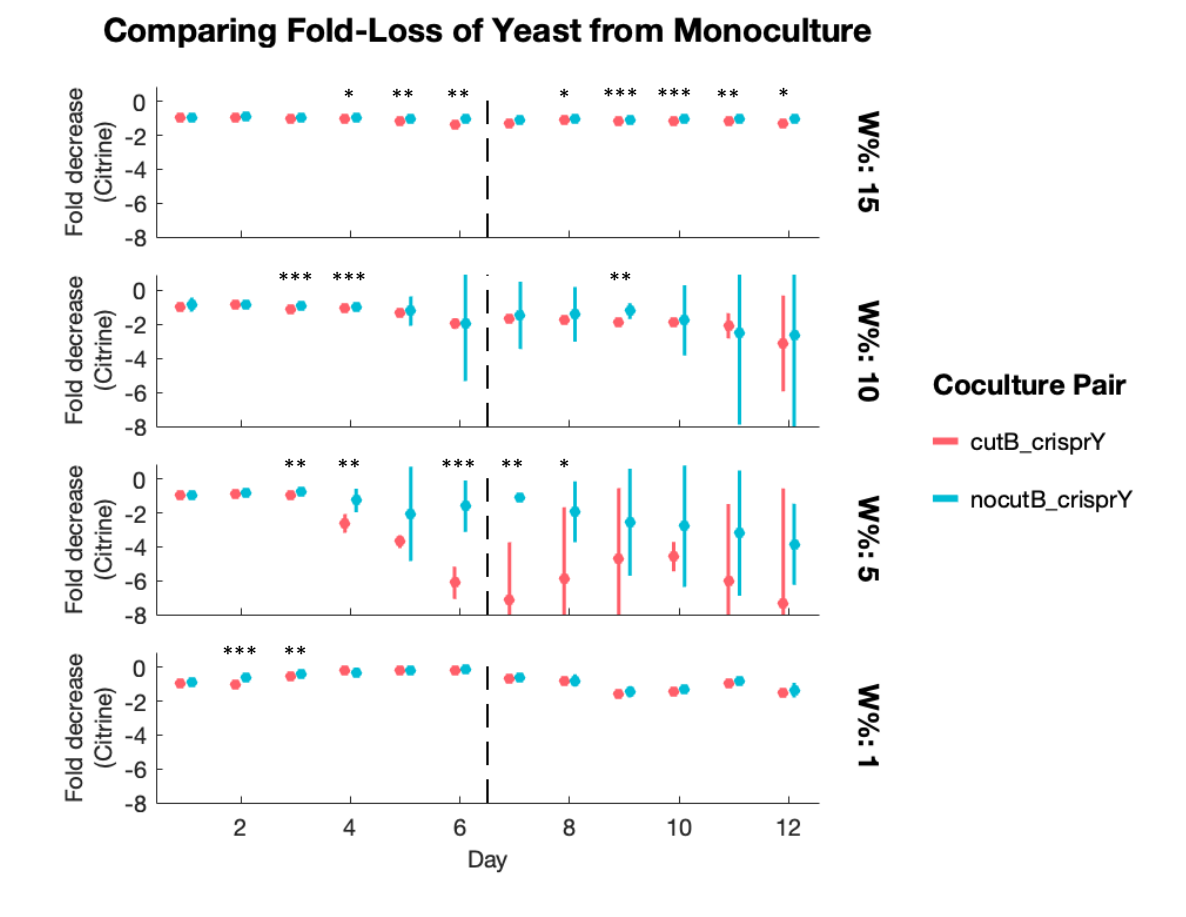
# C. Growth plots of co-cultures show TKC-killing in some conditions.

Day-end fluorescence measurements from 12 days of batch culturing of cell pairs at four concentrations of tryptophan (rows). Trp-auxotrophic recipients collapse for both pairings (cutting donor and no-*ori*<sup>T</sup> negative control donor) at 1% W, but only for the cutting donor at 5% W. Lines are means of three replicates, shaded region standard deviation. Mannose was added to experiment after day 6, shown as vertical dotted lines.



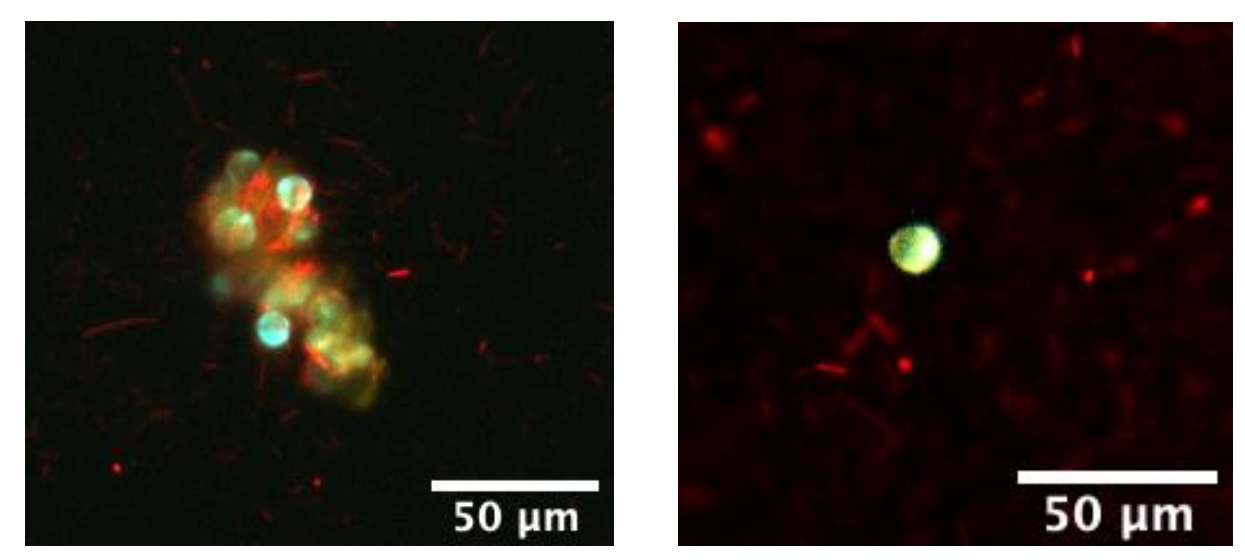
# D. Growth trajectories for TKC-killing assay.

Normalized fluorescence data for each cell pairing (columns) at four yeast-dependent amino acid concentrations (W%, rows), for 12 days' batch culturing. All samples shown are grown in 0% U such that yeast that receive the TKC-Cas9 plasmid are cut and can no longer grown. Bacterial (normalized mCherry) traces shown in red, yeast (normalized ymCitrine) counts in yellow. Solid lines represent co-culture traces, which are matched with each cell's monoculture traces (dotted) for comparison; shading is standard deviation (three replicates). Vertical dotted lines represent addition of mannose to media, after which yeast growth appears to level off.



# E. Comparing recipient population decline between co-cultures, monoculture.

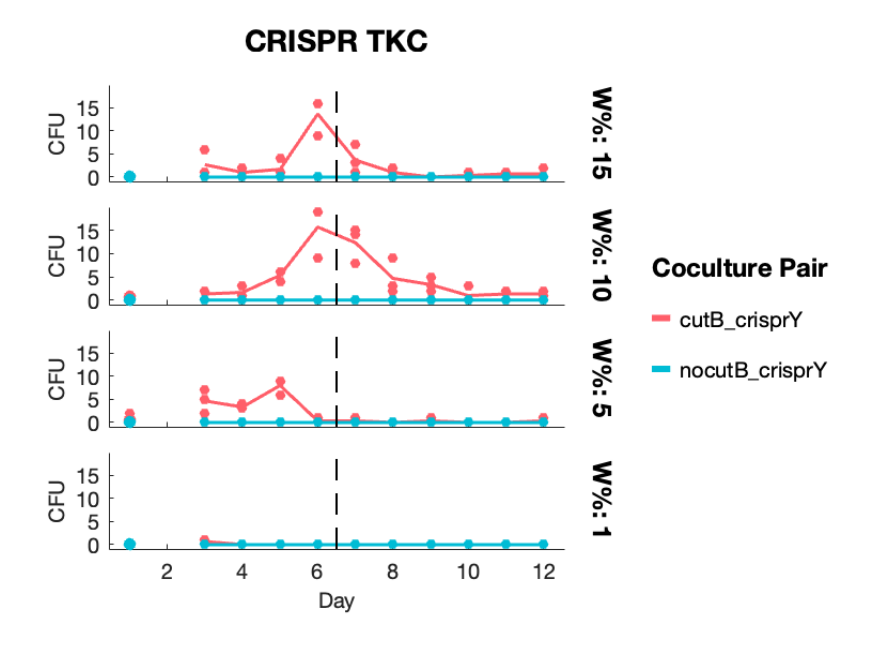
Fold-decreases in yeast growth, based on normalized fluorescence, from recipient yeast monoculture (left: cut-donor in red, negative control donor in blue) or negative-control co-culture (right: cut-donor in red). Fold decrease = -(Baseline Citrine) / (Measured Citrine), where "baseline" is either monoculture (left) or negative-control donor co-culture (right). Points are means of three replicates, bars 95% CI. Stars represent p-value significance from two-sample t-test, with no significance for time points lacking stars (p > 0.05). Vertical dotted lines designate addition of mannose at day 6.



F. Microscopy images of TKC-killing co-cultures pre and post mannose addition.

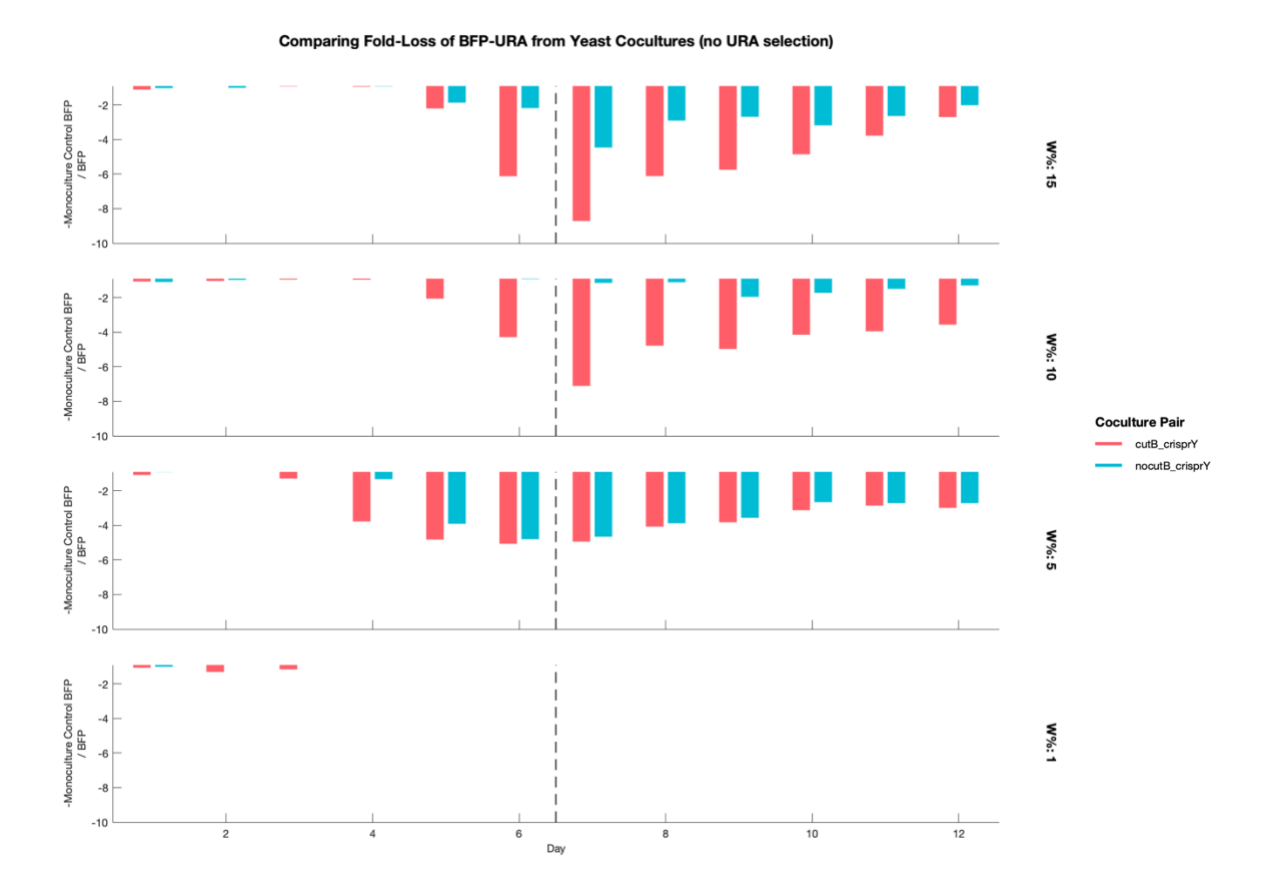
10x images of co-cultures from TKC-killing assay, showing clumping before mannose addition (left, day 5), vs. free cells after mannose addition (right, day 7); mannose was added after day 6. Cells shown are cut-donors and yMM1787, at 5% W 100% U. Brightness for each channel (red, yellow, and blue) was manually scaled to visualize cells most easily. Scale bar =  $50 \mu m$ .

(Return to results)



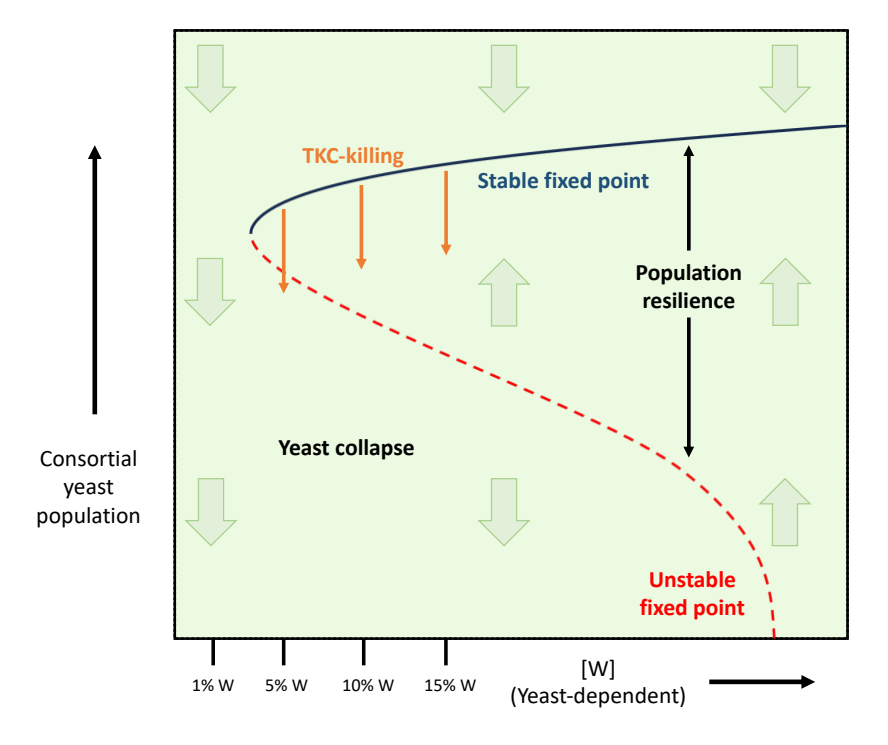
# G. Transient TKC counts show rise, mannose-initiated fall.

TKC counts (CFU) for both cell pairings (negative control donor, blue, is unable to transfer DNA, all counts = 0), over four W% (rows). After addition of mannose (vertical dotted line), most surviving co-cultures drop in TKC counts. Note that 5% W yeast population is coincidentally driven to extinction near day 6, and thus unaffected by mannose. TKC counts here are "transient" because transconjugants are terminal at 0% U, so transconjugants are unable to persist in co-culture across days.



H. Plasmid loss for TKC-killing assay without cut selection.

Fold-loss of BFP-URA3 plasmid in 100% U, for each co-culture relative to yMM1787 monoculture, at four different W% (rows) over 12 days' batch culture. Because yeast are prone to lose the BFP-URA3 plasmid without uracil selection, these demonstrate additional loss of this plasmid due to cutting. Fold decrease calculated by –(Monoculture BFP signal) / (Co-culture BFP signal). Note that cut-donors (red) drive yeast to extinction in 5% W at around day four, and so parity with negative-control donors (blue) after that is likely an artifact of overall low BFP signal. Vertical dotted lines denote addition of mannose.



#### I. Conceptual stable and unstable fixed points of yeast in consortium.

A conceptual map of auxotrophic yeast populations in consortium with bacteria (y-axis), based on concentration of tryptophan ([W]). For environmental perturbations to cell counts (changes in y) bordering a stable fixed point (dark blue line), the yeast population is likely to recover toward its consortial homeostasis (direction of green arrows), though less so when another species is capable of filling the ecological niche left by population loss. If a perturbation drops the population below the unstable fixed point (red dotted line), however, the yeast will not recover and will instead collapse. The distance between unstable and stable fixed points is defined as the resilience of the population. In our experiment, TKC-mediated killing decreases yeast counts (orange arrows) below the consortial steady state, but only drops the recipient population below the unstable fixed point at 5% W. Map is not meant to be to scale, and is based on Dai et. al. 2012<sup>118</sup>.

(Return to results)

(Return to top)

#### 4.5 Materials and Methods

### 4.5.1 Rescue growth model

To apply insights from the clumping model, rescue conditions were tested within the clumping model via the following modifications. Here, yeast cells are selected for TKC events, and there's no limitation of tryptophan (required externally by crossY). To account for this experimental change, the entire amino acid term for yeast growth was based upon limitations of uracil and histidine (required externally for both yeast strains, and carried by Mob1 plasmid)—a change accounted for in changes to input parameters G—but the entire amino acid term was removed from the transconjugant ODE, making them agnostic to terms G,  $\alpha$ , and P. Moreover, because we assume rescued yeast to not stay primarily clumped over a long period, the growth rate for transconjugants was assumed to fall somewhere between that of clumped yeast and free yeast. Finally, unlike previous transconjugant equations, in which transconjugants were primarily carrying-capacity limited by non-transconjugant yeast, here the opposite is likelier true, for any rescue conditions (that would allow yeast numbers to approach carrying capacity), so T is entered into carrying capacity limitation for free bacteria, free yeast, and transconjugants.

Modified growth equation for transconjugants (*T*) in rescue assay:

$$\frac{dT}{dt} = \left(\frac{R_{ly} + R_y}{4}\right) * T \left(1 - \frac{(Y + T + C_y)}{K_y} - \frac{c_b B}{K_b}\right) - D_y \left(\frac{T}{K_y}\right) + \gamma \left(\frac{B * Y}{B + Y}\right) + \gamma_c \left(\frac{C_b * C_y}{C_b + C_y}\right)$$

To model the phase space of transconjugant outcomes for a range of bacterial and yeast fitness, based on limited amino acids, concentrations of leucine (crossB-dependent) and uracil/histidine (all yeast-dependent) G were tested against other fixed parameter outcomes from the clumped-cell model. Because molar concentrations of uracil (crossY-dependent) and histidine (wtY-dependent)

are similar for 100% KS solution (0.0954 mM histidine, 0.178 mM uracil), both were assumed equal at 100% (0.100 mM). Monod terms k were modified to reflect amino-acid sensitivity differences from cross-fed coculture experiments, with crossB maintaining its value for leucine dependence, wtB maintaining its lack of sensitivity ( $k_b = 0$ ), and setting both yeast strains to the value found for crossY sensitivity to tryptophan (see Table S2), making both crossY and wtY equally sensitive to U or H.

Concentrations of amino acids were swept over the range of 0-15%, as per many experimental conditions, even though the rescue assay kept [L] at 0% (uracil and histidine ranged from 0% to 15%). Model anomalies arose when setting all amino acids at or near 0, in which TKC values far surpassed possible ranges (>10<sup>10</sup>), presumably due to small denominators in cell collision equation terms. To account for this, model outputs for which either bacterial or yeast counts dropped below 1 (after converting from fluorescence, for both clumped- and free-cells) were zeroed out for TKC at those times. This modification had no perceptible changes for amino acids not near 0%.

#### (Return to top)

#### 4.5.2 CRISPR-Cas9 plasmid and strain construction

For TKC-mediated CRISPR killing assay, the crossY, *ura3Δ0 hismx6Δ::HPHMX* strain yMM1786 was transformed with the plasmid pMM1360 containing *pTDH3-yeBFP URA3 CEN/ARS* without an *ori*<sup>T</sup> sequence. sgRNAs were designed to cut within the connector region of this plasmid (ConR1 from YTK), downstream of yeBFP, such that any YTK-assembled plasmid containing the ConR1 sequence could be a target in future experiments. CRISPR plasmids were assembled using Ellis lab plasmids<sup>120,121</sup>. Briefly, oligos for five sgRNA sequences targeting the ConR1 region were

designed using Benchling<sup>122</sup>, PNK-phosphorylated and annealed. Annealed oligos were then assembled into sgRNA entry vector pMM1340 via Golden Gate assembly and transformed into bacteria, selecting with carbenicillin. Purified and sequence-verified sgRNA plasmids were then digested with EcoRV to isolate the sgRNA sequences with homology arms matching the insertion site of the Cas9 plasmid. Plasmid pMM1341, which contains Cas9, GFP, and *HIS3*, was digested with BsmBI to remove GFP and leave homology arms for sgRNA at each end of the resultant linear DNA. The two pieces were combined via yeast recombinant cloning. Finally, *ori*<sup>T</sup> was inserted by ligating a modified version of the *ori*<sup>T</sup> sequence with the assembled Cas9-sgRNA after digesting with AatII and SacII.

(Return to top)

#### 4.5.3 Determination of TKC count

In most cases, transconjugant counts were assayed as in <u>Chapter 2 methods</u>. For rescue assay, due to higher counts, cultures after day 2 were serial-diluted up to 1:10,000, in increments of 10x dilutions, and frogged onto SC-UH 2% agar in a 245 mm BioAssay Dish (Corning cat # 431111). Countable microcolonies from frogging dilutions were averaged, based on dilution value; saturated microcolonies were ignored.

(Return to top)

#### 4.5.4 Batch culturing measurements

Generally, samples were batch cultured as per <u>Chapter 2 methods</u>, including dilutions, growth conditions, fluorimetry, and <u>flow cytometry</u>. For the TKC-killing assay, a couple of notable variations were employed. First, while flow cytometry was performed on these samples, days after

mannose addition (days 7-12) were measured by flow cytometry every other day, but due to a myriad of technical difficulties among the flow cytometers used, these results were discarded and Tecan fluorescence were used as the primary measurments of populations. Yeasts and bacteria were measured for fluorescence as in Chapter 2, but here yeBFP was also measured (Ex=381nm, Em=445nm, 20nm bandwidth, gain=60) for loss of plasmid from recipient population. Additionally, samples were measured every other day via fluorescence microscopy as per clump imaging in Chapter 2, with images of non-diluted and 50x diluted samples taken every other day for the 12-day time course.

#### (Return to top)

# 4.5.5 Table 2: Strains used in this study

ID	Species	Genetic features	Fluorescence	Source	Figures
yMM1585	Yeast	Leu <sup>++</sup> , Trp <sup>-</sup> , Ura <sup>-</sup>	ymCitrine, yCerulean	<sup>77</sup> , this work	1
yMM1636	Yeast	His <sup>-</sup>	ymCitrine	<sup>77</sup> , this work	1
yMM1720	Yeast	Leu <sup>++</sup> , Trp <sup>-</sup> , His <sup>-</sup>	ymCitrine, yCerulean	<sup>77</sup> , this work	2
yMM1786	Yeast	Leu <sup>++</sup> , Trp <sup>-</sup> , Ura <sup>-</sup> , His <sup>-</sup>	ymCitrine, yCerulean	<sup>77</sup> , this work	2
yMM1787	Yeast	Leu <sup>++</sup> , Trp <sup>-</sup> , Ura <sup>-</sup> , His <sup>-</sup> , pMM1360	ymCitrine, yCerulean, BFP	<sup>77</sup> , this work	2
kMM0011	Bacterium	None	None	90	1
kMM0127	Bacterium	Trp <sup>++</sup> , Leu <sup>-</sup>	None	<sup>90</sup> , this work	Both

#### 4.5.6 Table 3: Plasmids used in this study

ID	Species	Function / Features	Fluorescence	Source	Figures
pMM0819	Bacterium	pProD-mCherry	mCherry	Addgene 87144	Both
pMM0892	Bacterium	T4SS genes, Gent <sup>R</sup>	None	pTA-Mob 1.0 <sup>30</sup>	2
pMM1353	Both	T4SS genes, Gent <sup>R</sup> , URA3, HIS3,	None	pTA-Mob 2.0, Addgene 149662	1
		CEN/ARS, ori <sup>T</sup>		Addgene 149002	

pMM1340	Bacterium	sgRNA assembly vector, sfGFP	GFP	Addgene 90516	None
pMM1341	Bacterium	Cas9, sfGFP	GFP	Addgene 90519	None
pMM1342	Bacterium	sgRNA assembly, YTK target	None	This work	None
pMM1360	Both	yeBFP, URA3, CEN/ARS	BFP	<sup>95</sup> , this work	2
pMM1437	Both	yeBFP, <i>ori</i> <sup>T</sup> , HIS3, CEN/ARS	BFP	<sup>95</sup> , this work	2
pMM1438	Both	Cas9, ori <sup>T</sup> , sgRNA (YTK), HIS3	None	This work	2
pMM1439	Both	Cas9, sgRNA (YTK), HIS3	None	This work	2

(Return to top)

# Chapter 5: Optogenetic control of TKC

# 5.1 Introduction

In synthetic microbiology, a myriad of tools has been developed to control cells in space in time, but the majority of them involve diffused molecules added to the growth system, such as the commonly used sugar inducer arabinose. Optogenetics—the control of cell functions by light stimulation—adds a versatile control option, as light activation of gene expression is cheap and easily controlled for time, space, and intensity<sup>123</sup>. While the light used to activate microbial genes (in yeast) was initially red/far red<sup>124</sup>, most systems currently in use in bacteria utilize blue-light inducible photoreceptors, including the histidine kinase-driven pDawn system<sup>125</sup> used here. Activation by blue light limits utilization in any future TKC-based probiotics, since blue light, unlike red light, doesn't readily penetrate mammalian tissues<sup>126,127</sup>. Still, options exist for internal (blue) optogenetic stimulation, whether by nanoparticles that can convert infrared light to blue light<sup>128,129</sup>, or bioluminescent generation of blue light<sup>130</sup>. Moreover, blue-light optogenetic-driven probiotics could readily be applied to perturb surface-associated fungi, such as those in oral cavity or skin infections, or the rhizosphere (see Introductory remarks), where light stimulation would be much more accessibly achieved.

Optogenetic activation of TKC could have many other applications in synthetic biology, moreover, not least as dosage control of T4SS genes to discern its regulation, which is still little understood<sup>57</sup>. Several studies have used optogenetics to control spatial growth patterns—whether in yeast cooperator-cheater systems by activating production of a public good<sup>131</sup>, or by optogenetic patterning of bacteria by stimulated adhesion between cells<sup>132,133</sup>—which could be used to control TKC by engineering population boundaries. Moreover, with the findings presented above (see

<u>Chapter 2 results</u>), optogenetic control of mannoprotein binding via Type I fimbriae expression could hypothetically directly control adhesion between *E. coli* and *S. cerevisiae*, and thus TKC, in culture as well as colonies. Finally, optogenetic control of the T4SS could more directly control any perturbations caused by TKC, and is the purpose of this chapter.

The pDawn system used here for bacterial light-activation of the T4SS is readily modified for gene of interest, has long "off" kinetics (once activated, it stays on for long periods), and enjoys previous validation in our BW25113 strain<sup>125,134</sup>. Briefly, symbiotic nitrogen fixation genes from Bradyrhizobium japonicum FixJ and FixL were modified to incorporate a Light Oxygen Voltage (LOV) domain of the Bacillus subtlis gene YtaV onto FixL, to form the chimeric histidine kinase YF1<sup>125,135</sup>. In the absence of light, YF1 phosphorylates FixJ, which then drives the promoter FixK2. In the similar pDusk system, a gene of interest is placed under the control of pFixK2, enabling light-sensitive repression (gene turns off in blue light), whereas in pDawn, a geneinversion cassette is placed downstream of pFixK2. In pDawn, pFixK2 drives the λ phage repressor CI, which represses the strong promoter pR, under which the gene of interest is placed; thus, blue light turns off repression of the gene of interest, and thereby enables blue-light activation <sup>125</sup>. While this system was chosen in part for its ability to maintain activation even while not being stimulated (see Methods), more temporal control of gene de/activation could be achieved by switching to light-dimerizing systems<sup>136,137</sup>, or the well-studied light-DNA-binding EL222<sup>138</sup>, upon understanding the key determinants of optogenetic-TKC activation.

To incorporate optogenetic control of the T4SS, the first question is which of the 100+ gene(s) to modify in the pTA-Mob plasmids used in this study. As an initial target, I chose *TraJ*, due to its

essential role in the relaxosome, wherein it binds to the *ori*<sup>T</sup> sequence<sup>59,60</sup>, a decision that was recently validated by work from the Karas lab (the source of the pTA-Mob plasmids) that found increased TKC after mutating the *TraJ* promoter<sup>64</sup>. Thus, any opto-TKC scheme first required extensive plasmid construction, to 1) put TraJ under pDawn control, 2) construct a *trans*-acting conjugative plasmid (see <u>section 3.2.1</u>), and 3) delete *TraJ* from pTA-Mob 1.0, to allow exclusive optogenetic control of this essential relaxosome function.

#### (Return to top)

#### 5.2 Results

#### 5.2.1 pDawn shows prolonged activation with low intensity, short-pulsed light signal

Despite previous validation of the pDawn system with blue light, our automated batch culture system doesn't allow for simultaneous and prolonged optogenetic stimulation and culture shaking, so I first tested a range of light intensities and lengths for expression of pDawn-sfGFP<sup>132</sup>. Our lab previously developed a 96-well optogenetic stimulation array ("optoPlate")<sup>139</sup>, which we incorporated into our automated Tecan Fluent plate handling robot, such that plates can be transferred between a heated shaker ("Bioshakes"), the optoPlate, and a Tecan Spark fluorimeter (Fig 1a). For a first test, I grew cells containing pDawn-sfGFP at room temperature and no shaking, but constant light stimulation across the full range of available light intensities. The plate was transferred to the Spark and measured for GFP fluorescence and OD600 every 15 minutes for ~24 hours. At ~20 hours' growth, well after all sfGFP-containing cells had exceeded the fluorimeter's detection limit, I lowered the gain on the GFP channel to discern late-stage changes between light intensities. Results show all but the lowest light intensities fully saturated for green fluorescence by 5 hours' growth, and with roughly equivalent loss of growth from sfGFP expression after 5 hours (Fig 1b).

Next, I tested whether low light-activation times would yield similar expression, so that experiments could primarily be grown on the Bioshakes, to match other culture conditions. Instead of growing pDawn-sfGFP carrying cells on the optoPlate as before, I grew them on the Bioshakes, held at 30°C, and included a 1 min light activation step after every 15 min Spark read. Results generally recapitulate the previous results from constant stimulation (Fig 1c), verifying the long "off" time of the pDawn system. Subsequent experiments utilized light activation intensities of 50, since this was the lowest intensity to yield full green fluorescence—on par with the highest light doses—by 10 hours, and had the highest GFP/OD600, i.e., the highest fluorescence per cell density.

#### (Return to top)

#### 5.2.2 Deletion of *TraJ* from T4SS genes leads to reduced TKC, toward opto-control

To remove TraJ from pTA-Mob 1.0, both to put TraJ under optogenetic control and to make a negative control strain for optogenetic experiments,  $\lambda_{red}$  recombineering was used to edit the ~60 kbp plasmid<sup>91</sup> (Fig 2a). First, primers were designed to PCR amplify the kanamycin resistance gene flanked by flippase recognition targets (common to Keio collection strains, see section 2.5.1), along with 50 bp homology arms matching TraJ-proximal regions in pTA-Mob 1.0. Using  $\lambda_{red}$  genes, this cassette was transformed into pTA-Mob 1.0-carrying cells to create pTA-Mob 1.0 traJ:: $Kan^R$ . Then a flippase-expressing plasmid was used to excise  $Kan^R$ , creating pTA-Mob 1.0  $\Delta traJ$ . Simultaneously, TraJ was amplified from pTA-Mob 1.0 and assembled into the pDawn plasmid via Golden Gate assembly. For controls, pDawn-sfGFP was used in place of pDawn-TraJ, either with an intact pTA-Mob 1.0 (positive control) or with pTA-Mob 1.0  $\Delta traJ$  (negative control). All three strains additionally carried a plasmid carrying mCherry (see section 2.5.1) and a trans-

TKC reporter (see <u>section 3.2.1</u>) to be transferred to recipients, creating a four plasmid system in each case.

A head-to-head comparison between TKC from pTA-Mob 1.0 and pTA-Mob 1.0  $\Delta traJ$  showed that the latter, meant to be TKC-defective, did indeed transfer DNA to recipients, albeit ~100-fold less effectively (Fig 2b). While pDawn-sfGFP, included in both donor controls, didn't serve a conjugative function, bacterial maintenance of this pDawn variant was essential to prevent large changes in fitness between the strains, though its green fluorescence overlapped spectrally with yeast-expressing ymCitrine, and proved fitness-altering for bacterial growth (see below). Finally, while positive control donors did generally yield the most transconjugants regardless of light dose, as expected (Fig 3d), all donor strains performed poorly for TKC and for growth in co-culture, as is discussed in the following section.

(Return to top)

#### 5.2.3 Opto-TraJ donors fail to generate light-activated TKC

All "opto-donor" strains (opto-*TraJ*, positive and negative controls described above) were found to be very slow growing relative to strains used for other experiments, likely due to maintaining four plasmids simultaneously. While this lower growth rate didn't totally preclude growth of monoculture opto-donors in batch culture, growth of opto-donors in co-culture was near non-existent (Fig 3a). I made several attempts to overcome this hurdle, including screening various media ratios of SC and M9, testing mixed colonies, and combining cells after various days' growth and thus light stimulation (data not shown), none of which gave reliable bacterial growth in co-culture or significant TKC from positive controls, let alone opto-*TraJ*. One strategy—lowering the

concentration of tryptophan using crossY recipients, thus limiting yeast growth as in <u>section 4.2.2</u>—did result in better bacterial growth in co-culture (<u>Fig 3b</u>), and yielded some transconjugants, but TKC counts were still near zero and thus unconclusive (<u>Fig 3c</u>), while co-culture growth between the three donor strains was frustratingly variable (<u>Fig 3b</u>).

While overcoming the hurdles of co-culture growth for opto-donor strains, I also wanted to verify whether light control of TraJ allowed optogenetic control over conjugation, independent of the dynamics between these strains. To test this, I grew opto-donors with another *E. coli* strain lacking any antibiotic resistance markers carried by opto-donors. The recipient bacterial strain used carried chloramphenicol resistance, which opto-donors lack, allowing me to select for recipients only by plating cells onto LB-chloramphenicol, and then test for transconjugants by replica plating onto LB-carbenicillin (the *ori*<sup>T</sup>-carrying plasmid also encodes ampicillin resistance). I grew each donor strain in dark and light conditions prior to combining cells for co-culture, then grew each unique pairing in either dark or light conditions, resulting in six separate co-cultures. Results from this experiment, while not tabulated, clear show that opto-*TraJ* donors do not significantly increase conjugation with light, nor do they show significantly higher conjugation versus the negative control donor (Fig 3d). These results do, however, verify that the positive control donors conjugate more than the other strains.

# (Return to top)

#### 5.3 Discussion

My work to produce a light-controlled TKC system never came to fruition, but many avenues still exist to make it viable. Testing the opto-TKC system intraspecies demonstrated that, aside from the complexities of co-culture of bacteria and yeast, pDawn control of *TraJ* itself is either not

functional or not sufficient. While I was able to verify that pDawn was functionally activated by the light doses and co-culture conditions used, it's possible that the TraJ gene cloned to be under pDawn control is not being expressed and/or that its expression is frame shifted, etc. RT-PCR would readily ascertain TraJ is being transcribed in a light-dependent manner and verify that its sequence matches the encoded DNA. More likely culprits perhaps are either that *TraJ* expression requires a different level of expression (vs. highly induced), perhaps making the gene a poor lighttarget, or that conjugation is too infrequent in this system to successfully measure light-activation changes above the noise floor, especially given that the negative control (with pTA-Mob 1.0  $\Delta TraJ$ ) is "leaky" due to two copies of the gene present in pTA-Mob 1.0, and it's possible that only one copy was successfully knocked out. Repeating the intraspecies test for optogenetic conjugation over a range of light intensities would help discern regulation, while the accessibility of wholeplasmid sequencing would make verification of both TraJ knockouts from the ~60 kbp plasmid trivial. Increasing overall conjugation counts could also be achieved by making corresponding versions of the *cis*-acting pTA-Mob 2.0, which enjoys higher conjugation rates, a task that is trivial in planning albeit nontrivial experimentally.

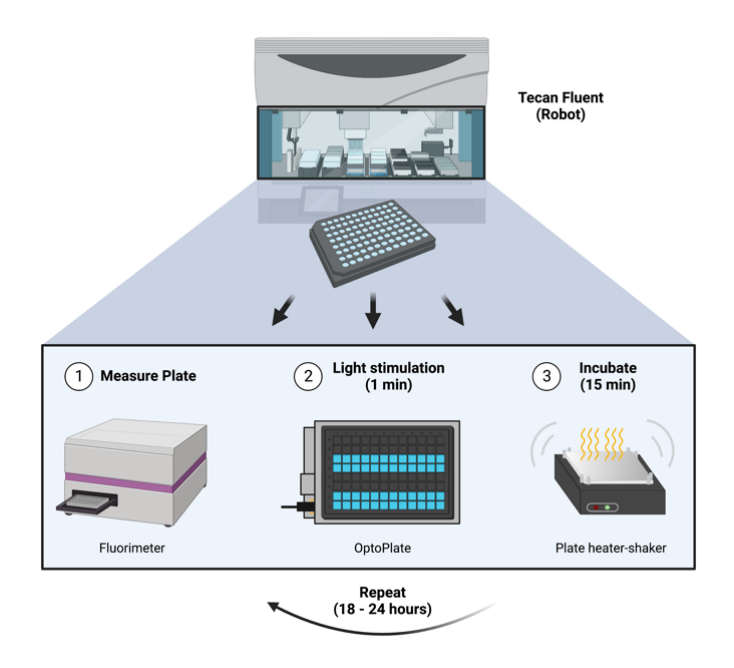
In interspecies co-culture, the opto-TKC system faced additional hurdles, as bacterial strains failed to grow as well as they did in monoculture. Likely this is, in part, due to the fitness costs of maintaining four separate plasmids, especially considering two of them likely share replicative machinery (*ori*<sup>V</sup>s ColE1 in the *trans*-TKC reporter and F1 in pDawn belong to the same incompatibility group<sup>140</sup>). And while it's unclear why there should be such a sudden change between monoculture and co-culture when switching from three to four plasmids, it's well known that plasmids impose a fitness burden due to maintenance<sup>141</sup>; even the three plasmids in *trans*-TKC

co-cultures (including pTA-Mob 1.0, constitutive mCherry, and trans-reporter) caused slower growth relative to two-plasmid cis-acting cells. Considerable effort went into lessening this burden by integrating the constitutive mCherry gene into either the cis-acting pTA-Mob 2.0 (see 3.2.1) or the genomes of my bacterial strains at the nupG locus, by following published methods<sup>142</sup>, but neither was successful for reasons still unknown. Yet other possibilities remain to lower the plasmid burden in this system, including the aforementioned modification of opto-TKC into a cisacting system (obviating the need for the trans-reporter plasmid); creating a new, compatible bacterial *ori* for the Yeast Toolkit, by which I generated the *trans*-reporter, or cloning mCherry into the pDawn plasmid. Additional hurdles still remain, however, as the growth rates between the opto-TraJ (experimental) donor strain and the two control donor strains were quite different (see 5.4.5.B). As was seen in early TKC-Cas9 experiments, in which my negative strain expressed GFP (not shown), different donor strain growth resulted in large effects on recipient strain growth in absence of any TKC function, which is to say, it's very important to have the strains growing at the same rate to avoid convolution between TKC function and co-culture dynamics. If my opto-TraJ strain shows high TKC counts in light, but the donors grow very poorly in light (allowing yeast to grow better), I might just be measuring a small fraction of a larger yeast population. This can be controlled for somewhat by measuring TKC-per-recipient frequencies, but if the counts are low for most conditions, noise can lead to false positives very easily. Thus, any renewed work would benefit from bringing parity to the donors, either by replacing the sfGFP currently used in controls with a mutated TraJ, or a strategy similar to the TKC-killing experiments, wherein the negative control simply lacked the *ori*<sup>T</sup> necessary to transfer DNA.

(Return to top)

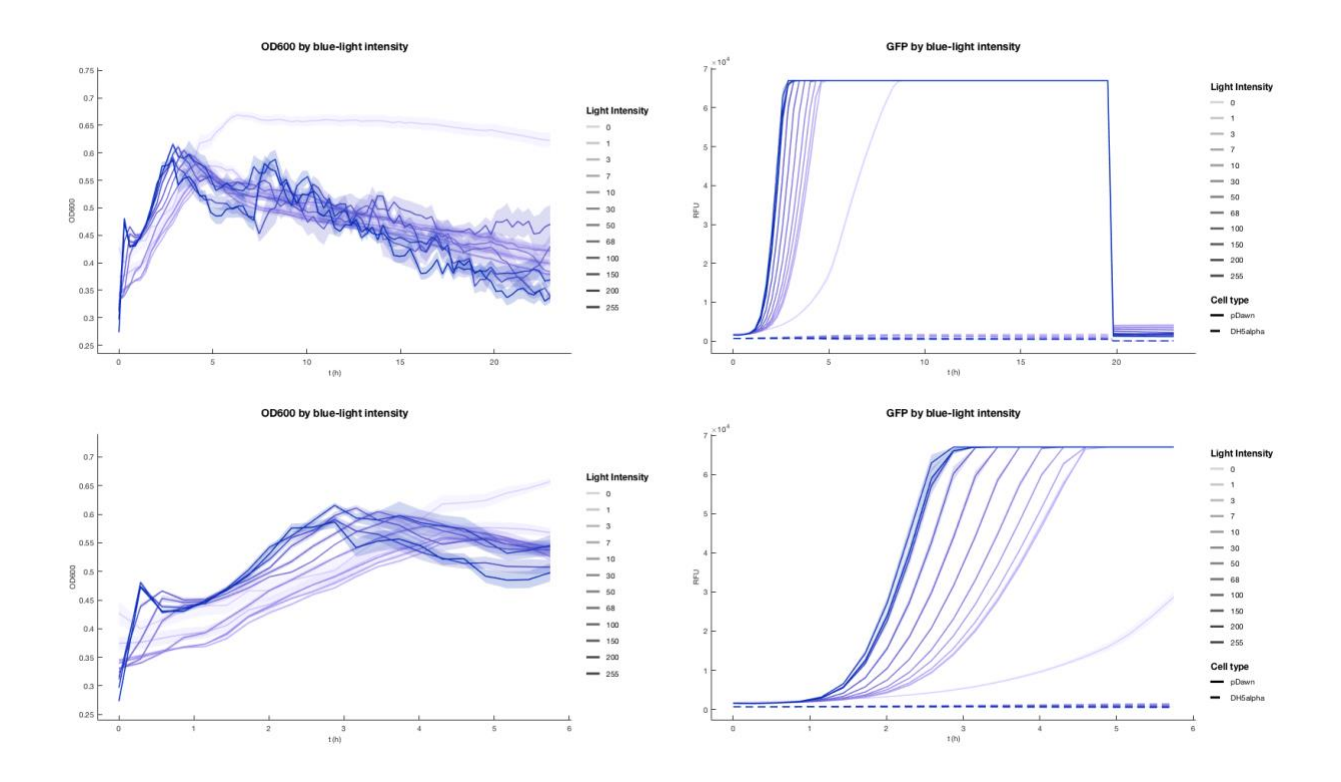
# 5.4 Figures

# 5.4.1 Figure 1: pDawn stimulation by automated blue-light batch culture system



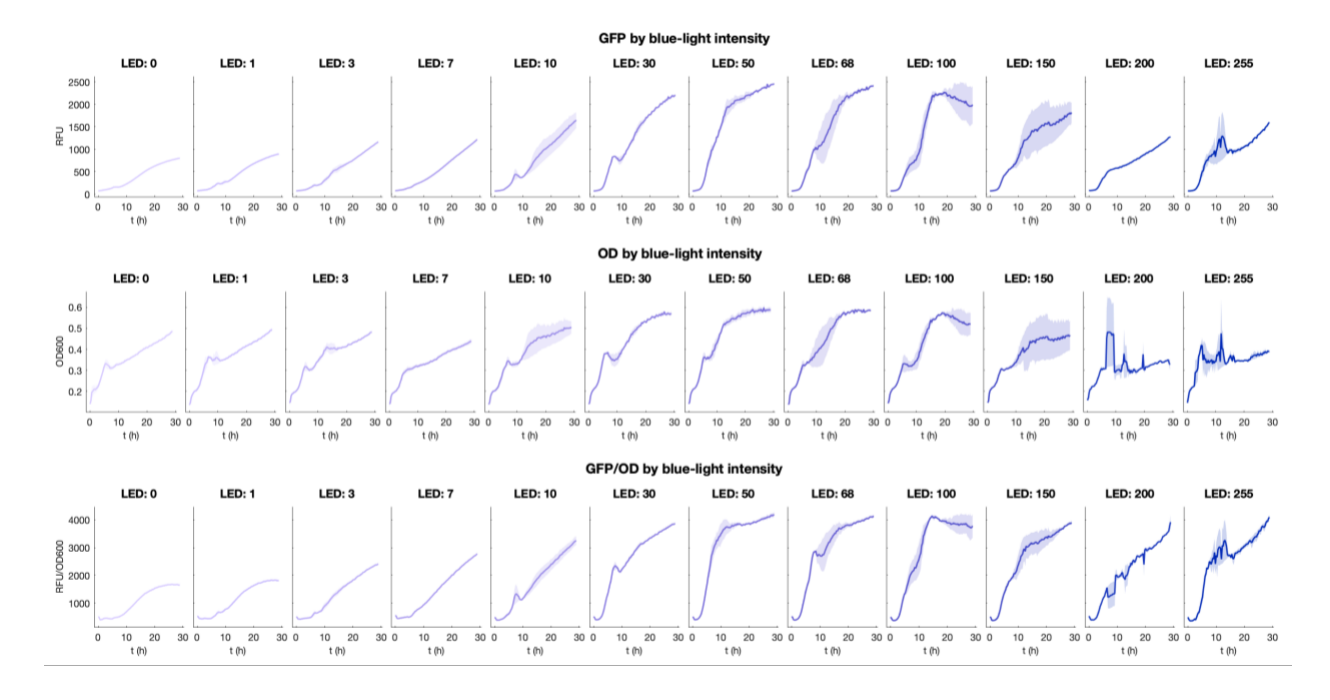
# A. Diagram of optoPlate batch culture system

Batch cultures spiked in 96-well plates were handled in the dark until initiated in Tecan Fluent automated plate handling system. Samples were first measured for fluorescence and OD600 via Tecan Spark, then transferred to programmed optoPlate, with varying levels of light intensities per well, for 1 min. Plates then grew on Bioshakes heated shaker for 15 min., after which the cycle repeated. Each days' growth continued this loop for ~18-24 hours before batch culture dilution and additional (TKC) measurement.



B. pDawn-sfGFP expression under a range of light intensities, with constant stimulation

OD600 (left column) and GFP (right column) measurements of pDawn-sfGFP containing cells (solid lines) over ~24 hr. growth, with constant light stimulation. LED intensities shown by trace lightness and color range, from 0 brightness (off) to 255 (max setting). Bottom row shows the same traces as the top row, zoomed in on the first 6 hr. growth. GFP gain setting was lowered after ~24 hr. DH5α (plasmid-free) negative control cells were measured for GFP autofluorescence, shown as dotted lines. Solid lines are means of six replicates, shading 95% CI.

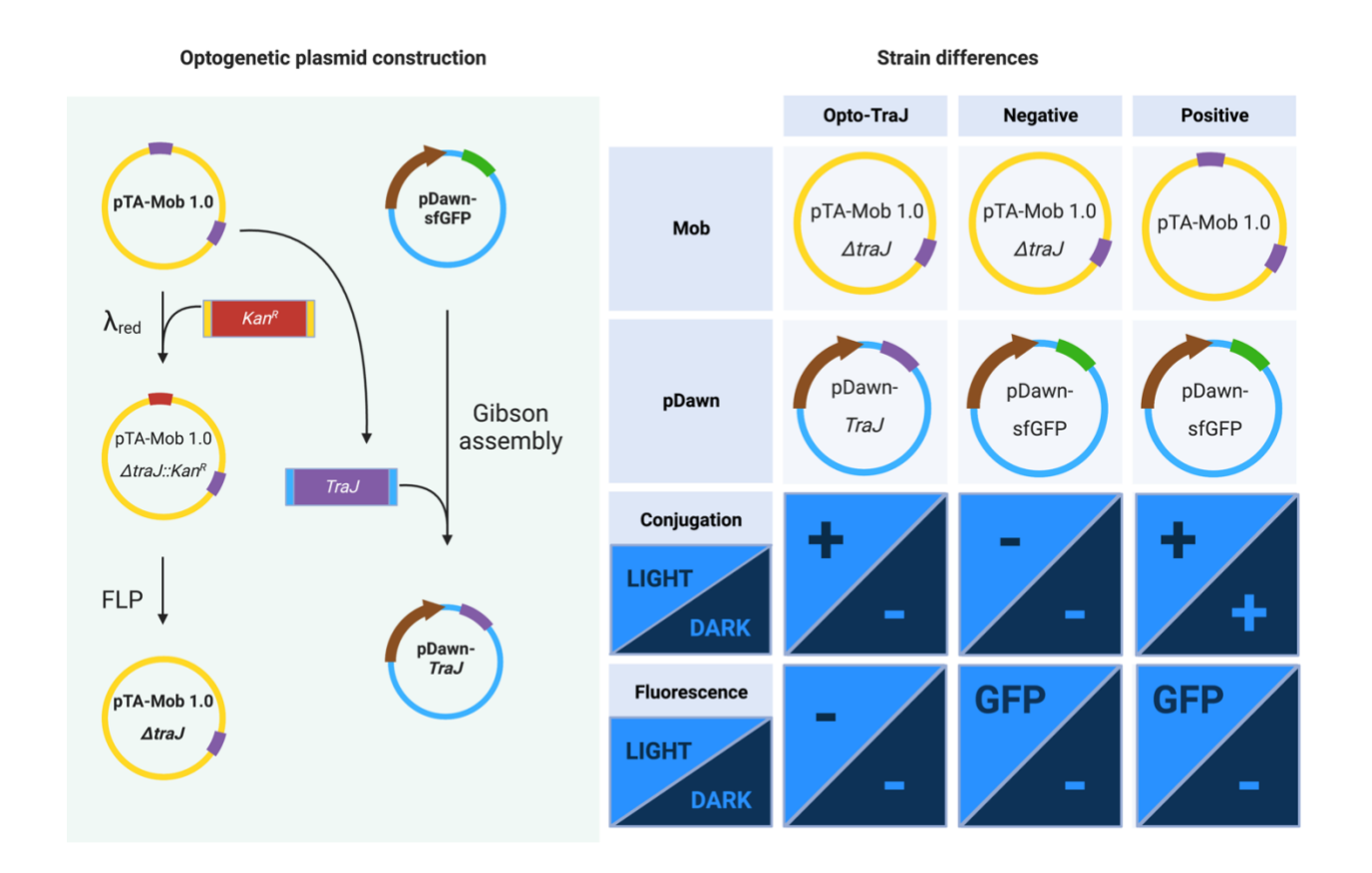


C. pDawn-sfGFP expression under a range of light intensities, with periodic stimulation

Traces of GFP (top row), OD600 (middle row), and calculated GFP / OD600 (bottom row) for cells containing pDawn-sfGFP over ~30 hours' growth, with periodic light activation: 1 min on, 15 min "off" (growing without light stimulation). LED intensities shown in columns and by color and lightness. LED 50 was chosen for subsequent experiments due to high pDawn activation (high GFP by 10 hr.), both in raw fluorescence and per capita fluorescence (GFP/OD600). Lines are means of two replicates, shading 95% CI.

(Return to results)

#### 5.4.2 Figure 2: Opto-TKC control construction



#### A. Construction scheme for opto-TraJ and control strains

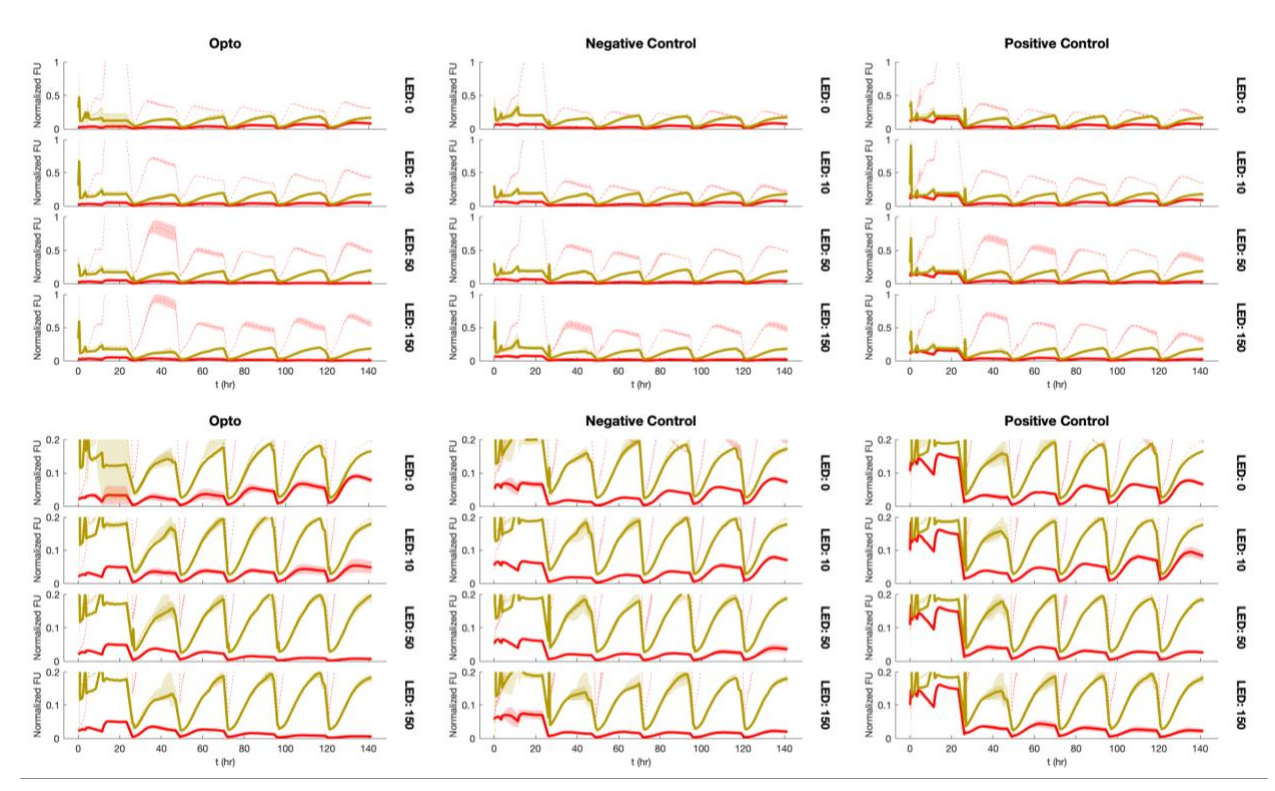
Left: construction of pTA-Mob 1.0 and pDawn variants. One copy of *TraJ* was replaced with kanamycin resistance plus homology arms via lambda red recombineering, which was then removed via flippase (FLP) to generate pTA-Mob 1.0 *AtraJ*, which bears only one copy of *TraJ*. *TraJ* was simultaneously amplified with homology to pDawn and assembled via Gibson assembly. Right: list of differences between experimental and control optogenetic strains. Experimental opto-*TraJ* and negative control both carry single knockout pTA-Mob 1.0 *AtraJ* but only the former carries pDawn-*TraJ*. Both controls contain pDawn-sfGFP and fluoresce green in light conditions. All three strains additionally carry *trans*-TKC reporter and mCherry plasmids, and the combination of three was generated for both WT bacterial donors and crossB crossfeeding donor strains.



# B. Mob ΔtraJ results in ~100-fold lower TKC

TKC-selective plates show different transfer rates between unmodified pTA-Mob 1.0 (left) and single-knockout pTA-Mob 1.0  $\Delta traJ$  (right), with ~100-fold fewer transconjugants for the knockout variant. (Plate titles pertain to intended use with TKC-killing system and don't relate to optogenetic experiments). TKC was performed with equal numbers of donors and recipients, based on OD measurements.

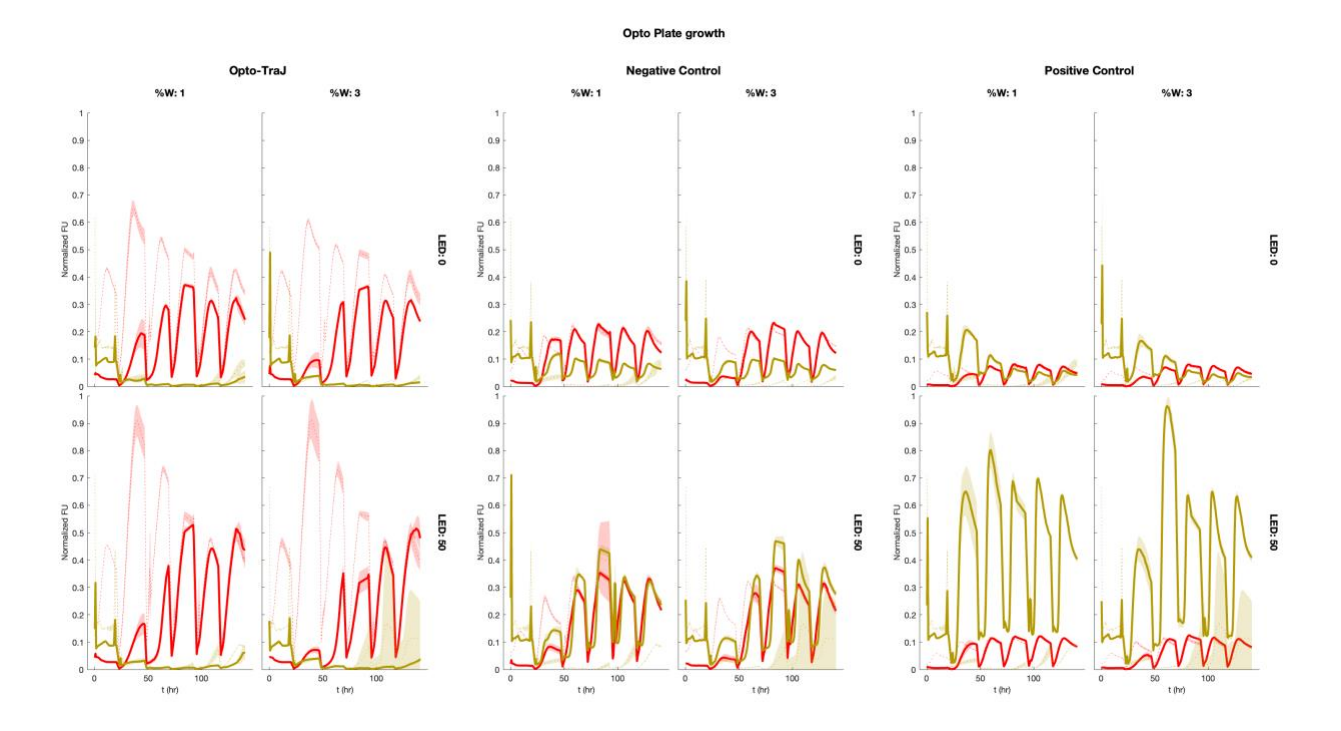
(Return to results)



5.4.3 Figure 3: Opto-TKC donors fail to conjugate with light activation

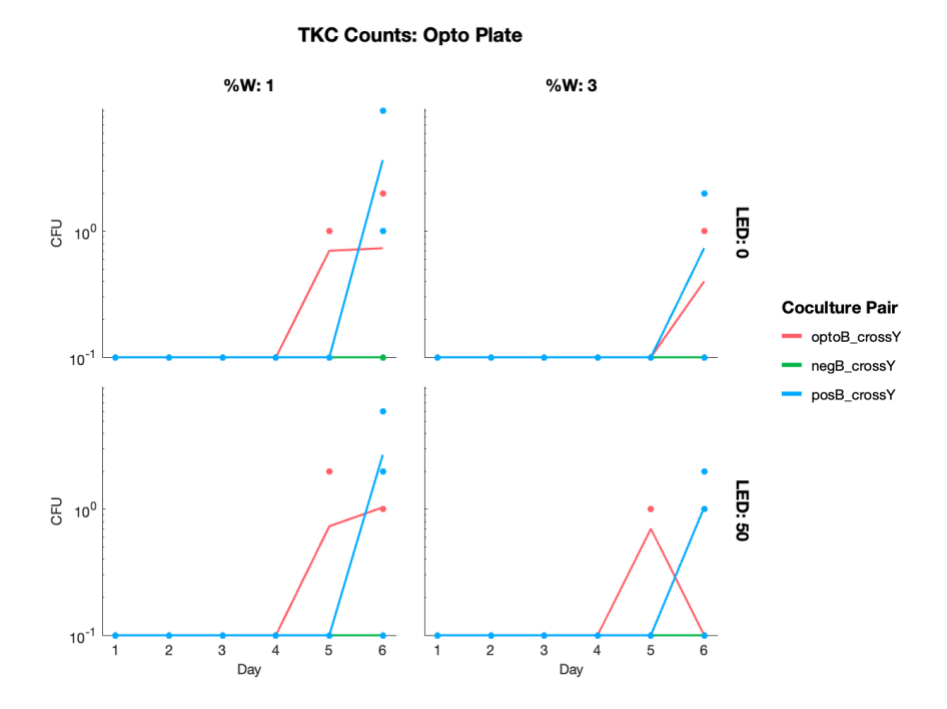
A. Opto-donors are unable to grow sufficiently in co-culture.

Normalized fluorescence traces (normalized to max fluorescence per channel after day 1) for bacteria (red) and yeast (yellow) over six days of batch culturing, measured every 15 min. Opto-*TraJ* donors (light-activated TKC), negative and positive control donors shown in columns, over four different light intensities, including no light (rows). Co-culture traces shown via solid lines, corresponding monocultures via dotted lines; note that while solid red lines (co-cultured bacteria) are consistently low across all conditions (including dark), dotted red lines (monoculture bacteria) grow well. Bottom plots are zoomed in along y-axis. Lines are means of three replicates, shading standard deviation.



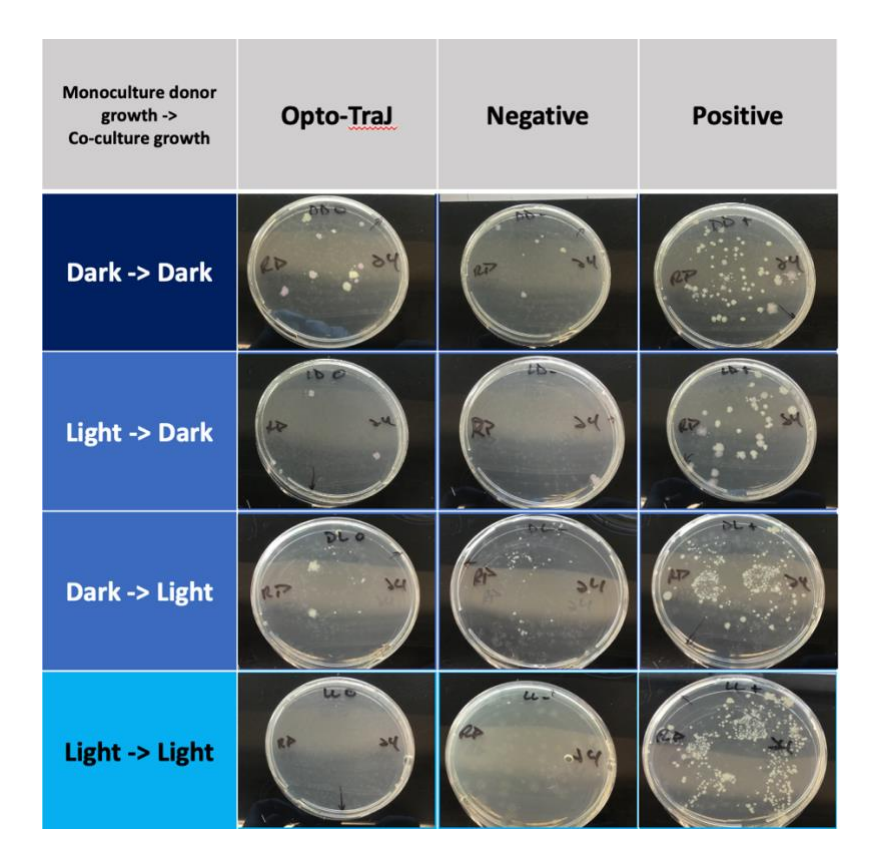
B. Limiting growth of yeast in co-culture allows opto-donor growth.

Normalized fluorescence traces (normalized to max fluorescence per channel after day 1) for bacteria (red) and yeast (yellow) over six days of batch culturing, measured every 15 min. Opto-*TraJ* donors (light-activated TKC) on left, negative control donors in center, and positive control donors shown on right, over two tryptophan concentrations (columns) and two different light intensities, including no light (rows). Co-culture traces shown via solid lines, corresponding monocultures via dotted lines; note that while solid red lines (co-cultured bacteria) are consistently low across all conditions (including dark), dotted red lines (monoculture bacteria) grow well. Note that, while all donor strains are able to grow in co-culture, the extent of that growth varies both by strain and by light dose.



# C. TKC from tryptophan-limited optogenetic co-cultures shows few transconjugants.

Colony forming units of transconjugants from W-limited optogenetic co-culture experiments shown in Fig 3b. Cell pairings given by colors, for two different W% (columns) and two light dosages (rows). Note that, while both opto-*TraJ* and positive control donors give TKC counts, as hypothesized, opto-*TraJ* donors show transconjugants in dark conditions (LED = 0), and positive control TKC is zero for most days, including those with non-zero TKC from opto-*TraJ* donors, making these results inconclusive.



D. Opto-donors in intraspecies co-culture shows failure of light-activated conjugation.

Replica plates of bacterial transconjugants, for various light conditions and donor strains, after 24 hours of co-culture. Letter labels pertain to light ("L"=light, "D"=dark) condition of opto-donors prior to combination in co-culture, and light condition of co-culture; e.g. "LD" or "Light->Dark" donors were grown in light prior to combination, but the combined co-culture was grown in the dark. Note that while positive controls generally have higher conjugation events across conditions, negative controls show a significant number, and experimental (opto) donors do not exceed negative controls.

(Return to results)

#### 5.5 Materials and Methods

# 5.5.1 Construction of opto-strains

Bacterial cells carrying pTA-Mob 1.0 and pMM0820—encoding inducible λ<sub>red</sub> genes—were electroporated with a linear DNA cassette of Kan<sup>R</sup> flanked by flippase recognition targets (FRT) and  $\sim 50$  bp homology to one copy of TraJ on pTA-Mob 1.0, after induction of  $\lambda_{red}$  genes via arabinose<sup>91</sup>. Successful gene replacements (pTA-Mob 1.0 \( \Delta traJ::Kan^R \)) were selected by growth on kanamycin media, after which pMM0820 was heat cured by sub-culturing at 40°C. The flippase-encoding pMM0821 was then transformed into these cells, with transformants selected for with chloramphenicol (resistance via pMM0821) and gentamycin (resistance via pTA-Mob 1.0), then replica plated onto kanamycin media. Any colonies that grew on chloramphenicol and gentamycin, but did not grow on the kanamycin replica plate were presumed to have lost Kan<sup>R</sup> (pTA-Mob 1.0 ∆traJ), were sequence-verified and heat cured of pMM0821 via growth at 40°C. Simultaneously, pDawn-sfGFP was linearized via PCR such that sfGFP was removed from the resultant linear DNA. PCR of TraJ from pTA-Mob 1.0, with 50 bp homology arms for the linearized pDawn, allowed Gibson assembly of TraJ under pDawn control (pDawn-TraJ). Both kMM0011 and kMM0127 were then transformed with combinations of these plasmids as per Fig 2a).

#### (Return to top)

#### 5.5.2 Blue-light stimulation in batch culture

Batch cultures were grown, measured for fluorescence and TKC as per <u>Chapter 2 methods</u>, though here, we made some modifications to account for light sensitivities. Overnight donor cultures were grown in opaque black 15 mL conical tubes, with loosely attached lids, in a dark incubator, to

prevent any preemptive light stimulation. Any cell transfers—washing and inoculating the initial batch culture plate, and all other dilutions, washes, and transfers—were performed in red light that doesn't activate the pDawn system, and plates were kept in aluminum foil while being handled in the light. The automated Tecan Fluent plate handler was covered with a felt cloth to prevent ambient light from reaching samples in during batch culturing. In batch culture, plates were first measured for fluorescence and OD600—thus the first measurement had no light stimulation—then transferred to a light-stimulating optoPlate for 1 min, then to a Bioshakes heated shaker, where samples grew at 30°C for 15 min, as per other batch cultures. The optoPlate was programmed for constant light intensity at each well location via a custom MATLAB script, with the specific intensity values demonstrated in each figure.

#### (Return to top)

#### 5.5.3 Intraspecies opto-TKC experiment

As in TKC batch culture experiments, donor and recipient cells were grown overnight prior to combination in co-culture. Here, though, opto-donor strains were grown in both light and dark conditions overnight, in a clear 24-well culture plate, which allowed light stimulation via a 24-well Light Plate Apparatus<sup>144</sup> (LPA). The recipient bacterial strain, bMM1221, was chosen for its maintenance of chloramphenicol resistance, which wasn't carried by any of the opto-donors. Cells of each strain from overnight cultures were washed, diluted and added to culture as per TKC batch culture experiments, except here cells were grown in 1 mL LB with no antibiotics, in clear 24-well culture plates. As per overnight cultures, co-culture plates were grown on LPAs with either no light stimulation (also protected by aluminum foil) or full light stimulation. At 1 hr, 5 hr, and 24 hr from co-culture start, co-cultures were diluted 1:1000, and 100 μL of each dilution was plated on LB

plates with chloramphenicol and 2% agar, to select for recipients. These were grown overnight at 37°C, at which point plates were replica-plated onto LB plates with carbenicillin and 2% agar, to select for transconjugants out of the recipient population.

# (Return to top)

# 5.5.4 Table 1: Strains used in this study

ID	Species	Genetic features	Fluorescence	Source	Figures
yMM1636	Yeast	His-	ymCitrine	<sup>77</sup> , this	2-3
				work	
yMM1720	Yeast	Leu <sup>++</sup> , Trp <sup>-</sup> , His <sup>-</sup>	ymCitrine, yCerulean	<sup>77</sup> , this	3
				work	
yMM1787	Yeast	Leu <sup>++</sup> , Trp <sup>-</sup> , Ura <sup>-</sup> , His <sup>-</sup> ,	ymCitrine, yCerulean,	<sup>77</sup> , this	2b
		pMM1360	BFP	work	
kMM0127	Bacterium	Trp <sup>++</sup> , Leu <sup>-</sup>	None	<sup>90</sup> , this	All
				work	
bMM1221	Bacterium	Chloramphenicol-	None	<sup>90</sup> , this	All
		resistance plasmid		work	

# 5.5.5 Table 2: Plasmids used in this study

ID	Species	Function / Features	Fluorescence	Source	Figures
pMM0819	Bacterium	pProD-mCherry	mCherry	Addgene 87144	All
pMM0820	Bacterium	$\lambda_{red}$ genes	None	91	None
pMM0821	Bacterium	Flippase	None	91	None
pMM0892	Bacterium	T4SS genes, Gent <sup>R</sup>	None	pTA-Mob 1.0 <sup>30</sup>	2-3
pMM1019	Bacterium	pDawn	None	<sup>125</sup> , Addgene 43796	None
pMM1020	Bacterium	pDawn-sfGFP	GFP	<sup>125</sup> , Addgene 107741	1
pMM1230	Bacterium	T4SS genes, Gent <sup>R</sup> ,	None	This work	None
		∆traJ::Kan <sup>R</sup>			
pMM1231	Bacterium	T4SS genes, Gent <sup>R</sup> ,	None	This work	2-3
		∆traJ			
pMM1339	Bacterium	pDawn-TraJ	None	This work	2-3
pMM1437	Both	yeBFP, <i>ori</i> <sup>T</sup> , HIS3,	BFP	<sup>95</sup> , this work	3
		CEN/ARS			
pMM1438	Both	Cas9, ori <sup>T</sup> , sgRNA	None	This work	2b
		(YTK), HIS3			

# (Return to top)

# Chapter 6: Discussion

# 6.1 Summary of major findings, in brief

- The primary interaction regime of *E. coli* and *S. cerevisiae* is competition, though auxotrophic *E. coli* can form commensal relationships with prototrophic *S. cerevisiae*
- TKC is highest in commensal co-cultures of *E. coli* and *S. cerevisiae*, apparently due to an optimal combination of growth rates and competitive interactions (e.g. pH, toxicity) that yields a low steady-state donor-to-recipient ratio
- Mannoprotein adherence of *E. coli* to *S. cerevisiae* drives TKC and allows commensal relationship with auxotrophic *E. coli*
- Population dynamics in culture including TKC behave in a mostly deterministic manner,
   even with adherence between cells
- Mixed colonies of *E. coli* and *S. cerevisiae* mostly separate from each other spatially—apparently due to competition—though the degree of separation is modifiable through engineered interactions
- TKC events in colonies correlate positively with spatial population overlap
- The number of transconjugant cells in a colony largely depends on the ability of newly conjugated recipients to form a spatial niche in expanding growth
- Poorly growing recipient cells can be returned to normal growth ("rescued") via TKC if donor cells are (low-growing) commensals of recipients
- Cas9-cutting of episomal DNA without a repair sequence allows selectable cutting function in yeast
- TKC-delivered Cas9 can depress and/or collapse recipient cell populations in some conditions

Mannose supplementation in growth media can interrupt ongoing TKC functions
 (Return to top)

#### 6.2 Future directions and opportunities

#### 6.2.1 ... In this system

Many of the findings presented here are merely in introductory phases: the basics have been established, but there's incredible space for exploring nuances and applying these findings in new ways. Before undertaking such efforts, however, any would-be researcher would do well to switch to the TKC system recently published to have higher conjugation efficiency via a mutated *TraJ* promoter, easily available now on Addgene<sup>64</sup>. This increased capacity would greatly ease experiments looking into range of conjugative function from any angle, by increasing the effective signal-to-noise ratio. The effects of mannose on both preventing and interrupting TKC—surprising in their robustness—would be fascinating to explore further. Testing different concentrations of mannose could reveal the extent of interruptibility, or potentially even reversibility, and adding mannose at various times in co-culture could elucidate the minimum time needed for TKC to occur before neutralization. Further, the well-studied type I fimbriae that binds to mannoproteins provides an excellent alternative for optogenetic control, a la other systems that have used optogenetics to control adhesion-based patterning in consortia<sup>132,133</sup>, except in this case it would simultaneously drive adhesion and bolster TKC.

Many additional experiments would be enabled by finishing work on a TKC-reporter that allows reliable measurement of TKC events in time and space, not least those involving mixed colonies. Short of completely overhauling the fluorophores used to track donors and recipients—if need be,

donors would be the easier to change given mCherry's maintenance on a plasmid—more work could be done with a 2μ *trans*-reporter, vs. the *CEN/ARS* centromeric yeast replication machinery currently used, since 2μ plasmids have significantly higher copy numbers in yeast<sup>143</sup>; such a plasmid carrying yeBFP has already been constructed and only needs further testing to determine if it would work better than the current reporter. This would enable dynamic measurements of TKC events in culture (versus the day-end TKC measurements used here) via fluorimetry cytometry, help parse the differences between free and clumped transconjugants via fluorescence microscopy of cultures, and resolved spatial distribution of transconjugants in mixed colonies.

While I was able to deterministically model growth of this consortia in culture, modeling mixed colonies proved more elusive. Multiple collaborations toward spatially modeling growth (let alone TKC), whether by reaction-diffusion-like PDEs or adapting agent-based models<sup>145,146</sup> have yet to bear fruit. Of course, much more experimental work identifying and controlling mixed colony morphology would greatly aid such an endeavor, especially with a functional TKC-reporter. Further pursuit of agar pad data could "expand" our understanding of spatial founding effects, the extent to which each strain is able to grow proximal to the other, and where conjugative events occur and persist. It would also be fascinating to run functional TKC assays—those designed to alter recipient populations, e.g. those in Chapter 4—in a mixed colony setting. The rescue assay, for example, could show not only where recipient populations are susceptible to TKC-supported growth, it also has the benefit of amplifying any conjugation signal, by selecting for it; indeed this strategy was attempted for optogenetics experiments, to test whether low-frequency conjugation events were going undetected. If rescue or killing proved successful in colony settings, it would also be relevant to treatment applications to test a range of initial donor conditions: adding bacterial

cells at later times or at various distances from initial yeast colonies, to test donors' ability to alter established growth.

Finally, a logical expansion of these experiments would be to change the function of the DNA delivered to yeast recipients. Perhaps most in line with this work would be a strategy whereby TKC events shift the phase space (see 4.5.1.G) for subsequent TKC, e.g., including a feedback resistant leucine gene with high copy number in the conjugative DNA, such that transconjugants overproduce leucine at much higher rates, supporting donor growth beyond low, commensal levels. If effective, such a strategy could open the door to TKC-mediated circuit functions of these consortia, in this example causing oscillation between low donor growth pre-TKC, high donor growth upon sufficient leucine production, and lower donor growth again after leucine producing yeast are competed to low levels; any success engineering the consortia to self-regulate steadystate ratios via conjugative DNA would be huge. Alternatively, TKC-delivered functions could focus on modifying the bioproduction of some valuable product produced by S. cerevisiae, especially since we already have some information on which genes differentiate lab yeasts from, say, brewer's, baker's, or bioproduction yeast strains<sup>147</sup>. An initial test could focus on shifting a lab strain toward increased production on par with one of these industrial strain types—e.g. increased ethanol production—toward either new engineered yeasts or modification of wild yeasts in consortial bioproduction (domesticated versions of these species have already been used for consortial bioproduction of ethanol<sup>148</sup>).

#### 6.2.2 ... In a new system

I expect that many of the findings presented here could be reproduced for other fungal species, especially since so many fungi have mannoprotein-rich cell walls<sup>74</sup> that would cause aggregation<sup>72,73</sup>, and since *E. coli* are likely to grow faster than many fungi, opening the door to nutrient-limited donor growth control. Indeed, in an exploratory co-culture of *E. coli* with the pathogenic fungi *Candida albicans*, I found aggregates similar to those occurring with *S. cerevisiae*. But the first step toward any probiotic use with such fungal pathogens would be to verify and explore conjugative functions with the well-studied probiotic strain *E. coli* Nissle 1917 (EcN), which has been safely demonstrated for human probiotic use in several contexts<sup>149</sup>. The most commonly used Nissle strain, EcNc, is thankfully plasmid-free<sup>150</sup>, allowing more options for introduction of TKC components, but it's uncertain whether such introduction would be trivial, as other EcN's are poor recipients of several classes of Inc-type plasmids via conjugation, and it's unclear whether that's a function of resisting conjugation or failure to maintain conjugative plasmids (see Table IX, ref <sup>151</sup>).

In terms of targeting a more clinically-relevant pathogenic fungal recipient, *C.albicans* would be an unlikely starting point, despite its pathogenicity<sup>3</sup> and having tested co-cultures already, because the species is diploid<sup>152</sup>, adding a layer of unnecessary complexity to recipient maintenance of conjugated DNA (complexity that, to be clear, would be valuable to sort out at some future point). Contrastingly, opportunistic fungal pathogens such as *Candida glabrata*, *Aspergillus fumigatus*, or the cutaneous *Malassezia restricta*—which has been associated with Crohn's disease<sup>4</sup>—are all haploid and would all provide more suitable starting points for TKC-mediation<sup>153–155</sup>. All of these species would benefit from research targeting competitive exclusion by *E. coli* (perhaps especially

C.glabrata, as EcN's could be deployed to coat medical equipment commonly associated with candidiasis and prevent fungal colonization), or TKC-mediated killing by programming sgRNAs specific to each strain. C.glabrata and A.fumigatus would additionally benefit from TKC-mediated disruption of biofilm factors for adhesion, hyphal growth, etc., as C.glabrata is an opportunistic pathogen and A. fumigatus plays important roles in carbon cycling, so preventing virulence without killing recipients could be valuable<sup>7,156</sup>. M. restricta, given its ubiquity along skin surfaces, would perhaps benefit the most from spatially-resolved experiments of TKC intervention, as well as any successful optogenetic control. Any work that expands TKC to other fungal recipients would also benefit greatly from verifying orthogonality: explicitly targeting TKC expression in one fungal species and testing in a three-species system including the target recipient strain and another yeast e.g. S. cerevisiae. While I mention this as a bit of an afterthought, it's worth noting that it'd be incredibly nontrivial to establish such a three-species system in a reliable way, to verify singlespecies conjugative expression. Short of achieving this, a TKC system targeting a new fungal pathogen could be independently tested against S. cerevisiae and, for that matter, mammalian cells, for lack of expression.

The possible functions of TKC with fungi extend well beyond human pathogens, too. A wide range of fungi play huge roles in soil microbiomes—environments accessible for probiotic treatments—including plant pathogens<sup>6</sup>, and beneficial arbuscular mycorrhizal fungi (AMF)<sup>157</sup>. The broad host range, plant rot forming species *Botrytis cinerea* and *Sclerotinia sclerotiorum* both exist predominantly as haploids and can be cultured in lab settings, and both are recalcitrant to fungal treatments while infecting hundreds of valuable plants species worldwide<sup>158–160</sup>. Because such species have variable hosts, which in turn have variable resistance capacities, a TKC treatment that

interrupts a common source of pathogenicity—say, oxalic acid production in *S. sclerotiorum*<sup>161</sup>—could prove generically useful in a range of agricultural settings. Moreover, such cultivatable fungi could hypothetically be studied in controlled settings that allow cell visualization during plant root interactions, such as EcoFAB<sup>162</sup>, though it's not clear to me whether this system has been adapted for fungal growth. AMFs, on the other hand, require much more complex culture conditions on account of being obligate biotrophs with plants<sup>157</sup>, but would be no less interesting to study for TKC compatibility. A putative goal of such work might be to increase the secretion of so-called "Myc" factors produced by AMFs, which induce plant root growth toward establishing symbioses<sup>163</sup>, the genetic regulation of which seems uncertain in AMFs. Research using *A. fumigata* recipients might serve to straddle such soil-focused work and pathogen-focused work, since the ubiquitous fungus plays a role in carbon cycling and can be found in many a compost pile<sup>164</sup>. Specifically interrupting pathogenic routes—e.g. conidial virulence factors such as CcpA<sup>165,166</sup> or body temperature tolerance via CgrA<sup>7</sup>—could yield compost treatments that keep the fungi serving their saprophytic roles instead of causing respiratory illness.

#### (Return to top)

#### 6.3 Concluding remarks

In this research, I set out to merge two major and large-scale goals: *in situ* microbiome perturbation and new tools for engineering fungi (in consortia). Because these goals are broad and span the studies of microbiology, ecology, and a large diversity of research methods—engineered cross-feeding, expansion assay dynamics, population modeling, optogenetics, etc.—I dedicated a great deal of effort to establishing foundational data. How do the cells interact? What does a multi-species, let alone a multi-*kingdom* colony front look like? What does it mean to sustainably modify

a recipient population in situ? Thus, I consider this work to have laid the groundwork for similar research in some ways, highlighting useful principles such as the relationship between population dynamics and TKC events, or the capacity to alter recipients meaningfully, while at the same time, hopefully highlighting some caveats to avoid, such as the importance of basal interactions in building synthetic consortia, and the limitations in engineering consortial dynamics (certainly I'm not the first to realize this). I expect that some of these findings will readily pertain to other research, such as mannoprotein-binding and its correlation to TKC, or the effect that optimizing the consortial fitness of each strain has on maximizing TKC, though in the latter case, the usefulness of this "foundational" principle will only extend so far as commensalism—or another manifestation of these consortial fitness differences—is common among basal interactions with other species. Additionally, I would be fascinated for additional research on mixed colony ecology, and one day tying it to mixed biofilm ecology in a predictable and even controllable way, as it's my belief that the 3D geography of consortial distribution holds numerous keys to understanding microbial interactions, and there's ample space for discovery for anyone with the means of effectively studying it. Finally, it's my hope that others grow upon the repertoire of TKC and HGTbased perturbations to microbial populations, and that these future insights and tools are used for restoring health—in humans, in ecosystems, among plant life—and make up for myriad disturbances to the vast world of natural microbiomes that we're still just uncovering, even if we also use such tools for contained artificial ecosystems (e.g. synthetic bioproduction) that don't further exacerbate disruptions to natural systems caused by the Anthropocene.

## 7 References

- 1. Huffnagle, G.B., and Noverr, M.C. (2013). The emerging world of the fungal microbiome. Trends Microbiol *21*, 334–341. 10.1016/j.tim.2013.04.002.
- 2. Casadevall, A. (2018). Fungal Diseases in the 21st Century: The Near and Far Horizons. Pathog Immun *3*, 183–196. 10.20411/pai.v3i2.249.
- 3. Pappas, P.G., Lionakis, M.S., Arendrup, M.C., Ostrosky-Zeichner, L., and Kullberg, B.J. (2018). Invasive candidiasis. Nat Rev Dis Primers *4*, 18026. 10.1038/nrdp.2018.26.
- 4. Limon, J.J., Tang, J., Li, D., Wolf, A.J., Michelsen, K.S., Funari, V., Gargus, M., Nguyen, C., Sharma, P., Maymi, V.I., et al. (2019). Malassezia Is Associated with Crohn's Disease and Exacerbates Colitis in Mouse Models. Cell Host Microbe *25*, 377-388.e6. 10.1016/j.chom.2019.01.007.
- 5. Aykut, B., Pushalkar, S., Chen, R., Li, Q., Abengozar, R., Kim, J.I., Shadaloey, S.A., Wu, D., Preiss, P., Verma, N., et al. (2019). The fungal mycobiome promotes pancreatic oncogenesis via activation of MBL. Nature *574*, 264–267. 10.1038/s41586-019-1608-2.
- 6. Doehlemann, G., Ökmen, B., Zhu, W., and Sharon, A. (2017). Plant Pathogenic Fungi. Microbiology Spectrum *5*, 10.1128/microbiolspec.funk-0023–2016. 10.1128/microbiolspec.funk-0023-2016.
- 7. Dagenais, T.R.T., and Keller, N.P. (2009). Pathogenesis of Aspergillus fumigatus in Invasive Aspergillosis. Clinical Microbiology Reviews *22*, 447–465. 10.1128/cmr.00055-08.
- 8. McBride, J.A., Gauthier, G.M., and Klein, B.S. (2017). Clinical manifestations and treatment of blastomycosis. Clin Chest Med *38*, 435–449. 10.1016/j.ccm.2017.04.006.
- 9. Tumin, R. (2023). 1 Dead and Nearly 100 Sickened in Fungal Outbreak at Paper Mill. The New York Times.
- 10. Roemer, T., and Krysan, D.J. (2014). Antifungal Drug Development: Challenges, Unmet Clinical Needs, and New Approaches. Cold Spring Harb Perspect Med *4*, a019703. 10.1101/cshperspect.a019703.
- 11. Reddy, G.K.K., Padmavathi, A.R., and Nancharaiah, Y.V. (2022). Fungal infections: Pathogenesis, antifungals and alternate treatment approaches. Curr Res Microb Sci *3*, 100137. 10.1016/j.crmicr.2022.100137.
- 12. Costa-de-Oliveira, S., and Rodrigues, A.G. (2020). Candida albicans Antifungal Resistance and Tolerance in Bloodstream Infections: The Triad Yeast-Host-Antifungal. Microorganisms 8, 154. 10.3390/microorganisms8020154.
- 13. de Oliveira Santos, G.C., Vasconcelos, C.C., Lopes, A.J.O., de Sousa Cartágenes, M. do S., Filho, A.K.D.B., do Nascimento, F.R.F., Ramos, R.M., Pires, E.R.R.B., de Andrade, M.S., Rocha, F.M.G., et al. (2018). Candida Infections and Therapeutic Strategies: Mechanisms of

- Action for Traditional and Alternative Agents. Front Microbiol *9*, 1351. 10.3389/fmicb.2018.01351.
- 14. Balcha, F.B., and Neja, S.A. (2023). CRISPR-Cas9 mediated phage therapy as an alternative to antibiotics. Animal Diseases *3*, 4. 10.1186/s44149-023-00065-z.
- 15. Lacroix, B., and Citovsky, V. (2016). Transfer of DNA from Bacteria to Eukaryotes. mBio 7, e00863-16. 10.1128/mBio.00863-16.
- 16. Steffan, B.N., Venkatesh, N., and Keller, N.P. (2020). Let's Get Physical: Bacterial-Fungal Interactions and Their Consequences in Agriculture and Health. J Fungi (Basel) *6*, 243. 10.3390/jof6040243.
- 17. Shirtliff, M.E., Peters, B.M., and Jabra-Rizk, M.A. (2009). Cross-kingdom interactions: Candida albicans and bacteria. FEMS Microbiol Lett *299*, 1–8. 10.1111/j.1574-6968.2009.01668.x.
- 18. Bamford, C.V., d'Mello, A., Nobbs, A.H., Dutton, L.C., Vickerman, M.M., and Jenkinson, H.F. (2009). Streptococcus gordonii Modulates Candida albicans Biofilm Formation through Intergeneric Communication. Infect Immun 77, 3696–3704. 10.1128/IAI.00438-09.
- 19. Cornelison, C.T., Keel, M.K., Gabriel, K.T., Barlament, C.K., Tucker, T.A., Pierce, G.E., and Crow, S.A. (2014). A preliminary report on the contact-independent antagonism of Pseudogymnoascus destructans by Rhodococcus rhodochrous strain DAP96253. BMC Microbiol *14*, 246. 10.1186/s12866-014-0246-y.
- 20. Wu, N.C., Cramp, R.L., Ohmer, M.E.B., and Franklin, C.E. (2019). Epidermal epidemic: unravelling the pathogenesis of chytridiomycosis. Journal of Experimental Biology *222*, jeb191817. 10.1242/jeb.191817.
- 21. Mittermeier, F., Bäumler, M., Arulrajah, P., García Lima, J. de J., Hauke, S., Stock, A., and Weuster-Botz, D. (2023). Artificial microbial consortia for bioproduction processes. Engineering in Life Sciences *23*, e2100152. 10.1002/elsc.202100152.
- 22. Parapouli, M., Vasileiadis, A., Afendra, A.-S., and Hatziloukas, E. (2020). Saccharomyces cerevisiae and its industrial applications. AIMS Microbiol *6*, 1–31. 10.3934/microbiol.2020001.
- 23. Villarreal-Soto, S.A., Beaufort, S., Bouajila, J., Souchard, J.-P., and Taillandier, P. (2018). Understanding Kombucha Tea Fermentation: A Review. Journal of Food Science *83*, 580–588. 10.1111/1750-3841.14068.
- 24. Ponomarova, O., Gabrielli, N., Sévin, D.C., Mülleder, M., Zirngibl, K., Bulyha, K., Andrejev, S., Kafkia, E., Typas, A., Sauer, U., et al. (2017). Yeast Creates a Niche for Symbiotic Lactic Acid Bacteria through Nitrogen Overflow. Cell Systems *5*, 345-357.e6. 10.1016/j.cels.2017.09.002.

- 25. Sheth, R.U., Cabral, V., Chen, S.P., and Wang, H.H. (2016). Manipulating Bacterial Communities by in situ Microbiome Engineering. Trends in Genetics *32*, 189–200. 10.1016/j.tig.2016.01.005.
- 26. Klein, T.A., Ahmad, S., and Whitney, J.C. (2020). Contact-Dependent Interbacterial Antagonism Mediated by Protein Secretion Machines. Trends in Microbiology *28*, 387–400. 10.1016/j.tim.2020.01.003.
- 27. Green, E.R., and Mecsas, J. (2016). Bacterial Secretion Systems: An Overview. Microbiology Spectrum *4*, 4.1.13. 10.1128/microbiolspec.VMBF-0012-2015.
- 28. Singh, R.P., and Kumari, K. (2023). Bacterial type VI secretion system (T6SS): an evolved molecular weapon with diverse functionality. Biotechnol Lett *45*, 309–331. 10.1007/s10529-023-03354-2.
- 29. Kreitz, J., Friedrich, M.J., Guru, A., Lash, B., Saito, M., Macrae, R.K., and Zhang, F. (2023). Programmable protein delivery with a bacterial contractile injection system. Nature *616*, 357–364. 10.1038/s41586-023-05870-7.
- 30. Soltysiak, M.P.M., Meaney, R.S., Hamadache, S., Janakirama, P., Edgell, D.R., and Karas, B.J. (2019). Trans-Kingdom Conjugation within Solid Media from Escherichia coli to Saccharomyces cerevisiae. International Journal of Molecular Sciences *20*, 5212. 10.3390/ijms20205212.
- 31. Villa, T.G., Feijoo-Siota, L., Sánchez-Pérez, A., Rama, JL.R., and Sieiro, C. (2019). Horizontal Gene Transfer in Bacteria, an Overview of the Mechanisms Involved. In Horizontal Gene Transfer: Breaking Borders Between Living Kingdoms, T. G. Villa and M. Viñas, eds. (Springer International Publishing), pp. 3–76. 10.1007/978-3-030-21862-1\_1.
- 32. Brophy, J.A.N., Triassi, A.J., Adams, B.L., Renberg, R.L., Stratis-Cullum, D.N., Grossman, A.D., and Voigt, C.A. (2018). Engineered integrative and conjugative elements for efficient and inducible DNA transfer to undomesticated bacteria. Nature Microbiology *3*, 1043–1053. 10.1038/s41564-018-0216-5.
- 33. Ronda, C., Chen, S.P., Cabral, V., Yaung, S.J., and Wang, H.H. (2019). Metagenomic engineering of the mammalian gut microbiome in situ. Nat Methods *16*, 167–170. 10.1038/s41592-018-0301-y.
- 34. Our Solutions | Atterx Biotherapeutics https://www.atterx.com/gn-4474.
- 35. Razzaq, A., Saleem, F., Kanwal, M., Mustafa, G., Yousaf, S., Imran Arshad, H.M., Hameed, M.K., Khan, M.S., and Joyia, F.A. (2019). Modern Trends in Plant Genome Editing: An Inclusive Review of the CRISPR/Cas9 Toolbox. International Journal of Molecular Sciences 20, 4045. 10.3390/ijms20164045.
- 36. Rubin, B.E., Diamond, S., Cress, B.F., Crits-Christoph, A., Lou, Y.C., Borges, A.L., Shivram, H., He, C., Xu, M., Zhou, Z., et al. (2022). Species- and site-specific genome editing in complex bacterial communities. Nat Microbiol *7*, 34–47. 10.1038/s41564-021-01014-7.

- 37. Bourras, S., Rouxel, T., and Meyer, M. (2015). Agrobacterium tumefaciens Gene Transfer: How a Plant Pathogen Hacks the Nuclei of Plant and Nonplant Organisms. Phytopathology *105*, 1288–1301. 10.1094/PHYTO-12-14-0380-RVW.
- 38. Karas, B.J., Diner, R.E., Lefebvre, S.C., McQuaid, J., Phillips, A.P.R., Noddings, C.M., Brunson, J.K., Valas, R.E., Deerinck, T.J., Jablanovic, J., et al. (2015). Designer diatom episomes delivered by bacterial conjugation. Nature Communications *6*, 6925. 10.1038/ncomms7925.
- 39. Diner, R.E., Bielinski, V.A., Dupont, C.L., Allen, A.E., and Weyman, P.D. (2016). Refinement of the Diatom Episome Maintenance Sequence and Improvement of Conjugation-Based DNA Delivery Methods. Front. Bioeng. Biotechnol. *4*. 10.3389/fbioe.2016.00065.
- 40. Slattery, S.S., Diamond, A., Wang, H., Therrien, J.A., Lant, J.T., Jazey, T., Lee, K., Klassen, Z., Desgagné-Penix, I., Karas, B.J., et al. (2018). An Expanded Plasmid-Based Genetic Toolbox Enables Cas9 Genome Editing and Stable Maintenance of Synthetic Pathways in Phaeodactylum tricornutum. ACS Synth. Biol. 7, 328–338. 10.1021/acssynbio.7b00191.
- 41. Sharma, A.K., Nymark, M., Sparstad, T., Bones, A.M., and Winge, P. (2018). Transgene-free genome editing in marine algae by bacterial conjugation comparison with biolistic CRISPR/Cas9 transformation. Scientific Reports 8, 1–11. 10.1038/s41598-018-32342-0.
- 42. Waters, V.L. (2001). Conjugation between bacterial and mammalian cells. Nat Genet *29*, 375–376. 10.1038/ng779.
- 43. Heinemann, J.A., and Jr, G.F.S. (1989). Bacterial conjugative plasmids mobilize DNA transfer between bacteria and yeast. Nature *340*, 205–209. 10.1038/340205a0.
- 44. Nishikawa, M., and Yoshida, K. (1998). Trans-kingdom conjugation offers a powerful gene targeting: tool in yeast. Genetic Analysis: Biomolecular Engineering *14*, 65–73. 10.1016/S1050-3862(97)10003-1.
- 45. Nishikawa, M., Suzuki, K., and Yoshida, K. (1992). DNA integration into recipient yeast chromosomes by trans-kingdom conjugation between Escherichia coli and Saccharomyces cerevisiae. Curr Genet *21*, 101–108. 10.1007/BF00318467.
- 46. Inomata, K., Nishikawa, M., and Yoshida, K. (1994). The yeast Saccharomyces kluyveri as a recipient eukaryote in transkingdom conjugation: behavior of transmitted plasmids in transconjugants. J Bacteriol *176*, 4770–4773.
- 47. Suzuki, K., Moriguchi, K., and Yamamoto, S. (2015). Horizontal DNA transfer from bacteria to eukaryotes and a lesson from experimental transfers. Research in Microbiology *166*, 753–763. 10.1016/j.resmic.2015.08.001.
- 48. López-Igual, R., Bernal-Bayard, J., Rodríguez-Patón, A., Ghigo, J.-M., and Mazel, D. (2019). Engineered toxin—intein antimicrobials can selectively target and kill antibiotic-

- resistant bacteria in mixed populations. Nat Biotechnol *37*, 755–760. 10.1038/s41587-019-0105-3.
- 49. Hamilton, T.A., Pellegrino, G.M., Therrien, J.A., Ham, D.T., Bartlett, P.C., Karas, B.J., Gloor, G.B., and Edgell, D.R. (2019). Efficient inter-species conjugative transfer of a CRISPR nuclease for targeted bacterial killing. Nature Communications *10*, 1–9. 10.1038/s41467-019-12448-3.
- 50. Robledo, M., Álvarez, B., Cuevas, A., González, S., Ruano-Gallego, D., Fernández, L.Á., and de la Cruz, F. (2022). Targeted bacterial conjugation mediated by synthetic cell-to-cell adhesions. Nucleic Acids Research *50*, 12938–12950. 10.1093/nar/gkac1164.
- 51. Kominek, J., Doering, D.T., Opulente, D.A., Shen, X.-X., Zhou, X., DeVirgilio, J., Hulfachor, A.B., Groenewald, M., Mcgee, M.A., Karlen, S.D., et al. (2019). Eukaryotic Acquisition of a Bacterial Operon. Cell *176*, 1356-1366.e10. 10.1016/j.cell.2019.01.034.
- 52. Lacroix, B., and Citovsky, V. (2018). Beyond Agrobacterium-Mediated Transformation: Horizontal Gene Transfer from Bacteria to Eukaryotes. In Agrobacterium Biology: From Basic Science to Biotechnology Current Topics in Microbiology and Immunology., S. B. Gelvin, ed. (Springer International Publishing), pp. 443–462. 10.1007/82\_2018\_82.
- 53. Sysoeva, T.A., Kim, Y., Rodriguez, J., Lopatkin, A.J., and You, L. (2020). Growth-stage-dependent regulation of conjugation. AIChE Journal *66*, e16848. 10.1002/aic.16848.
- 54. Thomas, C.M. (1981). Molecular genetics of broad host range plasmid RK2. Plasmid *5*, 10–19. 10.1016/0147-619X(81)90074-3.
- 55. Sen, D., Van der Auwera, G.A., Rogers, L.M., Thomas, C.M., Brown, C.J., and Top, E.M. (2011). Broad-Host-Range Plasmids from Agricultural Soils Have IncP-1 Backbones with Diverse Accessory Genes ▼. Appl Environ Microbiol 77, 7975–7983. 10.1128/AEM.05439-11.
- 56. Bates, S., Cashmore, A.M., and Wilkins, B.M. (1998). IncP Plasmids Are Unusually Effective in Mediating Conjugation of Escherichia coli and Saccharomyces cerevisiae: Involvement of the Tra2 Mating System. J Bacteriol *180*, 6538–6543.
- 57. Waksman, G. (2019). From conjugation to T4S systems in Gram-negative bacteria: a mechanistic biology perspective. EMBO reports 20, e47012. 10.15252/embr.201847012.
- 58. Pansegrau, W., Lanka, E., Barth, P.T., Figurski, D.H., Guiney, D.G., Haas, D., Helinski, D.R., Schwab, H., Stanisich, V.A., and Thomas, C.M. (1994). Complete nucleotide sequence of Birmingham IncP alpha plasmids. Compilation and comparative analysis. J Mol Biol *239*, 623–663. 10.1006/jmbi.1994.1404.
- 59. Pansegrau, W., Balzer, D., Kruft, V., Lurz, R., and Lanka, E. (1990). In vitro assembly of relaxosomes at the transfer origin of plasmid RP4. Proc Natl Acad Sci U S A *87*, 6555–6559. 10.1073/pnas.87.17.6555.

- 60. Ziegelin, G., Fürste, J.P., and Lanka, E. (1989). TraJ protein of plasmid RP4 binds to a 19-base pair invert sequence repetition within the transfer origin. J Biol Chem *264*, 11989–11994.
- 61. Ou, J.T. (1975). Mating signal and DNA penetration deficiency in conjugation between male Escherichia coli and minicells. Proceedings of the National Academy of Sciences 72, 3721–3725. 10.1073/pnas.72.9.3721.
- 62. Christie, P.J. (2016). The Mosaic Type IV Secretion Systems. EcoSal Plus 7. 10.1128/ecosalplus.ESP-0020-2015.
- 63. Schröder, G., Schuelein, R., Quebatte, M., and Dehio, C. (2011). Conjugative DNA transfer into human cells by the VirB/VirD4 type IV secretion system of the bacterial pathogen Bartonella henselae. Proc Natl Acad Sci U S A *108*, 14643–14648. 10.1073/pnas.1019074108.
- 64. Cochrane, R.R., Shrestha, A., Severo de Almeida, M.M., Agyare-Tabbi, M., Brumwell, S.L., Hamadache, S., Meaney, J.S., Nucifora, D.P., Say, H.H., Sharma, J., et al. (2022). Superior Conjugative Plasmids Delivered by Bacteria to Diverse Fungi. BioDesign Research *2022*. 10.34133/2022/9802168.
- 65. Miller, C., Ho, J.M.L., and Bennett, M.R. (2019). Bacterial Killers Engineered to Exterminate Pathogenic Microbes. Molecular Cell 75, 5–6. 10.1016/j.molcel.2019.06.027.
- 66. Getino, M., and Cruz, F. de la (2018). Natural and Artificial Strategies To Control the Conjugative Transmission of Plasmids. Microbiology Spectrum *6*. 10.1128/microbiolspec.MTBP-0015-2016.
- 67. Filutowicz, M., Burgess, R., Gamelli, R.L., Heinemann, J.A., Kurenbach, B., Rakowski, S.A., and Shankar, R. (2008). Bacterial conjugation-based antimicrobial agents. Plasmid *60*, 38–44. 10.1016/j.plasmid.2008.03.004.
- 68. Lawrence, J.G., and Retchless, A.C. (2009). The Interplay of Homologous Recombination and Horizontal Gene Transfer in Bacterial Speciation. In Horizontal Gene Transfer: Genomes in Flux Methods in Molecular Biology., M. B. Gogarten, J. P. Gogarten, and L. C. Olendzenski, eds. (Humana Press), pp. 29–53. 10.1007/978-1-60327-853-9\_3.
- 69. Moriguchi, K., Yamamoto, S., Ohmine, Y., and Suzuki, K. (2016). A Fast and Practical Yeast Transformation Method Mediated by Escherichia coli Based on a Trans-Kingdom Conjugal Transfer System: Just Mix Two Cultures and Wait One Hour. PLOS ONE *11*, e0148989. 10.1371/journal.pone.0148989.
- 70. Hoek, T.A., Axelrod, K., Biancalani, T., Yurtsev, E.A., Liu, J., and Gore, J. (2016). Resource Availability Modulates the Cooperative and Competitive Nature of a Microbial Cross-Feeding Mutualism. PLOS Biology *14*, e1002540. 10.1371/journal.pbio.1002540.

- 71. Zhou, K., Qiao, K., Edgar, S., and Stephanopoulos, G. (2015). Distributing a metabolic pathway among a microbial consortium enhances production of natural products. Nat Biotechnol *33*, 377–383. 10.1038/nbt.3095.
- 72. Jann, K., Schmidt, G., Blumenstock, E., and Vosbeck, K. (1981). Escherichia coli adhesion to Saccharomyces cerevisiae and mammalian cells: role of piliation and surface hydrophobicity. Infect Immun *32*, 484–489.
- 73. Ofek, I., and Beachey, E.H. (1978). Mannose Binding and Epithelial Cell Adherence of Escherichia coli. Infection and Immunity *22*, 247–254.
- 74. Gow, N.A.R., Latge, J.-P., and Munro, C.A. (2017). The Fungal Cell Wall: Structure, Biosynthesis, and Function. Microbiology Spectrum *5*, 10.1128/microbiolspec.funk-0035–2016. 10.1128/microbiolspec.funk-0035-2016.
- 75. Dal Co, A., van Vliet, S., Kiviet, D.J., Schlegel, S., and Ackermann, M. (2020). Short-range interactions govern the dynamics and functions of microbial communities. Nature Ecology & Evolution *4*, 366–375. 10.1038/s41559-019-1080-2.
- 76. Scarinci, G., and Sourjik, V. (2023). Impact of direct physical association and motility on fitness of a synthetic interkingdom microbial community. ISME J *17*, 371–381. 10.1038/s41396-022-01352-2.
- 77. Muller, M.J.I., Neugeboren, B.I., Nelson, D.R., and Murray, A.W. (2014). Genetic drift opposes mutualism during spatial population expansion. Proceedings of the National Academy of Sciences *111*, 1037–1042. 10.1073/pnas.1313285111.
- 78. Cavalieri, D., and Polsinelli, M. Tri uoroleucine resistance and regulation of a-isopropyl malate synthase in Saccharomyces cerevisiae. 9.
- 79. Wu, F., Lopatkin, A.J., Needs, D.A., Lee, C.T., Mukherjee, S., and You, L. (2019). A unifying framework for interpreting and predicting mutualistic systems. Nat Commun *10*. 10.1038/s41467-018-08188-5.
- 80. Zhang, B., DeAngelis, D.L., and Ni, W.-M. (2021). Carrying Capacity of Spatially Distributed Metapopulations. Trends in Ecology & Evolution *36*, 164–173. 10.1016/j.tree.2020.10.007.
- 81. Levin, B.R., Stewart, F.M., and Rice, V.A. (1979). The kinetics of conjugative plasmid transmission: Fit of a simple mass action model. Plasmid *2*, 247–260. 10.1016/0147-619X(79)90043-X.
- 82. Simonsen, L., Gordon, D.M., Stewart, F.M., and Levin, B.R. (1990). Estimating the rate of plasmid transfer: an end-point method. Microbiology, *136*, 2319–2325. 10.1099/00221287-136-11-2319.

- 83. Zhao, Z.-J., Zou, C., Zhu, Y.-X., Dai, J., Chen, S., Wu, D., Wu, J., and Chen, J. (2011). Development of l-tryptophan production strains by defined genetic modification in Escherichia coli. J Ind Microbiol Biotechnol *38*, 1921–1929. 10.1007/s10295-011-0978-8.
- 84. Volkova, V.V., Lu, Z., Lanzas, C., Scott, H.M., and Gröhn, Y.T. (2013). Modelling dynamics of plasmid-gene mediated antimicrobial resistance in enteric bacteria using stochastic differential equations. Scientific Reports *3*, 2463. 10.1038/srep02463.
- 85. Pande, S., Shitut, S., Freund, L., Westermann, M., Bertels, F., Colesie, C., Bischofs, I.B., and Kost, C. (2015). Metabolic cross-feeding via intercellular nanotubes among bacteria. Nature Communications *6*, 6238. 10.1038/ncomms7238.
- 86. Moriguchi, K., Edahiro, N., Yamamoto, S., Tanaka, K., Kurata, N., and Suzuki, K. (2013). Transkingdom Genetic Transfer from Escherichia coli to Saccharomyces cerevisiae as a Simple Gene Introduction Tool. Appl Environ Microbiol *79*, 4393–4400. 10.1128/AEM.00770-13.
- 87. Zhong, X., Droesch, J., Fox, R., Top, E.M., and Krone, S.M. (2012). On the meaning and estimation of plasmid transfer rates for surface-associated and well-mixed bacterial populations. Journal of Theoretical Biology *294*, 144–152. 10.1016/j.jtbi.2011.10.034.
- 88. Germerodt, S., Bohl, K., Lück, A., Pande, S., Schröter, A., Kaleta, C., Schuster, S., and Kost, C. (2016). Pervasive Selection for Cooperative Cross-Feeding in Bacterial Communities. PLOS Computational Biology *12*, e1004986. 10.1371/journal.pcbi.1004986.
- 89. Preussger, D., Giri, S., Muhsal, L.K., Oña, L., and Kost, C. (2020). Reciprocal Fitness Feedbacks Promote the Evolution of Mutualistic Cooperation. Current Biology *30*, 3580-3590.e7. 10.1016/j.cub.2020.06.100.
- 90. Baba, T., Ara, T., Hasegawa, M., Takai, Y., Okumura, Y., Baba, M., Datsenko, K.A., Tomita, M., Wanner, B.L., and Mori, H. (2006). Construction of Escherichia coli K-12 in-frame, single-gene knockout mutants: the Keio collection. Mol Syst Biol *2*, 2006.0008. 10.1038/msb4100050.
- 91. Datsenko, K.A., and Wanner, B.L. (2000). One-step inactivation of chromosomal genes in Escherichia coli K-12 using PCR products. Proc Natl Acad Sci U S A *97*, 6640–6645.
- 92. Hosoda, K., Suzuki, S., Yamauchi, Y., Shiroguchi, Y., Kashiwagi, A., Ono, N., Mori, K., and Yomo, T. (2011). Cooperative Adaptation to Establishment of a Synthetic Bacterial Mutualism. PLoS One *6*. 10.1371/journal.pone.0017105.
- 93. Davis, J.H., Rubin, A.J., and Sauer, R.T. (2011). Design, construction and characterization of a set of insulated bacterial promoters. Nucleic Acids Res *39*, 1131–1141. 10.1093/nar/gkq810.
- 94. pCDF-mcherry1 was a gift from Michael Lynch (Addgene plasmid # 87144; http://n2t.net/addgene:87144; RRID:Addgene 87144).

- 95. Lee, M.E., DeLoache, W.C., Cervantes, B., and Dueber, J.E. (2015). A Highly Characterized Yeast Toolkit for Modular, Multipart Assembly. ACS Synth. Biol. *4*, 975–986. 10.1021/sb500366v.
- 96. Morel, P. (2018). Gramm: grammar of graphics plotting in Matlab. Journal of Open Source Software *3*, 568. 10.21105/joss.00568.
- 97. Tolker-Nielsen, T., and Molin, S. (2000). Spatial Organization of Microbial Biofilm Communities. Microb Ecol *40*, 75–84. 10.1007/s002480000057.
- 98. Cao, Z., Zuo, W., Wang, L., Chen, J., Qu, Z., Jin, F., and Dai, L. (2023). Spatial profiling of microbial communities by sequential FISH with error-robust encoding. Nat Commun *14*, 1477. 10.1038/s41467-023-37188-3.
- 99. Blanchard, A.E., and Lu, T. (2015). Bacterial social interactions drive the emergence of differential spatial colony structures. BMC Systems Biology 9, 59. 10.1186/s12918-015-0188-5.
- 100. Korolev, K.S., Avlund, M., Hallatschek, O., and Nelson, D.R. (2010). Genetic demixing and evolution in linear stepping stone models. Rev Mod Phys 82, 1691–1718. 10.1103/RevModPhys.82.1691.
- 101. Hallatschek, O., Hersen, P., Ramanathan, S., and Nelson, D.R. (2007). Genetic drift at expanding frontiers promotes gene segregation. Proc Natl Acad Sci U S A *104*, 19926–19930. 10.1073/pnas.0710150104.
- 102. Korolev, K.S., Xavier, J.B., Nelson, D.R., and Foster, K.R. (2011). A Quantitative Test of Population Genetics Using Spatiogenetic Patterns in Bacterial Colonies. Am Nat *178*, 538–552. 10.1086/661897.
- 103. Korolev, K.S., Müller, M.J.I., Karahan, N., Murray, A.W., Hallatschek, O., and Nelson, D.R. (2012). Selective sweeps in growing microbial colonies. Phys Biol *9*, 026008. 10.1088/1478-3975/9/2/026008.
- 104. Freese, P.D., Korolev, K.S., Jiménez, J.I., and Chen, I.A. (2014). Genetic Drift Suppresses Bacterial Conjugation in Spatially Structured Populations. Biophys J *106*, 944–954. 10.1016/j.bpj.2014.01.012.
- 105. Stalder, T., and Top, E. (2016). Plasmid transfer in biofilms: a perspective on limitations and opportunities. npj Biofilms and Microbiomes 2, 16022. 10.1038/npjbiofilms.2016.22.
- 106. Fusco, D., Gralka, M., Kayser, J., Anderson, A., and Hallatschek, O. (2016). Excess of mutational jackpot events in expanding populations revealed by spatial Luria–Delbrück experiments. Nat Commun 7, 12760. 10.1038/ncomms12760.
- 107. Li, Q., Lau, A., Morris, T.J., Guo, L., Fordyce, C.B., and Stanley, E.F. (2004). A Syntaxin 1, Gαo, and N-Type Calcium Channel Complex at a Presynaptic Nerve Terminal: Analysis

- by Quantitative Immunocolocalization. J Neurosci *24*, 4070–4081. 10.1523/JNEUROSCI.0346-04.2004.
- 108. Kearns, D.B. (2010). A field guide to bacterial swarming motility. Nat Rev Microbiol 8, 634–644. 10.1038/nrmicro2405.
- 109. Yip, A., Smith-Roberge, J., Khorasani, S.H., Aucoin, M.G., and Ingalls, B.P. (2022). Calibrating spatiotemporal models of microbial communities to microscopy data: A review. PLoS Comput Biol *18*, e1010533. 10.1371/journal.pcbi.1010533.
- 110. Joyce, G., Robertson, B.D., and Williams, K.J. (2011). A modified agar pad method for mycobacterial live-cell imaging. BMC Res Notes *4*, 73. 10.1186/1756-0500-4-73.
- 111. Ivanusic, D., Madela, K., and Denner, J. (2017). Easy and low-cost stable positioning of suspension cells during live-cell imaging. J Biol Methods 4, e80. 10.14440/jbm.2017.203.
- 112. Shin, J., Kim, G., Park, J., Lee, M., and Park, Y. (2023). Long-term label-free assessments of individual bacteria using three-dimensional quantitative phase imaging and hydrogel-based immobilization. Sci Rep *13*, 46. 10.1038/s41598-022-27158-y.
- 113. Zhu, L., Chen, T., Xu, L., Zhou, Z., Feng, W., Liu, Y., and Chen, H. (2020). Effect and mechanism of quorum sensing on horizontal transfer of multidrug plasmid RP4 in BAC biofilm. Science of The Total Environment *698*, 134236. 10.1016/j.scitotenv.2019.134236.
- 114. Kurita, T., Otsu, N., and Abdelmalek, N. (1992). Maximum likelihood thresholding based on population mixture models. Pattern Recognition *25*, 1231–1240. 10.1016/0031-3203(92)90024-D.
- 115. Shade, A., Peter, H., Allison, S., Baho, D., Berga, M., Buergmann, H., Huber, D., Langenheder, S., Lennon, J., Martiny, J., et al. (2012). Fundamentals of Microbial Community Resistance and Resilience. Frontiers in Microbiology *3*.
- 116. Gardiner, G.E., Casey, P.G., Casey, G., Lynch, P.B., Lawlor, P.G., Hill, C., Fitzgerald, G.F., Stanton, C., and Ross, R.P. (2004). Relative Ability of Orally Administered Lactobacillus murinus To Predominate and Persist in the Porcine Gastrointestinal Tract. Appl Environ Microbiol 70, 1895–1906. 10.1128/AEM.70.4.1895-1906.2004.
- 117. Britton, R.A., and Young, V.B. (2012). Interaction between the intestinal microbiota and host in Clostridium difficile colonization resistance. Trends Microbiol *20*, 313–319. 10.1016/j.tim.2012.04.001.
- 118. Dai, L., Vorselen, D., Korolev, K.S., and Gore, J. (2012). Generic Indicators for Loss of Resilience Before a Tipping Point Leading to Population Collapse. Science *336*, 1175–1177. 10.1126/science.1219805.
- 119. Scheffer, M., Carpenter, S., Foley, J.A., Folke, C., and Walker, B. (2001). Catastrophic shifts in ecosystems. Nature *413*, 591–596. 10.1038/35098000.

- 120. Ryan, O.W., Skerker, J.M., Maurer, M.J., Li, X., Tsai, J.C., Poddar, S., Lee, M.E., DeLoache, W., Dueber, J.E., Arkin, A.P., et al. (2014). Selection of chromosomal DNA libraries using a multiplex CRISPR system. eLife *3*, e03703. 10.7554/eLife.03703.
- 121. Horwitz, A.A., Walter, J.M., Schubert, M.G., Kung, S.H., Hawkins, K., Platt, D.M., Hernday, A.D., Mahatdejkul-Meadows, T., Szeto, W., Chandran, S.S., et al. (2015). Efficient Multiplexed Integration of Synergistic Alleles and Metabolic Pathways in Yeasts via CRISPR-Cas. Cell Syst *1*, 88–96. 10.1016/j.cels.2015.02.001.
- 122. Design guide RNAs (gRNAs) (2022). Benchling. https://help.benchling.com/hc/en-us/articles/9684282104333-Design-guide-RNAs-gRNAs-.
- 123. Mazraeh, D., and Di Ventura, B. (2022). Synthetic microbiology applications powered by light. Current Opinion in Microbiology *68*, 102158. 10.1016/j.mib.2022.102158.
- 124. Shimizu-Sato, S., Huq, E., Tepperman, J.M., and Quail, P.H. (2002). A light-switchable gene promoter system. Nature Biotechnology *20*, 1041–1044. 10.1038/nbt734.
- 125. Ohlendorf, R., Vidavski, R.R., Eldar, A., Moffat, K., and Möglich, A. (2012). From Dusk till Dawn: One-Plasmid Systems for Light-Regulated Gene Expression. Journal of Molecular Biology *416*, 534–542. 10.1016/j.jmb.2012.01.001.
- 126. Rao, P., Wang, L., Cheng, Y., Wang, X., Li, H., Zheng, G., Li, Z., Jiang, C., Zhou, Q., and Huang, C. (2020). Near-infrared light driven tissue-penetrating cardiac optogenetics via upconversion nanoparticles in vivo. Biomed. Opt. Express, BOE *11*, 1401–1416. 10.1364/BOE.381480.
- 127. Matsubara, T., and Yamashita, T. (2021). Remote Optogenetics Using Up/Down-Conversion Phosphors. Frontiers in Molecular Biosciences 8. 10.3389/fmolb.2021.771717.
- 128. Cui, M., Sun, T., Li, S., Pan, H., Liu, J., Zhang, X., Li, L., Li, S., Wei, C., Yu, C., et al. (2021). NIR light-responsive bacteria with live bio-glue coatings for precise colonization in the gut. Cell Reports *36*, 109690. 10.1016/j.celrep.2021.109690.
- 129. Cui, M., Pang, G., Zhang, T., Sun, T., Zhang, L., Kang, R., Xue, X., Pan, H., Yang, C., Zhang, X., et al. (2021). Optotheranostic Nanosystem with Phone Visual Diagnosis and Optogenetic Microbial Therapy for Ulcerative Colitis At-Home Care. ACS Nano *15*, 7040–7052. 10.1021/acsnano.1c00135.
- 130. Sureda-Vives, M., and Sarkisyan, K.S. (2020). Bioluminescence-Driven Optogenetics. Life *10*, 318. 10.3390/life10120318.
- 131. Moreno Morales, N., Patel, M.T., Stewart, C.J., Sweeney, K., and McClean, M.N. (2021). Optogenetic Tools for Control of Public Goods in Saccharomyces cerevisiae. mSphere 6, e0058121. 10.1128/mSphere.00581-21.

- 132. Jin, X., and Riedel-Kruse, I.H. (2018). Biofilm Lithography enables high-resolution cell patterning via optogenetic adhesin expression. PNAS *115*, 3698–3703. 10.1073/pnas.1720676115.
- 133. Chen, F., and Wegner, S.V. (2020). Blue-Light-Switchable Bacterial Cell–Cell Adhesions Enable the Control of Multicellular Bacterial Communities. ACS Synthetic Biology *9*, 1169–1180. 10.1021/acssynbio.0c00054.
- 134. Jin, X., and Riedel-Kruse, I.H. (2018). High-resolution Patterned Biofilm Deposition Using pDawn-Ag43. JoVE (Journal of Visualized Experiments), e58625. 10.3791/58625.
- 135. Anthamatten, D., and Hennecke, H. (1991). The regulatory status of the fixL- and fixJ-like genes in Bradyrhizobium japonicum may be different from that in Rhizobium meliloti. Molec. Gen. Genet. *225*, 38–48. 10.1007/BF00282640.
- 136. Kennedy, M.J., Hughes, R.M., Peteya, L.A., Schwartz, J.W., Ehlers, M.D., and Tucker, C.L. (2010). Rapid blue-light-mediated induction of protein interactions in living cells. Nat Methods 7, 973–975. 10.1038/nmeth.1524.
- 137. Tabor, J.J., Levskaya, A., and Voigt, C.A. (2011). Multichromatic control of gene expression in Escherichia coli. J Mol Biol 405, 315–324. 10.1016/j.jmb.2010.10.038.
- 138. Motta-Mena, L.B., Reade, A., Mallory, M.J., Glantz, S., Weiner, O.D., Lynch, K.W., and Gardner, K.H. (2014). An optogenetic gene expression system with rapid activation and deactivation kinetics. Nat Chem Biol *10*, 196–202. 10.1038/nchembio.1430.
- 139. Grødem, E.O., Sweeney, K., and McClean, M.N. Automated calibration of optoPlate LEDs to reduce light dose variation in optogenetic experiments. Biotechniques *69*, 313–316. 10.2144/btn-2020-0077.
- 140. Morgan, K. Plasmids 101: Origin of Replication. https://blog.addgene.org/plasmid-101-origin-of-replication.
- 141. Carroll, A.C., and Wong, A. (2018). Plasmid persistence: costs, benefits, and the plasmid paradox. Can. J. Microbiol. *64*, 293–304. 10.1139/cjm-2017-0609.
- 142. Bryant, J.A., Sellars, L.E., Busby, S.J.W., and Lee, D.J. (2014). Chromosome position effects on gene expression in Escherichia coli K-12. Nucleic Acids Res *42*, 11383–11392. 10.1093/nar/gku828.
- 143. Karim, A.S., Curran, K.A., and Alper, H.S. (2013). Characterization of plasmid burden and copy number in Saccharomyces cerevisiae for optimization of metabolic engineering applications. FEMS Yeast Res *13*, 10.1111/1567-1364.12016. 10.1111/1567-1364.12016.
- 144. Sweeney, K., Moreno Morales, N., Burmeister, Z., Nimunkar, A.J., and McClean, M.N. (2019). Easy calibration of the Light Plate Apparatus for optogenetic experiments. MethodsX 6, 1480–1488. 10.1016/j.mex.2019.06.008.

- 145. Prestes Garcia, A. (2011). A first approach to individual-based modeling of the bacterial conjugation dynamics.
- 146. García, A.P., and Rodríguez-Patón, A. (2015). BactoSim An Individual-Based Simulation Environment for Bacterial Conjugation. In Advances in Practical Applications of Agents, Multi-Agent Systems, and Sustainability: The PAAMS Collection Lecture Notes in Computer Science., Y. Demazeau, K. S. Decker, J. Bajo Pérez, and F. de la Prieta, eds. (Springer International Publishing), pp. 275–279. 10.1007/978-3-319-18944-4 26.
- 147. Davydenko, S., Meledina, T., Mittenberg, A., Shabelnikov, S., Vonsky, M., and Morozov, A. (2020). Proteomics Answers Which Yeast Genes Are Specific for Baking, Brewing, and Ethanol Production. Bioengineering (Basel) 7, 147. 10.3390/bioengineering7040147.
- 148. Wang, L., York, S.W., Ingram, L.O., and Shanmugam, K.T. (2019). Simultaneous fermentation of biomass-derived sugars to ethanol by a co-culture of an engineered Escherichia coli and Saccharomyces cerevisiae. Bioresource Technology *273*, 269–276. 10.1016/j.biortech.2018.11.016.
- 149. Ou, B., Yang, Y., Tham, W.L., Chen, L., Guo, J., and Zhu, G. (2016). Genetic engineering of probiotic Escherichia coli Nissle 1917 for clinical application. Appl Microbiol Biotechnol *100*, 8693–8699. 10.1007/s00253-016-7829-5.
- 150. Schlee, M., Wehkamp, J., Altenhoefer, A., Oelschlaeger, T.A., Stange, E.F., and Fellermann, K. (2007). Induction of Human β-Defensin 2 by the Probiotic Escherichia coli Nissle 1917 Is Mediated through Flagellin. Infection and Immunity *75*, 2399–2407. 10.1128/iai.01563-06.
- 151. Sonnenborn, U., and Schulze, J. (2009). The non-pathogenic Escherichia coli strain Nissle 1917 features of a versatile probiotic. Microbial Ecology in Health and Disease *21*, 122–158. 10.3109/08910600903444267.
- 152. Jones, T., Federspiel, N.A., Chibana, H., Dungan, J., Kalman, S., Magee, B.B., Newport, G., Thorstenson, Y.R., Agabian, N., Magee, P.T., et al. (2004). The diploid genome sequence of Candida albicans. Proceedings of the National Academy of Sciences *101*, 7329–7334. 10.1073/pnas.0401648101.
- 153. Fidel, P.L., Vazquez, J.A., and Sobel, J.D. (1999). Candida glabrata: Review of Epidemiology, Pathogenesis, and Clinical Disease with Comparison to C. albicans. Clin Microbiol Rev *12*, 80–96.
- 154. Galagan, J.E., Calvo, S.E., Cuomo, C., Ma, L.-J., Wortman, J.R., Batzoglou, S., Lee, S.-I., Baştürkmen, M., Spevak, C.C., Clutterbuck, J., et al. (2005). Sequencing of Aspergillus nidulans and comparative analysis with A. fumigatus and A. oryzae. Nature *438*, 1105–1115. 10.1038/nature04341.
- 155. Vijaya Chandra, S.H., Srinivas, R., Dawson, T.L., and Common, J.E. (2021). Cutaneous Malassezia: Commensal, Pathogen, or Protector? Front Cell Infect Microbiol *10*, 614446. 10.3389/fcimb.2020.614446.

- 156. Rodrigues, C.F., Rodrigues, M.E., Silva, S., and Henriques, M. (2017). Candida glabrata Biofilms: How Far Have We Come? J Fungi (Basel) *3*, 11. 10.3390/jof3010011.
- 157. Parniske, M. (2008). Arbuscular mycorrhiza: the mother of plant root endosymbioses. Nat Rev Microbiol *6*, 763–775. 10.1038/nrmicro1987.
- 158. Atwell, S., Corwin, J., Soltis, N., Subedy, A., Denby, K., and Kliebenstein, D. (2015). Whole genome resequencing of Botrytis cinerea isolates identifies high levels of standing diversity. Frontiers in Microbiology 6.
- 159. Attanayake, R.N., Tennekoon, V., Johnson, D.A., Porter, L.D., del Río-Mendoza, L., Jiang, D., and Chen, W. (2014). Inferring outcrossing in the homothallic fungus Sclerotinia sclerotiorum using linkage disequilibrium decay. Heredity *113*, 353–363. 10.1038/hdy.2014.37.
- 160. Prova, A., Akanda, A.M., Islam, S., and Hossain, Md.M. (2018). Characterization of Sclerotinia sclerotiorum, an Emerging Fungal Pathogen Causing Blight in Hyacinth Bean (Lablab purpureus). Plant Pathol J *34*, 367–380. 10.5423/PPJ.OA.02.2018.0028.
- 161. Gill, R., Sandhu, P.S., Sharma, S., and Sharma, P. (2021). Pathogenicity Determinants of Sclerotinia sclerotiorum and Their Association to Its Aggressiveness on Brassica juncea. Plant Pathol J *37*, 365–374. 10.5423/PPJ.OA.03.2021.0036.
- 162. Zengler, K., Hofmockel, K., Baliga, N.S., Behie, S.W., Bernstein, H.C., Brown, J.B., Dinneny, J.R., Floge, S.A., Forry, S.P., Hess, M., et al. (2019). EcoFABs: advancing microbiome science through standardized fabricated ecosystems. Nat Methods *16*, 567–571. 10.1038/s41592-019-0465-0.
- 163. Sun, J., Miller, J.B., Granqvist, E., Wiley-Kalil, A., Gobbato, E., Maillet, F., Cottaz, S., Samain, E., Venkateshwaran, M., Fort, S., et al. (2015). Activation of Symbiosis Signaling by Arbuscular Mycorrhizal Fungi in Legumes and Rice. The Plant Cell *27*, 823–838. 10.1105/tpc.114.131326.
- 164. Kwon-Chung, K.J., and Sugui, J.A. (2013). Aspergillus fumigatus—What Makes the Species a Ubiquitous Human Fungal Pathogen? PLoS Pathog *9*, e1003743. 10.1371/journal.ppat.1003743.
- 165. Takahashi-Nakaguchi, A., Sakai, K., Takahashi, H., Hagiwara, D., Toyotome, T., Chibana, H., Watanabe, A., Yaguchi, T., Yamaguchi, M., Kamei, K., et al. (2018). Aspergillus fumigatus adhesion factors in dormant conidia revealed through comparative phenotypic and transcriptomic analyses. Cell Microbiol *20*, e12802. 10.1111/cmi.12802.
- 166. Voltersen, V., Blango, M.G., Herrmann, S., Schmidt, F., Heinekamp, T., Strassburger, M., Krüger, T., Bacher, P., Lother, J., Weiss, E., et al. (2018). Proteome Analysis Reveals the Conidial Surface Protein CcpA Essential for Virulence of the Pathogenic Fungus Aspergillus fumigatus. mBio *9*, e01557-18. 10.1128/mBio.01557-18.

- 167. Lauterjung, K.R., Morales, N.M., and McClean, M.N. (2020). Secrete to beat the heat. Nat Microbiol *5*, 883–884. 10.1038/s41564-020-0748-3.
- 168. Laman Trip, D.S., and Youk, H. (2020). Yeasts collectively extend the limits of habitable temperatures by secreting glutathione. Nat Microbiol *5*, 943–954. 10.1038/s41564-020-0704-2.
- 169. Clements, C.F., and Ozgul, A. (2018). Indicators of transitions in biological systems. Ecology Letters *21*, 905–919. 10.1111/ele.12948.
- 170. Allee, W. C., Emerson, A. E., Park, O., Park, T. & Schmidt, K. P. Principles of Animal Ecology (W. B. Saunders, 1949). In.
- 171. Artemova, T., Gerardin, Y., Dudley, C., Vega, N.M., and Gore, J. (2015). Isolated cell behavior drives the evolution of antibiotic resistance. Mol Syst Biol *11*. 10.15252/msb.20145888.
- 172. Veraart, A.J., Faassen, E.J., Dakos, V., van Nes, E.H., Lürling, M., and Scheffer, M. (2012). Recovery rates reflect distance to a tipping point in a living system. Nature *481*, 357–359. 10.1038/nature10723.
- 173. Thorsen, M., Jacobson, T., Vooijs, R., Navarrete, C., Bliek, T., Schat, H., and Tamás, M.J. (2012). Glutathione serves an extracellular defence function to decrease arsenite accumulation and toxicity in yeast. Molecular Microbiology *84*, 1177–1188. 10.1111/j.1365-2958.2012.08085.x.
- 174. Grant, C.M. (2001). Role of the glutathione/glutaredoxin and thioredoxin systems in yeast growth and response to stress conditions. Mol. Microbiol. *39*, 533–541. 10.1046/j.1365-2958.2001.02283.x.
- 175. Scheffer, M., Bascompte, J., Brock, W.A., Brovkin, V., Carpenter, S.R., Dakos, V., Held, H., van Nes, E.H., Rietkerk, M., and Sugihara, G. (2009). Early-warning signals for critical transitions. Nature *461*, 53–59. 10.1038/nature08227.
- 176. Stindt, K.R., and McClean, M.N. (2022). Give and take in the exometabolome. Nat Microbiol *7*, 484–485. 10.1038/s41564-022-01081-4.
- 177. Douglas, A.E. (2020). The microbial exometabolome: ecological resource and architect of microbial communities. Philosophical Transactions of the Royal Society B: Biological Sciences *375*, 20190250. 10.1098/rstb.2019.0250.
- 178. Zengler, K., and Zaramela, L.S. (2018). The social network of microorganisms how auxotrophies shape complex communities. Nat Rev Microbiol *16*, 383–390. 10.1038/s41579-018-0004-5.
- 179. Yu, J.S.L., Correia-Melo, C., Zorrilla, F., Herrera-Dominguez, L., Wu, M.Y., Hartl, J., Campbell, K., Blasche, S., Kreidl, M., Egger, A.-S., et al. (2022). Microbial communities

- form rich extracellular metabolomes that foster metabolic interactions and promote drug tolerance. Nat Microbiol 7, 542–555. 10.1038/s41564-022-01072-5.
- 180. Cullen, C.M., Aneja, K.K., Beyhan, S., Cho, C.E., Woloszynek, S., Convertino, M., McCoy, S.J., Zhang, Y., Anderson, M.Z., Alvarez-Ponce, D., et al. (2020). Emerging Priorities for Microbiome Research. Frontiers in Microbiology *11*.
- 181. Machado, D., Maistrenko, O.M., Andrejev, S., Kim, Y., Bork, P., Patil, K.R., and Patil, K.R. (2021). Polarization of microbial communities between competitive and cooperative metabolism. Nature Ecology & Evolution, 1–9. 10.1038/s41559-020-01353-4.
- 182. Maier, L., Pruteanu, M., Kuhn, M., Zeller, G., Telzerow, A., Anderson, E.E., Brochado, A.R., Fernandez, K.C., Dose, H., Mori, H., et al. (2018). Extensive impact of non-antibiotic drugs on human gut bacteria. Nature *555*, 623–628. 10.1038/nature25979.
- 183. Szappanos, B., Kovács, K., Szamecz, B., Honti, F., Costanzo, M., Baryshnikova, A., Gelius-Dietrich, G., Lercher, M.J., Jelasity, M., Myers, C.L., et al. (2011). An integrated approach to characterize genetic interaction networks in yeast metabolism. Nat Genet *43*, 656–662. 10.1038/ng.846.
- 184. Adamowicz, E.M., Muza, M., Chacón, J.M., and Harcombe, W.R. (2020). Cross-feeding modulates the rate and mechanism of antibiotic resistance evolution in a model microbial community of Escherichia coli and Salmonella enterica. PLOS Pathogens *16*, e1008700. 10.1371/journal.ppat.1008700.
- 185. Alam, M.T., Zelezniak, A., Mülleder, M., Shliaha, P., Schwarz, R., Capuano, F., Vowinckel, J., Radmaneshfar, E., Krüger, A., Calvani, E., et al. (2016). The metabolic background is a global player in Saccharomyces gene expression epistasis. Nat Microbiol *1*, 1–10. 10.1038/nmicrobiol.2015.30.
- 186. Morris, J.J., Lenski, R.E., and Zinser, E.R. (2012). The Black Queen Hypothesis: Evolution of Dependencies through Adaptive Gene Loss. mBio *3*, 10.1128/mbio.00036-12. 10.1128/mbio.00036-12.
- 187. USDA/NASS 2017 State Agriculture Overview for Wisconsin https://www.nass.usda.gov/Quick\_Stats/Ag\_Overview/stateOverview.php?state=WISCONSI N.
- 188. USDA (2018). Summary Report: 2015 National Resources Inventory. (Natural Resources Conservation Service, Washington, DC, and Center for Survey Statistics and Methodology, Iowa State University, Ames, Iowa.).
- 189. WI DATCP (2017b). Wisconsin Nutrient Management Update.
- 190. Issaka, S., and Ashraf, M.A. (2017). Impact of soil erosion and degradation on water quality: a review. Geology, Ecology, and Landscapes *1*, 1–11. 10.1080/24749508.2017.1301053.

- 191. Lal, R. (2004). Soil carbon sequestration to mitigate climate change. Geoderma *123*, 1–22. 10.1016/j.geoderma.2004.01.032.
- 192. Shuler, R.E., Roulston, T.H., and Farris, G.E. (2005). Farming practices influence wild pollinator populations on squash and pumpkin. J Econ Entomol *98*, 790–795. 10.1603/0022-0493-98.3.790.
- 193. WI DATCP (2018b). Farmland Preservation Program Brochure.
- 194. WI DATCP (2018a). Farmland Preservation Program Landowner Survey Report.
- 195. WI Legislature Farmland Preservation. Chapter. Vol. 91.80.
- 196. WI Legislature Tillage Setback Performance Standard. NR. Vol. 151.03.
- 197. Arriaga, F.J. The Environmental and Economic Impact of Erosion in Wisconsin. 9.
- 198. WI DATCP (2016). Farmland Preservation Tax Credits FP Zoning and FP Agreements Signed OR Modified After JULY 1, 2009.
- 199. "CPI Inflation Calculator." n.d. (2019). https://data.bls.gov/cgibin/cpicalc.pl?cost1=1.00&year1=200901&year 2=201901.
- 200. WI DATCP (2017a). Farmland Preservation Bienniel Report 2015-2017.
- 201. Ruark, M.D., Kelling, K.A., and Good, L.W. (2014). Environmental Concerns of Phosphorus Management in Potato Production. Am. J. Potato Res. *91*, 132–144. 10.1007/s12230-014-9372-1.
- 202. Lauer, J. (2016). Strip-Tillage: How does it affect yield in Wisconsin? | Integrated Pest and Crop Management. http://ipcm.wisc.edu/blog/2016/05/strip-tillage-how-does-it-affect-yield-in-wisconsin/.
- 203. Zemlicka, J. (2014). Banding Vs. Broadcast: Saving Fuel And Fertilizer With Strip-Till Application. https://www.striptillfarmer.com/articles/1295-banding-vs-broadcast-saving-fuel-and-fertilizer-with-strip-till-application.

# Appendix A: Secrete to Beat the Heat (News & Views Article)

Published in Nature Microbiology June 2020<sup>167</sup>.

#### A.1 Body text

Cooperative behaviour enables populations of yeast cells to survive high temperatures.

Temperature affects growth rate, metabolism, morphology and reproduction in microorganisms. At optimal temperatures, growth and reproduction are efficient. But as temperatures increase, reactive oxygen species are produced and proteins denature, resulting in oxidative stress, growth cessation and death. A microorganism has upper and lower temperature limits for growth with an optimum at some point between these two extremes. Saccharomyces cerevisiae (budding yeast) grows optimally at ~35 °C and ceases growth above 40 °C. In this issue of Nature Microbiology, Laman Trip and Youk find that between habitable (~38 °C) and uninhabitable (~40 °C) temperatures, growth at 39 °C is dependent on population density 168.

Laman Trip and Youk experimentally mapped population-level yeast growth as a function of temperature and initial density (Fig. 1). The resulting phase diagram revealed that all yeast populations fail to survive in temperatures above 40.3 °C. As this tipping-point temperature is approached, dense yeast populations continue to grow, less dense populations vary between some growing and some not growing, and sparse populations do not grow at all. Transitions between growth and non-growth were shown to be sensitive to additional stressors. For example, yeast that constitutively overexpress a fluorescent protein, and therefore demand more cellular resources, had a lower tipping-point temperature. Laman Trip and Youk ruled out selection for heat-tolerant

mutants or persister cells by demonstrating that sub-cultured survivors are not heat tolerant and that initial population decay rates are inconsistent with persister cells.

Laman Trip and Youk's results show that yeast are better equipped to survive high temperatures when surrounded by neighbouring cells. This finding is surprising, because the textbook view is that survival is influenced by each individual cell's response and fitness. Further, they find that the transition between habitable and uninhabitable temperature conditions is exquisitely sensitive to cell density. Such density-dependent behaviour has been observed in many ecological systems that demonstrate cooperativity<sup>169</sup>. Cooperation leads to an Allee effect, whereby at low densities, the population growth rate increases with population density<sup>170</sup>. This effect further leads to the catastrophic tipping point seen at 40.3 °C where a stable state of the system merges with the unstable state. Once past this tipping point, the only stable state available to the system is extinction. Similar behaviour is seen in many ecological systems<sup>119</sup>, including microbial populations that demonstrate cooperativity<sup>171,172</sup>. One particularly relevant example, also in budding yeast, is the cooperative metabolism of sucrose by secreted invertase. Dilution of yeast populations growing on sucrose results in a strikingly similar pattern of density-dependent growth and a tipping point at high dilution rates<sup>118</sup>.

Harmful reactive oxygen species are produced when cells are exposed to high temperatures. Therefore, Laman Trip and Youk hypothesized that glutathione, an important yeast antioxidant 173,174, might enable cooperative thermoprotection. They showed that glutathione accumulates in yeast cultures grown at high temperatures. Furthermore, spent media from these cultures or high concentrations of pure glutathione enabled growth when added to cultures that

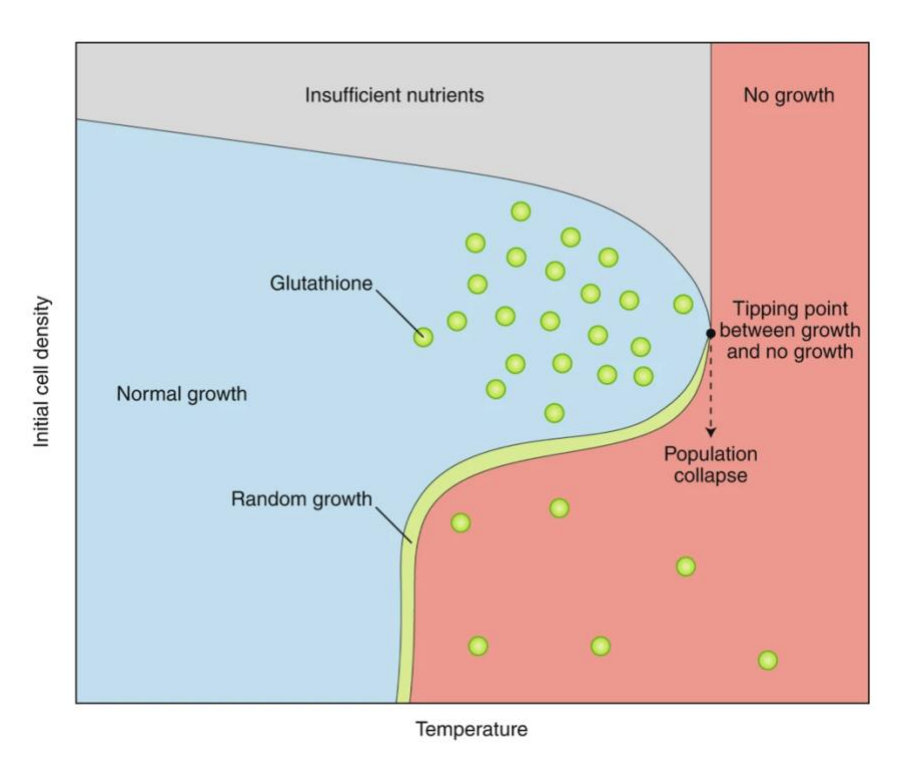
were otherwise too dilute to thrive at higher temperatures. Laman Trip and Youk generated and analysed mutations in genes known to be involved in glutathione transport and production, further demonstrating that the production and export of glutathione is essential to maintain growth at high temperatures, whereas importation is not. This suggests that the protection mechanism operates in the extracellular space. The authors built a stochastic mathematical model of yeast growth, in which the probability of replication is nonlinearly dependent on extracellular glutathione concentration. This model predicts population growth for different initial densities and temperatures, and fully recapitulates their experimental findings.

The authors' results suggest several research questions that could be investigated in the future. Although their data suggest that glutathione accumulation is necessary and sufficient for growth at high temperatures, it would be interesting to examine if other unidentified cooperative interactions also have a role. The mechanisms that allow some populations, but not others, to grow at higher temperatures could be examined in the context of variability in cell age, expression capacity and other factors. Thermotolerance in experimentally tractable yeast might be an interesting model system for examining early warning signals of population collapse<sup>175</sup>, particularly in the context of global warming and climate change.

The study by Laman Trip and Youk updates the conventional view of how yeast combat heat stress. More broadly, it also challenges a view of microbial biology based on autonomous cells and instead indicates that we need to adopt a systems biology framework — on par with the dynamical systems of macroecology — for even the simplest and most well-understood behaviours. In the simple intraspecies system examined by Laman Trip and Youk, intercellular interactions give rise to

emergent population-level phenotypes. In more complex communities, including multispecies communities or monospecies communities with metabolic specialization, more complicated interactions are possible, with correspondingly difficult-to-predict behaviours at the population level. Further experimental and theoretical research connecting measurable interactions with the ecology of microbial populations represents an important frontier in microbiology and carries many important implications for human and environmental health.

A.2 Figure 1: Cooperative secretion of glutathione extends the habitable temperature range for yeast.



The growth of yeast populations was measured by Laman Trip and Youk as a function of initial cell density and temperature1. These conditions result in normal growth (blue region), random growth (populations that sometimes grow and sometimes do not; green region), no growth (red region) or no growth due to nutrient depletion (grey region). Past a catastrophic tipping point, where the stable fixed point (the boundary between normal growth and nutrient-limited regions) and the unstable fixed point (random growth region) collide, no growth is possible. Secretion of

glutathione (green circles) by yeast leads to density-dependent growth at intermediate temperatures. Glutathione acts as an antioxidant, protecting yeast from cellular damage by reactive oxygen species. Too few cells results in insufficient amounts of glutathione produced and cells thus failing to divide (no growth/collapse). At higher cell densities, the cooperative production of glutathione protects yeast from heat damage and extends the habitable temperature range, resulting in growth.

# Appendix B: Give and Take in the Exametabolome (News & Views Article)

Published in Nature Microbiology March 2022<sup>176</sup>.

#### B.1 Body text

Metabolic changes in auxotrophs enrich the microbial community exometabolome and increase drug resistance.

Metabolic exchange between microorganisms affects microbial community formation, structure, physiology and resilience<sup>177</sup>. Auxotrophs, microorganisms that lack essential metabolic pathways, occur at high frequencies in naturally occurring microbial communities, which suggests that they are crucial for community assembly and function<sup>178</sup>. However, it is not clear how the presence of auxotrophs benefits the entire community, let alone how auxotrophs benefit prototrophs — cells that have the necessary metabolic pathways to synthesize all needed nutrients. In this issue of Nature Microbiology, Alam et al. report on the use of synthetic, self-establishing metabolically cooperating communities (SeMeCos) of Saccharomyces cerevisiae yeast to examine how auxotrophs contribute to community function<sup>179</sup>. They show that metabolic changes in auxotrophs affect all community members and influence metabolism, growth and drug resistance in prototrophs.

Much of what is known about the species composition and metabolic capabilities of microbial communities is derived from bioinformatic analyses of sequence data collected from naturally occurring communities<sup>180</sup>. In their study, Alam et al. take a complementary approach, and utilize SeMeCos to pose targeted research questions about metabolism and drug resistance in microbial communities that harbour both auxotrophs and prototrophs. The SeMeCos work by encoding

essential genes required for the biosynthesis of leucine (L), histidine (H), uracil (U) and methionine (M) on separate plasmids that randomly segregate during cell division, resulting in some yeast cells that are prototrophs whereas others lack one or more of the plasmids, which renders them auxotrophic (Fig. 1a). Each plasmid also encodes a different fluorescent reporter, which enabled Alam et al. to quantify and isolate different auxotrophs in the mixed community using high-throughput microscopy and fluorescence-activated cell sorting (FACS).

The drug tolerance of microbial communities is increasingly understood as an emergent community-level property, affected by myriad interactions within the community. An outstanding question is how community auxotrophs, and their interactions with other community members, affect drug resistance and tolerance. Alam and colleagues analysed data from the Earth Microbiome Project (EMP), a global crowd-sourced repository of microbiomes <sup>179</sup>, using genome-scale metabolic modelling developed by Machado et al. to identify auxotrophs <sup>181</sup>. They confirmed that a high frequency of amino-acid biosynthesis-related auxotrophies exists in all microbial communities, but noted that the highest fraction of these dependences is present in host-associated communities. In addition to containing a rich nutritional environment, host-associated microbiomes are more likely to be exposed to bioactive drugs. The authors next focused their analysis on growth data of 40 gut microbiome bacteria exposed to bioactive drugs <sup>182</sup>. They showed that microbiome members with auxotrophies in essential amino-acid biosynthetic pathways (15 of 40) fared better than or equal to their prototrophic counterparts in the presence of growth-suppressing drugs.

Resistance is particularly problematic in fungi, for which there are few classes of drugs and drug resistance is on the rise. To better understand the role of auxotrophs in drug tolerance, and to evaluate whether the same principles apply to fungal members of microbial communities, Alam et al. exposed the SeMeCos to 900 US Food and Drug Administration (FDA)-approved drugs, thereby allowing differences in drug tolerance to be directly associated with specific auxotrophies. Two groups of the FDA-approved drugs increased the auxotrophic composition of the SeMeCos, indicating that a target-independent drug robustness mechanism may exist within the auxotrophs relative to prototrophs. This was notably true for azoles, and analysis using an additional panel of five azoles and statins (both target the ergosterol biosynthetic pathway in yeast) confirmed this finding.

Auxotrophies, by definition, influence an individual organism's metabolism. Alam et al. combined computational and experimental approaches to understand the connection between individual auxotrophies and community-level metabolism. A flux balance analysis (FBA), building on an existing yeast genome-scale metabolic model<sup>183</sup>, revealed that community auxotrophs had (on average) more reactions with increased flux. Indeed, the number of auxotrophies present correlated with the number of metabolic pathways exhibiting altered flux. In addition, proteomic analysis of cells that are auxotrophic for a single amino acid or uracil confirmed results from the FBA analysis. Alam and collaborators then applied targeted metabolomics to measure the concentrations of amino acids and uracil in cells and in the exometabolome. Counterintuitively, reduction of the required metabolite in the presence of the corresponding auxotrophs was not usually observed. Rather, auxotrophs were shown to have increased export activity, thus resulting in metabolic enrichment of the exometabolome and drug tolerance in the SeMeCos. They use the cationic

carbocyanine dye DiOC5(3), which passively diffuses into cells and is subsequently exported alongside other nutrients, to show that auxotrophic cells export more metabolites than prototrophs in the SeMeCos. In keeping with this finding of ramped up export, auxotrophs show reduced intracellular concentration of the drug uniconazole relative to prototrophs.

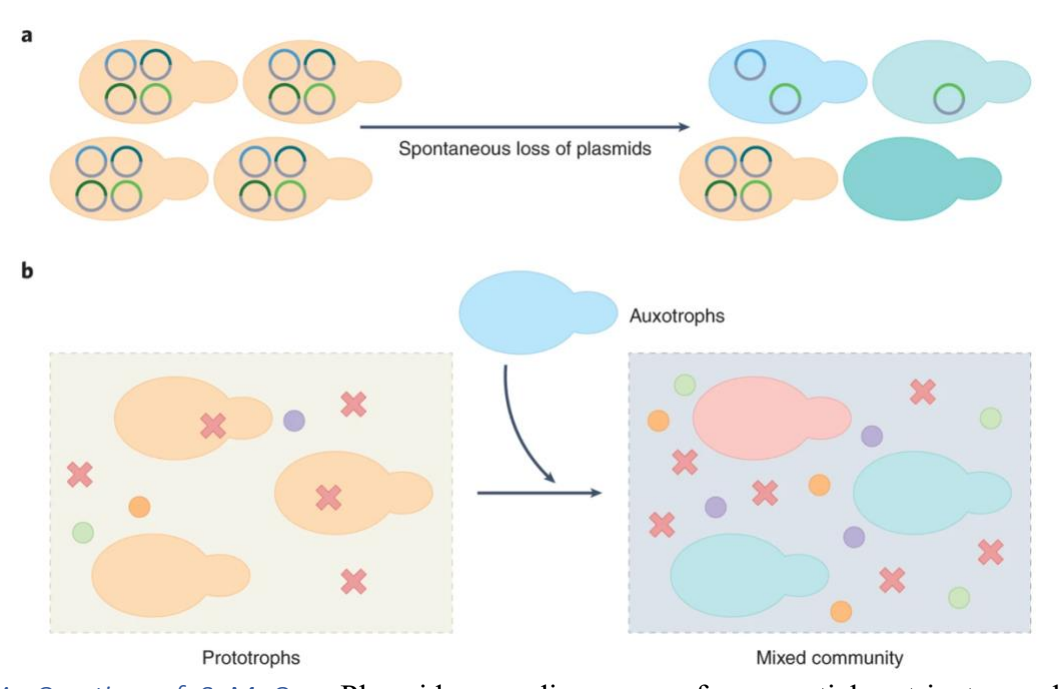
Finally, when protein expression of prototrophs from the mixed SeMeCos was compared with a wholly prototrophic community, prototrophs in the SeMeCos show altered protein expression, including increased expression of proteins involved in growth-related processes.

Taken together, the authors interpret their findings to hypothesize that the metabolisms of both auxotrophs and prototrophs totally reconfigure in microbial communities. Alam et al. find that the sheer abundance of extracellular nutrients exported by auxotrophic community members correlates with increased azole resistance and tolerance for prototrophic yeasts over a range of supplemented nutrient compositions and concentrations. It seems that increased metabolite export in communities that harbour auxotrophs creates a rich exometabolome that also provides auxotrophs with a target-independent drug-resistance mechanism. Indeed, simply supplementing the media with higher concentrations of H, L, U and M encoded by SeMeCo plasmids — nutrients that are present in higher concentrations in auxotroph-containing exometabolomes — is sufficient for prototrophic yeasts to exhibit higher drug robustness on both solid and liquid media.

Understanding how, and why, communities support individual organisms that lack the capacity to survive on their own, is important in microbiology, synthetic biology, evolution and ecology<sup>178</sup>. The findings by Alam et al. are valuable and build on other recent findings that demonstrate the

correlation of metabolomes to antibiotic resistance and the adaptability of said metabolomes to the community environment<sup>184,185</sup>. While much work is yet needed to establish a consistent and causative link between community composition and resistance, Alam's research suggests a surprising new avenue for exploration on this front. Most striking are the effects of auxotrophs on prototrophs. The mere presence of auxotrophs can benefit community functions, which adds a twist to the canonical view that prototrophs 'bear the burden' of mixed communities by producing shared resources that auxotrophs can exploit. It seems that the Black Queen Hypothesis<sup>186</sup>, which states that auxotrophs enjoy increased fitness in the right environments due to decreased cellular burden, and thus act as either commensals or parasites on their prototrophic neighbours, is perhaps more complex than originally proposed.

### B.2 Figure 1: SeMeCos to determine the effects of auxotrophs.



A. Creation of SeMeCos. Plasmids encoding genes for essential nutrients render yeast cells prototrophic (orange, left). Cells spontaneously lose these plasmids over generations, resulting in

a mixed population of prototrophs (orange, right) and auxotrophs (shades of blue, right), which lack one or more of these essential genes.

B. Exometabolome and community drug resilience. Relative to a community of wildtype prototrophic yeast (orange), inclusion of auxotrophic cells (blue) rewires both the extracellular metabolic environment through increased export and the metabolisms of prototrophs (red) in SeMeCos. This community adaptation not only increases shared nutrients in the extracellular space (coloured circles), but also increases community drug resilience by exporting intracellular drugs (red crosses).

# Appendix C: Protecting Soil Resources by Improving the Wisconsin Farmland Preservation Program (Policy Memo)

Published in Journal of Science Policy & Governance, October 2019.

#### C.1 Executive Summary

Soil erosion is a continuing problem in Wisconsin (WI), with erosion rates at double the national standard and increasing over time. Among other environmental concerns, this erosion impairs cropland productivity and pollutes waterways. Wisconsin's Farmland Preservation (FP) program is the state's largest program for maintaining soil erosion conservation standards. To combat soil erosion, we recommend improvements to the FP program incentives and conservation standards. The FP program sees substantial enrollment loss from contract expirations, so we recommend changing FP timespan from 15-year contracts to 5-year segments with automatic renewal. Additionally, to further increase enrollment in FP, we recommend increasing enrollment incentives by scheduling annual increases in FP tax credits indexed to inflation. Finally, we recommend tilling conservation standards be added to FP guidelines to require no-till or strip-till farming on enrolled acreage as a major step to decrease soil erosion.

#### C.2 Soil erosion and Wisconsin

Soil erosion decreases the acreage and quality of farmland, negatively impacts waterways, and increases flooding risk. WI has over 7 million acres operating as cropland <sup>187</sup> and approximately 34 million tons of cropland soil eroded due to runoff in 2015 <sup>188</sup>. Erosion in WI was almost double the national average in 2015, and, while national erosion rates are decreasing over time, WI rates are increasing <sup>188</sup>. It can take between 100 to 500 years for an inch of lost topsoil to form, and it's

estimated that nutrient loss through soil erosion can cost farmers \$51 to \$64 per acre in manure to compensate 189. Erosion comes with many other costs, including:

- Waterway pollution, causing algal blooms at the detriment of aquatic ecosystems <sup>190</sup>
- Decreases in amount of prime farmland in WI<sup>188</sup>
- Decreases in soil carbon sequestration, which increases dangerous greenhouse gasses in the atmosphere<sup>191</sup>
- Decreases in pollinator bee populations <sup>192</sup>

#### C.3 Farmland Preservation Program

Wisconsin's Farmland Preservation (FP) program is the largest state-run program that addresses soil erosion and prevents active soil acreage loss to commercial development<sup>193</sup>. FP enrolls farmers in 15-year contracts to zone acreage as farmland and to apply conservation standards within those acres. However, enrollment has decreased from 2.9 million acres of WI farmland in 2010 to 2.3 million in 2017 due to contract expirations without renewal<sup>194</sup>. According to a 2017 survey, farmers are not renewing because they do not want to limit the use of their land for 15 years (57% of farmers), and the tax credit is not high enough (31% of farmers)<sup>194</sup>.

#### C.4 Farmland Preservation lacks sufficient tilling standards

Farmers must demonstrate compliance with state conservation standards to qualify for FP, but these guidelines scarcely address a major contributor of soil erosion: conventional tilling practices <sup>195,196</sup>. The alternative tilling practices of no-till and strip-till, where none or only the portion of soil containing the seed row is tilled, prevent soil erosion and slow land degradation by minimizing soil disruption. In addition, these minimal tilling methods decrease time and diesel costs to farmers; strip tilling uses about half-asmany gallons of diesel per acre as conventional methods<sup>197</sup>. While usage of minimal tillage practices have increased since 2012, approximately

40% of WI cropland still undergoes conventional tilling, with corn accounting for the largest share of conventional tilling by acreage<sup>187</sup>.

#### C.5 Policy recommendations

Below we provide three major options to mitigate the many effects of soil erosion by increasing conservation efforts among farmers.

- i. Change FP timespan from 15-year contracts to 5year segments with automatic renewal Enrollment lasts indefinitely but could be cancelled at the end of any 5-year segment.
  - Advantages: Decreased length of time commitment for the farmer. State maintains enrollment by preventing loss from contract expiration.
  - *Disadvantages*: Higher administrative resources to handle 5-year segments. Farmers may cancel the contract earlier.
- ii. Schedule annual increases in FP tax credits by indexing to inflation Tax credits for FP are set at \$5, \$7.5, and \$10 per acre over three categories, but have not been updated since July 2009<sup>198</sup>. As of January 2019, indexing tax credits would increase credits to \$5.85, \$8.28, and \$11.7.

Advantages: Farmers would be assured a tax credit that scales over time and policy-makers would not need to adjust the credit continuously for inflation. Higher incentives should increase enrollment.

*Disadvantages:* Greater cost to the state; payments would cost an additional 17% in 2019<sup>199</sup>, or \$2.72 million extra based on 2016 payments<sup>200</sup>.

iii. Include tilling standards for FP (Chapter 91) to require no-till or strip-till farming on enrolled acreage We recommend stipulating no-till or strip-till practices for farmers to receive FP funds.

Advantages: Decreased soil erosion and associated benefits explained above. If all cropland complied with these standards, we estimate that erosion would decrease by more than half (tons per acre) in the first year and continue to improve in subsequent years as soil health increases<sup>201</sup>.

*Disadvantages:* High start-up costs associated with mechanical changeover. Costs to farmers can be mitigated by committing additional state funding.

Wisconsin's FP program is the best tool for improving soil health sustainably, and here we outline improvements to the three main problem areas of the program. We recommend implementing all three policy options to maximize conservation efforts and soil health.

# C.6 Appendix

#### Potential problems and solutions with minimal tilling

The scope of the above changes is restricted to FP participants by modifying Chapter 91 to include tilling standards that are stricter than NR 151<sup>196</sup>. As a more robust option, changes to statewide conservation standards could apply to all farmland in the state by modifying NR 151. NR 151 of the Wisconsin Administrative Code for the Dept. of Natural Resources only includes restrictions on tilling adjacent to waterways but could be expanded to require minimal tilling. Resistance to minimal tilling practices is largely due to a stressed planting timeline at the end of winter. Tilling turns up the soil, drying out the top layer to allow more rapid seeding, but also decreasing soil health. Our proposal would still allow strip-tilling, which also allows for rapid seeding, though only in very limited areas, with the intent to address this concern. Another widespread misconception of minimal tilling relates to expected drops in crop yields. Data shows that while a small drop does occur for both methods in the first year, continued use of minimal tilling actually increases crop yields relative to conventional tilling<sup>202</sup>. Mechanical changeover costs can run up

to \$100,000 to begin strip-tilling operations, but savings in fertilizer and diesel costs could make up this amount in only a few years depending on the size of the farm<sup>203</sup>. As stated in the memo, we recommend financial incentives to help farmers purchase, lease, or share equipment.